

ON LUBRICATION AND FRICTION IN SOFT ROUGH  
CONFORMAL SLIDING CONTACTS

Experimental and theoretical contributions to the discussion  
on elastomer shaft seal tribology

Von der Fakultät für Maschinenbau  
der Gottfried Wilhelm Leibniz Universität Hannover  
zur Erlangung des akademischen Grades  
Doktor-Ingenieur  
genehmigte  
Dissertation

von  
Dipl.-Ing. BENGT WENNEHORST

2016







ON LUBRICATION AND FRICTION IN SOFT ROUGH  
CONFORMAL SLIDING CONTACTS

Experimental and theoretical contributions to the discussion  
on elastomer shaft seal tribology

Von der Fakultät für Maschinenbau  
der Gottfried Wilhelm Leibniz Universität Hannover  
zur Erlangung des akademischen Grades  
Doktor-Ingenieur  
genehmigte  
Dissertation

von  
Dipl.-Ing. BENGT WENNEHORST

2016

1. Referent: Prof. Dr.-Ing. G. Poll  
2. Referent: Prof. Dr.-Ing. B. Glasmacher  
Vorsitzender: Prof. Dr.-Ing. B.-A. Behrens  
Tag der Promotion: 22.12.2016

Bengt Wennehorst: *On lubrication and friction in soft rough conformal sliding contacts—Experimental and theoretical contributions to the discussion on elastomer shaft seal tribology*, Dissertation, © 2016

*To my family*





---

## ABSTRACT

---

Conformal surfaces in parallel sliding lack a macroscopic hydrodynamic pressure and fluid film formation mechanism. However, such a mechanism still exists on a microscopic level due to roughness. It is common to translate roughness into a variation of fluid film thickness which in turn yields a hydrodynamic pressure distribution resulting in a net hydrodynamic lift. Reynolds equation and a suitable cavitation algorithm suffice to describe this effect mathematically. In case one surface consists of a compliant material with low modulus of elasticity, the deformation of asperities due to pressures and shear stresses in the fluid cannot be neglected—in fact, besides cavitation, it significantly contributes to the net hydrodynamic lift. Therefore, a coupling between fluid dynamics and elastic solid body deformations needs to be introduced. An additional complication arises when the hydrodynamic lift and the subsequent separation of the mean lines of the contacting rough surfaces is not enough to prevent asperity contacts completely. This situation is known as mixed lubrication where part of the normal load is transmitted at asperity contacts. These contacts are commonly treated as solid body contacts with a Coulomb-like friction law. However, when considering asperities as contraformal Hertzian contacts, elastic deformation may allow for the existence of thin micro-elastohydrodynamic lubricant films preventing direct solid body contact even at speeds which otherwise would be regarded as deep within the mixed lubrication regime close to boundary lubrication. These films may not be able to prevent wear completely, but may reduce friction significantly in comparison to dry friction. In this dissertation, the existence of such effects is demonstrated both by experiments with elastomeric radial lip seals and by simulation. The experimental work involved combined laser-induced fluorescence measurements of lubricant film thickness and measurements of seal friction torque. In the finite element based fluid–structure interaction soft micro-elastohydrodynamic mixed lubrication model developed in this work, no additional empirical parameters, such as the boundary friction coefficient, are needed. Thus, no additional experimental effort is required prior to any computation. Instead, the model entirely relies on geometry and material parameters that can be determined separately. The findings of this dissertation are not limited to the elastomer shaft seal application, but may also prove useful for studies of other soft rough conformal sliding contacts as, e.g., found in bio-tribological systems such as natural synovial joints and artificial joint replacements.

---

## ZUSAMMENFASSUNG

---

Konforme Oberflächen in parallel gleitendem Kontakt besitzen keinen makroskopischen hydrodynamischen Druckaufbau- und Schmierfilmbildungsmechanismus. Auf Grund der Oberflächenrauheit existiert ein solcher Mechanismus dennoch auf mikroskopischer Skala. Die Oberflächenrauheit wird üblicherweise in eine entsprechende örtlich veränderliche Schmierfilmhöhe überführt. Aus dieser wiederum ergibt sich eine hydrodynamische Druckverteilung, welche eine hydrodynamische Tragkraft zur Folge hat. Die Reynoldsgleichung sowie ein geeigneter Kavitationsalgorithmus genügen, um diesen Effekt mathematisch zu beschreiben. In dem Fall, dass eine der Oberflächen aus einem nachgiebigen Material mit geringem Elastizitätsmodul besteht, kann die Verformung der Rauheiten infolge der im Schmierstoff auftretenden Drücke und Schubspannungen nicht vernachlässigt werden; vielmehr trägt diese Verformung neben der Kavitation wesentlich zur hydrodynamischen Tragkraft bei. Daher ist es erforderlich, das Strömungsverhalten des Schmierstoffs und die elastischen Verformungen der Festkörper miteinander zu koppeln. Eine weitere Komplikation tritt auf, wenn die hydrodynamische Tragkraft und die sich daraus ergebende Abstandsvergrößerung der Bezugslinien der in Kontakt befindlichen rauhen Oberflächen nicht ausreicht, um Rauheitskontakte vollständig zu verhindern. Diese Situation ist als Mischreibung bekannt, wobei ein Teil der Normallast an Rauheitskontakten übertragen wird. Diese Kontakte werden üblicherweise als Festkörperkontakte mit einem Coulomb-artigen Reibungsansatz behandelt. Werden die Rauheiten jedoch als kontraforme Hertzsche Kontakte angesehen, so können elastische Verformungen die Ausbildung dünner mikro-elastohydrodynamischer Schmierfilme ermöglichen, welche einen direkten Festkörperkontakt sogar bei Gleitgeschwindigkeiten verhindern, die sonst als tief im Mischreibungsgebiet, nahe der Grenzreibung, liegend angenommen würden. Diese Schmierfilme zweiter Ordnung mögen nicht in der Lage sein, den Verschleiß vollständig zu verhindern, können jedoch die Reibung im Vergleich zur trockenen Reibung erheblich verringern. In der vorliegenden Arbeit wird die Existenz derartiger Effekte sowohl durch Experimente an elastomeren Radialwellendichtungen als auch durch Simulation aufgezeigt. Die experimentellen Arbeiten umfassten Schmierfilmdickenmessungen mit der Methode der laser-induzierten Fluoreszenz und die gleichzeitige Erfassung des Dichtungsreibmoments. In dem im Rahmen dieser Arbeit entwickelten Finite-Elemente-basierten Fluid-Struktur-Interaktionsmodell für die weiche mikro-elastohydrodynamische Mischreibung werden kei-

ne weiteren empirischen Parameter, wie beispielsweise der Grenzreibungskoeffizient, benötigt. Für Berechnungen ist somit kein weiterer vorheriger experimenteller Aufwand erforderlich. Das Modell basiert stattdessen vollständig auf Geometrie- und Materialparametern, die unabhängig voneinander bestimmt werden können. Die Ergebnisse dieser Arbeit sind nicht auf den Anwendungsfall des elastomeren Radialwellendichtrings beschränkt, sondern können sich ebenfalls als nützlich für die Untersuchung anderer weicher rauher konformer Gleitkontakte erweisen, wie sie beispielsweise in bio-tribologischen Systemen wie Gelenken oder künstlichem Gelenkersatz anzutreffen sind.

Keywords: Soft micro-elastohydrodynamic lubrication, mixed lubrication, friction in lubricated elastomeric contacts, elastomeric radial lip seal, fluid–structure interaction

Schlagworte: Weiche mikro-elastohydrodynamische Schmierung, Mischreibung, Reibung in geschmierten Elastomerkontakten, elastomere Radialwellendichtring, Fluid–Struktur-Interaktion



---

## PUBLICATIONS

---

This dissertation provides a summary of an ongoing series of research activities focusing on the tribological characteristics of elastomeric radial lip seals. Many ideas and figures have appeared previously in the following publications:

### CONFERENCE PAPERS, RESEARCH REPORTS AND ARTICLES

- [Weno8] WENNEHORST, B.: Wälzlagerdichtungen: Schutzdichtungen für Wälzlager; Forschungsvorhaben Nr. 432 I der FVA / Forschungsvereinigung Antriebstechnik e.V. Frankfurt a.M., 2008 (Nr. 876). – Forschungsheft
- [WEP11] WENNEHORST, B. ; ENGELKE, E. ; POLL, G.W.G.: Modelling radial lip seal friction — A multi-scale mixed lubrication approach. In: FLITNEY, R. (Ed.): *Proc. 21st International Conference on Fluid Sealing*, BHR Group, Cranfield, 2011
- [WPO6] WENNEHORST, B. ; POLL, G.W.G.: Optische Untersuchungen zu Vorgängen im Dichtspalt von Wellendichtungen. In: *Radialwellendichtringe: VI. Hamburger Dichtungstechnisches Kolloquium Dynamische Dichtungen*. Hamburg-Harburg, 2006
- [WPO7] WENNEHORST, B. ; POLL, G.W.G.: Einfluss von Schmierstoffkontaminationen auf Lebensdauer und Betriebseigenschaften von Wälzlagern. In: *Tribologie und Schmierungstechnik* 54 (2007), Issue 5, p. 11–17
- [WPO8] WENNEHORST, B. ; POLL, G.W.G.: Optical Investigations into the Dynamic Sealing Gap of Radial Shaft Seals. In: BARTZ, W.J. (Ed.): *Lubricants, materials and lubrication engineering: 16th International Colloquium Tribology, 15–17 January 2008, Ostfildern, Germany*, TAE, Technische Akademie Esslingen, 2008
- [WPO9a] WENNEHORST, B. ; POLL, G.W.G.: Optical Investigations into Dynamic Radial Sealing Contacts With a Special Emphasis on the Application of the Laser Induced Fluorescence Method. In: *Proceedings of the 4th World Tribology Congress 2009* Japanese Society of Tribologists, 2009
- [WPO9b] WENNEHORST, B. ; POLL, G.W.G.: Untersuchungen zur Tribologie von RWDR — Ergebnisse von Schmierfilmhöhen- und Reibungsmessungen. In: *Radialwellendichtringe: VII.*

*Hamburger Dichtungstechnisches Kolloquium Dynamische Dichtungen*. Hamburg-Harburg, 2009

- [WP09c] WENNEHORST, B. ; POLL, G.W.G.: Investigations into the tribological characteristics of radial lip seals — LIF and friction measurements. In: FLITNEY, R. (Ed.): *Proc. 20th International Conference on Fluid Sealing, 7–9 October 2009, Nottingham (UK)*, BHR Group, 2009, p. 213–229
- [WP10] WENNEHORST, B. ; POLL, G.W.G.: Investigations into the Tribological Characteristics of Radial Lip Seals — Results of Combined Lubricant Film Thickness and Friction Measurements. In: *Sealing systems - cutting edge technology in the smallest envelope: 16th ISC, International Sealing Conference* Fachverband Fluidtechnik im VDMA e.V., 2010
- [WP11] WENNEHORST, B. ; POLL, G.W.G.: Investigations Into the Tribological Characteristics of Radial Lip Seals: Results of LIF and Friction Measurements. In: *KGK-Kautschuk Gummi Kunststoffe* 64 (2011), Issue 4, p. 19
- [WP13a] WENNEHORST, B. ; POLL, G.W.G.: Modeling Radial Lip Seal Friction — A FEM-based Multi-Scale Soft Micro-Elastohydrodynamic Lubrication Approach. In: *5th World Tribology Congress 2013* Italian Tribology Association, 2013
- [WP13b] WENNEHORST, B. ; POLL, G.W.G.: Revisiting Soft Micro-Elastohydrodynamic Lubrication: A FEM-based Multi-Scale Approach for Modeling Radial Lip Seal Friction. In: *22th International Conference on Fluid Sealing*, BHR Group, Cranfield, 2013
- [WP14] WENNEHORST, B. ; POLL, G.W.G.: Soft micro-elastohydrodynamic lubrication and friction at rough conformal contacts. In: *Proceedings of the Institution of Mechanical Engineers, Part J: Journal of Engineering Tribology* 1350650114558322 (2014). <http://dx.doi.org/10.1177/1350650114558322>. – DOI 10.1177/1350650114558322. – Published online before print November 4, 2014
- [WP15] WENNEHORST, B. ; POLL, G.W.G.: Bi-sinusoidal roughness modeling for soft micro-elastohydrodynamic asperity lubrication in rough conformal contacts. In: *Proceedings of the 42nd Leeds–Lyon Symposium on Tribology*. Lyon, France, 2015

#### CO-AUTHORED CONTRIBUTIONS

- [OWP10] OTTINK, K. ; WENNEHORST, B. ; POLL, G.: Analysis of Rod Seals by Application of the Light Induced Fluorescence

Method. In: *Sealing systems — cutting edge technology in the smallest envelope: 16th ISC, International Sealing Conference* Fachverband Fluidtechnik im VDMA e.V., 2010

- [OWP11] OTTINK, K. ; WENNEHORST, B. ; POLL, G.: Analysis of the Lubricant Film Thickness on Rod Seals by Application of the Fluorescence Method. In: *66th Annual Meeting and Exhibition, Society of Tribologists and Lubrication Engineers (STLE)* Society of Tribologists and Lubrication Engineers, 2011
- [OWP13] OTTINK, K. ; WENNEHORST, B. ; POLL, G.: Untersuchungen zum Systemverhalten abgedichteter Wälzlager. In: *10. VDI-Fachtagung Gleit- und Wälzlagerungen. Gestaltung, Berechnung, Einsatz*, VDI, 2013

#### INTERNAL REPORTS

- [Weno4a] WENNEHORST, B.: *Untersuchung der Gas- und Flüssigkeitsförderung an Wälzlagerschutzdichtungen—Entwicklung geeigneter Versuchseinrichtungen; English title: Investigations on gas and fluid exchange at protective seals for rolling element bearings—development of test facilities*, Institut für Maschinenkonstruktion und Tribologie (IMKT), Leibniz Universität Hannover, Project Work, 2004
- [Weno4b] WENNEHORST, B.: *Entwicklung einer optischen Einrichtung zur Untersuchung des dynamischen Dichtspalts von Stangen- und Wellendichtungen; English title: Design of an optical device for investigations into the dynamic sealing gap of rod and rotary shaft seals*, Institut für Maschinenkonstruktion und Tribologie (IMKT), Leibniz Universität Hannover, Diplom thesis, 2004





---

## ACKNOWLEDGMENTS

---

This work would not have been possible without the efforts of many.

First I wish to thank my supervisor Prof. Dr.-Ing. Gerhard Poll, head of the Institute for Machine Design and Tribology at Gottfried Wilhelm Leibniz Universität Hannover, for his enthusiastic encouragement and guidance throughout my research work. I am also grateful to Prof. Dr.-Ing. Birgit Glasmacher, head of the Institute for Multiphase Processes & Centre for Biomedical Engineering, Gottfried Wilhelm Leibniz Universität Hannover, for her friendly interest in this thesis and for agreeing to act as second examiner, and to Prof. Dr.-Ing. Bernd-Arno Behrens, head of the Institute for Forming Technology and Machines, for chairing the examination committee.

With regard to my first research project on protective seals for rolling element bearings (German title: “Schutzdichtungen für Wälzlager”), I gratefully acknowledge the institutional and financial support of the Research Association for Drive Technology (Forschungsvereinigung Antriebstechnik e.V. – FVA) and the German Federation of Industrial Research Associations (Arbeitsgemeinschaft industrieller Forschungsvereinigungen “Otto von Guericke” e.V. – AiF). One of the test rigs set up during this project was later modified and used for the combined radial lip seal friction and lubricant film thickness measurements described in this dissertation, and I am grateful to SKF ERC, Nieuwegein, the Netherlands, for funding these further investigations.

Regarding the above mentioned protective seals project, I wish to thank my former student, and later colleague, Ingo Dewitz for his many enthusiastic contributions (far exceeding what can be expected of a student assistant), in particular for preparation of the cross-sectional seal micrographs. Moreover, as representatives of the mechanical and the electronic workshops, I would like to thank Manfred Hormann and Hermann Könemann for their support during the setup of the various experimental facilities.

Furthermore, with regard to the modeling work, I am highly indebted to the entire ELMER Multiphysics development team at CSC – IT Center for Science, Espoo, Finland, especially Peter Råback for tirelessly answering questions and implementing additional features asked by the users, and Mika Malinen for implementing the neo-Hookean material law.

I am also grateful to Marius Schüller for helping with the seal contact temperature measurements.

Many thanks go to Norbert Bader for English proofreading, and for resolving a number of  $\TeX$  technical issues.

I wish to add a further, personal and heartfelt, thanks to Prof. Poll for giving me the opportunity to continue the modeling work on a part-time position. This gave me the flexibility to both develop the ELMER fluid–structure interaction soft micro-EHL model, and to provide extensive data processing, as well as statistical R programming and analysis support for my wife’s medical PhD research project, which was facing unforeseen resource bottlenecks after several years of ongoing work. It is due to Prof. Poll’s understanding and generous patience that these difficulties could be resolved, thus enabling my wife to continue with her PhD work.

Finally, I am particularly indebted to my parents for their overwhelming encouragement and support.

Last but certainly not least, I owe my deepest gratitude to my wife Katharina for her love, support, encouragement, patience, and understanding, and, while I was away writing this thesis, for taking care of our wonderful baby son Jonas Rasmus.

Hannover, October 2016  
Bengt Wennehorst

---

## CONTENTS

---

1	INTRODUCTION	1
1.1	Radial lip seal design	2
1.1.1	Seal design evolution	2
1.1.2	Sealing element geometry	3
1.1.3	Shaft surface characteristics	5
1.2	Fundamentals of radial lip seal operation	5
1.2.1	Sealing hypotheses	5
1.2.2	Lubrication and friction of radial lip seals	8
1.3	Experimental approaches in radial lip seal research	19
2	AIMS AND SCOPE	27
3	EXPERIMENTAL APPROACH	29
3.1	Experimental set-up	30
3.2	Optical methods	31
3.2.1	Total internal reflection sealing contact visualization	31
3.2.2	Laser Induced Fluorescence	33
3.3	Test seal characteristics	43
3.4	Characteristics of the lubricating oil	48
4	EXPERIMENTAL RESULTS	53
4.1	Results of Total Internal Reflection Sealing Contact Visualization	53
4.2	Results of Lubricant Film Thickness and Seal Friction Torque Measurements	54
4.2.1	Results of optical lubricant film thickness measurements	54
4.2.2	Results of seal friction torque measurements	59
4.3	Results of additional seal contact temperature measurements	61
5	SEMIEMPIRICAL COMPUTATION OF VISCOUS LUBRICANT FRICTION	67
5.1	Preliminary Computational Fluid Dynamics simulations	67
5.2	Simplified numerical approach	70
6	MODELING LUBRICATION AND FRICTION OF RADIAL LIP SEALS	79
6.1	Revisiting the concept of soft micro-elastohydrodynamic asperity lubrication	79
6.2	Deterministic model of seal lip surface	81

6.3	Soft micro-EHL film thickness computation	86
6.4	Finite-element-based lubrication models	88
6.4.1	Preliminary study neglecting hydrodynamic effects	88
6.4.2	Sensitivity analysis	93
6.4.3	Fully coupled fluid–structure interaction approach	93
6.4.4	Application to the run-in seal	100
6.4.5	Further validation on a steel shaft	108
7	CONCLUSION AND OUTLOOK	111
	BIBLIOGRAPHY	115

---

## NOMENCLATURE

---

### NOTATION

$a$	m	amplitude of sinusoidal roughness model
$b$	m	seal contact width
$c$	mol/m <sup>3</sup>	molar concentration
$d$	m	shaft diameter
$f$	N	friction force
$h$	m	lubricant film thickness
$i$	1	running index
$p$	Pa	pressure
$r_h$	1	ratio of hydrodynamic lifting force to external load
$u$	m/s	sliding velocity
$u_e$	m/s	mean entrainment velocity
$A$	m <sup>2</sup>	base area
$E$	Pa	Young's modulus of elasticity
$E'$	Pa	equivalent elastic constant
$F$	N	normal load
$F_r$	N	seal radial force
$G$	Pa	shear modulus
$H_{cen}$	1	dimensionless central film thickness
$I$	W/m <sup>2</sup>	intensity
$K$	Pa	bulk modulus
$MW$	kg/kmol	lubricant molecular weight
$N_y$	1	number of undulations across seal contact
$P$	W	power

$R_q$	m	root mean square roughness of the counter-face
$R_e$	m	effective radius of curvature in direction of lubricant entrainment (undeformed geometry)
$R_s$	m	effective radius of curvature in direction of lubricant side-leakage (undeformed geometry)
$R_x$	m	radius of curvature in circumferential direction
$R_y$	m	radius of curvature in axial direction
$S_q$	m	root mean square roughness of the seal lip surface
$T$	N m	friction torque
$U_e$	1	dimensionless speed parameter
$W_e$	1	dimensionless load parameter
$\beta_x^*$	m	correlation length in circumferential ( $x$ ) direction
$\beta_y^*$	m	correlation length in axial ( $y$ ) direction
$\beta_\theta^*$	m	correlation length in $\theta$ direction
$\Delta A$	m <sup>2</sup>	shaft surface area increment
$\Delta_{r.m.s.,x}$	1	root mean square roughness slope in circumferential direction
$\Delta_{r.m.s.,y}$	1	root mean square roughness slope in axial direction
$\Delta y$	m	width of axial lubricant slices
$\epsilon(\lambda)$	m <sup>2</sup> /mol	molar absorption coefficient
$\eta$	Pa s	dynamic viscosity
$\gamma$	1	ellipticity ratio
$\dot{\gamma}$	1/s	shear strain rate
$\lambda_{r.m.s.,x}$	m	effective wavelength in circumferential direction

$\lambda_{r.m.s.,y}$	m	effective wavelength in axial direction
$\mu$	1	coefficient of friction
$\nu$	1	Poisson's ratio
$\nu_{40/100}$	mm <sup>2</sup> /s	(kinematic) reference viscosities at 40 °C and 100 °C
$\rho_{15}$	kg/m <sup>3</sup>	lubricant density at 15 °C
$\tau$	Pa	fluid shear stress
$\vartheta$	°C	temperature
$\Phi$	1	quantum efficiency

## SUBSCRIPTS

av	average
cav	relating to cavitation
cen	relating to central elastohydrodynamic film thickness
contact	relating to sealing contact zone
el	elastic
em	relating to fluorescence emission
ex	relating to fluorescence excitation
fluo	relating to fluorescence
hd	hydrodynamic
max	maximum
rel	relative
visc	relating to lubricant viscosity
RUC	relating to roughness unit cell

## ABBREVIATIONS

ACF	Auto-Correlation Function
CCD	Charge Coupled Device
DPSS	Diode Pumped Solid State
EHL	Elastohydrodynamic Lubrication
FKM	Fluorocarbon Rubber
FSI	Fluid-Structure Interaction
GV	Gray Value
LIF	Laser Induced Fluorescence
M	Mean
PMMA	Polymethylmethacrylate
PTFE	Polytetrafluorethylene
SD	Standard Deviation
TIR	Total Internal Reflection
UHMW-PE	Ultra-high-molecular-weight polyethylene
100Cr6	Bearing steel containing 1 % of carbon and 1.5 % of chromium



---

## INTRODUCTION

---

The primary purpose of a radial lip seal for rotating shaft and hub applications (Figure 1.1) is to retain lubricants within a sump or cavity, while excluding contaminants. Lip seals are also used to separate fluids and to confine pressure. They are used throughout industry in a variety of applications with widely varying operating conditions. These conditions can vary from high speed shaft rotation with a light oil mist, no pressure in a clean environment to a completely flooded low speed application in a muddy environment. External temperatures can range from  $-50^{\circ}\text{C}$  in the Arctic to  $50^{\circ}\text{C}$  in the tropics. Sump temperatures can reach  $150^{\circ}\text{C}$  or higher. The advantages of radial lip seals include low cost, small space requirements, easy installation and an ability to seal a wide variety of applications.

To be effective, a radial lip seal must maintain an adequate interference between the elastomeric lip member and the rotating part. A garter spring is used to augment the sealing force supplied by the elastomeric member and to help maintain the sealing force throughout the life of the seal. An interference fit must also be maintained between the seal outside diameter and the bore inside diameter to prevent seal outside diameter leakage, to prevent the seal from spinning in the bore housing and to ensure seal retention within the bore housing in low pressure applications [CR92].

During standstill, due to the interference between the seal lip and the rotating part, these seals provide static tightness. During shaft rotation, though, a hydrodynamic load supporting lubricant film can develop drastically reducing seal friction and wear. Moreover, a microscopic reverse pumping effect may provide dynamic tightness even if dynamic sealing contacts are subject to pressure gradients. Even though the overall system design parameters being the precondition of these effects are well-known by experience<sup>1</sup>, both the mechanisms constituting the reverse pumping effect as well as the lubricant film formation and the frictional characteristics are still subject of fundamental studies. So far, a number of different hypotheses have been developed each being capable of explaining certain aspects of observed radial lip seal operating characteristics<sup>2</sup>.

---

<sup>1</sup> See, e. g., [CR92], and JOHNSTON [Joh99].

<sup>2</sup> For a comprehensive review, the reader may refer, e. g., to SALANT [Sal99].

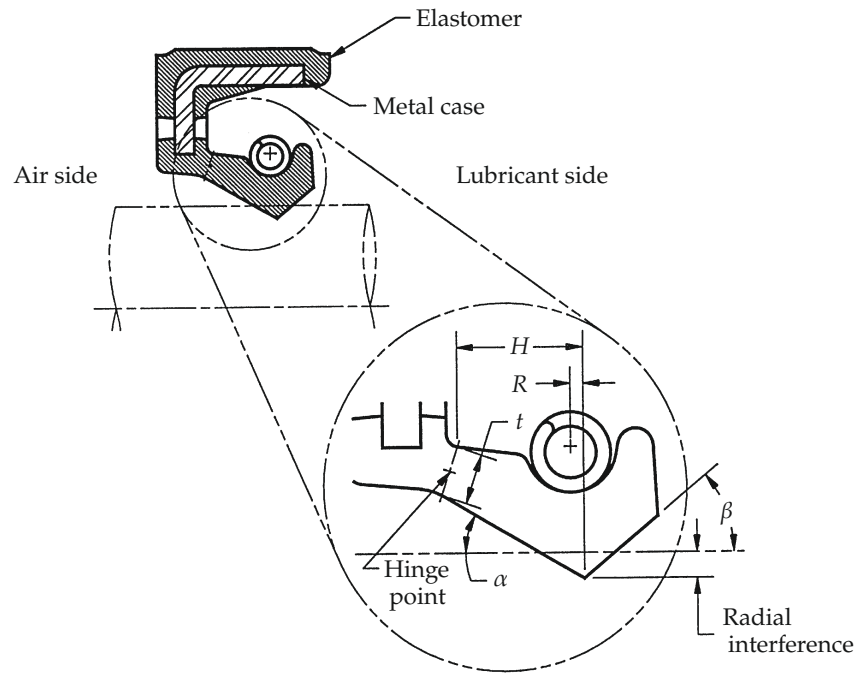


Figure 1.1: Basic construction of a radial shaft seal. Reproduced from JOHNSTON [Joh99] with permission of SAGE.

### 1.1 RADIAL LIP SEAL DESIGN

While many different seal designs and lip configurations are used to meet all of the various application conditions<sup>3</sup>, the basic operating principles for these different configurations are the same. Based on the prototypical case of the standard oil seal shown in Figure 1.1, this section introduces the key design aspects that are mainly responsible for reliable, i. e., leakage-free operation of a radial lip seal.

#### 1.1.1 Seal design evolution

The earliest seals were leather straps used at the end of wheel axles to hold grease or animal fat in place. The 18th Century Industrial Revolution created demands for more sophisticated lubrication and sealing systems. Packings and rope were used successfully as seals, even though some leakage occurred. Higher shaft speeds and higher and lower operating temperatures demanded improvements. About 1927, leather oil seals were produced with sealing surfaces that could follow shaft eccentricities. These assembled seals were compact, self-contained units. They could be press-fitted easily into a housing bore.

A major improvement in leather seal design occurred around 1934. Leather was clinched in an outer case with either a finger spring or

<sup>3</sup> See, e. g., [CR92], and FLITNEY [Fli14].

a garter spring added to provide uniform loads. The garter spring proved to be more effective in providing reliable sealing.

As lubrication problems became more complex, oil replaced grease as a lubricant. Operating temperatures increased. Seal design and materials were modified to prevent leakage. Leather treatments were introduced to prevent light oil seepage through leather fibers.

The development of the world's first oil-resistant rubbers led to synthetic rubber oil seals in the early 1940's. Early synthetic rubber seal designs were actually assembled leather seal designs, with rubber simply replacing leather. A trim knife was used to form a sealing edge.

By 1945, bonding cements were developed to bond rubber directly to a metal case. Seals had to have large bonding areas. Additional improvements in seal bonding systems have been made since the late 1940's. Today, seals are designed with cemented joints that are actually stronger than the rubber. Assembled seals are no longer recommended because of their high cost, internal leakage, and lack of dimensional control [CR92].

Modern seal designs can have a molded sealing lip that eliminates trimming, but seals with a trimmed sealing edge are also on the market. Many further improvements that enable radial lip seals to meet increasingly demanding application requirements are due to the development of heat and chemically resistant elastomers [Joh99].

### 1.1.2 Sealing element geometry

The functioning of the radial lip seal, i. e., the reverse pumping action that provides dynamic tightness under lubricated conditions, stems from the asymmetric geometry of the sealing element. When installed on the shaft, the axial seal lip contact pressure distribution is also asymmetric. To provide the reverse pumping action, the contact pressure distribution is required to be skewed such that the maximum is nearer to the oil side<sup>4</sup>. The following two aspects contribute to this asymmetry [Joh99]:

- A. the different seal lip angles on the air and oil side,  $\alpha$  and  $\beta$  respectively, with  $\alpha < \beta$ , and
- B. the displacement  $R$  of the garter spring and its attendant force to the air side of the seal lip contact band (see Figure 1.1).

Typical seal lip angles are in the range of 25° to 30° for the air-side angle  $\alpha$ , and 40° to 45° for the oil-side angle  $\beta$  when the seal is in the free state. When installed on the shaft, the rotational movement of the lip amounts to about 10°, yielding seal lip angles in the working

<sup>4</sup> Figure 3.8, p. 48, shows the axial seal lip contact pressure distribution of the seal type studied in this work.

condition of approximately  $20^\circ$  and  $50^\circ$ . The oil-side angle should be great enough to allow a scraping action. If it is too low, the desired axial contact pressure distribution will not be generated and leakage will occur. The air-side angle should be small to allow a meniscus of the lubricant film to form, and large enough that the element may follow runout. If the air-side angle is too low, accelerated wear will occur on the air side which shortens seal life. If the angle is too high, the proper contact pressure distribution will not be generated, resulting in seal leakage.

A further contribution to the skewed axial seal lip contact pressure distribution is governed by the axial distance  $R$  between the seal lip contact band and the centerline of the spring. This offset, which should be positive, i. e., toward the air side of the seal, typically amounts to approximately 10% of the lip length,  $H$ . If the  $R$  value becomes negative, e. g., due to a combination of manufacturing and installation tolerances, the spring can cause the axial seal lip contact pressure distribution to switch around, which may result in instant leakage. If the  $R$  value is greater than approximately 0.75 mm in the positive direction, the spring may cause the sealing element to collapse, resulting in accelerated wear and shortened life.

The flexibility of the seal is governed by the lip length,  $H$ , and the flex thickness,  $t$ , at the hinge point. The lip length is the axial distance between the lip contact point and the base of the flex thickness. A short lip length will tend to increase the radial load and increase the wear of the element. A long beam length will increase the flexibility of the element, e. g., to cope with larger than usual dynamic shaft eccentricities. Lip lengths are normally 2 mm to 5 mm, depending upon the application and the seal size. The flex section is the area that deforms when the seal is installed and governs the seal load and followability. In general, the flex thickness,  $t$ , should be designed with sufficient thickness to reduce the tendency of the elastomer element to "wrap" around the shaft. In addition, the flex thickness must be thin enough that the element may follow runout. Normally, the flex thickness is of the order of 40% of the lip length. For seals designed to operate at pressure, or for seals installed in a rotating housing, the flex thickness may be increased and the lip length shortened. This, however, will reduce the runout capability of the seal.

The garter spring is a helically coiled wire with its ends connected to form a ring. It is normally used in tension for maintaining a radial sealing force between the sealing element of a radial lip seal and the shaft [CR92, Joh99].

### 1.1.3 Shaft surface characteristics

The sealing system is typically formed by a radial lip seal and a steel shaft with a plunge-ground surface<sup>5</sup>. The shaft surface finish is critical to seal function. A common specification is  $0.25\ \mu\text{m}$  to  $0.50\ \mu\text{m}$  ( $R_a$ ) with  $(0.00 \pm 0.05)^\circ$  lead angle. With a molded seal this finish will wear away the rubber skin from the sealing lip and create asperities in the wear track of the seal lip. The asperities support a lubricating film that protects the lip from further wear. If the shaft surface is initially too smooth, the seal may not break in properly and leakage will occur. If the shaft surface is initially too rough, gross lip wear may occur before the protective lubricating film develops, and leakage will result. The molded skin at the seal lip is broken very quickly as the shaft rotates (1 hour or less) and a wear track begins to develop. If there are no large quantities of external or internal contaminants present the width of the seal lip wear track will typically stabilize within 100 hours. During the life of the seal, the shaft becomes smooth and burnished even though very little material is removed from the seal lip [Hor91, CR92].

## 1.2 FUNDAMENTALS OF RADIAL LIP SEAL OPERATION

As opposed, e.g., to journal bearings, where the hydrodynamic lubricant film formation is governed by the wedge-shaped macro-geometry of the lubricated sliding contact, the seal lip surface is in parallel sliding contact with the shaft and, therefore, lacks a macroscopic hydrodynamic pressure and fluid film formation mechanism. However, such a mechanism still exists on a microscopic level due to roughness. In circumferential, i.e., sliding, direction, the corresponding micro-hydrodynamic effects manifest in the frictional characteristics of the seal. At the same time, the net axial component of the viscous lubricant drag flow governs the sealing function, i.e., the capability of the seal lip to provide dynamic tightness under lubricated conditions<sup>6</sup>. Obviously, this requires the axial net flow across the sealing contact to be directed toward the oil side.

### 1.2.1 Sealing hypotheses

Initially, it was believed that the seal lip prevents leakage by cutting through the oil film, and that this cutting mechanism could be enhanced by increasing the radial force exerted on the seal lip. How-

<sup>5</sup> The surface roughness of the circumferentially ground shafts is considerably smaller along the circumferential, i.e., the sliding, direction than along the axial direction (see KUNSTFELD [Kun05], and the author's own results presented in Section 6.4.5).

<sup>6</sup> It is tempting to assume that seal friction and axial flow rates are therefore correlated with each other. However, experimental results are inconsistent, and the existence of such a correlation is controversial (see, e.g., SATO ET AL. [SSSY03]).

ever, early work of LEIN [Lei54] indicated that there was always an oil film between the seal lip and the shaft due to capillary forces; this oil film could not be cut or squeezed away, even when the radial force was appreciably increased. JAGGER [Jag57b] then proposed that surface tension prevents the fluid from leaking through the sealing gap. JAGGER AND WALKER [JW67] observed that successful seals developed “microasperities” in the seal lip contact area, and that the shaft surface became smooth. The surface tension concept was further developed by INY AND CAMERON [IC61], RAJAKOVICS [Raj71], and by JAGGER AND WALLACE [JW73]. The surface tension concept proposed by JAGGER AND WALLACE [JW73] was disputed by several researchers. As pointed out by SALANT [Sal99], a sealing mechanism based on surface tension forces requires the oil meniscus on the air side of the seal to be convex, while experimental observations, e. g., by STAKENBORG [Sta88a, Sta88b], indicated that the meniscus is concave. Sealing mechanisms based on surface tension have, therefore, not been further pursued<sup>7</sup>.

Based on the observation that oil drops placed on the air side of the seal were soon transported across the sealing contact into the sump, and that successful seals leaked when installed conversely, it was generally agreed that seal function depends upon an inherent reverse pumping ability. KAWAHARA ET AL. [KAHM78] conducted experiments to quantify this reverse pumping effect and demonstrated that the oil flow out of the conversely installed seal was dependent upon shaft speed, fluid viscosity and lip wear track surface condition. NAKAMURA ET AL. [NK84, NKK85, Nak87], who analyzed the contact pattern of the rubber lip on a glass shaft, confirmed the existence of microasperity contacts and demonstrated that the characteristics of the microasperity contact pattern were related to sealing performance.

Later it was generally agreed that radial lip seal leakage is prevented by a positive pumping action originating from both the seal lip surface micro-geometry in combination with the asymmetric axial seal lip contact pressure distribution. HORVE [Hor91] established a relationship between microasperity formation, pumping ability, service reliability, and the formulation of the elastomeric material. He demonstrated that materials can be formulated that will not develop microasperities in the wear track of the sealing lip (Figure 1.2, Material A). These seals were shown to have poor pump rates and service reliability. When the wear tracks of these materials were artificially roughened, the pump rates increased dramatically for a short time and then decayed as the artificially induced microasperities were worn away. Materials can also be formulated to quickly develop an

<sup>7</sup> However, recent work by SCHULER [Sch14] suggested that the wetting behavior of the lubricant and surface combinations might have an impact on the dynamic sealing mechanism, depending on the operating conditions.

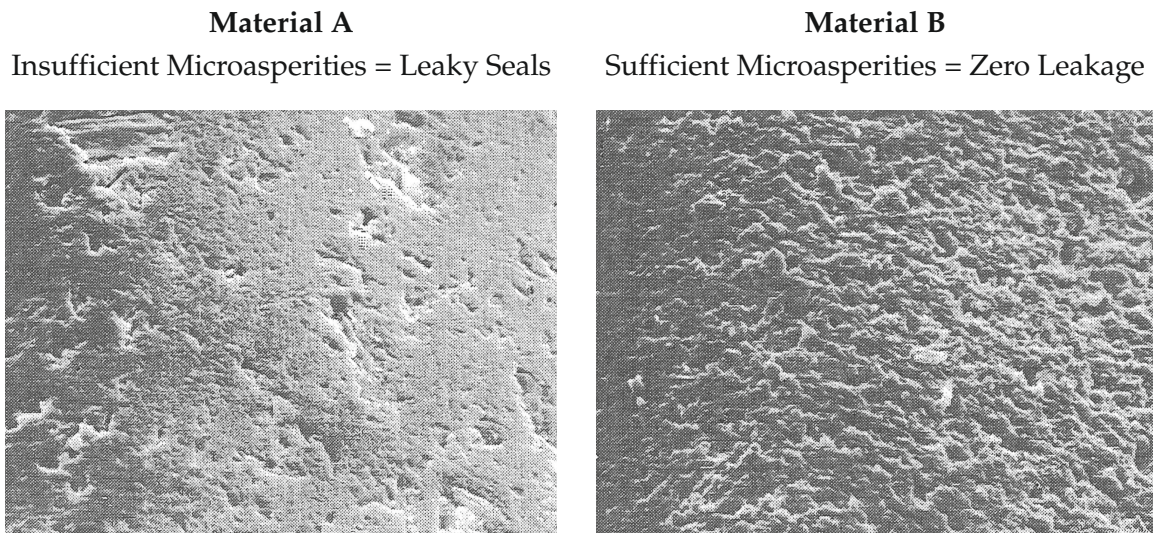


Figure 1.2: Microasperities in the seal wear track; 300X – 17 hours, shaft surface worn smooth.  
Reprinted from HORVE [Hor91] with permission from SAE International.

abundance of microasperities in the wear track (Figure 1.2, Material B). Seals made with these materials were shown to have high pump rates with excellent service reliability.

As shown by KAMMÜLLER [Kam86] and VAN LEEUWEN AND WOLFERT [LW97], due to the skewed axial contact pressure distribution, the shear forces induced by the rotating shaft yield a corresponding asymmetric tangential deformation of the seal lip contact zone. KAMMÜLLER [Kam86] described axially striated, or, helical, patterns of asperities in the seal wear track. Under dynamic conditions, these undulated wear structures deform into a topography of ridges and valleys inclined to the axial direction. The ridges were considered to act as a microscopic visco-pump, the net axial flow of which is directed toward the oil side<sup>8</sup>. Undulated axial wear structures are not routinely found on seal wear tracks. Nevertheless, the concept of microscopic visco-pumps can also be applied to isotropic seal lip surface roughness. MÜLLER [Mül87] proposed a “cascade pumping side flow mechanism”, where the reverse pumping action is assumed to originate from viscous drag flow around flattened hemispherical seal lip surface asperities. Due to the asymmetric axial seal lip contact pressure distribution, the total cascade pumping side flow will be larger on the air side of the contact pressure maximum than on the oil side, thus yielding a net axial flow which is directed toward the oil side. SPONAGEL ET AL. [SKS87] argued that a hemispherical seal lip surface asperity within the seal lip contact zone will become oriented when the seal lip surface is subjected to a tangential deformation that varies with the axial position across the contact zone. The asperities deform into shapes and orientations such that they act like

<sup>8</sup> See also WENK ET AL. [WSLW16].

viscous pumps. Due to the asymmetry of the tangential seal lip surface deformation, the net axial flow is directed toward the oil side<sup>9</sup>. STAKENBORG [Sta88a, Sta88b] argued that in a steady-state situation the reverse pumping action of the seal is counterbalanced by the capillary forces of the oil–air interface, i. e., the oil meniscus, on the air side of the sealing contact.

Macroscopic effects were also demonstrated to contribute to the reverse pumping phenomenon. OTT [Ott83] and QU [Qu93] described a dynamic sealing effect due to Görtler-Taylor vortices generated in the oil sump at the rotating shaft surface. These vortices created an inward pumping effect that compensated the hydrostatic pressure, thereby preventing leakage. The phenomenon was demonstrated with a rigid model seal that had a wide gap between the rotating shaft and the seal inner diameter. GAWLINSKI [Gaw81], and GAWLINSKI AND KONDERLA [GK84], proposed that the reverse pumping effect was due to an axial scrubbing action of the seal lip that results from dynamic shaft eccentricity. Tests, e. g. by HORVE [Hor87], however, showed that small amounts of reciprocating motion without rotary shaft motion will not induce the amount of pumping observed when the shaft rotates. PRATI [Pra87], and AMABILI ET AL. [ACP00], demonstrated that gross leakage will result when combinations of dynamic shaft eccentricity and shaft speed exceed the ability of the seal lip design and material combination to follow the shaft. BRINK AND HORVE [BH73] reported that a molded lip seal design with a wavy sealing edge pumped more than conventional seal designs with a straight sealing edge. Increasing the amplitude of this wave and the number of waves increased the pump rate. This macroscopic pumping effect was later mathematically described by HORVE [Hor87]. HERMANN AND SEFFLER [HS85] reported that tilting the shaft from the horizontal yielded a one-cycle wave seal contact band, which resulted in an increased pumping ability. These secondary macroscopic effects are generally agreed to be superimposed onto the natural microscopic pumping effect which is related to microasperity formation.

### 1.2.2 *Lubrication and friction of radial lip seals*

As described in Section 1.2.1, early work of LEIN [Lei54] indicated that there was always an oil film between the seal lip and the shaft due to capillary forces; this oil film could not be cut or squeezed away, even when the radial force was appreciably increased. Instead, the radial force increase just resulted in a high seal friction torque, with a correspondingly increased shaft wear and a high contact temper-

<sup>9</sup> SALANT AND FLAHERTY [SF95] presented a numerical elastohydrodynamic analysis of this concept. The computation of reverse pump rates (and seal friction) was later generalized to mixed microelastohydrodynamic lubrication models where the sealing surface of the lip was modeled as a quasi-random surface, see, e. g., SHI AND SALANT [SS00, SS01], and SALANT [Sal01].



ature that destroyed the elastomer seal lip, thereby causing leakage. LEIN [Lei54] presented seal friction torque curves where the friction torque started from a non-zero value and then increased at a declining rate with increasing rotational speed<sup>10</sup>. Based on the fact that a radial lip seal lacks the converging fluid film known from journal bearings, LEIN argued that the oil film, even though causing viscous friction, will not be capable of providing hydrodynamic load support; therefore, the seal radial force will be carried by asperity contacts that will cause boundary friction from molecularly thin lubricant films, as well as dry friction. He then concluded that the entire seal friction is generally composed of a constant boundary (and, partially, dry) friction component and a speed-dependent viscous lubricant friction part.

JAGGER [Jag57a] used the results of seal pressure leakage and seal friction force measurements to indirectly estimate the lubricant film thickness within the seal lip contact zone. In order to vary the contact load between the seal and the counterface, JAGGER used an axial seal lip design such that the loading was changed from the radial direction to the axial direction. The contact load was changed by adding or removing weights. In order to globally characterize the lubrication condition of the seal lip, and to directly measure the oil film thickness, JAGGER [Jag57a] used an electrical capacitance method<sup>11</sup>. The average film thickness values obtained for a range of loads and speeds were of the order of 2.5  $\mu\text{m}$ , which was consistent with the indirect film thickness estimates. Moreover, the measurements of electrical capacity showed that, even at the lowest rotational speeds, the seal lip and the counterface were separated by a coherent oil film that disappeared as soon as the shaft became stationary, but built up again immediately movement was started. JAGGER argued that the lubricant film was generally much thicker than the molecular films of boundary lubrication and yet it was much thinner than the usual hydrodynamic films found in journal bearings, where the film thickness was on the order of 25  $\mu\text{m}$ ; compared to these thick films, owing to the smaller film thickness, shear rates were often higher, giving rise to higher coefficients of friction<sup>12</sup> and more pronounced temperature effects.

Further indirect evidence for the formation of a continuous lubricant film came from observations of JAGGER [Jag57b], JOHNSTON [Joh78], and HORVE [Hor91], who reported that, under lubricated conditions, the width of the seal lip wear track remains virtually constant after a very short initial break-in period.

---

<sup>10</sup> Very similar seal friction torque curves were also reported by JOHNSTON [Joh78], and JOHNSTON AND VOGT [JV95].

<sup>11</sup> For a discussion of this technique, see, e. g., VISSCHER [Vis92], and TOURNERIE ET AL. [TLF93].

<sup>12</sup> The friction coefficient  $\mu = (2T)/(dF_r)$ , where  $T$  is seal friction torque,  $F_r$  is seal radial force at oil sump temperature, and  $d$  is shaft diameter, may easily exceed 0.5 under normal operating conditions, see, e. g., ENGELKE [Eng11].

HIRANO ET AL. [HIK61] correlated the friction coefficient  $\mu$  with the dimensionless hydrodynamic Duty Parameter  $G = \eta ub/F$  (where  $\eta$  is lubricant viscosity,  $u$  is shaft surface speed,  $b$  is seal lip contact width, and  $F$  is total contact load), and found that  $\mu = \Phi G^{1/3}$ , where  $\Phi$  is a characteristic proportionality factor for seal friction. Because  $\mu$  increased with increasing  $G$ , the authors concluded that the seals were hydrodynamically lubricated and that a lubricant film existed, even though  $\Phi$  was found to decrease at higher sliding speeds. This speed dependence was attributed to the viscoelastic properties of the seal material. Later, LINES ET AL. [LLO66] demonstrated that  $\Phi$  was independent of velocity when the effect of the underlip temperature on the viscosity was taken into account, thereby providing further evidence for the occurrence of hydrodynamic lubrication. LINES ET AL. also found that friction measurements indicated boundary lubrication at very low values of  $G$ . Similar results were presented by SCHNÜRLE AND UPPER [SU73] who directly compared the frictional characteristics of radial lip seals to the hydrodynamics of journal bearings. Within this classical concept, as illustrated in Figure 1.3, at very low values of  $G$  hydrodynamic pressure build-up effects do not yet significantly contribute to the overall load support, and the friction is therefore governed by boundary, or even dry friction caused by asperity contacts. When approaching the region of minimum friction, the friction coefficient decreases noticeably with an increase in  $G$ . Under these mixed lubrication conditions, hydrodynamic effects will increasingly contribute to the overall load support, but part of the normal load is still transmitted at asperity contacts. At higher values of  $G$ , beyond the friction minimum, the hydrodynamic pressure build-up suffices to entirely carry the external load and to separate the surfaces. Thus, owing to the fact that asperity contacts are completely avoided under these hydrodynamic full-film lubrication conditions, no wear will occur, and the further increase in friction is purely viscous.

The classical Stribeck curve concept has since become the standard approach to radial lip seal lubrication, even though its applicability is not unquestioned. For example, in a large study comprising 64 seals, JOHNSTON AND VOGT [JV95] concluded that the hydrodynamic Duty Parameter  $G$  does not provide a universal description of the behavior of an individual seal over a broad spectrum of running conditions. Approximately 50% of the seals did not show the typical Stribeck curve (i. e., an initial drop in friction followed by a rise). On the contrary, these seals showed a steep rise in friction from the very beginning<sup>13</sup>. Extrapolating these curves backwards to  $G = 0$  gave intercepts with the ordinate axis which were significantly displaced from the origin, with friction coefficients ranging from about 0.12 to

<sup>13</sup> Similar friction curves were also previously reported by JOHNSTON [Joh78] and LEIN [Lei54]. The reader may remember that, as detailed above, LEIN [Lei54] had therefore concluded that there is always a boundary friction component being independent of sliding speed.

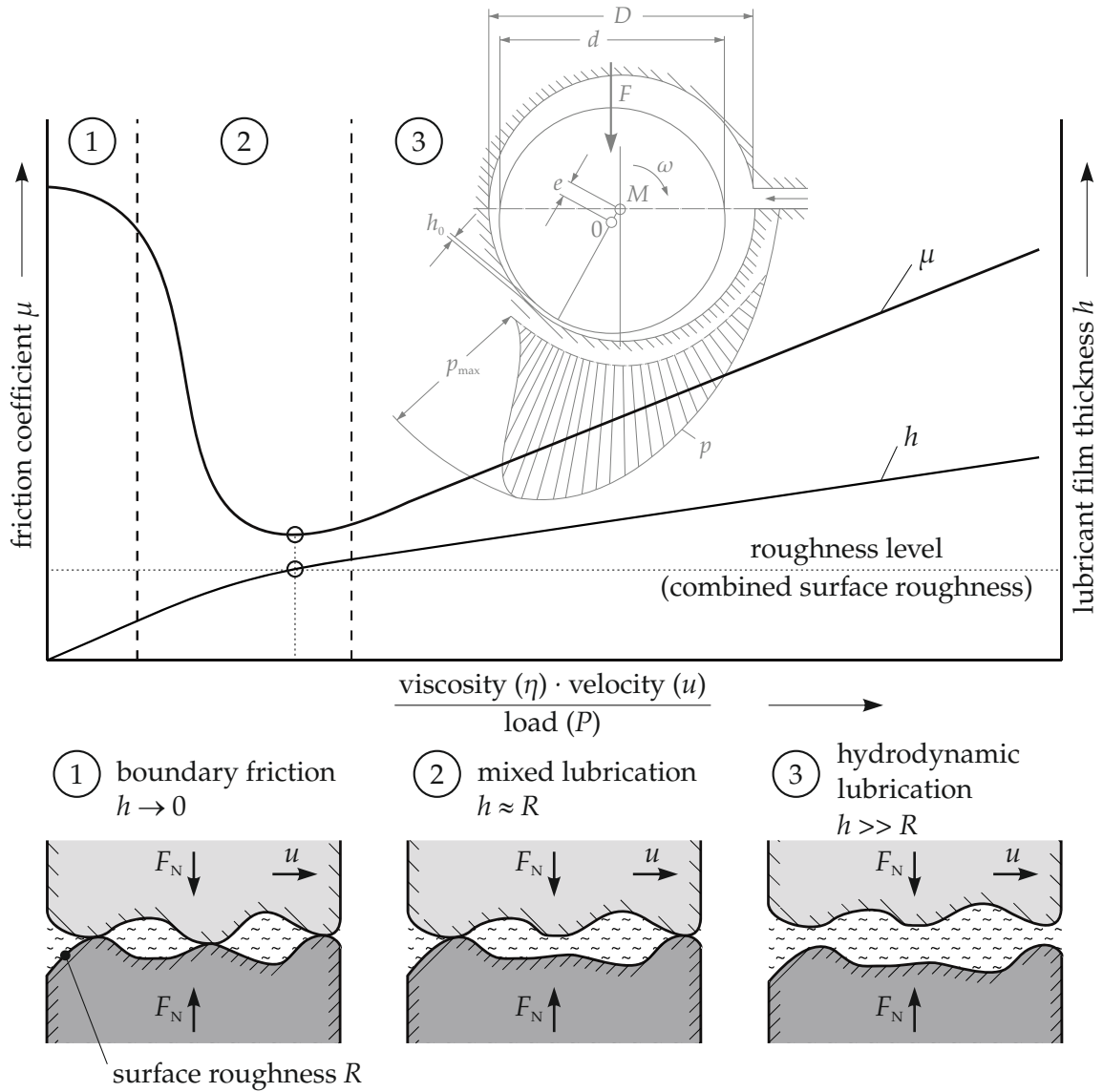


Figure 1.3: Hydrodynamic lubrication of a journal bearing; schematic of classical Stribeck curve concept.

0.4. Generally, there was a wide spread in frictional levels between seals at higher values of  $G$  that was not only attributable to the different ordinate intercepts but also to vastly differing starting slopes and curvatures of the graphs. JOHNSTON AND VOGT argued that although the Duty Parameter takes into account the fluid viscosity and seal radial load, it can only represent a limited aspect of the conditions within the sealing gap. The authors concluded that both the run-in surface structures of the shaft and the seal lip must play equally important roles in the frictional characteristics but cannot be quantitatively considered in a graphical representation which is solely based on the Duty Parameter  $G$ .

The first explanation of the load support came from HIRANO AND ISHIWATA [HI65], who assumed that the seal lip was sliding over asperities on the shaft surface. They used foil bearing theory, accounting for the viscoelasticity of the seal lip, to predict the frictional characteristics of the seal. This concept has been abandoned, as it was demonstrated by JAGGER AND WALKER [JW67], and, later, by HORVE [Hor91], that, during running, the shaft is polished and becomes much smoother than the seal lip.

JAGGER AND WALKER [JW67]<sup>14</sup> suggested that the oil film was able to carry the radial load by virtue of a micro-asperity lubrication mechanism where the elastomer seal lip surface asperities are treated as lubricated contraformal Hertzian contacts; here, the compliance of the rubber allows for the formation of a second order micro-elastohydrodynamic lubricant film between the flattened asperity tops and the smooth shaft. The average thickness of these second order under-asperity lubricant films was calculated to be about  $0.25\ \mu\text{m}$ . The calculated friction coefficients agreed fairly well with experimental results. The basic idea of this lubrication concept was later revisited by GABELLI [Gab89, Gab91], who developed a combined hydrodynamic and micro-elastohydrodynamic lubrication model that was generalized to the parallel sliding contact between two rough surfaces; here, second order micro-elastohydrodynamic lubricant film formation due to asperity contacts was modeled using the soft micro-elastohydrodynamic film thickness formula developed by CHITTENDEN ET AL. [CDT87]. GABELLI presented results of a parameter study, but there was no comparison with experimental data.

Mainly motivated by hard surface asperity lubrication models originally developed for mechanical face seals, it has become common practice to attribute the load support in radial lip seals primarily to first order hydrodynamic pressure generation by seal lip surface asperities, in combination with inter-asperity cavitation<sup>15</sup>. Based on this

<sup>14</sup> See also JAGGER AND WALLACE [JW70].

<sup>15</sup> See, e.g., HAMILTON ET AL. [HWA66], and ANNO ET AL. [AWA68]. Later, however, LEBECK [Leb87] arrived at the conclusion that 'micro asperity lubrication does not account for the apparent hydrodynamic load support observed in many practical cases', and is 'not a powerful enough effect to provide the load support observed'.

general agreement, within the last three decades a number of radial lip seal lubrication models have been developed. Starting out from basic hydrodynamic approaches with undulated and bi-sinusoidal deterministic representations of the seal lip surface roughness, these models have evolved to fast flow factor based codes which account for random roughness of the seal lip surface and mixed lubrication conditions, allowing for the computation of reverse seal pump rates, seal friction and lubricant film thickness<sup>16</sup>. The available mixed lubrication models<sup>17</sup> are based on the assumption of a classical Stribeck curve-like transition from partial to full-film lubrication as shown in Figure 1.3. Under conditions where the first order hydrodynamic pressure generation does not suffice to completely separate the seal lip surface from the shaft, these mixed lubrication models, therefore, comprise partial lubricant film rupture that is formally treated with a Coulomb-type boundary friction component.

Besides the micro-hydrodynamic effects due to seal lip surface asperities, there are secondary mechanisms that can also contribute to the load support. For example, due to the viscoelastic behavior of the seal lip, radial oscillations, resulting, e. g., from dynamic shaft eccentricity or shaft runout, may appreciably enhance the hydrodynamic lubricant film formation<sup>18</sup>. It has also been hypothesized that the non-Newtonian behavior of the lubricant could impact the lubricant film formation and reverse pumping mechanism of radial lip seals<sup>19</sup>.

Regarding the lubrication condition of the seal lip, both the results of seal friction torque and leakage (or pump rate) measurements have been used to indirectly estimate the lubricant film thickness within the sealing contact zone<sup>20</sup>, yielding values that were well below the film thickness expected in hydrodynamic full-film lubrication.

McCLUNE AND TABOR [MT78] studied the lubrication of annular rubber specimens that were carefully aligned and mounted concentrically over a rotating glass disc, a set-up similar to that used by JAGGER [Jag57a]. Measurements of the coefficient of friction indicated that the frictional behavior could be explained in terms of elasto-

16 See, e. g., GABELLI [Gab89, Gab91], GABELLI AND POLL [GP92], SALANT [Sal92], SALANT AND FLAHERTY [SF95], SHI AND SALANT [SS00], SHI AND SALANT [SS01], HARP AND SALANT [HS01], HARP AND SALANT [HS02], HAJJAM AND BONNEAU [HB04], HAJJAM AND BONNEAU [HB06a], HAJJAM AND BONNEAU [HB06b], SHEN AND SALANT [SS06], MAOUI, HAJJAM AND BONNEAU [MHB07], MAOUI, HAJJAM AND BONNEAU [MHB08], SALANT [Sal10], SCARAGGI AND CARBONE [SC12], ZHOU ET AL. [ZLS<sup>+</sup>12], GUO ET AL. [GJS<sup>+</sup>13], ZHOU ET AL. [ZLTA13], and MIZUTA AND SUGIMURA [MS13].

17 See, e. g., SHI AND SALANT [SS00], SHI AND SALANT [SS01], SHEN AND SALANT [SS06], SALANT [Sal10], SCARAGGI AND CARBONE [SC12], and GUO ET AL. [GJS<sup>+</sup>13].

18 See, e. g., INY AND CAMERON [IC61], STAKENBORG ET AL. [SLH90], VAN LEEUWEN AND STAKENBORG [LS90, LS91], and GABELLI AND POLL [GP92].

19 See, e. g., DE OLIVEIRA [Oli95], and BAART ET AL. [BLP10, BLP14], for the special case of grease-lubricated radial lip seals.

20 See, e. g., JAGGER [Jag57a], JOHNSTON [Joh78], and VAN LEEUWEN AND WOLFERT [LW97].

hydrodynamic lubrication at individual asperities, as was first suggested by JAGGER AND WALKER [JW67]. Using more detailed equations than were available at the time of their work, MCCLUNE AND TABOR compared the theoretical and experimental frictional behavior over a range of velocities, lubricant viscosities, and surface roughnesses, and, on the whole, found a good agreement.

Both the lubricant film formation and the frictional characteristics of radial lip seals have since been extensively studied directly.

OGATA ET AL. [OFS87] used an electrical resistance technique in order to measure the oil film breakdown ratio, i. e., the fraction of the lubricant film that is broken down and allows contact between the seal lip and the shaft<sup>21</sup>. The seal friction was also measured. In these experiments, the temperature of the lubricating oil was controlled to a constant value of 30 °C at the position of the seal lip surface. The results led the authors to conclude that at speeds less than 0.0026 m s<sup>-1</sup> there is dry friction including stick-slip, at speeds of 0.0026 m s<sup>-1</sup> to 0.18 m s<sup>-1</sup> there is boundary lubrication involving a thin fluid film, and at speeds above 0.18 m s<sup>-1</sup> there is a mode of fluid film lubrication including thin boundary oil films. The authors further referred to a previous study showing that the oil film breakdown ratio increased remarkably in the high-speed region when the temperature of the lubricating oil was not controlled to a constant value. Using the operating conditions of the seal, the oil film thickness within the sealing contact zone was indirectly estimated to be in the range of approximately 0.1 μm to 1 μm. Therefore, the authors suggested the application of elastohydrodynamic lubrication theory considering surface roughness.

BINNINGTON [Bin91] used a laser induced fluorescence technique and a microphotographic method to measure the lubricant film thickness in the contact zone of elastomeric radial lip seals running on a hollow glass shaft. Here, the optical density of the photographic film, being an indirect measure of the local fluorescence intensity, was calibrated to known lubricant film thickness values. The measurements yielded film thicknesses ranging from approximately 1.1 μm at 106 min<sup>-1</sup> to 2.5 μm at 1512 min<sup>-1</sup>. BINNINGTON concluded that the seals were operating under conditions of mixed lubrication, i. e., the surfaces of the seal lip and the shaft were not completely separated, but the radial load was shared by both the flattened seal lip surface micro-asperities, the hydrodynamic action of the micro-asperities, and the squeezing of the lubricant entrapped within the seal lip surface cavities.

POLL AND GABELLI [PG92] (see also GABELLI AND POLL [GP92]) used a film thickness measurement method based on magnetic fluids.

<sup>21</sup> It is worth mentioning that the electrical detection of fluid film breakdown does not necessarily imply the presence of dry contacts. Fluid film breakdown may also be falsely detected in the presence of a very thin, yet coherent oil film, if the local electric field strength exceeds a critical value, and dielectric breakdown occurs.

The average lubricant film thickness was found to increase quickly with rotational speed, reaching values (up to approximately  $10\ \mu\text{m}$  for a sliding speed of  $1.43\ \text{m s}^{-1}$ ) that were considered to be indicative of hydrodynamic lubrication. The authors, however, noted that the experiments were especially set up to get high values of the lubricant film, i. e., low contact pressure, high viscosity, wide contact area and shaft eccentricity<sup>22</sup>, in order to check the capability of the measurement methods while maintaining isothermal conditions inside the contact.

POLL ET AL. [PGBQ92] described a microscopic fluorescence setup implementing a CCD<sup>23</sup> camera, thus allowing for a dynamic digital mapping of rotary lip seal lubricant films. The test seal was run on a hollow glass shaft. The measurements yielded an average film thickness of approximately  $0.35\ \mu\text{m}$  at a maximum sliding velocity of  $0.12\ \text{m s}^{-1}$ . The speed-dependent changes in film thickness were very small; when starting up after a standstill period there was a tendency for film thickness to increase, whereas it appeared to stay almost constant when reducing the speed to zero. The authors argued that this behavior had been expected from the almost linear increase of friction torque measured at the same time. When starting up after a standstill period, minimum seal friction was observed at a very low sliding speed below  $10\ \text{mm s}^{-1}$ .<sup>24</sup> Using a straightforward mixed lubrication approach similar to that previously proposed by LEIN [Lei54], the measured seal friction was considered to be composed of a constant and a speed-dependent viscous (Newtonian) lubricant friction part. The constant part was hypothesized to be due to boundary friction in some regions of the contact area, or to non-Newtonian behavior of very thin second order micro-elastohydrodynamic lubricant films forming under the asperity tips. It was assumed to equal the friction torque at very small decreasing speeds.

Based on previous work by VISSCHER [Vis92], VAN LEEUWEN AND WOLFERT [LW97] used an optical open-loop focus error signal detection technique to measure the lubricant film thickness within the sealing contact of a radial lip seal running on a hollow glass sleeve. These measurements yielded film thicknesses ranging from  $1\ \mu\text{m}$  at  $0.035\ \text{m s}^{-1}$  to  $4.5\ \mu\text{m}$  at  $0.35\ \text{m s}^{-1}$ . However, given the much smaller film thickness estimates indirectly derived from additional seal friction torque measurements, the authors concluded that the averaged film thickness had been appreciably overestimated in the measurements. Additionally, they noted that the signal to noise ratio was too low.

---

22 Regarding the impact of dynamic shaft eccentricity on leakage and friction of elastomeric radial lip seals, see, e. g., PRATI [Pra87], AMABILI ET AL. [ACP00], and SILVESTRI ET AL. [SPT06, SPT07].

23 CCD Charge Coupled Device

24 Very similar frictional characteristics were later also described by POLL [Pol00].

SATO ET AL. [STNY00a] described a laser induced fluorescence setup implementing a laser-scanning unit, similar to confocal laser scanning microscopes, to qualitatively map the lubricant film thickness within the contact zone of radial lip seals running on a glass shaft. The measurements were conducted at rotational speeds ranging from  $100 \text{ min}^{-1}$  to  $1000 \text{ min}^{-1}$ , considering both regular sealing as well as pumping, i. e., fully flooded, conditions. Under sealing conditions, with increasing speed the relative fluorescence intensity increased slightly on the oil side of the sealing contact zone. On the air side of the contact, however, there were regions where the lubricant film was nearly nonexistent. With increasing speed, the size of these regions tended to increase towards the oil side. This behavior was explained with a speed-dependent increase of the reverse pumping action, leading to different axial equilibrium positions of the lubricant film on the air side of the sealing contact. Under fully flooded conditions, the lubricant film was appreciably thicker on both sides of the sealing contact, compared to that obtained under sealing conditions. However, only small differences were found within the central region of the sealing contact. Under fully flooded conditions, there was no distinct influence of sliding speed on the qualitative axial film thickness profiles.

In another paper [STNY00b], SATO ET AL. described a calibration method for quantitative film thickness measurements. It was demonstrated that the fluorescence intensity decayed appreciably with increasing lubricant temperature, especially at temperatures above  $60^\circ\text{C}$ . In order to continuously monitor the temperature within the seal lip contact zone, a thermocouple was implemented into the seal lip. Finally, the duration of each film thickness measurement was kept below 10 s to consistently prevent the seal lip temperature from exceeding  $50^\circ\text{C}$ . Using the calibration curves obtained at room temperature, film thickness measurements under sealing conditions yielded axial film thickness profiles that were qualitatively similar to those seen in the previous study; towards the oil side, however, the film thickness far exceeded  $10 \mu\text{m}$ . The authors noted that these film thickness values were appreciably higher than those measured and estimated by others. Using the defocused laser spot to qualitatively map the lubricant distribution and the lubricant flow within a larger portion of the sealing contact zone, the authors finally arrived at the conclusion that the measured film thickness predominantly originated from the fluid filled seal lip surface cavities and microchannels; however, the lubricant film thickness observed under the flattened seal lip surface micro-asperities, i. e., within the actual contact zones, was appreciably smaller. The thickness of these second order under-asperity lubricant films was estimated to be below  $1 \mu\text{m}$ , thus being similar to previously published findings.



Using the same calibration technique and a further improved fluorescence setup with a hollow glass shaft, SATO ET AL. [SSSY03] later obtained qualitatively similar results. The measurements were conducted at rotational speeds ranging from  $20 \text{ min}^{-1}$  to  $1150 \text{ min}^{-1}$ , corresponding to sliding speeds of  $0.0942 \text{ m s}^{-1}$  to  $5.4192 \text{ m s}^{-1}$ . Seal friction torque and pump rates were also measured. In order to continuously monitor the temperature within the seal lip contact zone, a thermocouple was implemented into the seal lip. Fluorescence calibration tests were done at temperatures ranging from room temperature to  $60^\circ\text{C}$ . No information was provided concerning the duration of each film thickness measurement or the corresponding seal lip temperature. Under sealing conditions, depending on the operating conditions, the average film thickness decreased axially from about  $10 \mu\text{m}$  on the oil side to approximately  $1 \mu\text{m}$  on the air side of the sealing contact. Even when the seals were preventing leakage, lubricant films thicker than  $1 \mu\text{m}$  were observed on the air side of the contact. Under pumping conditions, both sides of the sealing contact were fully flooded with lubricant, the axial film thickness profiles were rather symmetric, and the lubricant film was thicker than that observed under sealing conditions, particularly near the air side. Both under sealing, and under pumping conditions, there was no appreciable change in film thickness with circumferential position, nor did the film thickness change appreciably with the shaft speed; even when the shaft was stopped, the film thickness profiles did not change substantially. The coefficient of friction  $\mu$  under sealing and pumping conditions was proportional to  $G^n$  ( $G = \eta ub/P_r$ ), with the exponent  $n$  ranging from 0.25 to 0.5; the  $\mu - G$  characteristics differed from specimen to specimen. As opposed to previous findings, e. g., by KAWAHARA AND HIRABAYASHI [KH79], there was little or no correlation between pumping rate  $Q'$  and the coefficient of friction;  $\mu$  was appreciably different even when the  $Q' - G$  characteristics of the test seals were nearly the same. The authors also presented a hydrodynamic full-film lubrication model of a rigid bi-sinusoidal seal lip surface sliding against a smooth counterface. Using this simple model that also accounted for inter-asperity cavitation, it was demonstrated that at higher sliding velocities the hydrodynamic pressure generation could suffice to keep the surfaces separated, yielding estimates of viscous lubricant friction that qualitatively agreed with experimental results but tended to underestimate the measured friction. Due to the fact that surface contact was not allowed in this fully hydrodynamic model, it was not possible to consider low sliding speeds, and the computational results, therefore, covered only half of the experimental speed range. The computational results were shown to depend strongly on the amplitude and wavelength of the surface structure.

MIZUTA AND SUGIMURA experimentally [MS11] and theoretically [MS11, MS13] studied the effect of seal lip surface roughness on

the lubrication of radial lip seals. Seal friction torque measurements under pumping (i. e., completely flooded) conditions were conducted at sliding speeds ranging from  $0.0942 \text{ m s}^{-1}$  to  $4.7 \text{ m s}^{-1}$ . The seal lip surface roughness was characterized by means of laser scanning microscopy. The experimental results indicated that a seal having a larger root mean square roughness, longer correlation distance, and smaller mean peak curvature in the direction of sliding, showed lower friction. In order to numerically study the lubrication of the seal lip, the authors developed a hydrodynamic full-film lubrication model of a bi-sinusoidal seal lip surface sliding against a smooth counterface. While essentially based on previous work by SATO ET AL. [SSSY03], this model additionally accounted for linear elastic deformation of the seal lip due to hydrodynamic pressure. The distortion of the “asperities” due to viscous shear force was not included<sup>25</sup>, but the effect of the “asperity” orientation was considered by using different wavelengths in circumferential and axial direction. In addition, in axial direction the seal lip surface was given an asymmetrically curved shape the minimum of which was located towards the oil side. The computations were carried out for sliding speeds ranging from  $0.1 \text{ m s}^{-1}$  to  $10 \text{ m s}^{-1}$ , “asperity” amplitudes ranging from  $0.5 \mu\text{m}$  to  $2.0 \mu\text{m}$ , and “asperity” wavelengths of  $32 \mu\text{m}$ ,  $64 \mu\text{m}$ , and  $128 \mu\text{m}$ . The numerical results qualitatively confirmed the experimental findings that seals having a larger root mean square roughness, longer correlation distance, and smaller mean peak curvature, showed lower friction. However, realistic estimates of measured seal friction were obtained only when using the “smallest” wavelength and, at the same time, applying the highest sliding speeds. With decreasing speed, the measured seal friction was increasingly underestimated. Due to the fact that surface contact was not allowed in this fully hydrodynamic approach, this specific model was not able to capture sliding speeds below approximately  $1 \text{ m s}^{-1}$ , where the hydrodynamic pressure generation did not suffice to keep the surfaces separated. When using the larger “asperity” wavelengths, the applicable speed range was appreciably increased; at the same time, however, the measured friction coefficients were even more severely underestimated<sup>26</sup>. The authors concluded that the seal friction was apparently affected by other mi-

<sup>25</sup> The corresponding asperity “micro-wedge” formation, however, may contribute appreciably to the hydrodynamic load bearing capacity. Therefore, the described modeling approach is expected to systematically overestimate the viscous friction.

<sup>26</sup> It is interesting to note the similarity of these findings to the results of VAN BAVEL [Bav97] who developed a hydrodynamic full film lubrication model of a bi-sinusoidal seal lip surface subjected to asymmetric tangential displacement. Here, the clearance between the seal lip and the shaft was fixed, and the model parameters were based on average values of published results. The asperity wavelength was set to  $10 \mu\text{m}$  in both directions, according to observations of KAMMÜLLER [Kam86]. Both the computed average hydrodynamic pressure and the friction torque were appreciably lower than the expected values.

crotopographical features of the seal lip that had not been covered in this hydrodynamic modeling approach.

FOWELL ET AL. [FMSK14] used fluorescence microscopy to measure the lubricant film thickness within the highly conformal contact of a relatively rough FKM (fluorocarbon) O-ring sliding against a concave glass lens, a geometry that was deemed similar to that found in elastomeric seals. Results were presented for sliding speeds ranging from  $14.1 \text{ mm s}^{-1}$  to  $105.0 \text{ mm s}^{-1}$ . The average film thickness was low within the nominal elliptical contact area and the lubricant film consistently remained below  $1 \mu\text{m}$ . Throughout the contact patch distributed areas of local minima in lubricant film thickness were observed, the size of which decreased as entrainment speed increased. The presence and behavior of these discrete minima suggested that the roughness of the elastomer sample dominated the film behavior under the applied conditions, and that micro-films were likely forming on asperity contacts.

### 1.3 EXPERIMENTAL APPROACHES IN RADIAL LIP SEAL RESEARCH

From a practical point of view, both measurements of seal friction torque (see Section 1.2.2) and leakage, as well as life tests, are useful as they allow for a global assessment of the sealing system's frictional losses and reliability, including the compatibility of the elastomer compound and the lubricant formulation<sup>27</sup>.

Pump rate measurements are of less direct interest to the user<sup>28</sup>. This is mainly due to the fact that during these measurements the sealing contact requires to be completely flooded, either through converse installation of the seal, or by adding a known volume of oil to the low contact angle side (i. e., the "air side") of the sealing contact. These conditions differ from those in the regular oil seal application where, due to the reverse pumping action, the oil meniscus on the air side of the sealing contact may be ingested into the sealing zone when the shaft speed exceeds a critical value (see, e. g., SALANT [Sal97]). Under such conditions, this region of the sealing contact may be partially subject to starved lubrication, and seal friction will mostly be higher

<sup>27</sup> See, e. g., HIRANO ET AL. [HIK61], SCHNÜRLE AND UPPER [SU73], HORVE [Hor84], JOHNSTON [Joh86], JOHNSTON AND VOGT [JV95], CHIBA ET AL. [CSY98], AMABILI ET AL. [ACP00], and ENGELKE [Eng11].

<sup>28</sup> However, pump rate measurements have been widely used in previous studies on radial lip seal working principles. To name but a few, see, e. g., KAWAHARA ET AL. [KAHM78], KAWAHARA AND HIRABAYASHI [KH79], KAWAHARA ET AL. [KAH80], HORVE [Hor84], HORVE [Hor87], HORVE [Hor91], FRITZSCHE [Fri94], STEINHILPER AND FRITZSCHE [SF92] (measurement of air pump rates), KUNSTFELD [Kun05], NAKAOKA ET AL. [NSG<sup>+</sup>05] (gas pump rates measured with gas chromatography), BUHL [Buh06], MIZUTA ET AL. [MFS07] (pump rates measured with fluorescence spectrometry), WENNEHORST [Wen08], LEIS ET AL. [LHRP10], OTTINK [Ott13], and GUO ET AL. [GJL<sup>+</sup>14].

compared to the fully flooded case, depending on the lubricant viscosity. Nevertheless, these measurements provide important information for developers of elastomeric radial lip seals as they allow the reverse pumping mechanism to be assessed, and optimized, as a function of the operating conditions and the seal design parameters. As described above, these parameters include, e. g., the cross-sectional seal lip design, the seal radial force, the location and the characteristics of the garter spring, the resulting axial contact pressure distribution, and the seal lip surface roughness characteristics. Moreover, pump rate measurements can help quantify the relative impact of the counterface on the entire sealing system's sealing capability; in many cases, e. g., non-standard counterface materials or manufacturing processes, it is not the seal that causes leakage, but the sealing system fails due to a superimposed axial viscous drag flow resulting from directional surface microstructures on the counterface. Depending on the orientation of these structures<sup>29</sup>, such a counterface will either enhance or reduce the reverse seal pump rate compared to that measured on a regular non-pumping (i. e., standard) shaft; in the worst case, the pump rate changes sign, and leakage occurs.

Measurements of the seal lip contact temperature not only provide information about thermal impact that are helpful for material selection<sup>30</sup>. They also allow the actual lubricant viscosity within the sealing contact zone to be determined, which is a crucial variable in any theoretical approach to radial lip seal lubrication and friction<sup>31</sup>.

Both the electrical capacitance and resistance methods, as well as the magnetic resistance technique (see Section 1.2.2) are integrating methods and, therefore, do not allow for a locally resolved investigation of the sealing contact zone. Invaluable direct insight into dynamic sealing contacts, down to the roughness scale, has been provided by experimental studies applying optical methods. Starting out with the entire macroscopic sealing system including the oil sump, transparent housing components have been employed to visually study the effect of rotational oil flow generated by the shaft on the rate of leakage through the gap formed by rigid seals and the shaft (see OTT [Ott83], and QU [Qu93])<sup>32</sup>.

<sup>29</sup> The direction of rotation should not be changed as the run-in process at a constant speed may induce permanent directional conditioning effects of the seal lip surface. If the direction of rotation is then inverted after the run-in, the tangential deformations of the seal lip surface are not perfectly elastic, and the original reverse pumping action might not be reestablished. Then, leakage may occur irrespective of the surface characteristics of the counterface.

<sup>30</sup> See, e. g., HORVE [Hor76], and HORVE [Hor84].

<sup>31</sup> See, e. g., LEIN [Lei54], HIRANO ET AL. [HIK61], LINES ET AL. [LLO66], UPPER [Upp68], KAWAHARA AND HIRABAYASHI [KH79], KAWAHARA ET AL. [KAH80], HORVE [Hor87], WOLLESEN [Wol93], SATO ET AL. [STNYoob], ENGELKE [Eng11], and GUO ET AL. [GJL<sup>+</sup>14].

<sup>32</sup> Both authors used rigid seals with a geometry typical for radial lip seals, i. e., the oil side angle was larger than the air side angle. The rigid seals used by QU [Qu93] were made of plexiglass (polymethylmethacrylate); transparent seal components

GUO ET AL. [GJL<sup>+</sup>14] described the use of a non-contacting optical coordinate measuring instrument to analyze the change in the profile of the seal lip resulting from wear. Here the lip profiles were measured in a free state, and the seal lip was not subject to any force during the measurement.

Non-contact optical techniques, such as optical interferometry and confocal laser scanning microscopy, are routinely used today in order to characterize the surface roughness of the seal lip. Here, due to the poor reflectivity of many elastomer compounds, it may be necessary to use impression methods, e. g., based on polyurethane (see GUO ET AL. [GJL<sup>+</sup>14]), and to measure the roughness of the resulting impression.

Besides the surface roughness characteristics, the contact width of the seal lip is another important parameter required in theoretical studies of the sealing contact. It increases with wear, which leads to a gradual redistribution of the initial seal lip contact pressure distribution. The seal lip contact width has been routinely measured using transparent sleeves having the same diameter as the actual counterface<sup>33</sup>. A prism, or a tilted mirror, which is fixed in the sleeve at 45°, is used to redirect the optical path<sup>34</sup>, and microscopic imaging techniques are employed to determine the seal lip contact width. In order to account for the effect of rubber viscoelasticity, the contact photographs are usually taken several hours after installation of the seal.

Transparent hollow shafts, mostly made of glass, have been used to study the radial lip seal contact under lubricated dynamic conditions. LINES ET AL. [LLO66] used a hollow glass shaft to measure the contact width at various rotational speeds. JAGGER AND WALKER [JW67] also used a glass shaft to photograph the lubricated seal lip contact area through a microscope by electronic flash. A notable feature common to all the seals observed in their study was that the general dark tone of the contact band became lighter when the shaft was rotating. The authors believed this to be caused by a multitude of tiny cavitation pockets, smaller than the distance between asperities. Regarding the occurrence of inter-asperity cavitation, similar findings were later described by JENISCH [Jen91], who additionally used a custom-made

---

were also used by HAAS [Haa86] in order to study the lubricant flow within non-contacting (e. g., labyrinth) seals.

<sup>33</sup> See, e. g., HIRANO ET AL. [HIK61], LINES ET AL. [LLO66], OTT [Ott83], KAMMÜLLER [Kam86], WOLF [Wol87] (who studied the axial deformation and contact behavior of pressurized and axially undulated radial lip seals), JENISCH [Jen91], FRENZEL [Fre00] (with application to pressurized reciprocating seals made of polyurethane), RUHL [Ruh01], ENGELKE [Eng11], and GUO ET AL. [GJL<sup>+</sup>14].

<sup>34</sup> In order to measure the contact width of lip seals made of polytetrafluorethylene (PTFE), FLITNEY [Fli82] used a mandrel made of plexiglass with a polished conical bore, utilizing total reflection to observe the sealing contact. A similar set-up was also used by STAKENBORG [Sta88a] to visually inspect the contact zone of elastomeric radial lip seals.

microscope that was attached to the hollow glass shaft and therefore rotating with the same speed. Using this setup, JENISCH studied circumferential irregularities and waviness of the seal lip contact band arising, e. g., from the manufacturing process or misaligned installation of the seal.

NAKAMURA ET AL. [NK84, NKK85, Nak87] used videotapes to record the actual microscopic contact between the seal lip and a hollow glass shaft as a distribution of dark spots. The intensity values within these spots were calibrated to seal lip contact pressure and, according to the classification of darkness, groups of contour lines were drawn by means of digital image processing. Regions of cavitation were distinguished as bright patterns. Upon statistical analysis of a large number of such processed contact images, the authors arrived at a set of statistical criteria, mainly based on the axial location and the area fraction of the maximum seal lip contact pressure, for a non-leaking radial lip seal<sup>35</sup>.

POLL ET AL. [PGBQ92] described a total internal reflection contact visualization technique that drastically improved the contrast of the seal lip contact images, especially under dry conditions. Here, the light was fed into the hollow glass shaft at an oblique angle through the front side of the shaft. Due to total internal reflection at the glass-air interfaces, the incoming light is reflected back and forth until it reaches the actual sealing contact. Here, only the actual rubber-glass contacts are optically coupled and thus visible as bright spots, whereas areas without contact remain dark. Similar to the method described by NAKAMURA ET AL. [NK84, NKK85, Nak87], intensity values correspond to the local seal lip contact pressure distribution. In another study, GABELLI ET AL. [GPP92] used this technique to visualize the axial seal lip contact pressure redistribution resulting from the normal run-in process of a radial lip seal.

KAMMÜLLER [Kam86] used a hollow shaft made of plexiglass to study the asymmetric tangential distortion of the seal lip contact zone resulting from the asymmetric axial seal lip contact pressure distribution. The local displacements of the seal lip were reconstructed by comparing the positions of high reflectance features observed under static conditions with those observed during shaft rotation. The high reflectance features were produced by vapor depositing a thin film of gold (approximately 20 nm thick) onto the seal lip. The torsional deformation of the seal lip bulk material was determined using two spatially fixed steel needles that served as reference points. Similar approaches were later described by VAN LEEUWEN AND WOLFERT [LW97], who vapor deposited chromium layers (below 40 nm thick) onto the seal lip and used digital image processing techniques, and by OTTINK [Ott14], who used thin diamond-like carbon

<sup>35</sup> The same methodology was used by CHIBA ET AL. [CSH91], who studied the sealing phenomena of a lip-type seal for an automotive air conditioning compressor.

films (a few nanometers thick) that were chemically vapor deposited onto the seal lip. VAN LEEUWEN ET AL. [LPM11] used time-resolved digital microscopic imaging to study the stick-slip behavior of the rubber asperity contacts within the dry contact between an axial lip seal and a rotating coated flat optical disk. Irregularities in the rubber were used as targets and their position was determined with time.

STAKENBORG [Sta88a, Sta88b] microscopically observed the oil–air interfaces, the lubricant distribution, and cavitation within the sealing contact zone through a small glassfibre bundle implemented into a fixed hollow steel shaft. The end of this glassfibre bundle was given the same radius as the shaft surface. Using this setup, the thermal boundary conditions, i. e., the heat transfer properties of the shaft, were largely preserved and much more realistic compared to glass or plexiglass shafts with their lower thermal conductivities. An important disadvantage of this approach, however, is that, in the case of a rotating seal, the contact conditions of the seal lip are influenced by centrifugal forces, whereas in most practical situations the shaft rotates and the seal is fixed.

Based on the same thermal rationale, GABELLI AND POLL [GP92] microscopically observed the sealing contact through a glass window implemented into a hollow steel shaft. In order to achieve high-contrast imaging of the lubricant behavior within the sealing contact, a fluorescent dye was dissolved in the oil and the blue light induced fluorescence method was applied. Utilizing the total internal reflection contact visualization technique described by POLL ET AL. [PGBQ92], the reflected fluorescence excitation light was simultaneously used to study the contact pattern of the seal lip surface micro-asperities.

Optical approaches have also been used to microscopically study the sealing contacts regarding the transport and aggregation of solid particles carried with the lubricating oil, and to study local flow phenomena. TAMURA AND OBAYASHI [TO00], and CHIBA ET AL. [CSY98] directly observed the reflectance and scatter of solid particles to study the impact of solid lubricant contamination on the occurrence of seal leakage. BAUER [Bau08], in a similar approach, used metallic particles to study the lubricant flow within the contact of spiral groove lip seals made of PTFE. HIDROVO AND HART [HH99] used a laser induced fluorescence (LIF) setup and a mixture of fluorescent particles and dust to visualize the progression and clustering of contaminant particles in the seal–shaft interface of a spiral groove lip seal. SATO ET AL. [STNY00a] used a LIF setup and fluorescent microparticles made of polymethylmethacrylate (PMMA) to study the local flow<sup>36</sup> near the contact of a radial lip seal with hydrodynamic pumping aids having

<sup>36</sup> This is the basic principle of microscopic particle image velocimetry ( $\mu$ -PIV), which has become a standard method in experimental fluid mechanics (see, e. g., ADRIAN [Adf91], SANTIAGO ET AL. [SWM<sup>+</sup>98], MEINHART ET AL. [MWS99], MEINHART ET AL. [MWG00], and WERELEY AND MEINHART [WM05, WM10]).

the form of protruding helical ribs. WENNEHORST AND POLL [WPo6] used fluorescent microparticles made of melamin resin and observed spiral particle movement and particle clustering in the direct vicinity of a standard elastomer seal lip contact and within the contact of a spiral groove lip seal made of PTFE.

Optical interferometric approaches have been used to measure the lubricant film thickness within the sliding contact of elastomer seals for both rotating and reciprocating motion of the counterface. These approaches, however, have been largely limited to lubricated sliding contacts between plane pad- or band-shaped model seal lips and rotating glass discs<sup>37</sup>, or reciprocating glass plates<sup>38</sup>. The application of this technique to study rough elastomer contacts turned out to be challenging, as the production of interferometric photographs requires that a specular surface exist on the seal, and that the amount of light reflected from the oil–seal interface produce satisfactory interference with the light from the glass–oil interface. McCLUNE AND TABOR [MT78] studied the lubrication of annular rubber specimens that were carefully aligned and mounted concentrically over a rotating glass disc, a set-up similar to that used by JAGGER [Jag57a]. When using rough elastomer specimens, the optical interference technique could not be used because the interference colors were so broken that it was impossible to interpret the results. KRAUTER [Kra82], who measured the oil film thickness within the contact of elastomeric Stirling engine rod seals, used a thin elastic lacquer coating on the seal to increase the amount of light reflected from the oil–seal interface. When discussing results, however, KRAUTER believed this optical coating to have influenced the measurements. LIMING [Lim01] used a pad-shaped model seal lip to measure the lubricant film build-up due to hydrodynamic pumping aids having the form of protruding helical ribs. In order to enhance the reflectance of the elastomer surface, the model seals were produced using extremely smooth molds. Moreover, in order to avoid diffuse reflections, the elastomer compounds did not contain any colored additives.

Fluorescence techniques for the measurement of thin liquid films, as originally described by SMART AND FORD [SF74], have been actively pursued in the field of internal combustion engine research, mainly focusing on the oil film thickness between the piston rings and the cylinder wall or cylinder liner<sup>39</sup>. Fluorescence techniques have also been used to measure the lubricant film thickness, e. g., on

<sup>37</sup> See, e. g., LIMING [Lim01, Lim03].

<sup>38</sup> See, e. g., KANZAKI ET AL. [KKK97] and KANETA ET AL. [KFKK97, KTN<sup>+</sup>00, KTT<sup>+</sup>05].

<sup>39</sup> See, e. g., FORD AND FOORD [FF78], TING [Tin80], HOULT ET AL. [HLWB88, HLWB89], LUX ET AL. [LHO91], WONG AND HOULT [WH91], RICHARDSON AND BORMAN [RB91], SHAW ET AL. [SIHW92], SANDA ET AL. [SSKN93], KONOMI ET AL. [KNMS93], INAGAKI ET AL. [ISMK95], TAKIGUCHI ET AL. [TNFY98], THIROUARD AND HART [TH00], WEIMAR AND SPICHER [WS03], and DHUNPUT ET AL. [DTA07] (who studied the development of cavitation in the lubricant film of piston-ring assemblies).



hard magnetic memory disks (TANIMOTO AND RABINOWICZ [TR92]), in axial spiral groove bearings (ZOU ET AL. [ZTL<sup>+</sup>05]), and in metal forming processes (AZUSHIMA [Azu06]). SUGIMURA ET AL. [SHY00], and REDDYHOFF ET AL. [RCSG10] applied fluorescence microscopy to study lubricant film thickness and lubricant flow within the macroscopic elastohydrodynamic contact between a steel ball and a glass disc. MYANT ET AL. applied fluorescence microscopy to measure the lubricant film thickness in macroscopic compliant point contacts (stationary elastomer hemisphere pressed against a glass disc) under conditions of steady sliding [MRS10], and during transient sliding motion [MFC14]. KASSFELDT [Kas87] used a laser induced fluorescence technique to measure the lubricant film thickness within the contact of hydraulic cylinder seals<sup>40</sup>. With regard to reciprocating sealing applications, fluorescence-based lubricant film thickness measurements were also described, e. g., by DEBLER ET AL. [DGP03], and OTTINK ET AL. [OWP10]. HIDROVO AND HART [HH99] used a laser induced fluorescence technique to qualitatively study the lubricant film thickness within the sealing contact of a spiral groove lip seal. SATO ET AL. [STON99] used a laser induced fluorescence technique to qualitatively study the lubricant behavior within the sealing contact of a radial lip seal with hydrodynamic pumping aids having the form of protruding helical ribs. MIZUTA ET AL. [MAS07] used a fluorescence setup, essentially based on previous work of SATO ET AL. [SSSY03], to study the impact of elevated oil sump pressure on the seal lip contact width, the lubricant film thickness, and the frictional characteristics of radial shaft seals specifically designed for pressurized applications. Fluorescence techniques were also used by BINNINGTON [Bin91], POLL ET AL. [PGBQ92], SATO ET AL. [STNY00b], SATO ET AL. [SSSY03], and MIZUTA AND SUGIMURA [MS11] to quantitatively study the lubricant film formation in standard radial lip seals, and by FOWELL ET AL. [FMSK14], who measured the lubricant film thickness within the highly conformal contact of a relatively rough O-ring sliding against a concave glass lens, a geometry that was deemed similar to that found in elastomeric seals. The main findings of these investigations are described in Section 1.2.2.

---

<sup>40</sup> A description of this technique can also be found in JACOBSON [Jac91], pp. 219–227.



# 2

---

## AIMS AND SCOPE

---

As detailed in Section 1.2.2, the tribological characteristics of radial lip seals are currently not completely understood. Measured seal friction coefficients have been shown to vary vastly from specimen to specimen, even under conditions that, based on the hydrodynamic Duty Parameter  $G$ , can be deemed comparable from a classical hydrodynamic standpoint, i. e., when the  $\mu - G$  curve looks like a Stribeck curve, and when the value of  $G$  formally indicates hydrodynamic full-film lubrication with a complete separation of the surfaces. Consequently, for the typical case of a shaft being much smoother than the elastomer seal lip, the observed differences (for a given seal material and lubricant) have been ascribed to the run-in surface micro geometry of the lip. The roughness influence follows directly from the fact that the parallel sliding contact between the lip and the shaft lacks a macroscopic pressure and lubricant film formation mechanism, and that the generation of load support is, therefore, limited to micro-hydrodynamic effects on the roughness scale. Within the classical Stribeck curve concept, for an individual seal there might be a value of  $G$  where the initially flattened elastomer seal lip surface asperities separate completely from the shaft due to first order micro-hydrodynamic pressure generation; then, the seal lip lifts off, the boundary friction component vanishes, and the fully established lubricant film gives rise to purely viscous friction. However, combined seal friction and lubricant film thickness measurements have provided evidence that seal friction may be at a minimum at very low sliding speeds where there is apparently no speed-dependent lubricant film build-up at all. A number of researchers have arrived at the conclusion that radial lip seals may consistently run in a mode of mixed lubrication where first order micro-hydrodynamic effects do not suffice to eliminate asperity contact completely, even when the seal friction curve passes through a minimum and, therefore, formally resembles a classical Stribeck curve. To make the situation even more confusing, many seal friction curves simply do not resemble a classical Stribeck curve but instead show rising friction from the very beginning, and the friction curves, when extrapolated backwards to  $G = 0$ , are not passing through the origin as would be expected for purely viscous friction. Instead, these extrapolated curves intersect

the ordinate axis at friction values larger than zero, thus indicating a contribution of boundary friction.

This dissertation aims at contributing to a better understanding of the lubricant film formation mechanism and the frictional characteristics of elastomeric radial lip seals. It provides a summary of a series of ongoing experimental and theoretical work and is organized as follows:

**EXPERIMENTAL WORK** The first step involves combined measurements of seal friction torque and lubricant film thickness, using newly developed experimental facilities. The axial lubricant film thickness distribution is measured optically using the fluorescence method. In order to study the impact of the seal lip surface micro-geometry on the lubricant film formation, two different test seals are used that nominally differ only in the wear condition of the seal lip. To account for the influence of temperature on the lubricant viscosity, seal lip contact temperatures are additionally measured on a separate test rig. The experimental approach is described in Chapter 3, and the results of the experimental investigations are presented in Chapter 4.

**SEMIEMPIRICAL APPROACH** In order to gain further insight into the measured overall seal friction, a novel semiempirical approach is developed using the measured axial lubricant film thickness profiles as input in complementary computations of the viscous lubricant friction component. This work is described in Chapter 5.

**MODELING WORK** Based on the experimental and semiempirical results, mixed lubrication models are developed that rely on the concept of second order micro-elastohydrodynamic asperity lubrication. This work, as well as the comparison of computed and measured seal friction, are described in Chapter 6.

Within the scope of this work, only the “pumping” condition is considered where the sealing contacts are fully flooded. This decision was made in order to ensure a well-defined lubrication condition of the entire sealing contact throughout the measurements; moreover, this basic configuration can more readily serve as a starting point for modeling than the “sealing” condition, where the air-side region of the sealing contact may be partially subject to starved lubrication and the theoretical treatment is more complex.

# 3

---

## EXPERIMENTAL APPROACH

---

As detailed in Section 1.2.2, experimental investigations into the lubrication of elastomer shaft seals have been previously performed mainly at relatively high sliding velocities chosen for a better comparability with the actual oil seal application. Optical approaches have been based mainly on transparent hollow shafts made of glass. Due to the poor thermal conductivity of glass and the corresponding heat accumulation within the sealing contact zone, tribological investigations may be easily biased by thermal effects, which can impact both the tribological system under investigation as well as the measurement system itself. For example, an unrealistic drop of the lubricant viscosity directly affects the overall lubricant film formation and viscous lubricant friction; in fluorescence-based lubricant film thickness measurements, depending on the characteristics of the fluorescent dye, the fluorescence intensity at a given film thickness may decay noticeably with increasing temperature. These effects occur at the same time and impair the interpretation of the experimental results, as the actual speed-dependent lubricant film build-up may be considerably underestimated.

The combined lubricant film thickness and friction torque measurements in this work are, therefore, based on the following general considerations:

- use of a sapphire hollow shaft (having high thermal conductivity similar to steel) in order to avoid unrealistic heat accumulation within the sealing contact zone;
- limitation to low sliding speeds in order to minimize thermal effects;
- use of in situ calibration to monitor the impact of thermal effects on the fluorescence signal;
- use of test seals having low radial force to ease the build-up of the lubricant film;
- use of a high viscosity oil in order to enhance the build-up of the lubricant film.

## 3.1 EXPERIMENTAL SET-UP

Based on the author's previous work<sup>1</sup>, the optical test rig according to Figure 3.1 was set up. A stereo microscope is adopted to a modified seal test bench<sup>2</sup> via a cross table for adjustment. For radial observation of the sealing contact region a transparent hollow shaft made of sapphire in combination with a further optimized Laser Induced Fluorescence (LIF) set-up ("LIF device" in Figure 3.1, see also Section 3.2.2) is used. In order to avoid gravitational effects during standstill periods, as well as for laser safety reasons, the optical point of measurement is at the lower position of the sealing contact. The newly implemented sapphire hollow shaft (outer diameter: 82 mm) features a realistic surface roughness ( $R_q \approx 0.03 \mu\text{m}$ ) being similar to that of an actual run-in steel counterface. Thanks to the high thermal conductivity of sapphire being of the same order as that of steel<sup>3</sup>, heat accumulation within the sealing contact is substantially reduced, providing better comparability with the real tribosystem compared to glass shafts. The overall radial and axial dynamic run-out of the hollow shaft is less than  $10 \mu\text{m}$ . At the axial location of the test seal lip, through diligent alignment of the sapphire adaptor, the optimized run-out amounts to approximately  $1 \mu\text{m}$ , the corresponding influence on the measurements (axial reciprocation of the seal lip during shaft rotation) therefore being negligible. A cooled and temperature-controlled<sup>4</sup> 12 bit black and white CCD camera (SENSICAM, PCO AG, Kelheim, Germany) is used for digital image acquisition. A triggering system allows for image acquisition at a well-defined circumferential shaft position, while continuous imaging at frame rate is used for time-resolved measurements. The maximum spatial resolution of the imaging system amounts to  $0.85 \mu\text{m}/\text{pixel}$  in both horizontal and vertical direction. At the same time as the optical investigations are performed, the friction torque is measured implement-

- 
- 1 See WENNEHORST [Weno4b], WENNEHORST AND POLL [WPo6], WENNEHORST [Weno8], and WENNEHORST AND POLL [WPo8].
  - 2 The test rig was originally set up for measuring friction and pump rates of protective seals for rolling element bearings under pressurized conditions, see WENNEHORST [Weno8]. The pressure gradients applied to the contact of a single seal were obtained on a modified FE8 test rig by measuring the pressure within a completely sealed full-scale ball bearing subjected to rotational speed and temperature ramps. The modular design of the seal test rig also allowed for optical investigations into the dynamic sealing contacts utilizing the optical white light and fluorescence prototype set-up previously developed by WENNEHORST [Weno4b]. In later projects, thermally controlled versions of the pump rate test rig were used, additionally allowing for measurements at elevated oil sump temperatures (see LEIS ET AL. [LHRP10], VON HOLLEN ET AL. [HLPR11], and OTTINK [Ott13, Ott14]). The final optical set-up described in this work was later used by OTTINK [Ott13, Ott14].
  - 3 This similarity applies in particular to the temperature range of approximately 300 K to 400 K (see, e. g., INCROPERA ET AL. [IDBL07]), which is also relevant to typical radial lip seal applications, especially regarding the upper limit.
  - 4 The CCD sensor is cooled to  $-15^\circ\text{C}$  to minimize thermal dark current noise.

ing a high-precision telemetric torque sensor (HBM, 5 N m measuring range, 0.1 % accuracy). For temperature stability reasons, two equal seals are mounted each on the hollow shaft, the resulting ring gap (according to the close-up depicted in Figure 3.1) being completely filled with oil. Since the experiments are limited to low sliding velocities, no additional fluid circulation equipment is used. The sealed volume is vented via three small bores in the outer seal adaptor, one of them being the feedthrough for the temperature sensor. The oil sump temperature is measured in the vicinity of the sealing contact. The two outer contact angle sides of the test seals are wetted continuously with oil during the experiments in order to maintain the fully flooded lubrication condition. The measurements are quasi-stationary with stepwise change of rotational speed, allowing for a relaxation period of at least 5 min at each speed level. Both the seal friction torque and the oil sump temperature are taken as the average over the last 60 s of the corresponding speed step.

### 3.2 OPTICAL METHODS

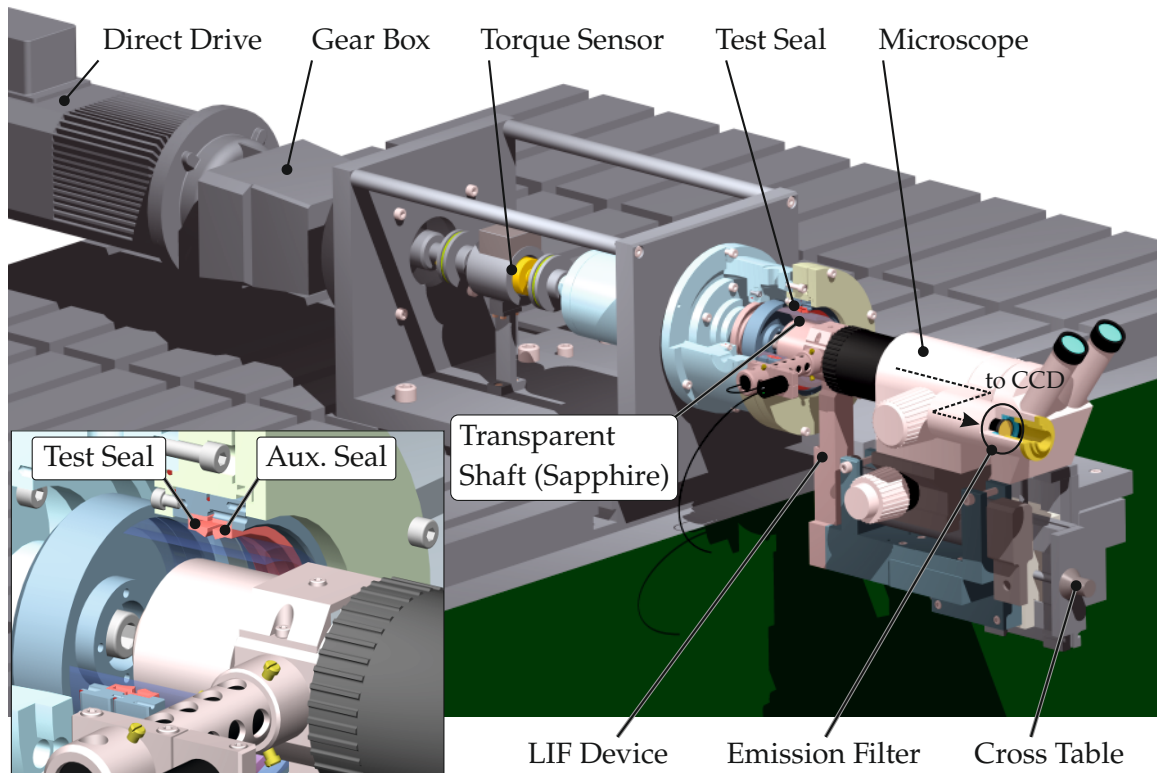
The optical test facility combines different optical methods which, as a whole, allow for comprehensive investigations into dynamic sealing contacts. The white light and fluorescence based methods applied in this work are described below.

#### 3.2.1 *Total internal reflection sealing contact visualization*

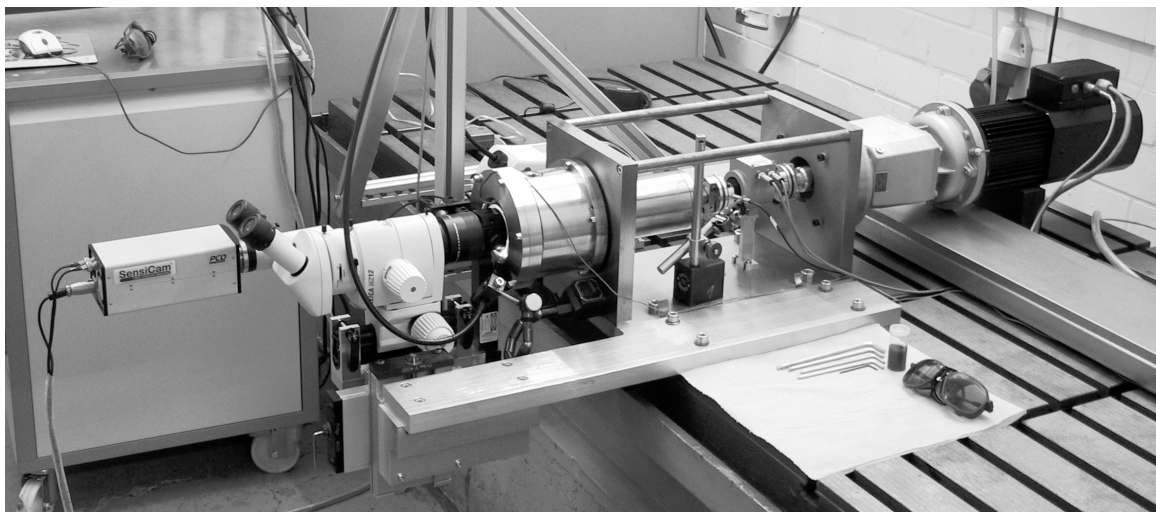
Basic observations of sealing contact regions, in particular for alignment of the region of interest, are carried out using white light of a cold light source. High contrast visualization of the sealing contact is achieved by feeding the light into the transparent hollow shaft at an oblique angle through the front side of the shaft, as shown in Figure 3.2, according to POLL ET AL. [PGBQ92].

Due to total internal reflection (TIR) at the sapphire–air interfaces, the incoming light is reflected back and forth until it reaches the actual sealing contact, similar to fiber optics or liquid light guides<sup>5</sup>. At a first glance light is reflected only by the actual rubber–sapphire contacts whereas areas without contact remain dark. Looking at the TIR method in detail though, optical coupling of the elastomer surface can occur up to a distance of few hundred nanometers, depending on the wavelength and the angle of incidence. This optical coupling is due to the propagation of an evanescent wave, the electric field intensity of which exponentially decays with perpendicular distance

<sup>5</sup> Under lubricated conditions, depending on the refraction index of sapphire and the lubricant, total internal reflection may also occur at sapphire–oil interfaces. As previously demonstrated by WENNEHORST [Weno8], this may be a useful method for qualitative investigations into lubricant film formation.



(a) Experimental set-up, conceptual illustration based on CAD model.



(b) Experimental set-up, photograph.

Figure 3.1: Experimental set-up. (a) reproduced according to WENNEHORST AND POLL [WP09c].



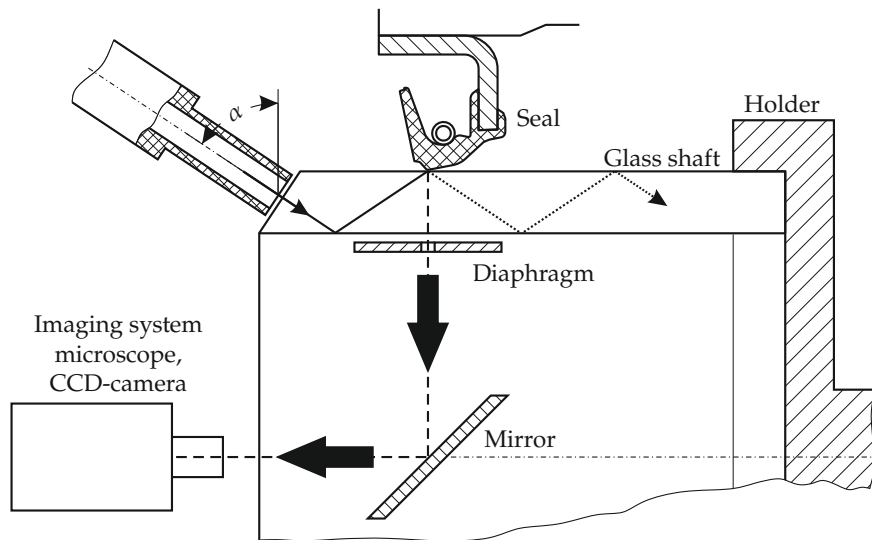


Figure 3.2: Total Internal Reflection technique according to POLL ET AL. [PGBQ92]. Reproduced with permission of Springer.

from the TIR interface. These effects could be utilized for quantitative topographical distance mapping within the sealing contact<sup>6</sup>; the experimental implementation of such a measuring principle, however, is challenging. When used qualitatively, the TIR method allows for high-contrast visualization of the actual contact pattern especially under dry conditions, which is particularly useful for the determination of the seal contact width and the assessment of the wear condition. Considering the multi-scale nature of surface roughness, the different reflectance light intensity levels can be directly associated with the local contact pressure distribution resulting from the elastomer contact topography.

### 3.2.2 Laser Induced Fluorescence

For investigations into the lubricant distribution within sealing contacts and quantitative lubricant film thickness measurements, respectively, the Laser Induced Fluorescence method (LIF) is applied, as illustrated in Figure 3.3. A fluorescent dye dissolved in the lubricant emits fluorescence radiation during excitation by light with appropriate wavelength. Due to Stoke's shift, the maximum fluorescence emission is shifted towards longer wavelengths, so that fluorescence can be selectively captured by means of suitable optical filters, fluorescence intensity thereby being a direct measure for lubricant film thickness. The short recombination time of the optically excited dye molecules, which is of the order of nanoseconds, allows for the investigation of highly dynamic processes.

<sup>6</sup> See, e.g., HARRICK [Har62].

### 3.2.2.1 Fundamentals of fluorescence

Fluorescence is a type of photoluminescence, i. e., emission of light that is not resulting from heat but from absorption of photons. As detailed, e. g., by GUILBAULT [Gui90], light, a form of electromagnetic radiation the propagation of which is regarded as a wave phenomenon, is characterized by a wavelength  $\lambda$  and a frequency  $\nu$  interrelated by

$$\nu = \frac{c_0}{\lambda} \quad (3.1)$$

where  $c_0 = 3 \times 10^8$  m/s is the velocity of light.

Upon striking matter, light can either pass through with no absorption occurring, or it can be absorbed by matter, either entirely or in part. In the latter case energy is transferred to the molecule in the absorption process. Absorption of energy must occur in integral units, called quanta or photons. The quanta–energy relationship can be expressed by the equation

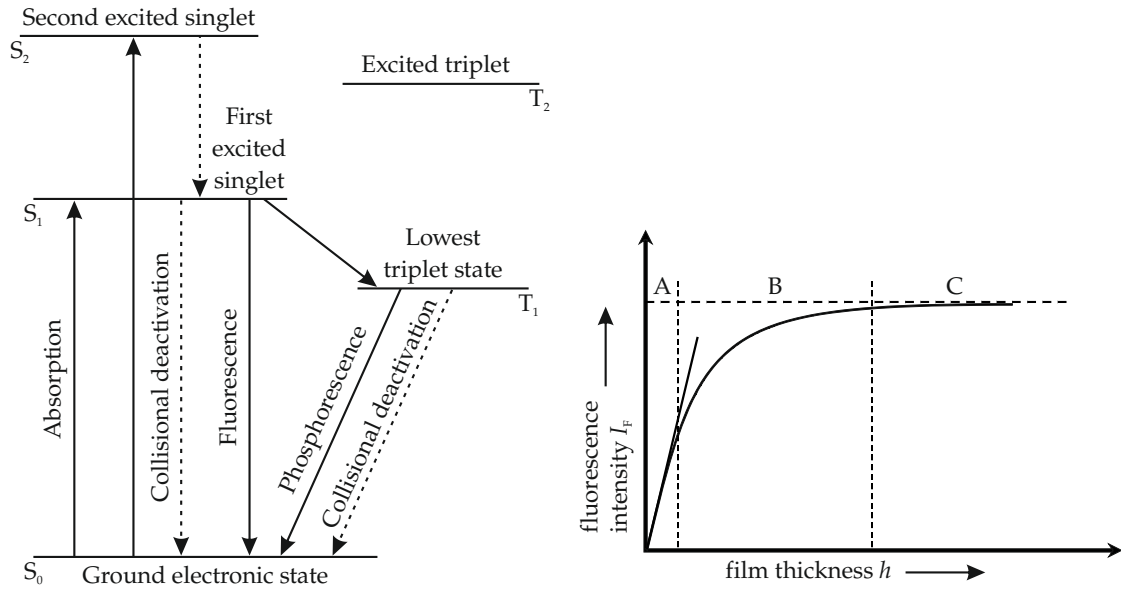
$$E = h\nu = \frac{hc_0}{\lambda} \quad (3.2)$$

where  $E$  is energy and  $h = 6.626 \times 10^{-34}$  J s is Planck's constant.

Every molecule possesses a series of closely spaced energy levels and can go from a lower to a higher energy level by the absorption of a discrete quantum of light, equal in energy to the difference between the two energy states (see Figure 3.3a). Only a few molecules interact with light and are raised to this higher excited state, thus being able to exhibit luminescence.

When a quantum of light impinges on such a molecule, it is absorbed in about  $10^{-15}$  s, and a transition to a higher electronic state takes place (see Figure 3.3a). This absorption of radiation is highly specific, and radiation of a particular energy is absorbed only by a characteristic structure. The electron is raised to an upper excited singlet ( $S_1$ ,  $S_2$ , etc.) via ground-to-singlet state transitions, which are responsible for the visible and ultraviolet absorption spectra observed for molecules. Absorption transitions usually originate in the lowest vibrational level of the ground electronic state ( $S_0$ ).

During the very short time the molecule can spend in the excited state (typically  $1 \times 10^{-9}$  s to  $10 \times 10^{-9}$  s, see also HIDROVO AND HART [HH02]), some energy in excess of the lowest vibrational energy level is rapidly dissipated. The lowest vibrational level of the excited singlet state,  $S_1$ , is attained. If all the excess energy is not further dissipated by collisions with other molecules (collisional deactivation, or “quenching”), the electron returns to the ground electronic state  $S_0$ , with the emission of energy. This phenomenon is called fluorescence. Because some energy is lost in the brief period before emission can occur, the emitted energy (fluorescence) is of longer wavelength than



(a) Schematic energy level (Jablonski) diagram for a diatomic molecule. (b) Fluorescence intensity vs. film thickness.

Figure 3.3: Illustration of LIF measuring principle. (a) reproduced from GUILBAULT [Gui90] with permission of M. DEKKER, via Copyright Clearance Center; (b) reproduced from WENNEHORST AND POLL [WP09c].

the energy that was absorbed. This difference in energy is called the Stoke's shift and it allows separation of the excitation light from the fluorescent emission. The ratio of the number of molecules returning to the ground state by fluorescent emission over the total number of fluorophore molecules excited is termed the fluorescence quantum yield [HH02].

The phenomenon of phosphorescence involves an intersystem crossing, or transition, from the singlet to the triplet state (see Figure 3.3a). Transition times of  $10^{-4}$  s to 10 s are observed in phosphorescence, so a characteristic feature is an afterglow, i. e., emission continues even after the exciting radiation is removed. Because of the relatively long lifetime of the triplet state, molecules in this state are much more susceptible to radiationless deactivation processes, and only substances dissolved in a rigid medium phosphoresce [Gui90].

### 3.2.2.2 Fluorescence-based measurement of lubricant film thickness

When a rectangular differential volume element of fluid mixed with a fluorescent dye with cross-sectional area  $A$  and thickness  $dx$  is irradiated by light (normal to the area  $A$ ) with uniform intensity  $I_{ex}$ , the

total fluorescence,  $P_{\text{fluo}}$ , emitted by this differential volume is given by [HH01, HH02]

$$P_{\text{fluo}} = I_{\text{ex}}\epsilon(\lambda_{\text{ex}})c\Phi A dx . \quad (3.3)$$

Fluorescence is, therefore, dependent on:

1. the excitation light intensity  $I_{\text{ex}}$ , i. e., the amount of light available to produce molecular transitions to higher, excited levels;
2. the molar absorption coefficient  $\epsilon(\lambda_{\text{ex}})$ , which determines how much of the incident light per molecule produces actual molecular transitions;
3. the dye concentration  $c$ , which is a measure of the number of dye molecules present;
4. the quantum efficiency  $\Phi$ , which is the ratio of the energy emitted by the energy absorbed, and is a measure of how much of the energy stored in the higher electronic states is emitted as fluorescent light, when the molecules return to their ground state; and,
5. the volume  $A dx$  of the element, which is the control volume over which excitation and fluorescence takes place.

Since the thickness of the differential volume element is infinitesimally small, dividing equation (3.3) by the area  $A$ , the fluorescence intensity normal to the area  $A$  is obtained. If, according to HIDROVO AND HART [HH01, HH02], the area  $A$  is assumed to be the projected area of a single pixel, the intensity  $I_{\text{fluo}}$  collected by a CCD pixel from this differential fluorescent element is given by

$$I_{\text{fluo}} = I_{\text{ex}}\zeta\epsilon(\lambda_{\text{ex}})c\Phi dx \quad (3.4)$$

where  $\zeta$  is the “monitoring efficiency” of the imaging system, accounting for the fact that in reality, since the fluorescent light is pointed in all directions, only a fraction of the total fluorescence emitted by a differential volume element is collected by the CCD detector. The “monitoring efficiency” is a function of the size of the aperture of the collecting system and the distance from the emission location to the aperture. If the thickness and sample half-width over which fluorescence takes place are much smaller than the distance from the fluorescent sample to the collecting system aperture, the “monitoring efficiency” is approximately a constant (between 0 and 1) over the entire thickness of the sample. Both of the previous conditions are achieved with the use of a long working distance lens.

According to equation (3.4), pixel intensity is proportional to the excitation intensity, monitoring efficiency, dye characteristics, dye concentration, and thickness of the fluid element. This representation is accurate only for infinitesimally thin fluid films. A more general and accurate description of the fluorescence response can be obtained from Beer–Lambert’s Law of Absorption<sup>7</sup>, which accounts for the absorption of the excitation light by the finite fluid through which it travels:

$$I_{\text{ex}}(x) = I_0 e^{-\epsilon(\lambda_{\text{ex}})cx} . \quad (3.5)$$

Here,  $I_0$  is the excitation light intensity at  $x = 0$  (i. e., incident light intensity).

When considering a differential element within a region of finite film thickness, the fluorescence intensity collected by the CCD from this fluid element is

$$dI_{\text{fluo}} = I_{\text{ex}} \xi \epsilon(\lambda_{\text{ex}}) c \Phi dx . \quad (3.6)$$

Thus, from equations (3.5) and (3.6):

$$dI_{\text{fluo}} = I_0 e^{-\epsilon(\lambda_{\text{ex}})cx} \xi \epsilon(\lambda_{\text{ex}}) c \Phi dx . \quad (3.7)$$

For a given fluid film thickness,  $h$ , the total intensity collected by the CCD is

$$I_{\text{fluo}}(h) = \int_0^h dI_{\text{fluo}} = \int_0^h I_0 e^{-\epsilon(\lambda_{\text{ex}})cx} \xi \epsilon(\lambda_{\text{ex}}) c \Phi dx \quad (3.8)$$

such that (see also Figure 3.3b)

$$I_{\text{fluo}}(h) = I_0 \xi \Phi \left\{ 1 - e^{-\epsilon(\lambda_{\text{ex}})ch} \right\} . \quad (3.9)$$

For small values of  $h$  (thin films), equation (3.9) can be approximated as

$$I_{\text{fluo}}(h) \approx I_0 \xi \epsilon(\lambda_{\text{ex}}) c \Phi h . \quad (3.10)$$

This is identical to equation (3.4) and is the basis for the concepts of optically thin and optically thick systems. The fluorescence’s dependence on film thickness is quasi-linear for optically thin systems, while it is exponential for optically thick systems. What is considered a thin or thick film thickness depends on the product  $\epsilon(\lambda_{\text{ex}})c$  [HHo1, HHo2].

According to POLL ET AL. [PGBQ92], the fluid film can be separated into three sectors (see Figure 3.3b):

<sup>7</sup> See also SMART AND FORD [SF74], and POLL ET AL. [PGBQ92].

SECTOR A In sector A, within the film thickness, almost all the fluorescent particles are excited, and the incident light intensity is more than can be absorbed and transformed into fluorescence. The emitted fluorescent light intensity should then mainly depend on the amount  $n$  of fluorescent particles:

$$I_{\text{fluo}} = f(n) ,$$

and thus on the film thickness and the dye concentration.

SECTOR B In sector B, transient region, the film thickness increases to a point where, depending on the incident light intensity, there is not enough light left in some parts of the film to excite all particles. Here, the slope of the fluorescent intensity curve decreases: the fluorescent intensity is now not only a function of the number of fluorescent particles but also of the intensity of the incident light:

$$I_{\text{fluo}} = f(I_0, n) .$$

SECTOR C In sector C, practically all the incident light is used for fluorescent emission or transformed into heat in a distance shorter than the total film thickness. Particles in the film outside this zone will not be excited any more. The fluorescent intensity should now mainly be a function of the incident light intensity:

$$I_{\text{fluo}} = f(I_0) .$$

In practice, according to POLL ET AL. [PGBQ92], there is a considerable influence of the fluorescent dye concentration as well, although less strong as in sector A and B. A possible explanation is that for a given incident light intensity the average travelling distance of the incident as well as the fluorescent radiation will decrease with fluorescent particle concentration. That way, it becomes less probable that light is lost by absorption and transformation into other forms of energy rather than fluorescence.

At very high particle concentrations re-absorption will have an adverse effect: a part of the fluorescent radiation may then strike other fluorescent particles, thereby being transformed into radiation of longer wavelengths (e. g., heat). These particles are then no longer available for fluorescence. Two conclusions of the above findings are [PGBQ92]:

- for very thin films such as the ones investigated here, the intensity of the incoming light is of minor importance;
- an improvement of accuracy and resolution of a film thickness measurement in this range can only be achieved by optimizing the fluorescent dye concentration and the excitation wavelength.

As a first step in the implementation of the fluorescence method, a fluorescent dye must be selected which is highly soluble in the lubricant. Then, for a given exposure time of the CCD sensor, the dye concentration is gradually increased from a very low value until the quasi-linear section of the calibration curve (“sector A” in Figure 3.3b) coincides with the expected film thickness range, thus yielding optimum sensitivity for this specific film thickness range. At lower dye concentrations, the quasi-linear section of the calibration curve extends to beyond the expected film thickness range, and sensitivity will be lower within the expected film thickness range. At higher dye concentrations, sensitivity will be further improved, but the quasi-linear section of the calibration curve will cover only part of the expected film thickness range. Generally, the dye concentration should be kept as low as possible so as to avoid alteration of the lubricant characteristics.

### 3.2.2.3 LIF implementation

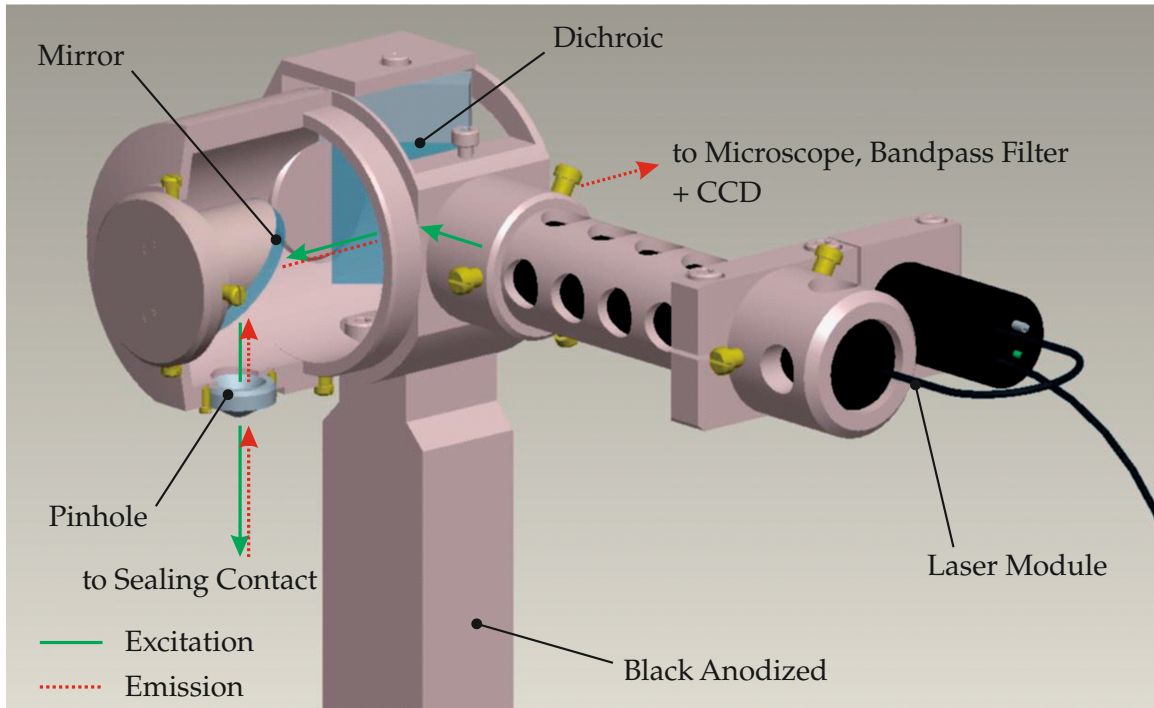
For LIF<sup>8</sup> lubricant film thickness measurements, as shown in Figure 3.4, the light of a stabilized green emitting DPSS<sup>9</sup> laser module<sup>10</sup> (STOCKERYALE LASIRIS,  $\lambda = 532$  nm, 5 mW diode power) is coupled into the optical axis via a tilted dichroic mirror. Radial redirection of the optical path is achieved by means of another tilted mirror, thus allowing for exact vertical illumination and observation of the sealing contact. For fluorescent labeling, the dye *Fluorescent Yellow 131SC* is dissolved in the oil at a concentration of  $c = 690$  ppm.<sup>11</sup> Optical filtering of the fluorescence response is achieved by means of the dichroic and an additional narrow band pass filter (SEMROCK BRIGHT-LINE, 585 nm center wavelength, 40 nm bandwidth) mounted within the camera tube in front of the CCD sensor. The focus of the laser module (Gaussian beam profile) had been adjusted in preliminary experiments to yield a minimum excitation light intensity gradient within the region of interest.

<sup>8</sup> In this work, a laser was preferred over filtered light from incandescent lamps or vapor discharge lamps. This decision was mainly based on the fact that the use of a compact laser module appreciably simplified the optical setup that had to be custom made.

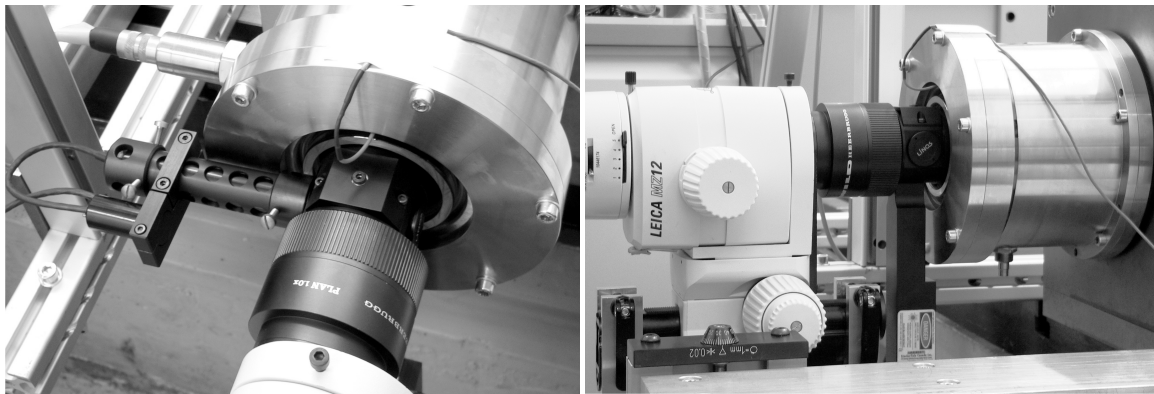
<sup>9</sup> DPSS Diode Pumped Solid State

<sup>10</sup> The laser generates output power stabilized by an internal photodiode. A green emitting laser was chosen to reduce photobleaching, i. e., the decay of the fluorescence intensity observed under prolonged irradiation of the same fluid film region. Photobleaching results from photodegradation of fluorophore molecules, and, therefore, depends on the energy, i. e., the wavelength, of the fluorescence excitation light. According to FORD AND FOORD [FF78], photobleaching is most pronounced when using ultraviolet excitation light, and can be appreciably reduced by using excitation light of longer wavelengths.

<sup>11</sup> As confirmed by external oil analysis (OELCHECK, Brannenburg, Germany), at this concentration the addition of the dye had no measurable impact on the oil viscosity.



(a) LIF device, conceptual illustration based on CAD model.



(b) LIF device, photograph.

Figure 3.4: Newly developed LIF device. (a) reproduced from WENNEHORST AND POLL [WP09c].



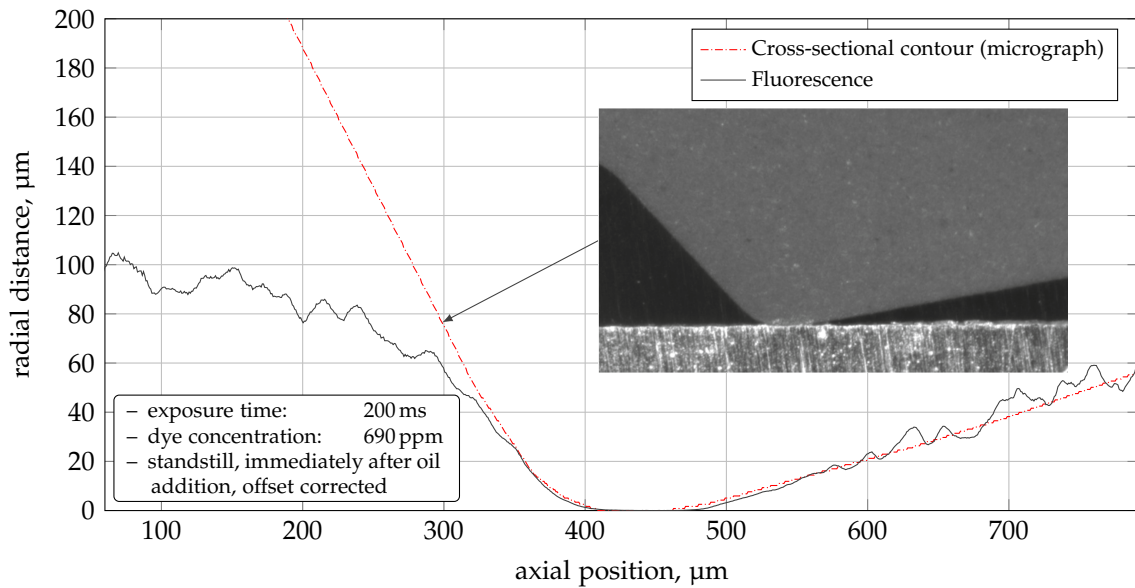


Figure 3.5: *In situ* LIF calibration approach. Reproduced from WENNEHORST AND POLL [WP09c].

For *in situ* calibration, the fluorescence intensity measured with a new seal under the conditions given in Figure 3.5 is aligned to the contour data derived from corresponding cross-sectional micrographs<sup>12</sup>. These cross-sectional micrographs (epoxy mold) were captured using the same imaging system and magnification. Fluorescence intensity values are thus converted to lubricant film thickness. The method is very similar to *in situ* or “dynamic” LIF calibration techniques being well-established in internal combustion engine research focusing on the piston ring–cylinder liner contact<sup>13</sup>.

Throughout all experiments, for each measuring point (i. e., rotational speed, including calibration during standstill) 10 successive images are captured. During shaft rotation, the image acquisition is triggered to capture exactly the same circumferential shaft position. For time-resolved measurements however successive images are acquired at frame rate (approximately 5 Hz, corresponding to 0.2 s exposure time). The fluorescence images are evaluated using MATLAB. In order to derive average film thickness profiles, in a first step the complete image series is averaged (time series). From the resulting average fluorescence image the average film thickness profile is then derived by further averaging over 10 image columns (spatial averaging in circumferential direction) and scaling with the calibration

<sup>12</sup> Several cross-sectional micrographs were produced, the variation in the seal lip contact angles proving to be negligible. Since the macroscopic seal lip contour was not measurably affected by the run-in processes occurring during the 50-hour FE8 tests (see WENNEHORST [Weno8]), the same calibration scale factor was also applied to the run-in test seals.

<sup>13</sup> See, e. g., HOULT ET AL. [HLWB88], WONG AND HOULT [WH91], SHAW ET AL. [SIHW92], TAKIGUCHI ET AL. [TNFY98], and WEIMAR AND SPICHER [WS03].

factor. The resulting film thickness profiles thus represent axial cross-sections of the (spatio-temporal) average lubricant volume within the sealing contact. Furthermore, single image columns are evaluated for each frame (one per shaft revolution) in order to provide non-averaged (i. e., “raw”) film thickness profiles. Offsets at nominal film thickness *zero* result from different superimposed effects, the most important of which are:

- the constant offset of the CCD camera<sup>14</sup>,
- reflected excitation light (negligible in case of appropriate optical filtering),
- auto-fluorescence of the seal elastomer within the fluorophore’s emission band (due to pigments or fillers),
- auto-fluorescence of lubricant residues within the elastomer surface (e. g., originating from run-in),
- slanting fluorescence originating from the oil bulk in the immediate vicinity of the sealing contact (systematically inherent due to the finite working distance of the microscope).

In order to compensate for such effects, causing a “wrong” lubricant film equivalent within the sealing contact, the complete static “calibration profile” (captured during standstill immediately after the addition of lubricant) is used for offset correction of the film thickness profiles obtained under dynamic conditions. Since the fluorescence intensity decreases with increasing temperature<sup>15</sup>, which leads to an apparent reduction of the seal lip contact angles, the static “calibration profile” can also be used to control for heating effects.

The calibration described above yields a nominal film thickness resolution of approximately 40 nm/GV. In reality, however, the minimum film thickness that can be resolved will be determined by the noise characteristics of the CCD camera. The total dark signal of the camera, measured when the aperture of the cooled camera is closed, amounts to  $(55.20 \pm 1.94)$  GV ( $M \pm SD$ ); here, the standard deviation, as a measure of the noise level, yields a film thickness equivalent of roughly 80 nm. When averaging 10 frames, the noise level is reduced to approximately 0.61 GV. Consequently, the achievable lower limit of measurements can be estimated to be in the range of 25 nm to 80 nm.

---

<sup>14</sup> CCD dark current noise can be minimized by maintaining a low detector temperature. Then, the total CCD dark signal noise is dominated by the CCD readout noise, i. e., the sum of electronic effects. Therefore, a default offset is additionally used in this CCD camera, allowing the statistical characteristics of the total CCD dark signal noise to be accurately assessed (i. e., the entire distribution of gray values (GV) both above and below the resulting total offset, without any truncations).

<sup>15</sup> See, e. g., SATO ET AL. [STNYoob].

## 3.3 TEST SEAL CHARACTERISTICS

The seals used in this work are plain radial lip seals made of a fluorocarbon compound (FKM) with a mineral filler. Here, the term “plain” refers to the most basic seal lip design involving only the reverse pumping effect originating from within the sealing contact zone. This means that there are no additional macroscopic surface structures next to the seal lip hydrodynamically augmenting the “natural” reverse pumping effect<sup>16</sup>. The seal type, the design of which is shown in Figure 3.6, has been studied and characterized extensively in previous investigations (see WENNEHORST [Weno8] and OTTINK [Ott13, Ott14]). Specifically designed as protective seals for grease lubricated rolling element bearings<sup>17</sup> (e.g., automotive hub units), the radial force<sup>18</sup> ( $F_r = (55.5 \pm 6.4) \text{ N/m } (M \pm SD), n = 10$ ) is roughly 50 % lower compared to standard oil seals<sup>19</sup>. This radial force reduction, on the one hand, is necessary in order to prevent the seals from being thermally damaged due to the poor thermal conductivity of the lubricating grease. On the other hand, due to the precise true-running of the bearing inner rings, the radial force of protective seals may be safely reduced without compromising the followability of the seal lip, and too high a radial force would unnecessarily increase the frictional losses. In the real application, the seals are used in a cassette type assembly utilizing a flinger element with an L-shaped cross-section as a counterface for the seal lip. When installed with a slight axial interference, a secondary sealing contact is thus established between the axially extended seal lip and the flinger that protects the main radial sealing contact from external contaminants. The lubrication of this auxiliary sealing contact is ensured by providing a grease reservoir between the two sealing contacts. It is worth noting that, in contrast to standard oil seals, the protective seals are

<sup>16</sup> See, e.g., SATO ET AL. [STON99], LIMING [Lim01], GORRINO ET AL. [GAC07], WEN ET AL. [WYHC11], and WEN ET AL. [WYTT11].

<sup>17</sup> The service life of rolling element bearings, besides the regime of lubrication, depends strongly on the cleanliness level of the lubricant (see, e.g., GABELLI ET AL. [GMEI08]). Depending on the application, the source of liquid and particulate contaminants may be external to the system (e.g., water, sand, or dust entering into an automotive hub unit), or the contaminants are generated within the system itself (e.g., hard wear debris from gears carried in the oil). As previously demonstrated by GABELLI ET AL. [GIM96], if lip-type protective seals are used in order to prevent hard particulate contaminants from entering into the elastohydrodynamic rolling contacts, the bearing life can be drastically increased. For a review of the impact of lubricant contaminations on the life performance and the operating characteristics of rolling element bearings, including the wear and fatigue related damage mechanisms, the reader may refer, e.g., to WENNEHORST AND POLL [WP07], or, OTTINK [Ott14].

<sup>18</sup> The seal radial force was measured at room temperature (see WENNEHORST [Weno8]) using the radial force measuring device according to DIN 3761 PART 9 [DIN3761-9] as detailed in DEBLER [Deb05] and ENGELKE [Eng11]. The results were later confirmed by OTTINK [Ott13, Ott14] who additionally conducted thermally controlled measurements demonstrating the temperature dependence of the seal radial force.

<sup>19</sup> See, e.g., JOHNSTON [Joh99].

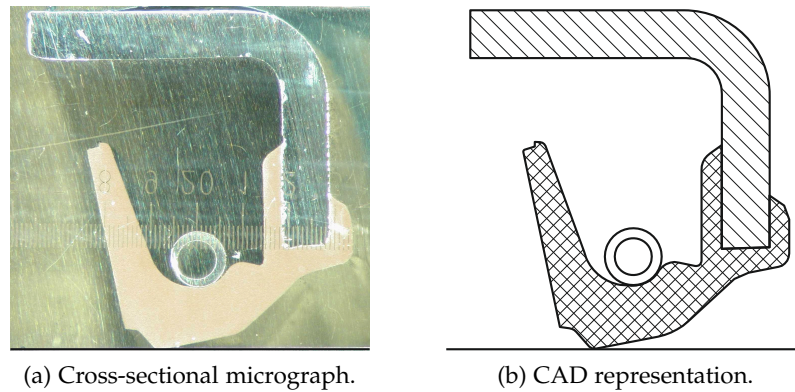


Figure 3.6: Test seal design; reproduced from WENNEHORST [Weno8].

installed conversely, i. e., such that the outward pumping of small amounts of base oil aids in preventing contaminants from entering into the sealing contact. During rotation, the flinger element acts as a dirt slinger, providing further protection against contamination from the surroundings. Corresponding to the previous investigations, only the radial main sealing contact (nominal diameter  $d = 82$  mm) is considered in this work.

Two pairs of nominally equal seals (the test seal and an auxiliary seal, see Section 3.1) are used in the experiments. All four seals originate from a research project on protective seals for rolling element bearings that was previously conducted by the author (see WENNEHORST [Weno8]). The first two seals are virtually new; they were run on the lubricated sapphire shaft only at low sliding speeds and only for a short time during the preparation of the measurements. Based on experience [CR92], it can be assumed that the thin molded skin at the seal lip is already broken, and that the filler particles and particle agglomerates closest to the surface are already worn away. Within the sealing contact region of the test seal, the root mean square roughness of the seal lip (measured with non-contacting optical profilometry as detailed in Section 6.2) amounts to  $4.37 \mu\text{m}$  ( $S_q$ ). In the following, this seal will be referred to as “short-term run seal”. The second pair of seals was used as protective seals in a completely sealed full-scale ball bearing that was subjected to rotational speed and temperature ramps on a modified FE8 test rig. In these experiments, grease (FUCHS *Renolit LX-OS3*) was used as lubricant, and the surrounding medium was air. The sliding speeds were in the range from  $0 \text{ m s}^{-1}$  to  $5 \text{ m s}^{-1}$ , and the temperatures applied to the bearing outer ring ranged from  $-15^\circ\text{C}$  to  $80^\circ\text{C}$ . The cumulative duration of the test programs was approximately 50 h. During this short time, neither the seal radial force nor the seal lip contour was measurably altered by the run-in process. Within the sealing contact region, the root mean square roughness of the seal lip, however, was appreciably

reduced to  $0.58\ \mu\text{m}$  ( $S_q$ ). In the following, this seal will be referred to as “run-in seal”.

Since neither elastic material data nor elastomer specimens were available for the test seals, in order to characterize the elastic properties of the test seal type, a hyperelastic material model was calibrated to the measured seal radial force by means of finite element analysis (FEA) of the seal assembly process (see also WENNEHORST [Wen08] for a similar approach). The elastomer material model was based on the Mooney-Rivlin strain energy function, which is the most widely used constitutive relationship for the non-linear stress analysis of elastomers (see, e. g., FINNEY [Fin01]). For the special case of uni-axial tension of a Mooney-Rivlin material, the stress–strain equation can be expressed as [Fin01]:

$$\sigma = 2(\lambda - \lambda^{-2})(C_1 + C_2(\lambda^{-1})) \quad (3.11)$$

where

$\sigma$  stress on original area, i. e., engineering stress,

$\lambda$  stretch ratio ( $1 + \Delta L/L$ ).

The initial (i. e., small-strain) shear modulus is related to the material constants by

$$G = 2(C_1 + C_2) . \quad (3.12)$$

If the material is assumed to be incompressible, then the initial tensile modulus (small-strain Young’s modulus) is given by

$$E = 6(C_1 + C_2) \quad (3.13)$$

or, for a compressible material with bulk modulus  $K$  and Poisson’s ratio  $\nu$ ,

$$E = \frac{9KG}{3K + G} = 2(1 + \nu)G . \quad (3.14)$$

As previously recommended by GABELLI ET AL. [GPP92] (see also FINNEY [Fin01]), the neo-Hookean Mooney-Rivlin material model was chosen where the second Mooney-Rivlin coefficient  $C_2$  is zero and equation (3.11) reduces to

$$\sigma = 2C_1(\lambda - \lambda^{-2}) . \quad (3.15)$$

As in [GPP92], the Poisson’s ratio of the compressible neo-Hookean Mooney-Rivlin material was set to 0.49. The simulations were conducted using the commercial FE code ABAQUS (v. 6.11, Simulia Inc.,

Providence, RI, USA). ABAQUS requires that the neo-Hookean material parameters be expressed in terms of C10 and D1. These parameters are related to the shear modulus  $G$  and the bulk modulus  $K$  by

$$C10 = \frac{G}{2}, \quad (3.16)$$

$$D1 = \frac{2}{K}. \quad (3.17)$$

When using the relation [Fino1]

$$K = \frac{E}{3(1-2\nu)}, \quad (3.18)$$

and equation (3.14), D1 can also be expressed in terms of C10, i. e., the shear modulus, and the Poisson's ratio:

$$D1 = \frac{6(1-2\nu)}{4(1+\nu)C10}. \quad (3.19)$$

In order to calibrate the neo-Hookean material model, axisymmetric simulations of the seal assembly process were conducted, which were based on the cross-sectional data (polished micrograph corresponding to Figure 3.6a) of an unmounted, i. e., stress-free, seal from which the garter spring had been removed. During this set of simulations, for the Poisson's ratio given above, the parameter C10 (and, at the same time, D1 according to equation (3.19)) was iteratively adjusted until the computed radial force contribution of the seal's elastomer body (due to bending of the seal lip and hoop stress formation) accurately agreed with the radial force measured with seals from which the garter spring had also been removed (76.6% of the radial force measured with garter spring). The steel part was considered to be rigid, and the nodes on the steel-elastomer interface were, therefore, completely constrained. The elastomer section was discretized with 20 585 4-node bilinear axisymmetric quadrilateral hybrid elements (CAX4H), with a fine mesh resolution in the bending and the contact regions. Within the seal lip contact zone, the final axial node distance in the deformed configuration amounted to approximately 2  $\mu\text{m}$ , allowing for accurate resolution of the axial seal lip contact pressure distribution. As in [GPP92], effects of tangential traction were neglected, and friction free boundary conditions were assumed for the study of the seal contact problem.

The coefficient C10 was found to be  $C10 = 0.749 \text{ MPa}$ , giving an initial (small-strain) Young's modulus  $E = 4.463 \text{ MPa}$ . The nominal uni-axial stress-strain curve of the neo-Hookean material model is shown in Figure 3.7. Here, the nominal, or, engineering, stress is

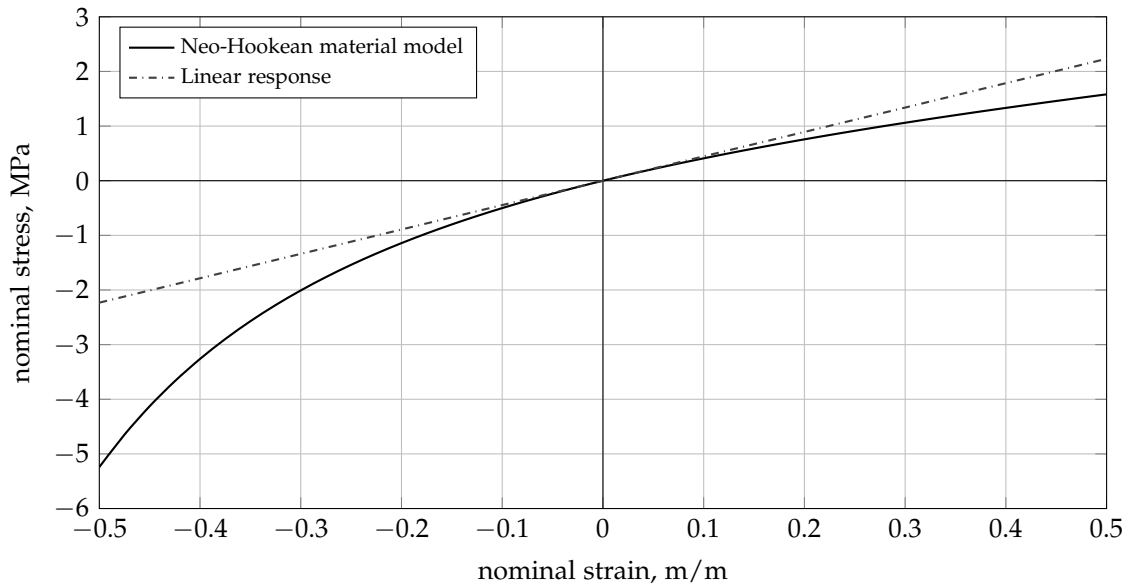


Figure 3.7: Nominal stress–strain curve of neo-Hookean material model, and linear material response based on small-strain Young’s modulus.

given as force per unit of original cross-sectional area, and the nominal strain is given as change in length per unit of original length. The stress–strain curve was generated by ABAQUS using the built-in material evaluation functionality. For comparison, the linear material response based on the small-strain Young’s modulus is also depicted.

After identification of the material parameters, the radial force contribution of the garter spring was finally imposed as a radial semi-elliptical distribution of pressure resting in the garter spring groove. Both the smooth macroscopic axial seal lip contact pressure distribution, as well as the seal lip contour are shown in Figure 3.8.

The computed seal contact width amounts to approximately  $103\ \mu\text{m}$ . Besides the seal radial force, it provides a further means to verify the material model. Indeed, as will be shown in Section 4.1, the seal contact width from the finite element analysis agrees well with the results of optical contact width measurements. As expected, the axial seal lip contact pressure distribution is asymmetric, with the contact pressure maximum being located towards the large contact angle side of the seal lip (i. e., towards the “oil side”, when considering the standard radial lip seal application). The axial seal lip contact pressure distribution, therefore, conforms to the empirical experience that in properly working elastomer radial lip seals the first moment of the seal lip contact pressure distribution is (initially) located towards the “oil side” (see NAKAMURA AND KAWAHARA [NK84], NAKAMURA ET AL. [NKK85], and NAKAMURA [Nak87]). However, it is worth noting that, as demonstrated by GABELLI ET AL. [GPP92], depending on the elastomer compound, just a few hours of running-in time may be sufficient to considerably increase the seal lip contact width, and to

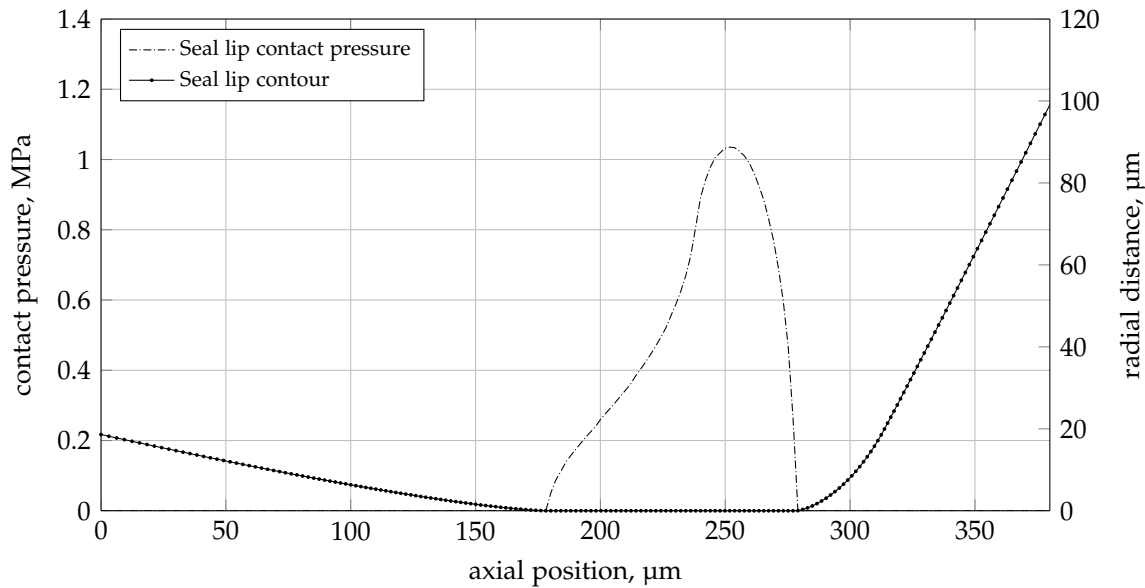


Figure 3.8: Smooth macroscopic axial contact pressure distribution and seal lip contour of a new seal, results of finite element analysis of seal assembly process (final configuration, including radial force contribution of garter spring).

change this contact pressure into an almost absolutely flat and symmetric distribution with a modest ridge located at each edge of the contact area<sup>20</sup>. Moreover, it should be remembered that the computed seal lip contact pressure distribution shown in Figure 3.8 is based on the smooth macroscopic seal lip contour. As recently demonstrated by WENK ET AL. [WSLW16], when including the measured seal lip surface roughness in three-dimensional finite element simulations of the seal assembly process, the pressure distribution within the sealing contact will be appreciably more complex.

### 3.4 CHARACTERISTICS OF THE LUBRICATING OIL

The lubricating oil used in this work is a pure mineral base oil without any additives<sup>21</sup>. The physical properties of the lubricant (kinematic reference viscosity at 40 °C and 100 °C, respectively, and lubricant

<sup>20</sup> Given the observation that the reverse pumping mechanism of the seals is not lost during such a standard short-time run-in process (molded seal lips even require this initial wear in order to roughen and start pumping), the authors even go as far as questioning the validity of the hypothesis that the working principle of lip seals could be explained by exploiting an assumed asymmetric characteristic of the sealing pressure (as previously suggested, e.g., by NAKAMURA AND KAWAHARA [NK84], NAKAMURA ET AL. [NKK85], KAMMÜLLER [Kam86], NAKAMURA [Nak87], HORVE [Hor87], LINDGREN [Lin87], TØNDER AND SALANT [TS92], and SALANT [Sal92]).

<sup>21</sup> This mineral oil is the base oil of the grease (FUCHS *Renolit LX-OS3*) used in the author's previous research on protective seals for rolling element bearings [Weno8].



Table 3.1: Physical properties of the lubricating oil.

Kinematic reference viscosity at 40 °C	$\nu_{40}$	171.92	mm <sup>2</sup> /s
Kinematic reference viscosity at 100 °C	$\nu_{100}$	13.35	mm <sup>2</sup> /s
Lubricant density at 15 °C	$\rho_{15}$	902	kg/m <sup>3</sup>

density at 15 °C, determined externally by OELCHECK, Brannenburg, Germany) are shown in Table 3.1.

The kinematic viscosity  $\nu$  is defined as<sup>22</sup>

$$\nu = \frac{\text{dynamic viscosity}}{\text{density}} = \frac{\eta}{\rho}. \quad (3.20)$$

While the kinematic viscosity is routinely measured with ease and great precision and is therefore preferred for characterizing lubricants, the dynamic (or “absolute”) viscosity is required for calculating hydrodynamic and elastohydrodynamic lubrication. The functional relationship for the temperature dependence of the dynamic viscosity can be determined by combining the temperature dependence of the kinematic viscosity with that of the density. According to DIN 51563:2011-04 [DIN51563], the temperature dependence of the kinematic viscosity of mineral oils can be determined from the UBBELOHDE-WALTHER equation

$$m_\nu = \frac{\lg(\lg(\nu_1 + 0.8)) - \lg(\lg(\nu_2 + 0.8))}{\lg T_2 - \lg T_1} \quad (3.21)$$

where

$m_\nu$  slope of logarithmically plotted  
viscosity–temperature curve,

$\nu_1, \nu_2$  kinematic viscosity at test temperatures  $T_1$  and  $T_2$ ,

$T_1, T_2$  test temperatures ( $\vartheta_1 = 40$  °C and  $\vartheta_2 = 100$  °C),  
given in K.

The kinematic viscosity at temperature  $\vartheta$  is then given by

$$\nu(\vartheta) = 10^{l_\nu} - 0.8 \quad (3.22)$$

where

$$l_\nu = 10^{(m_\nu(\lg T_1 - \lg(\vartheta + 273.15)) + \lg(\lg(\nu_1 + 0.8)))}.$$

<sup>22</sup> See, e. g., HAMROCK ET AL. [HS]04], p. 88.

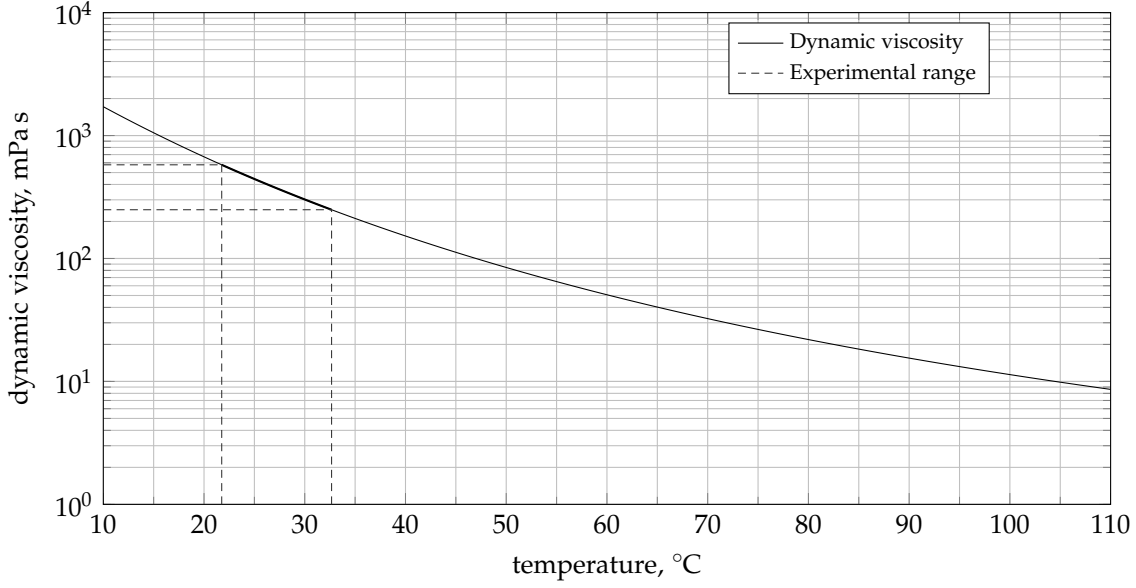


Figure 3.9: Temperature–viscosity characteristics of mineral base oil used in combined seal friction torque and lubricant film thickness measurements. Reproduced according to WENNEHORST ET AL. [WEP11].

The temperature dependence of the lubricant density (at atmospheric pressure<sup>23</sup>) can be determined according to DIN 51757:2011-01 [DIN51757] from<sup>24</sup>

$$\rho(\vartheta) = \rho_{15} - 0.605(\vartheta - 15) . \quad (3.23)$$

The dynamic viscosity as a function of temperature is shown in Figure 3.9, including the temperature and viscosity ranges encountered in this work.

Throughout this work, the lubricating oil is considered to be Newtonian with a constant dynamic viscosity [HSJ04]

$$\eta = \frac{\text{shear stress}}{\text{shear strain rate}} = \frac{f/A}{u/h} = \frac{\tau}{\dot{\gamma}} = \text{const} \quad (3.24)$$

where, assuming laminar flow in a fluid filled parallel gap (Couette flow) with a stationary bottom plane,

<sup>23</sup> In soft contacts, the operating pressures are low, and both the pressure dependence of the lubricant density, as well as the pressure dependence of the lubricant viscosity can be neglected.

<sup>24</sup> See also BARZ [Bar96].

- $f$  viscous friction force arising from intermolecular forces and internal friction as the lubricant molecules move past each other,
- $A$  area,
- $u$  sliding velocity of the upper plane,
- $h$  lubricant film thickness.

In lightly loaded contacts, when normal and shear stresses in the lubricant are low, the Newtonian model describes the behavior of many lubricating oils very well, i. e., the shear stress in the liquid increases linearly with the shear strain rate (see JACOBSON [Jac91], p. 53). However, when the surface velocity  $u$  (i. e., the shear strain rate) is increased to a certain value, the stress in the liquid reaches the limit of Newtonian behavior<sup>25</sup>, and the shear stress then increases at a declining rate<sup>26</sup>. According to BAIR [Baio7]<sup>27</sup>, the critical shear stress  $\tau_{\text{crit}}$  for the onset of non-Newtonian effects can be estimated by means of the Einstein–Debye relation for the rotational relaxation time for a molecule

$$\tau_{\text{crit}} = \frac{\rho R_g T}{MW} \quad (3.25)$$

where

- $\rho$  mass density in kg/m<sup>3</sup>,
- $R_g$  universal gas constant = 8314.34 Pa m<sup>3</sup>/(kmol K),
- $T$  lubricant temperature in K,
- $MW$  lubricant molecular weight in kg/kmol.

The mean molecular weight of petroleum oils can be estimated from the kinematic viscosity as described in ASTM standard D 2502–92 (reapproved 2004) [ASTM2502]. A more accurate estimate can be obtained using the Hirschler–Maroto equation (see MAROTO AND DE LAS NIEVES [MNo7] and MAROTO [Mar09]) which removes the interpolation errors arising from the use of the D 2502–92 (reapproved

<sup>25</sup> In typical elastohydrodynamic contacts, where the lubricated surfaces are hard, the pressure in the oil is of the order of 1 GPa. At these high pressures and under static conditions, the viscosity of lubricating oils increases by many orders of magnitude. As long as the shear stress in the oil is low, most mineral oils behave as Newtonian liquids, even at very high viscosities, but the stress level, where the oil no longer behaves as a Newtonian liquid, is reached at a much lower shear rate.

<sup>26</sup> This behavior is also known as shear-thinning. At high shear stresses, elastic shear deformation of the lubricant adds to the viscous deformation, so for the same total deformation of the lubricant the stress level will be lower. This decreases the traction compared to the case with a Newtonian oil [Jac91].

<sup>27</sup> See p. 133.

2004) ASTM viscosity–molecular weight chart. In both approaches, the mean molecular weight is calculated from kinematic viscosity measurements at 100 °F and 210 °F (37.78 °C and 98.89 °C). In the approach of MAROTO AND DE LAS NIEVES, in order to write the Hirschler–Maroto equation in a compact form, a viscosity slope factor ( $VSF$ ) is defined as [Mar09]

$$VSF = H(\nu(37.78\text{ °C})) - H(\nu(98.89\text{ °C})) \quad (3.26)$$

where  $\nu(37.78\text{ °C})$  and  $\nu(98.89\text{ °C})$  are the kinematic viscosities evaluated at 37.78 °C and 98.89 °C, respectively, and  $H(\nu)$  is a function, partially based on the Walther equation, that takes the form

$$H(\nu) = 870 \lg(\lg(\nu + 0.6)) + 154. \quad (3.27)$$

The mean molecular weight ( $MW$ ) can be expressed in terms of the previous parameters by means of the following equation

$$MW = 180 + S \times [H(\nu(37.78\text{ °C})) + 60] \quad (3.28)$$

where  $S$  is a function which depends on  $VSF$ :

$$S = 3.562 - 0.01129(VSF) - 1.857 \times 10^{-5}(VSF)^2 + 6.843 \times 10^{-8}(VSF)^3. \quad (3.29)$$

For the oil used in this work, the mean molecular weight can thus be estimated to be 487 kg/kmol. Therefore, according to equation (3.25) the critical shear stress  $\tau_{\text{crit}}$  for the onset of shear-thinning will be 4.52 MPa to 4.65 MPa for the experimental temperature range indicated in Figure 3.9.

Besides shear-thinning, shear cavitation should also be considered, which may occur due to the low operating pressures found in soft lubricated sliding contacts. According to the principal normal stress cavitation criterion introduced by WINER AND BAIR<sup>28</sup>, this departure from Newtonian constitutive behavior is predicted to occur when the lubricant is subjected to a shear stress that exceeds the pressure<sup>29</sup>.

<sup>28</sup> See BAIR [Bai07], p. 141, and KOTTKE ET AL. [KBW05].

<sup>29</sup> This phenomenon has the appearance of the limiting shear stress that has been observed in EHL traction where the shear stress averaged over the contact area becomes independent of sliding velocity and generally does not exceed some material specific fraction of the pressure averaged over the contact. The origins of these behaviors are, however, very different [Bai07].

# 4

---

## EXPERIMENTAL RESULTS

---

### 4.1 RESULTS OF TOTAL INTERNAL REFLECTION SEALING CONTACT VISUALIZATION

The results of the white light total internal reflection (TIR) sealing contact visualization are shown in Figure 4.1. The images were obtained under dry and static conditions ( $100\times$  magnification, lateral imaging resolution of  $0.85\ \mu\text{m}$  in both directions). Three-dimensional representations of these sealing contact images, obtained by three-dimensional mapping of the corresponding reflectance light intensity values<sup>1</sup>, are depicted in Figure 4.2. Moreover, in order to provide a clearer image of the elastomer contact roughness, i. e., without including the circumferential surface structure of the counterface, TIR images were also taken on a smooth part of the sapphire hollow shaft as shown in Figure 4.3.

Utilizing TIR, notable differences between the sealing contacts are found. At first, as can be seen in Figures 4.1 and 4.2, the circumferentially oriented roughness structure of the counterface is clearly reproduced within the contact patterns of both the short-term run and the run-in seal. As expected, the contact width of the run-in seal ( $b \approx 115\ \mu\text{m}$ ) is slightly larger than the contact width of the short-term run seal ( $b \approx 105\ \mu\text{m}$ )<sup>2</sup>. Furthermore, the reflectance light intensity distribution of the run-in seal is less “discrete” compared to the short-term run seal. Note that darker areas within the contact do not necessarily represent deep cavities within the elastomer surface, since the optical coupling by the evanescent wave shows exponential behavior, as described in Section 3.2. Even though the contact pattern of the run-in seal appears considerably more homogeneous, the fine circumferential surface structure of the counterface is still clearly visible. The reason for this different contact appearance is the run-in process, during which larger surface asperities are worn away and the elastomer surface topography flattens. This process leads to a sig-

---

<sup>1</sup> Here, the corresponding digital image processing, including lateral calibration of the microscopic imaging system, was carried out using the open source software *ImageJ* (Rasband, W.S., ImageJ, U.S. National Institutes of Health, Bethesda, Maryland, USA, <http://imagej.nih.gov/ij/>, 1997–2016).

<sup>2</sup> This agrees well with additional finite element analyses based on seal cross-sections and radial force data, see Section 3.3.

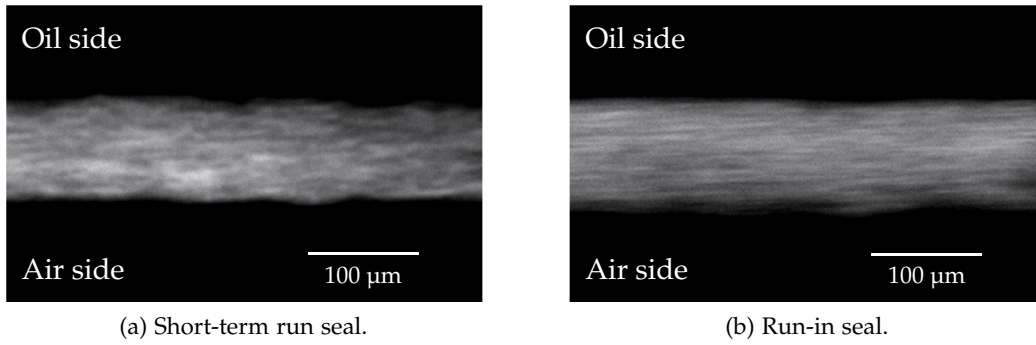


Figure 4.1: White light total internal reflection sealing contact visualization under dry, static conditions. Reproduced from WENNEHORST AND POLL [WP09c].

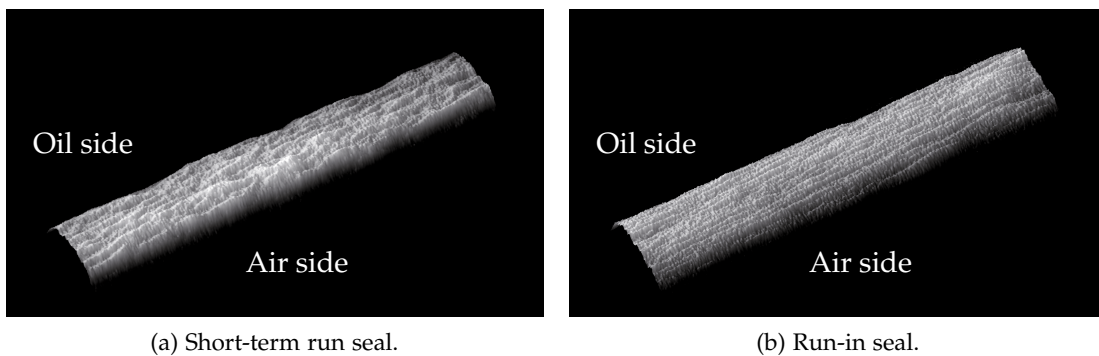


Figure 4.2: Three-dimensional representations of sealing contact images shown in Figure 4.1, obtained by three-dimensional mapping of corresponding reflectance light intensity values.

nificant increase of the actual contact area within the sealing contact. Wear structures oriented in axial direction, as originally described by KAMMÜLLER [Kam86], and, later, by STAKENBORG [Sta88b], were not observed. Depending on the seal elastomer, the radial force and the wear situation, however, such surface structures might exist on the nano scale and therefore well below the spatial resolution of the present imaging system.

## 4.2 RESULTS OF LUBRICANT FILM THICKNESS AND SEAL FRICTION TORQUE MEASUREMENTS

### 4.2.1 Results of optical lubricant film thickness measurements

With the short-term run and the run-in seals a series of experiments with stepwise change of rotational speed were conducted at low speeds ranging from  $0 \text{ min}^{-1}$  to  $100 \text{ min}^{-1}$ . At the same time as the optical lubricant film thickness measurements were conducted, the seal friction torque was determined (see Section 4.2.2). Due to the

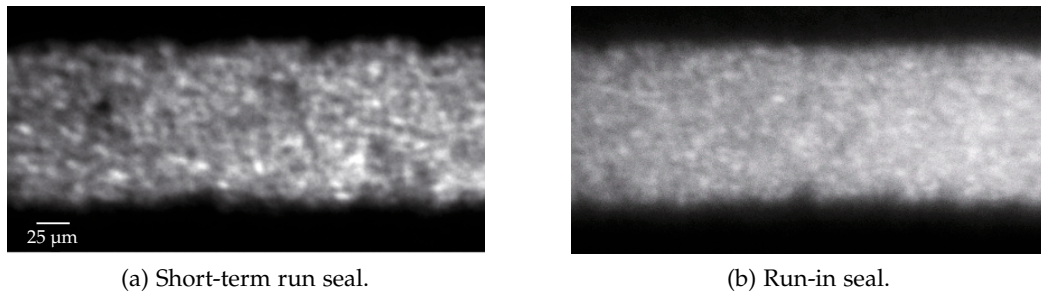


Figure 4.3: Total internal reflection sealing contact visualization on smooth part of sapphire hollow shaft under dry, static conditions.

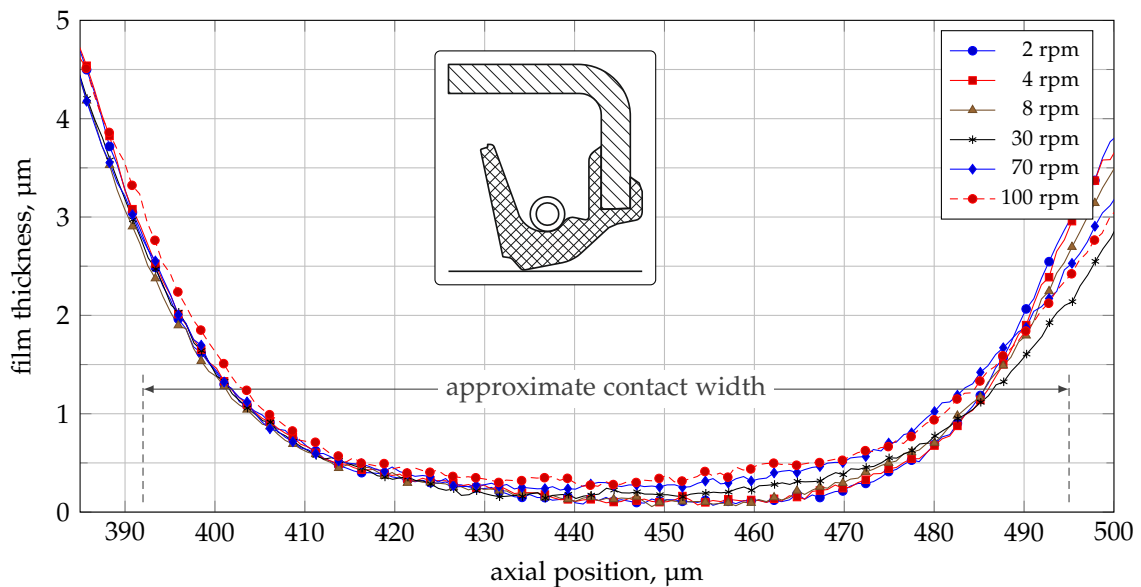


Figure 4.4: Average film thickness profiles of short-term run seal at different rotational speeds. Reproduced according to WENNEHORST AND POLL [WP09c].

low sliding velocities the rise of the oil bulk temperature was limited to only several degrees, the corresponding impact on the fluorescence signal being indiscernible.

Even though a large number of rotational speeds were evaluated, the results can be summarized using only a few speed levels. The average axial film thickness profiles of the short-term run and the run-in seal are depicted in Figures 4.4 and 4.5. Ten successive fluorescence images taken at the same angular position were used for evaluation of each speed level. Since photo bleaching was not observed under dynamic conditions, for reasons of stability and reproducibility the laser was operated continuously.

The most important result regarding the short-term run seal is the observation that the strongest speed-dependent increase of the lubricant film thickness is limited to the low contact stress area of the sealing contact (see Figure 3.8 in Section 3.3). As an explanation, viscous

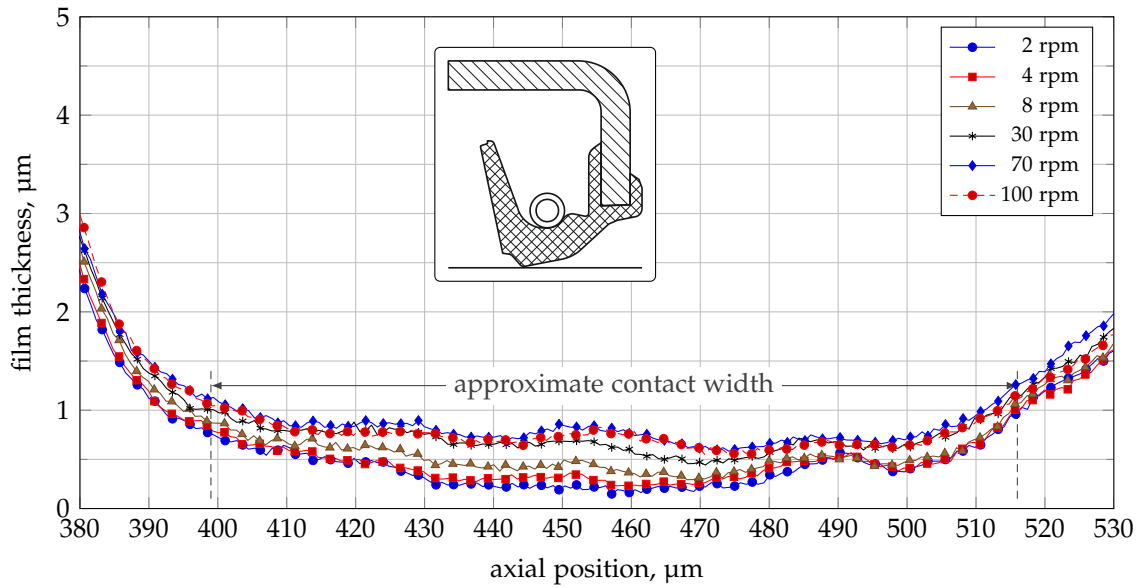


Figure 4.5: Average film thickness profiles of run-in seal at different rotational speeds. Reproduced according to WENNEHORST AND POLL [WP09c].

drag flow around elastomer surface asperities might be considered, the effect of which strongly depends on the contact topography, i. e., the local contact pressure distribution. With regard to the deformation of the elastomer surface asperities (radial as well as tangential), lubricant can be expected to be dragged into the contact much easier from the air side than from the oil side, as the contact topography is significantly “denser” in the high contact stress region. This mechanism obviously supports the reverse pumping mechanism by predominantly feeding lubricant into the sealing contact from the air side.

A completely different behavior is observed with the run-in seal. At first not only the low contact stress region, but the whole sealing contact is affected by the lubricant film build-up. Except for the lowest speeds, the lubricant films are considerably thicker compared to the short-term run seal. The most significant film thickness increase already occurs at very low speeds. Local film thickness maxima result from lubricant filled cavities within the contact (see darker areas in Figure 4.1b, and Figure 4.2b). These oil filled areas or “pockets” were oriented in circumferential direction and developed immediately after start-up. Even though noticeable temporal film thickness fluctuations were observed, these structures remained relatively constant throughout the course of the experiment.

Another important result regarding the run-in seal is the observation that — in contrast to the short-term run seal — the most pronounced film thickness increase is observed within the central region of the contact. Taking viscous drag flow into consideration as described above, another mechanism is obviously present leading to an



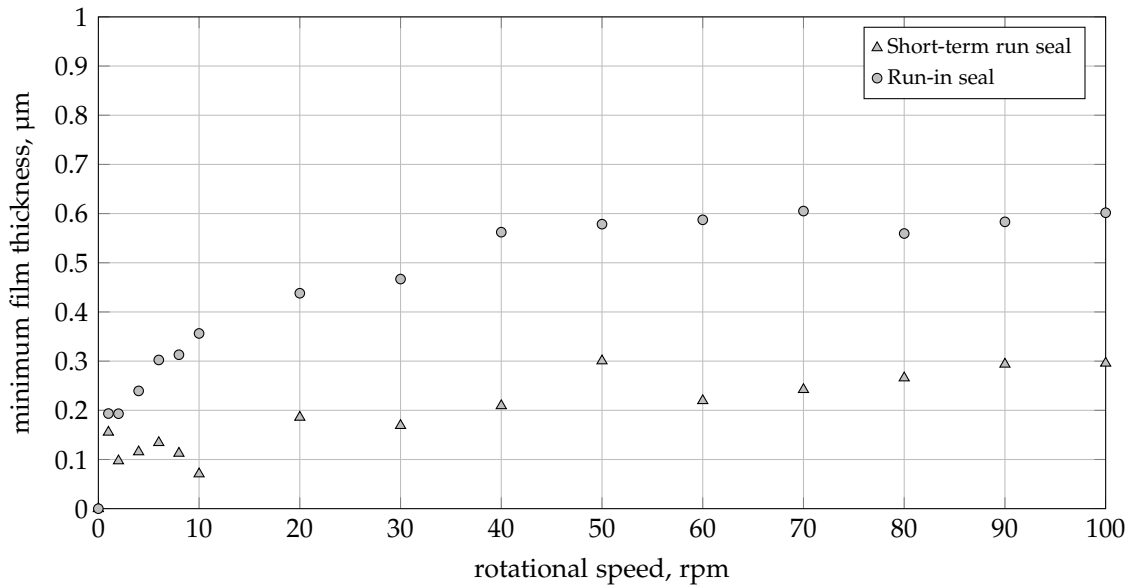


Figure 4.6: Minimum of average film thickness profiles vs. rotational speed for short-term run and run-in seal. Reproduced according to WENNEHORST AND POLL [WP09c].

improved pressure build-up capacity within the sealing contact. With the current experimental data alone this phenomenon cannot be explained. However, the formation of contact edge stresses during the run-in process, as previously proposed by GABELLI ET AL. [GPP92], and POLL [Pol00], is a reasonable approach to explain how lubricant can get entrapped within the contact path of the seal.

As a straightforward means of comparing the different lubricant film build-up capacities, the minimum film thickness values are shown in Figure 4.6. These values were derived by averaging over several film thickness values in the immediate vicinity of the absolute minimum, corresponding to an axial distance of approximately  $6\ \mu\text{m}$ .

In Figure 4.7, for each complete series of 10 fluorescence images taken at the same angular position (“triggered imaging”), the single film thickness profiles derived from the individual frames, as well as the corresponding total average film thickness profile (frame series average) are depicted. Here, negative values result from the offset correction using the average reference (i. e., calibration) profiles. Again, the enhanced lubricant film build-up of the run-in seal can be clearly observed. However, not only with the short-term run, but also with the run-in seal the speed-dependent minimum lubricant film thickness is always below the combined surface roughness of the seals and the counterface, thus indicating that the seals consistently operate under mixed lubrication conditions.

In order to obtain temporal information about the lubricant film of the run-in seal, time resolved measurements were additionally carried out utilizing the same exposure time as in the triggered image

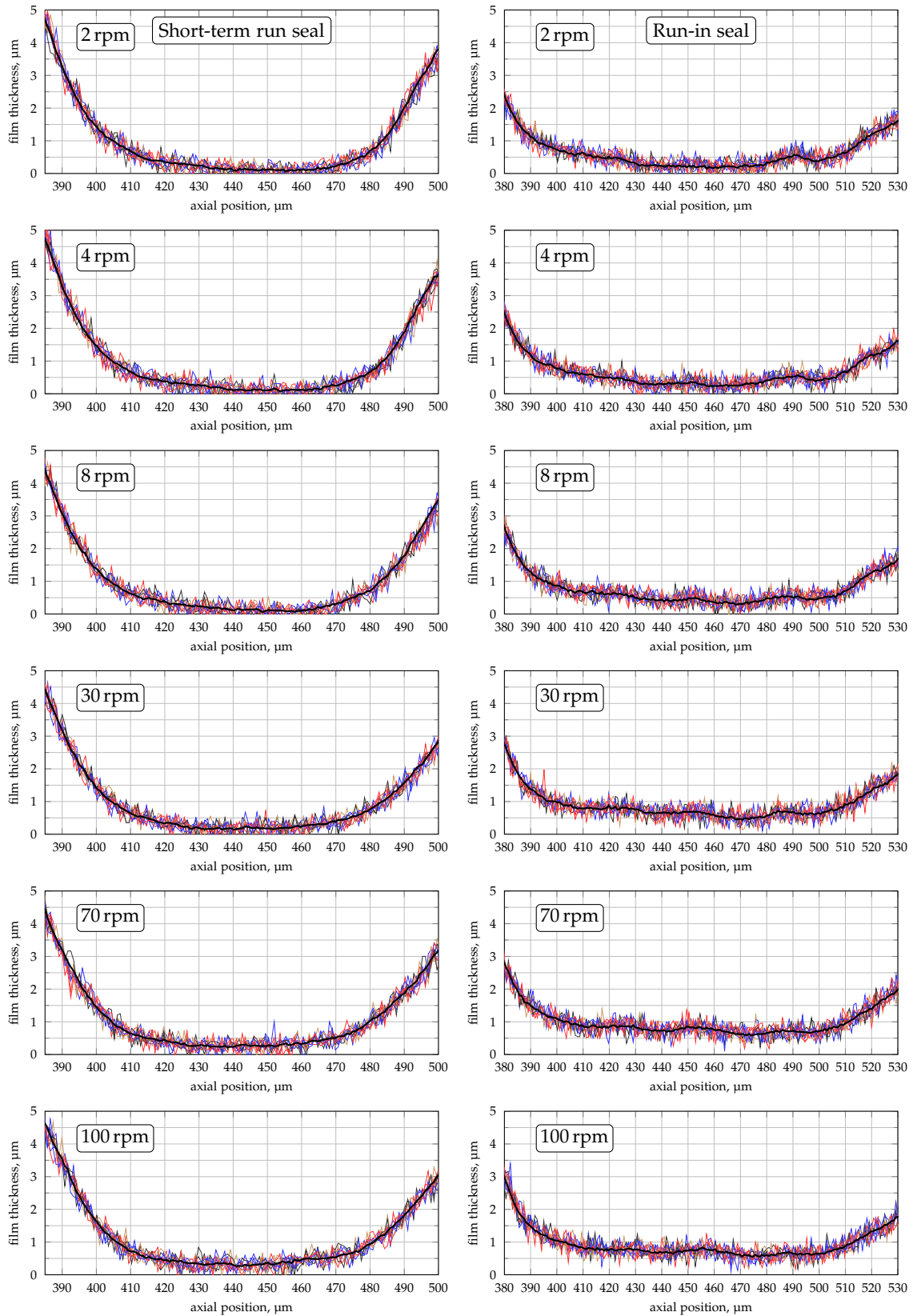


Figure 4.7: Total average film thickness profile and corresponding series of single profiles. Reproduced according to WENNEHORST AND POLL [WP09c].

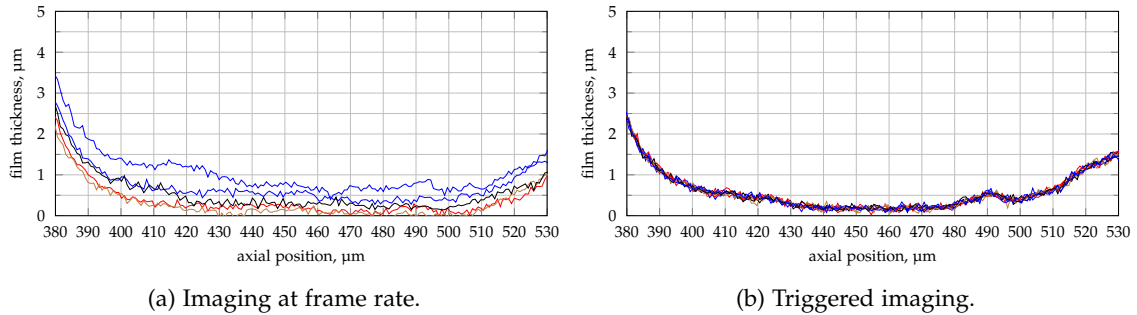


Figure 4.8: Average film thickness profiles at a rotational speed of  $1 \text{ min}^{-1}$ , obtained with imaging at frame rate and with triggered imaging, run-in seal. Reproduced according to WENNEHORST AND POLL [WP09c].

acquisition, i. e., at a frame rate of approximately 5 Hz. The evaluation of a large number of average film thickness profiles (average over 10 image lines) derived from successive single frames revealed that at the lowest speeds the sealing contact is subject to notable local lubricant film thickness fluctuations *not* affecting the contact contour as a whole. In Figure 4.8a, selected profiles are presented demonstrating the span of these spatio-temporal film thickness fluctuations observed at a rotational speed of  $1 \text{ min}^{-1}$ . In order to provide information about the film thickness variation with triggered imaging, the corresponding triggered average profiles are shown in Figure 4.8b. As described below in Section 4.2.2, at a rotational speed of approximately  $1 \text{ min}^{-1}$  (corresponding to approximately  $5 \text{ mm s}^{-1}$ ) minimum seal friction is observed and the lubricated contact changes from stick-slip to continuous sliding. Therefore, stick-slip effects at asperities, as described by VAN LEEUWEN ET AL. [LPM11], could serve as a reasonable explanation for the observed local film thickness fluctuations. As can be seen from the smaller variation in the lubricant film thickness profiles obtained with triggered imaging (Figure 4.8b), these effects might be periodically related to the angular shaft position. With increasing rotational speed, most probably due to the transition to sliding on a continuous lubricant film, the film thickness fluctuations decrease and the film thickness profiles obtained with triggered imaging, on average, approach those obtained successively at frame rate. It should, however, be noted that with increasing speed the arc captured during exposure time correspondingly increases, leading to a stronger averaging at higher speeds.

#### 4.2.2 Results of seal friction torque measurements

At the same time as the optical film thickness measurements were performed, friction torque measurements were conducted implementing a high-precision telemetric torque sensor. During the entire mea-

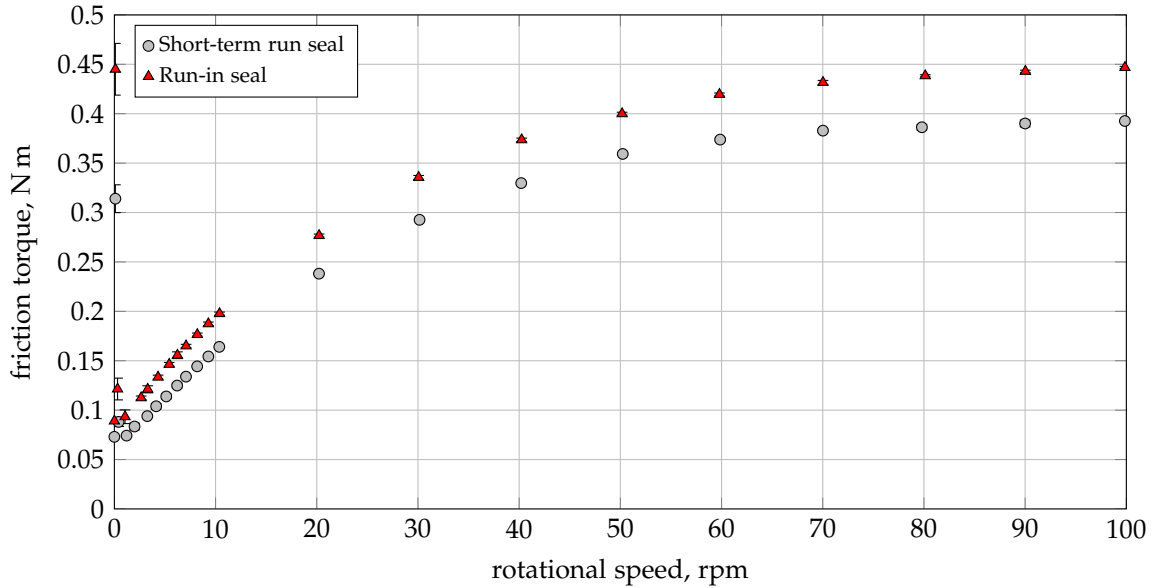


Figure 4.9: Friction torque of short-term run and run-in seal, quasi-stationary measurements with at least 5 min relaxation period at each speed level. Reproduced from WENNEHORST AND POLL [WP09c].

surement the friction losses of the low-friction test spindle (average  $T_{\text{spindle}} \approx 4 \text{ N mm}$ ) were subtracted from the measured overall friction torque. Based on the results of previous radial force measurements, the two seals can be assumed to contribute equally to the overall seal friction. The net torque values were thus divided by two in order to obtain the frictional losses of a single seal.

The results of the seal friction torque measurements are depicted in Figure 4.9. Generally, both the short-term run and the run-in seal show the same speed-dependent frictional characteristic with the overall friction torque level of the run-in seal being slightly higher compared to the short-term run seal. It should be noted that before the initial start-up, the friction torque of the unconstrained system was zero (see also Figure 5.2, p. 70). However, when reducing the speed to zero again after the experiment, a persisting torque is observed. As there is no more hydrodynamic lubricant film during standstill, this persisting torque is obviously due to friction forces between the sheared elastomer and the sapphire shaft in combination with the self-locking action of the gearbox. It can thus be interpreted as boundary friction. The friction torque of subsequent start-ups then consistently starts at this friction torque level<sup>3</sup>.

At very low sliding speeds noticeable stick-slip occurs and a pronounced friction maximum is observed (see Figure 4.10). The phenomenon is specific to rubber friction and, due to the temperature and frequency dependent complex modulus of the elastomer, origi-

<sup>3</sup> The same frictional characteristics were previously described by POLL [Pol00].

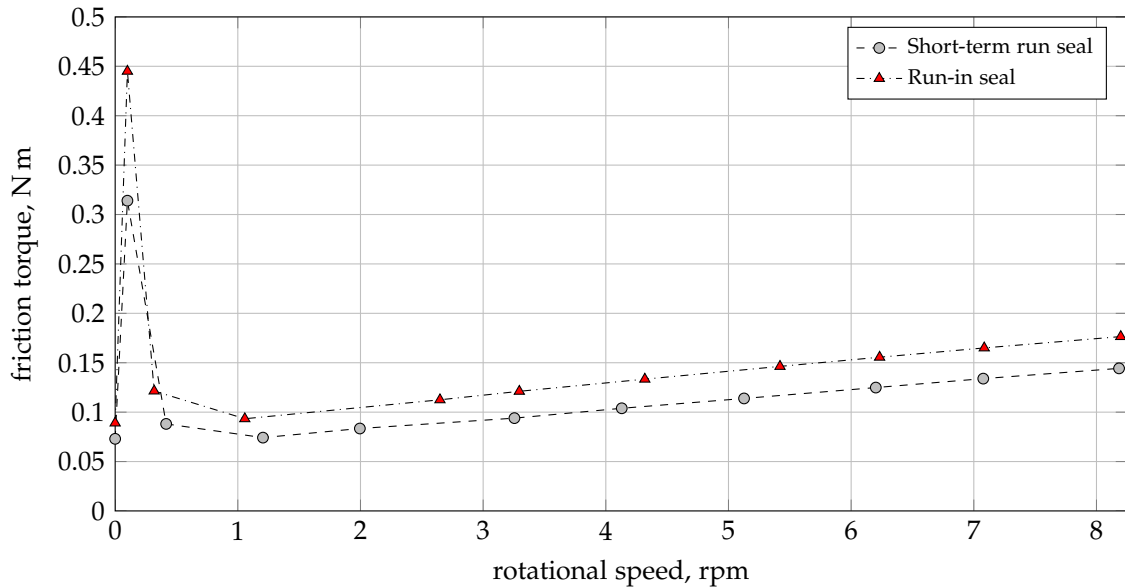


Figure 4.10: Friction torque of short-term run and run-in seal, close-up at low rotational speeds. Reproduced according to WENNEHORST AND POLL [WP09c].

rates from the interaction of the rubber with the rough counterface<sup>4</sup>. During speed step experiments with decreasing rotational speed, the above described friction curves were reproduced in the opposite direction.

At a rotational speed of approximately  $1 \text{ min}^{-1}$  (corresponding to approximately  $5 \text{ mm s}^{-1}$ ) minimum friction is measured followed by a linear friction torque increase up to approximately  $7 \text{ min}^{-1}$ . As the rotational speed increases further, the friction torque increase is strongly degressive. Below approximately  $40 \text{ min}^{-1}$  the degressive trend of friction might be explained by the still increasing film thickness, beyond mainly thermal effects, and, possibly, non-Newtonian fluid behavior should be considered.

#### 4.3 RESULTS OF ADDITIONAL SEAL CONTACT TEMPERATURE MEASUREMENTS

In order to further investigate the temperature influence, simultaneous measurements of seal under-lip temperature and seal friction torque were additionally carried out on another test rig according to ENGELKE [Eng11], the basic set-up of which is shown in Figure 4.11. Corresponding to the basic mechanical concept of the optical test rig the seal friction torque is determined using a telemetric torque sensor.

<sup>4</sup> See also Section 6.4.1, including references to friction models for rubber sliding on rough substrates. Further experimental results concerning rubber friction on rough and apparently smooth surfaces under dry and lubricated conditions can be found, e. g., in PERSSON ET AL. [PAT<sup>+</sup>04], PERSSON AND VOLOKITIN [PV06], LE GAL [LG07], MOFIDI ET AL. [MPPA08], and MOFIDI AND PRAKASH [MP08].

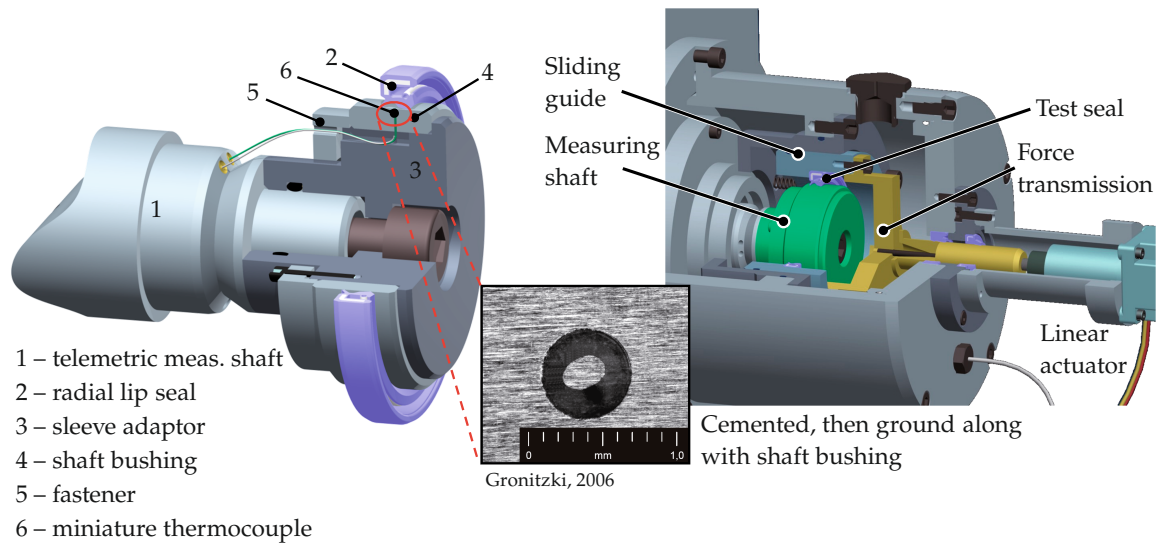


Figure 4.11: Set-up for measurement of seal under-lip temperature (see WOLLESEN [Wol93], GRONITZKI [Gro06], and ENGELKE [Eng11]). Reproduced according to WENNEHORST ET AL. [WEP11].

As on the optical test rig, the small torque offset of the low-friction test spindle is accurately determined by means of reference experiments without test seal and can thus be subtracted during data evaluation. For frictionless determination of the lubricant temperature within the sealing contact zone, a miniature thermocouple (diameter approximately 0.3 mm) is cemented into a shaft bushing being installed on a telemetric measuring shaft (see ENGELKE [Eng11]). The thermocouple is firstly cemented into and finally ground along with the shaft bushing in order to ensure the integrity of the seal counterface and to minimize the influence of the measuring system on the sealing contact configuration. Due to the thermocouple's small diameter being only slightly bigger than the seal contact width, the average lubricant viscosity within the sealing contact zone can be accurately determined. In order to ensure optimal axial alignment of the thermocouple and the sealing contact, a contact temperature pre-scan is carried out prior to the actual temperature measurements. At a constant rotational speed level, the pre-adjusted test seal is axially displaced relative to the shaft by means of an incremental linear actuator providing micron resolution. Using the maximum temperature in the resulting temperature–displacement chart as an indicator, the axial position corresponding to the optimal alignment of thermocouple and seal lip can be accurately determined. Finally the seal is positioned accordingly.

At various constant rotational speed levels within the range of zero up to approximately  $500 \text{ min}^{-1}$  the oil sump temperature and the seal under-lip temperature were determined. By way of example, in Figure 4.12 the results of a single temperature measurement are

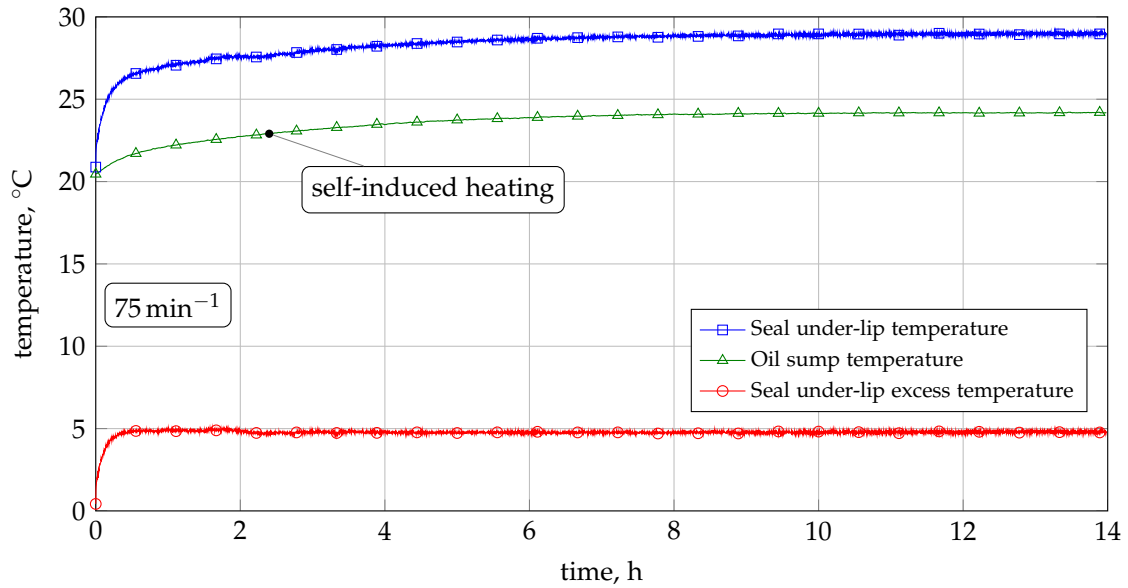


Figure 4.12: Seal under-lip temperature measurement;  $75 \text{ min}^{-1}$ , short-term run seal. Reproduced according to WENNEHORST ET AL. [WEP11].

depicted which was carried out with the short-term run seal at a constant rotational speed of  $75 \text{ min}^{-1}$ .

Corresponding to the optical measurements on the LIF test rig, no additional temperature control was applied. The oil sump temperature level slowly increases during the test run reaching thermal equilibrium within approximately 8 hours. A noteworthy result is the fact that the seal under-lip excess temperature, i. e., the difference between the under-lip temperature and the oil sump temperature, generally remains constant during the heating-up of the system. This is important as it allows for accurate transfer of the respective under-lip excess temperatures to the optical test rig (as described below) even though the heating-up characteristics of the two test rigs are different. The seal friction torques measured on the two different test rigs agreed to more than 90 %. Because of the similar thermal conductivity of steel and sapphire it may therefore be assumed that the excess temperatures in both systems are also very similar. The relationship between seal under-lip excess temperature (or “contact excess temperature”) and rotational speed was then derived applying curve fitting as illustrated in Figure 4.13. Using this relationship, the under-lip temperature during the fluorescence measurements can be determined from the respective oil sump temperature by further addition of the corresponding excess temperature. Finally, the dynamic viscosity during the fluorescence measurements is correspondingly adjusted using the known relation between viscosity and temperature described in Section 3.4.

Based on the above temperature and viscosity adjustment approach, the thermal conditions during the combined seal friction

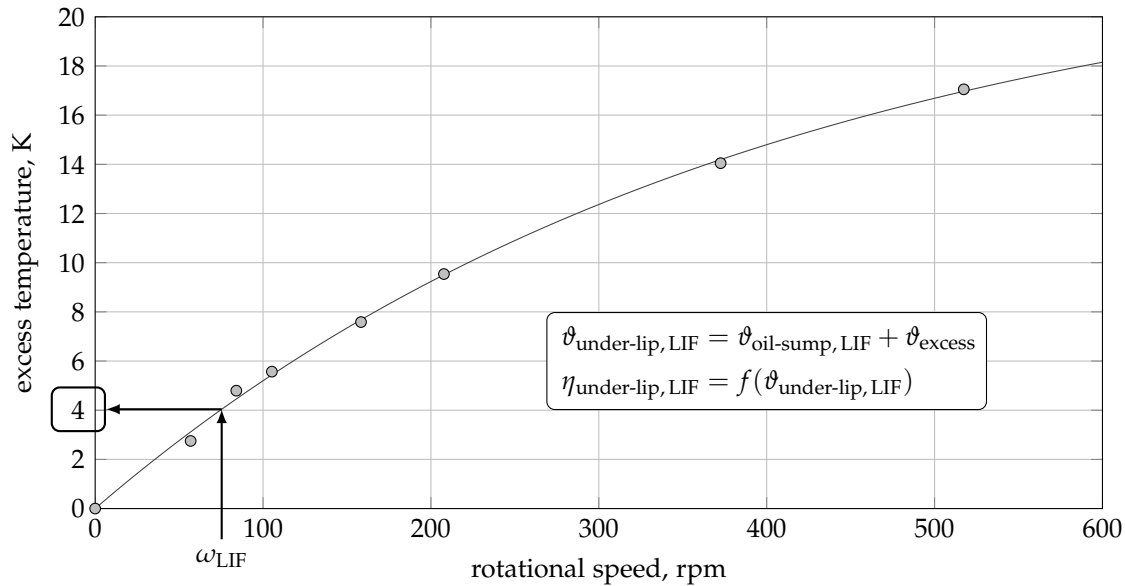


Figure 4.13: Relationship between under-lip excess temperature and rotational speed, short-term run seal (temperature test rig); determination of seal under-lip temperature during LIF measurements on optical test rig. Reproduced according to WENNEHORST ET AL. [WEP11].

torque and lubricant film thickness measurements, as well as the corresponding lubricant viscosity within the sealing contact zone, were derived for both the short-term run and the run-in seal; the results are summarized in Figures 4.14 and 4.15. The slightly different friction torque levels of the short-term run and the run-in seal may thus be explained by the difference observed in the overall oil sump temperature and, correspondingly, viscosity level in combination with the slightly larger contact width of the run-in seal. When comparing the frictional characteristics of the seals by means of the specific frictional heat, thereby eliminating the different sizes of the nominal seal contact area, it is interesting to note that, in this specific case, the specific frictional heat characteristics of both seals are nearly identical, irrespective of the run-in state. Over the entire rotational speed range the agreement is better than 95 %, with the maximum deviation observed at the highest rotational speed<sup>5</sup>.

Following the empirical thermal scale coupling approach proposed by ENGELKE [Eng11] (see also Section 5.2, and WENNEHORST ET AL. [WEP11]), a linearized relation between specific frictional heat and under-lip excess temperature was finally established with a pro-

<sup>5</sup> Given the higher viscosity during the measurements with the run-in seal, in order to yield comparable viscous lubricant friction losses, the speed-dependent lubricant film thickness increase within the contact of the run-in seal must be expected to be larger compared to that of the short-term run seal. This is indeed the case, as demonstrated in the LIF based lubricant film thickness measurements described in Section 4.2.1.



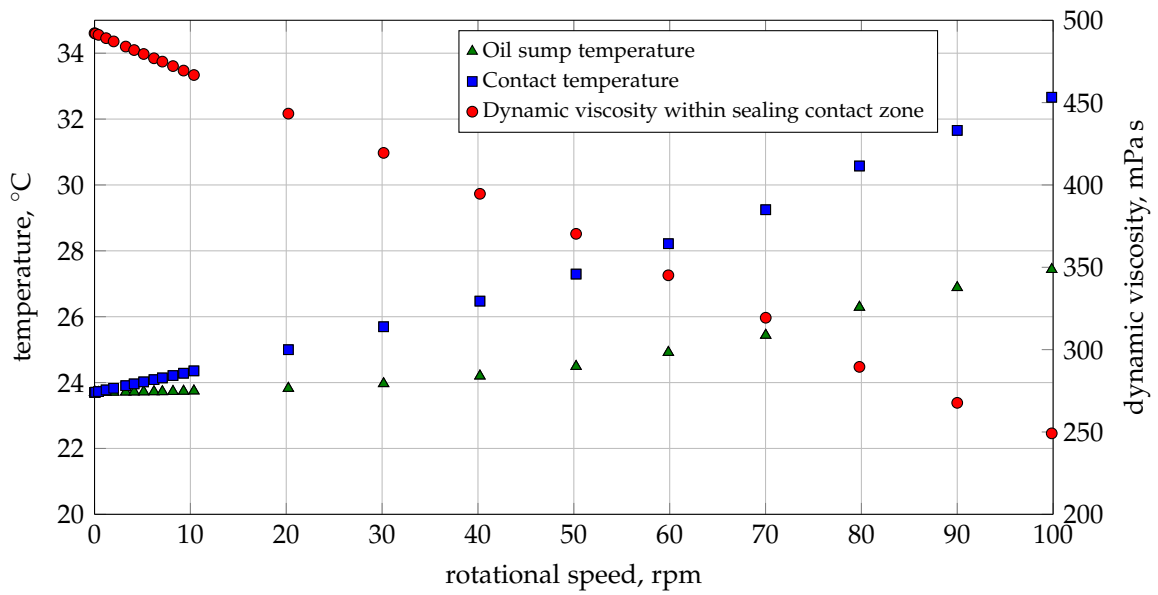


Figure 4.14: Thermal conditions during combined seal friction torque and lubricant film thickness measurements, and corresponding lubricant viscosity within sealing contact zone, short-term run seal. Reproduced according to WENNEHORST ET AL. [WEP11].

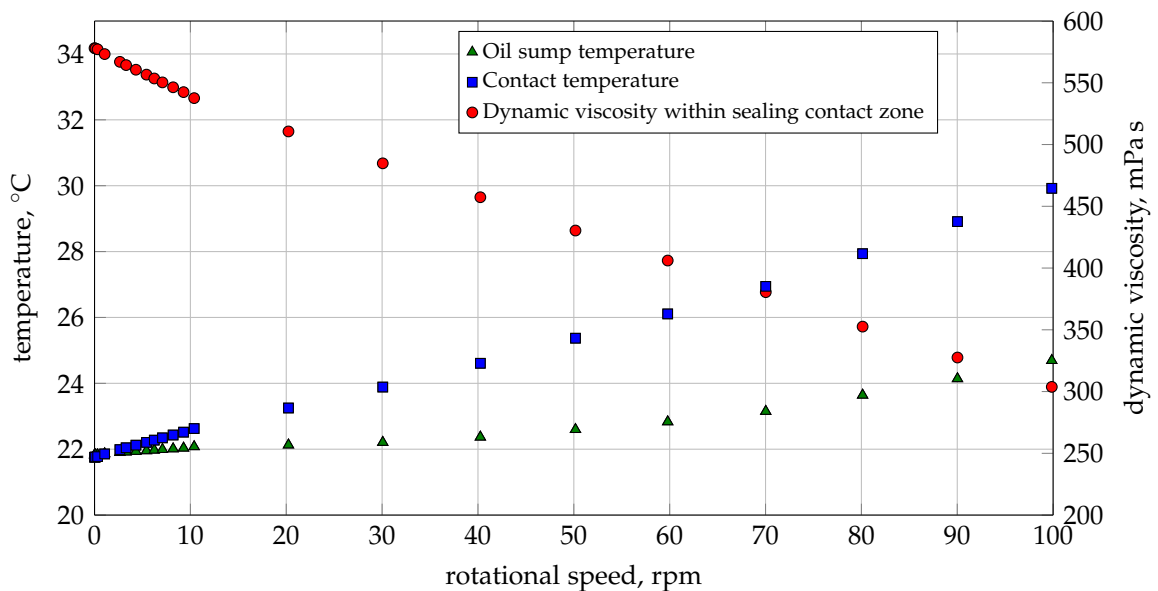


Figure 4.15: Thermal conditions during combined seal friction torque and lubricant film thickness measurements, and corresponding lubricant viscosity within sealing contact zone, run-in seal.

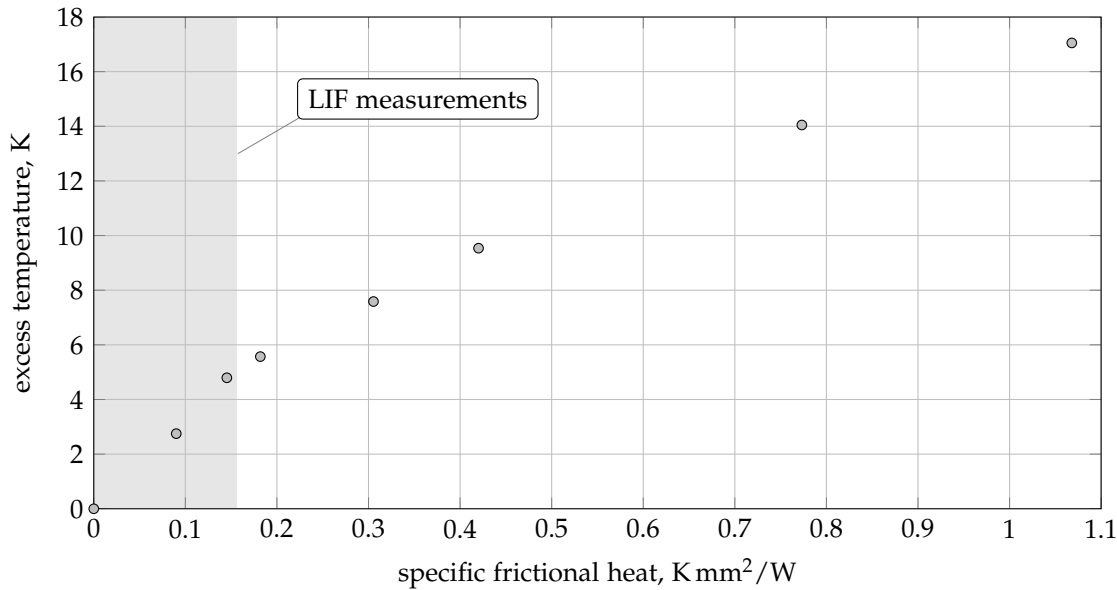


Figure 4.16: Under-lip excess temperature rise versus specific frictional heat, short-term run seal.

portionality factor amounting to approximately  $35\text{ K mm}^2/W$ . Utilizing this relation, frictional heating, and the corresponding changes of the lubricant viscosity, can be easily implemented into theoretical approaches for estimating seal friction. It is interesting to note that the above proportionality factor is appreciably larger than those obtained previously by OTTINK [Ott13, Ott14] and ENGELKE [Eng11]. Here, using the same contact temperature measurement system, the temperature increase factor, on average, was of the order of  $15\text{ K mm}^2/W$ . The difference results from the altered experimental conditions: while the previous measurements were conducted at higher sliding velocities up to  $10\text{ m s}^{-1}$ , applying temperature control and elevated oil sump temperatures ( $80^\circ\text{C}$  and above), the measurements in this work were carried out at low rotational speeds, and, for consistency with the measurements on the optical test rig, allowed for self-induced heating-up starting from ambient temperature. As shown in Figure 4.16, under these conditions the under-lip excess temperature rise versus specific frictional heat is steepest at the low rotational speeds used on the optical test rig, and then declines markedly. In the initial region the slope, i. e., the temperature increase factor, amounts to approximately  $33\text{ K mm}^2/W$ , thus being very close to that derived from the friction measurements on the optical test rig. With further increasing specific frictional heat the temperature increase factor then declines to values that are very similar to those previously reported by OTTINK [Ott13, Ott14] for the same seal type (approximately  $10\text{ K mm}^2/W$  to  $15\text{ K mm}^2/W$ ).

# 5

---

## SEMIEMPIRICAL COMPUTATION OF VISCOUS LUBRICANT FRICTION

---

As described in Section 4.2 (see also WENNEHORST AND POLL [WP09c]), the results of the combined seal friction torque and lubricant film thickness measurements indicate that, especially at the low sliding velocities corresponding to the observed seal friction minimum, the hydrodynamic lubricant film build-up is obviously insufficient to allow for a complete transition to full-film lubrication, i. e., a complete hydrodynamic unloading and lift-off of the compressed elastomer roughness. Therefore, even at higher sliding velocities beyond the friction minimum, the seals can be assumed to operate in the mixed lubrication regime.

In order to gain further insight into the measured overall seal friction, semiempirical approaches were developed coupling the LIF lubricant film thickness and the seal friction torque measurements by means of complementary LIF based computations of the viscous lubricant friction component. Here, the actual seal contact geometry determined by LIF, representing the spatio-temporal average cross-section of the lubricant volume within the sealing contact, was used as input. Using the measured film thickness, the roughness of the surfaces and their elastic deformations are implicitly taken into account.

### 5.1 PRELIMINARY COMPUTATIONAL FLUID DYNAMICS SIMULATIONS

In preliminary computations for the short-term run seal (see also WENNEHORST AND POLL [WP09c]), the open source computational fluid dynamics (CFD) package *OpenFOAM* was used which applies the finite volume method (see, e. g., JASAK [Jas96] and WELLER ET AL. [WTJF98]). The approach chosen to calculate the viscous lubricant friction component is illustrated in Figure 5.1. For each speed step simulation, the same axial region of the sealing contact was used with a maximum film thickness of approximately 10  $\mu\text{m}$ . With regard to the high number of elements needed to properly discretize the computational domain, this value proved to be an upper limit given the speed and memory of the computer used at that time. However, additional computations with a film thickness cut-off set at 2  $\mu\text{m}$  showed

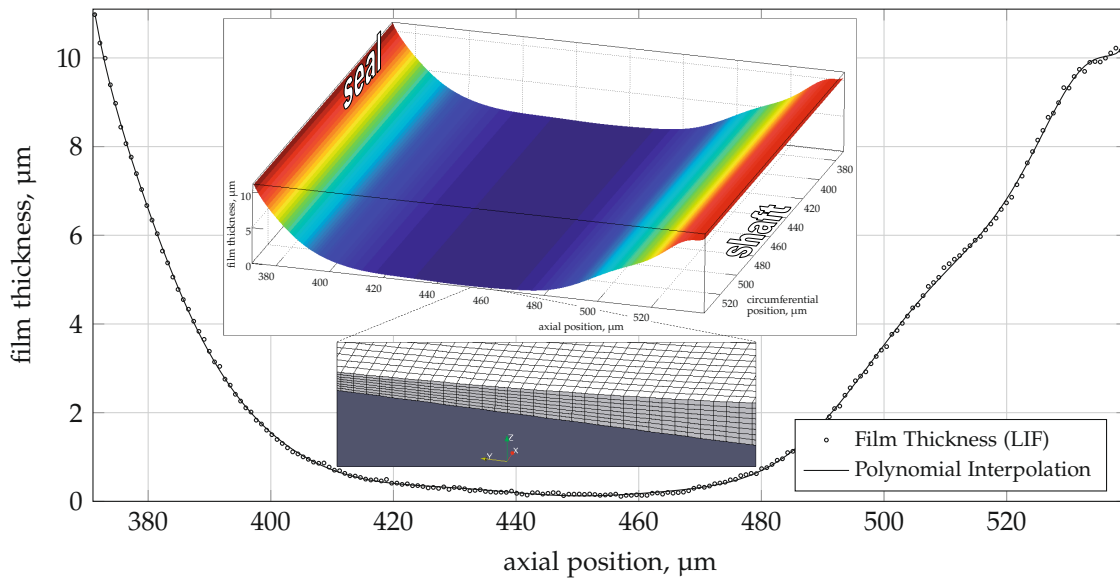


Figure 5.1: CFD approach for computation of viscous lubricant friction torque based on axial lubricant film thickness profiles (LIF measurement). Reproduced from WENNEHORST AND POLL [WP09c].

that the most important part of the friction clearly results from the small contact region with the thinnest lubricant films. The additional viscous shear stress contribution resulting from thicker films can thus be considered to be small.

In a first step, the film thickness profiles are smoothed by means of a high-order polynomial. The three-dimensional lubricant volume is reconstructed by circumferential extrusion of this polynomial, yielding a square computational domain with an edge length of approximately  $170\ \mu\text{m}$ . Since the lubricant film thickness is much smaller than the radius of the sealing contact, a Cartesian coordinate system is used. In this simplified model, the curved upper surface and the plane bottom surface represent the seal and the shaft surface, respectively. By means of additional MATLAB scripting, the geometrical data is translated into *OpenFOAM* specific ASCII format being the input for the *OpenFOAM* meshing module. The resulting high-quality structured meshes consist of approximately  $2.82 \cdot 10^6$  hexahedra. In Figure 5.1, a close-up view of such a mesh is depicted for a small subdomain of the lubricant film.

Both the seal and the shaft surface are considered to be smooth and rigid. As described above, the roughness of the surfaces and their elastic deformations are taken into account implicitly by using the measured averaged film profile as an input for the CFD computations. The no-slip boundary condition is applied to both surfaces. While the seal surface is fixed, the sliding velocities measured during the experiments are applied to the shaft in circumferential direction. The computations were conducted for the linear section of

the friction torque curve (Figure 4.9), i. e., rotational speeds in the range of  $1 \text{ min}^{-1}$  to  $7 \text{ min}^{-1}$ . The fluid flow is assumed to be isothermal, steady-state, incompressible and laminar, while the lubricant is assumed to be Newtonian. A solver implementing the SIMPLE<sup>1</sup> algorithm was used. At the time of this preliminary study, the kinematic viscosity was provided by the lubricant manufacturer, corresponding to the oil temperature measured during the experiment. The lubricant density was determined by means of additional measurements. In order to calculate the viscous lubricant friction torque, the viscous friction force is determined for the base patch integrating the wall shear stress over the corresponding domain. The resulting overall viscous friction torque can then easily be determined taking the entire length of the sealing contact and its radius into account:

$$T_{\text{visc}} = \left(\frac{d}{2}\right) \cdot \left(\frac{d \cdot \pi}{l_{\text{patch}}}\right) \cdot \int \tau_{\text{patch}} \, dA. \quad (5.1)$$

The validity of the above modeling approach was checked using a lubricant film with a uniform thickness of 200 nm (plane Couette flow), and proving that the simulation converged against the analytical solution.

In Figure 5.2, the computed viscous friction torque is compared to the measured overall friction torque.

Linear regression of the linear section of the measured friction torque curve yields a non-zero ordinate intercept at zero speed. As previously proposed by POLL [Pol00], this part of the overall friction should result from boundary friction, whereas the superimposed linear increase should be due to the sheared lubricant. Indeed, the best-fit line of the computed viscous friction torque accurately coincides with the experimental data applying a parallel shift according to this offset. At very low speeds, below the sliding speed at which minimum friction is observed, the increasing overall friction is apparently governed by rubber friction. The decreasing right-hand part of the low-speed friction torque maximum is most likely influenced by the onset of hydrodynamic lubricant film build-up effects. Nevertheless, the comparison of computed viscous friction and the measured overall seal friction supports the assumption of mixed lubrication within the linear section of the measured seal friction torque curve. Based on these results, the friction torque curves measured with the elastomer lip seals thus should not be interpreted as classical Stribeck curves with a complete transition to full-film lubrication.

<sup>1</sup> The SIMPLE (Semi-Implicit Method for Pressure-Linked Equations) algorithm allows to couple the Navier-Stokes equations with an iterative procedure (see, e. g., FERZIGER AND PERIC [FP01], and JASAK [Jas96]); here, the *simpleFoam* solver provided with *OpenFOAM* was used.

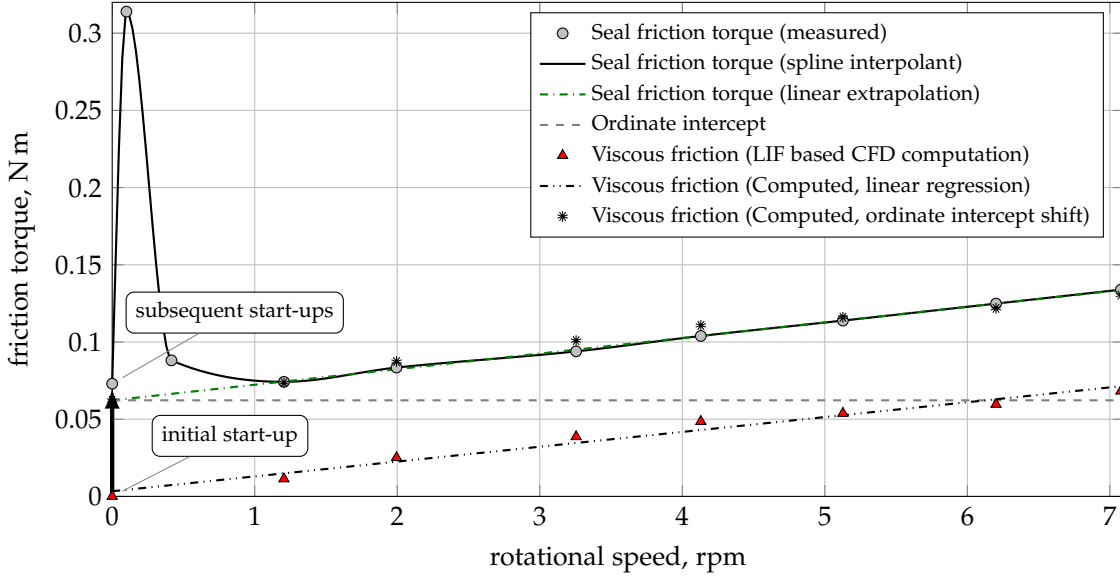


Figure 5.2: Comparison of measured overall seal friction torque and LIF based CFD computation of corresponding viscous lubricant friction part, short-term run seal. Reproduced from WENNEHORST AND POLL [WP09c].

## 5.2 SIMPLIFIED NUMERICAL APPROACH

Utilizing the temperature-corrected viscosities the complementary computations of the viscous lubricant friction component are resumed, now covering the entire rotational speed range applied during the optical measurements (see also WENNEHORST ET AL. [WEP11]). As in the CFD approach described above, the lubricant flow is considered to be isothermal, steady-state, laminar and incompressible with Newtonian fluid behavior. The surfaces of both shaft and seal are considered to be rigid with the no-slip boundary condition being applied. The viscous lubricant friction torque, however now is derived from the axial lubricant film thickness profiles by utilizing the laminar flow assumption and evaluating the wall shear stresses analytically. According to Figure 5.3 and equation (5.2) the frictional increments of axial lubricant slices are summed over the entire contact region by means of MATLAB scripting:

$$T_{\text{visc}} = \left(\frac{d}{2}\right) \cdot \sum_{i=1}^n \left(\frac{d \cdot \pi \cdot \Delta y \cdot \eta \cdot u}{h_{\text{av},i}}\right). \quad (5.2)$$

The axial width  $\Delta y$  of these slices equates to the maximum spatial resolution of the imaging system which amounts to  $0.85 \mu\text{m}/\text{pixel}$ . As illustrated in Figure 5.3, the radial height of each lubricant slice is set equal to the average of the associated film thickness values.

The lubricant film thickness profiles are evaluated over the complete axial field of view. Thus, not only the actual lubricant film

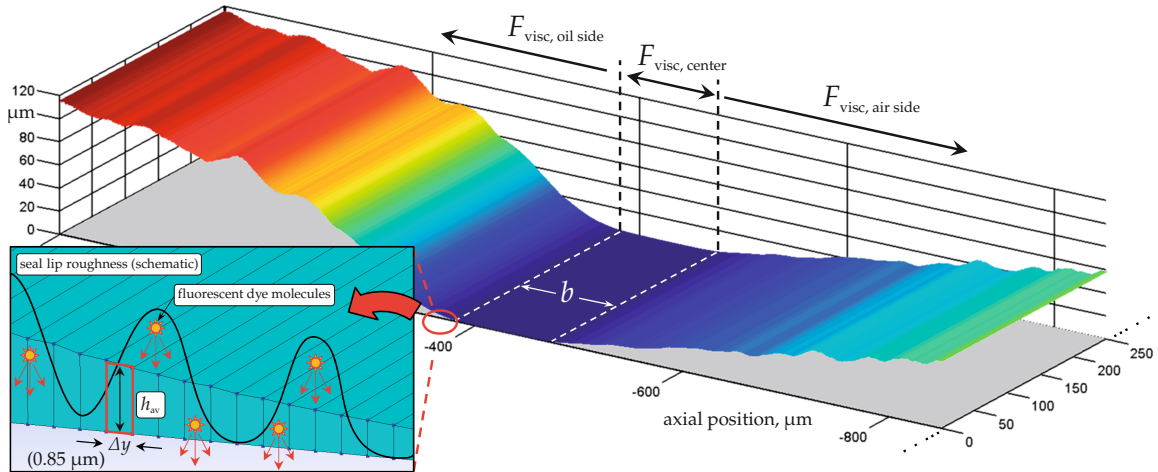


Figure 5.3: Computation of viscous lubricant friction torque based on axial lubricant film thickness profiles (LIF measurement). Reproduced from WENNEHORST ET AL. [WEP11].

within the seal lip contact band is considered but also the viscous friction components resulting from the oil-filled contact side areas (see Figure 5.3). A closer investigation of the resulting axial wall shear stress distribution clearly indicates that the additional shear stress contributions of the direct contact vicinity should not be neglected. Nevertheless, with further increasing lubricant film thickness the viscous lubricant friction rapidly decreases.

In Figure 5.4, the results of the friction computations are depicted for the film thickness profiles measured with the short-term run seal. Applying the simplified numerical approach, the results obtained above for the linear section of the friction torque curve are accurately reproduced. Moreover, as can be clearly seen from Figure 5.4, utilizing the temperature-corrected viscosities, the assumption of mixed lubrication is obviously justified for the entire friction torque curve. The friction torque offset observed on the right-hand side of the friction torque minimum appears largely unaffected by the sliding velocity. It is interesting to note that the magnitude of this offset apparently equates to the sealing system's boundary friction torque, given by the ordinate intercept of the extrapolated linear section of the seal friction torque curve, as shown in Figure 5.4, and previously argued by POLL [Poloo].

Generally, as shown in Figure 5.5, the same findings apply to the run-in seal. However, at higher rotational speeds the underestimation of the total measured seal friction becomes more pronounced. This is obviously due to local oil-filled surface cavities resulting from the run-in process as described in Section 4.2.1. Their cross-sectional contours appear in the film thickness profiles which are used as input in the axisymmetric computation of the viscous lubricant friction. Consequently, as they do not span the entire length of the sealing contact, the computed viscous shear forces are slightly underestimated.

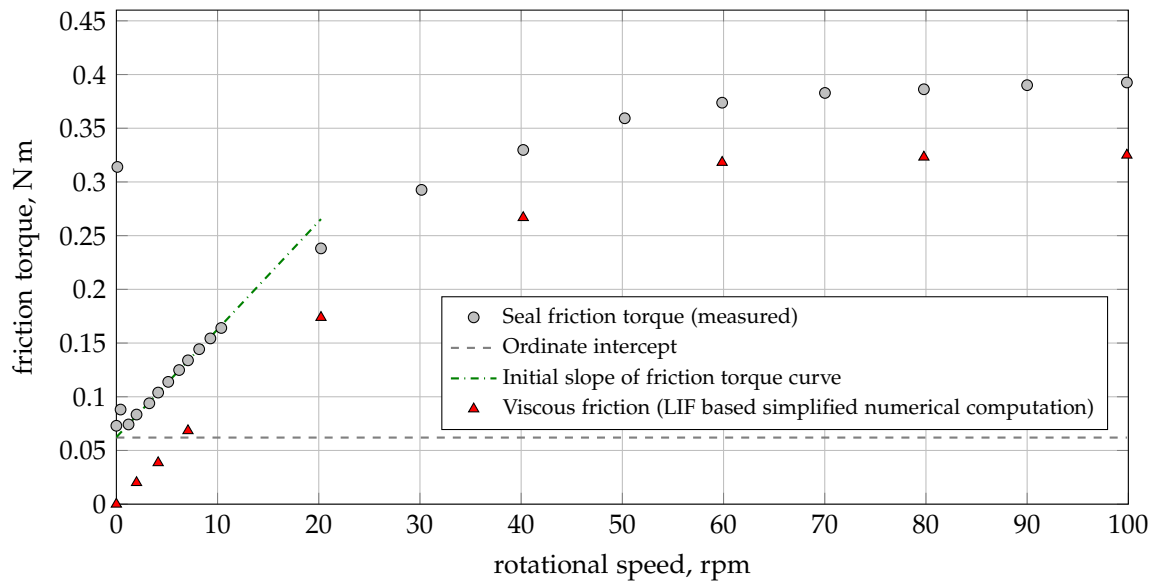


Figure 5.4: Comparison of measured overall friction torque and LIF based simplified numerical computation of corresponding viscous lubricant friction part; short-term run seal, temperature-corrected viscosities. Reproduced from WENNEHORST ET AL. [WEP11].

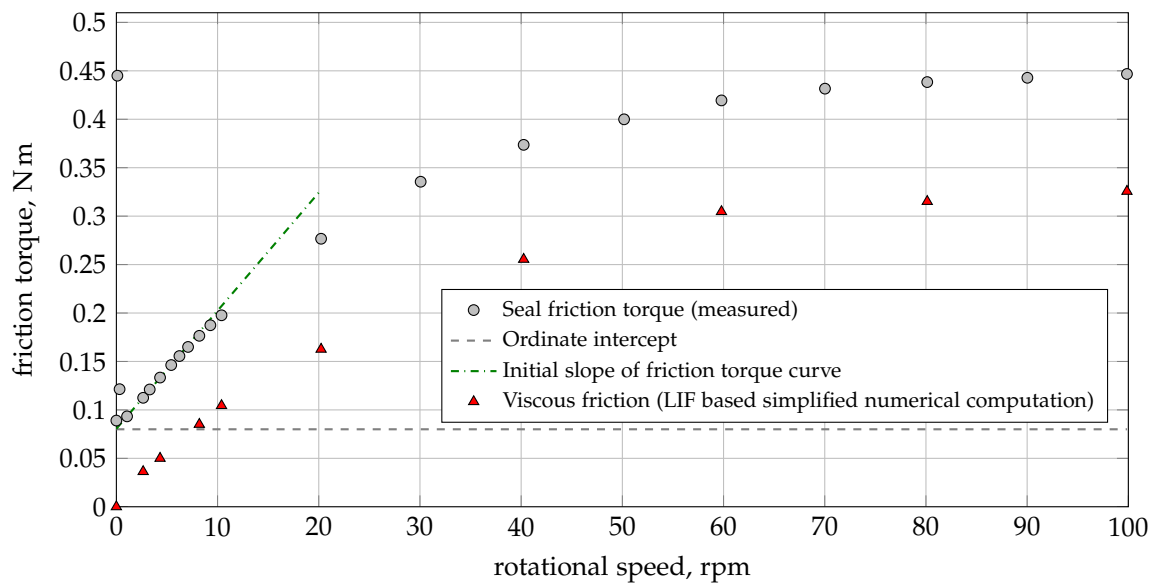


Figure 5.5: Comparison of measured overall friction torque and LIF based simplified numerical computation of corresponding viscous lubricant friction part; run-in seal, temperature-corrected viscosities. Reproduced from WENNEHORST ET AL. [WEP11].



Regarding the underestimation of seal friction observed with the above semiempirical computation of the viscous lubricant friction component, the most straightforward interpretation would be the assumption of mixed lubrication comprising a boundary friction component being roughly independent of sliding speed. Following this purely phenomenological approach previously suggested by LEIN [Lei54], and POLL ET AL. [PGBQ92], ENGELKE [Eng11] proposed a simple computational method for estimating radial lip seal friction and seal under-lip temperature. Here, the overall radial lip seal friction torque  $T_{\text{seal}}$  is assumed to be composed of a boundary friction component  $T_0$ , being independent of rotational speed  $n$ , and a speed-dependent viscous lubricant friction part  $T_\eta$ :

$$\begin{aligned} T_{\text{seal}}(\vartheta) &= T_0 + T_\eta \\ &= \mu_0 \cdot F_{\text{rad}} \cdot \left(\frac{d}{2}\right) + \eta(\vartheta) \cdot \frac{b}{h} \cdot \left(\frac{d}{2}\right)^3 \cdot \frac{(2 \cdot \pi)^2}{60} \cdot n. \end{aligned} \quad (5.3)$$

Boundary friction coefficients  $\mu_0$  were determined empirically for sliding speeds approaching zero. As seal radial forces may decrease significantly with increasing temperature<sup>2</sup>, the actual seal radial force  $F_{\text{rad}}$  measured at oil sump temperature was used in equation (5.3). As a simple estimate for the lubricant film thickness  $h$ , ENGELKE assumed  $h$  to be independent of speed, and roughly equal to the combined contact roughness of the seal and the shaft. Thus,  $h$  was calculated as the sum of the mean peak roughnesses  $R_p$  of both surfaces measured with a mechanical stylus instrument. The dynamic viscosity  $\eta$  depends on the lubricant temperature which, at the same time, itself depends on the frictional heat being generated within the sealing contact. Thus, both the seal friction torque and the contact temperature can be calculated by iteratively evaluating equation (5.3) utilizing an appropriate coupling between specific frictional heat and under-lip excess temperature. Utilizing a linearized relationship between these parameters that was determined empirically<sup>3</sup>, a spreadsheet-based

<sup>2</sup> See, e. g., ENGELKE [Eng11], and OTTINK [Ott14] who conducted additional temperature controlled radial force measurements with the seal type that was also used in this work.

<sup>3</sup> As detailed in WENNEHORST ET AL. [WEP11], it should be emphasized that this relationship de facto couples different scales: micro-scale frictional heat generation is coupled to the heat balance of the actual macro-scale sealing system assembly. Furthermore, it should be noted that this relation can also be established theoretically by means of thermal finite element analysis (see, e. g., ENGELKE ET AL. [EPSD11], and OTTINK [Ott14]) or conjugate heat transfer analysis (see, e. g., DAUBNER ET AL. [DWH10]). Provided that all relevant physical parameters are known to sufficient accuracy, it can be determined “synthetically” based on a limited set of simulations. Within the iteration scheme of the friction model, the corresponding relationship is then easily implemented by means of appropriate interpolation. The experimental effort thus could be reduced to a smaller number of tests needed for validation of the thermal model.

iteration scheme was set up by ENGELKE using the oil sump temperature as an initial value. The iterations were demonstrated to converge quickly, yielding the contact temperature (or contact excess temperature, respectively) and the seal friction torque as a function of rotational speed. The temperature and seal friction torque estimates obtained this way were shown to agree fairly well with experimental results.

Coming back to the underestimation of seal friction observed with the above semiempirical computation of the viscous lubricant friction component, another interpretation should also be considered which is based on a closer examination of the viscous shear stresses generated within the sealing contact zone. It is important to realize that, as illustrated in Figure 5.6 for a simple Couette flow, any local averaging of the actual lubricant film thickness distribution in rough contacts inherently leads to an underestimation of the total viscous friction force. This is due to the fact that the average of the lubricant film thickness does not adequately capture the viscous shear stress contributions resulting from very thin lubricant films. Besides the circumferential averaging of axial film thickness profiles, which is done prior to the idealized axisymmetric computation of the viscous lubricant friction, local averaging processes are inevitable due to the finite lateral resolution of the imaging system. Moreover, as indicated in Figure 5.3, averaging-like processes are also inherent to the fluorescence method due to the fact that fluorescence is emitted in all directions. Therefore, due to the finite working distance of the microscope, in rough contacts the low intensity fluorescence emitted from very thin lubricant films will be superposed with fluorescence originating from adjacent regions of thicker films, so that very thin films appear thicker than they are in reality. When calculating viscous lubricant friction semiempirically from the measured (i. e., laterally discretized) lubricant film thickness distributions, the combination of these averaging effects thus introduces a systematic error, the size of which can be expected to be strongly related to the lubrication condition<sup>4</sup> characterized by the ratio  $\Lambda$  of lubricant film thickness  $h$  to (combined) surface roughness<sup>5</sup>.

<sup>4</sup> It is interesting to note the similarity with the PATIR AND CHENG [PC78, PC79] approach for deriving average Reynolds type equations applicable to any general roughness structure. This "Average Flow Model" is based on defining empirical pressure and shear ("correction") flow factors such that the average lubricant flow can be expressed in terms of these flow factors and the mean quantities such as the mean pressure and the nominal film thickness. The flow factors are obtained by numerical flow simulations based on measured or numerically generated rough surfaces.

<sup>5</sup> A common definition of the dimensionless film parameter  $\Lambda$  used in elastohydrodynamic lubrication is  $\Lambda = h_{\min} / (R_{q,a}^2 + R_{q,b}^2)^{1/2}$ , where  $h_{\min}$  is the minimum film thickness in the (smooth) macroscopic elastohydrodynamic contact, and  $R_{q,a/b}$  are the root mean square surface finishes of the two surfaces  $a$  and  $b$ , respectively (see, e. g., HAMROCK ET AL. [HSJ04], p. 57). For a critical review of the  $\Lambda$  ratio, especially regard-

Evaluation based on global average:

$$\begin{aligned} F_{\text{visc, global av.}} &= A\eta u \frac{1}{h_{\text{av}}} \\ &= \left(\frac{5}{3}\right) A\eta u \frac{1}{h} \end{aligned}$$

Evaluation based on local film thickness values:

$$\begin{aligned} F_{\text{visc, lat. res.}} &= \left(\frac{A}{5}\right) \eta u \left(\frac{1}{1} + \frac{1}{2/5} + \frac{1}{1/5} + \frac{1}{2/5} + \frac{1}{1}\right) \frac{1}{h} \\ &= \left(\frac{12}{5}\right) A\eta u \frac{1}{h} \end{aligned}$$

Ratio:

$$\frac{F_{\text{visc, global av.}}}{F_{\text{visc, lat. res.}}} = 0.6944$$

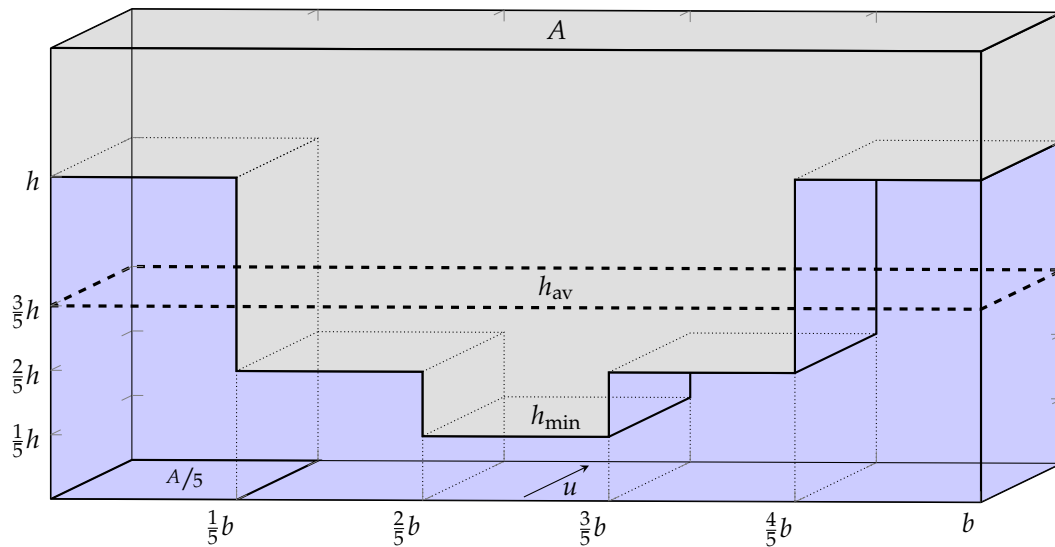


Figure 5.6: Underestimation of viscous lubricant friction due to film thickness averaging, arithmetic example.

Indeed, it can be demonstrated by means of simple theoretical considerations that the averaging error is most pronounced in the presence of very thin lubricant films, i. e., under conditions of mixed, or even thin film lubrication. However, when the separation of the surfaces increases, thereby approaching hydrodynamic full film lubrication, the averaging error rapidly decreases. This is illustrated in Figure 5.7, again applying the computational methodology shown in Figure 5.6, now varying the minimum film thickness in the range of 1 % to 100 % of the reference height  $h^6$ .

Therefore, if the seals were operating under conditions of full film lubrication, the semiempirical computations of the viscous lubricant friction would be expected to agree far better with the measured seal friction. As the measured seal friction is appreciably underestimated in the semiempirical computations, it may be concluded that the seals consistently operate under conditions of mixed lubrication. Here, the term “mixed lubrication” does not necessarily involve partial rupture of the lubricant film and a corresponding Coulomb-type boundary friction component, as it is commonly presumed in the case of hard surfaces. Instead, the compliance of the elastomer (i. e., its low modulus of elasticity) may allow for the formation of thin micro-elastohydrodynamic lubricant films separating the compressed elastomer asperities and the counterface<sup>7</sup>. The thickness of these films will be appreciably smaller than the contact roughness of the elastomer seal lip surface. Within this notion of mixed lubrication, the viscous lubricant friction originating from such films could in principle make up for the difference observed between the measured seal friction and the results of the semiempirical computations. Therefore, this alternative approach to mixed lubrication in soft rough contacts will be studied in detail in Chapter 6.

---

ing its applicability under conditions of mixed lubrication and thin film lubrication, see, e. g., CANN ET AL. [CJL94], and ZHU AND WANG [ZW12].

6 By applying the same computational methodology to pseudo-random roughness profiles with a Gaussian height distribution and an exponential autocorrelation function (see, e. g., PATIR [Pat78]), these findings were also generalized to more realistic height distributions (data not shown).

7 Further experimental evidence for the formation of such soft micro-elastohydrodynamic lubricant films may be found, e. g., in McCLUNE AND TABOR [MT78], KANETA ET AL. [KTN<sup>+</sup>00, KTT<sup>+</sup>05], and in FOWELL ET AL. [FMSK14].

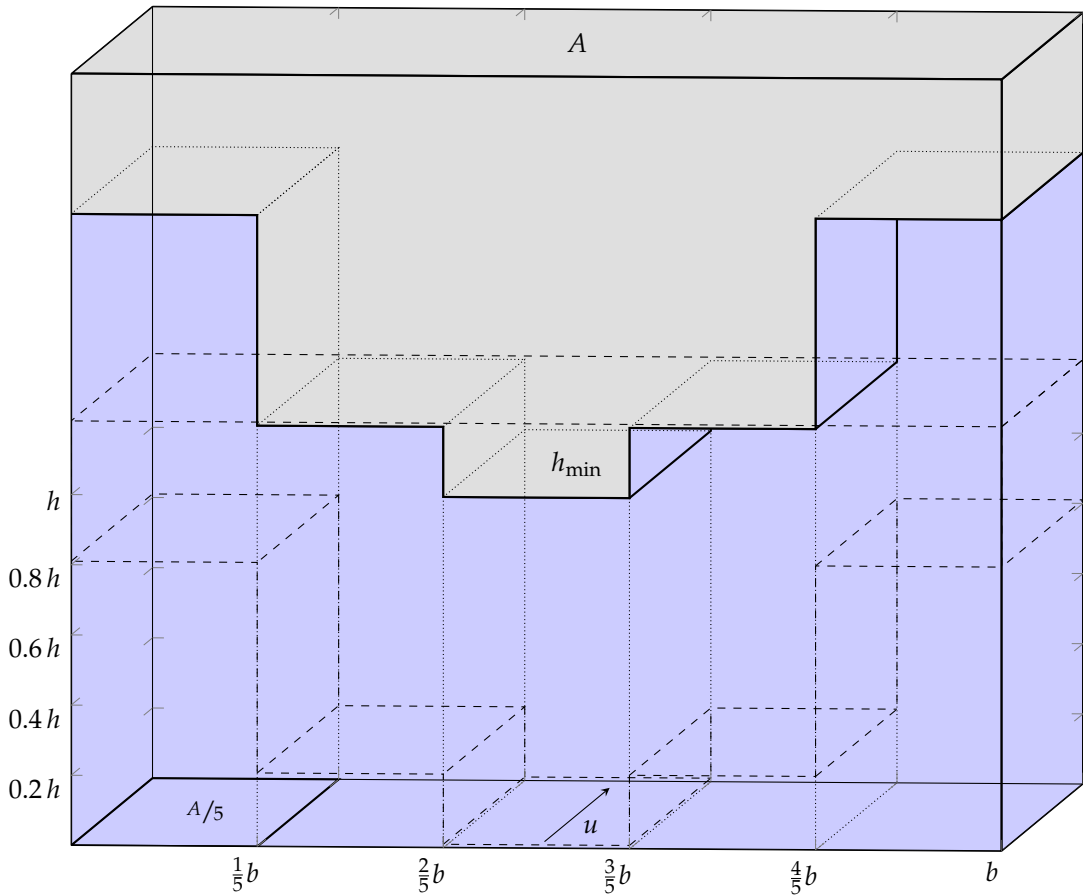
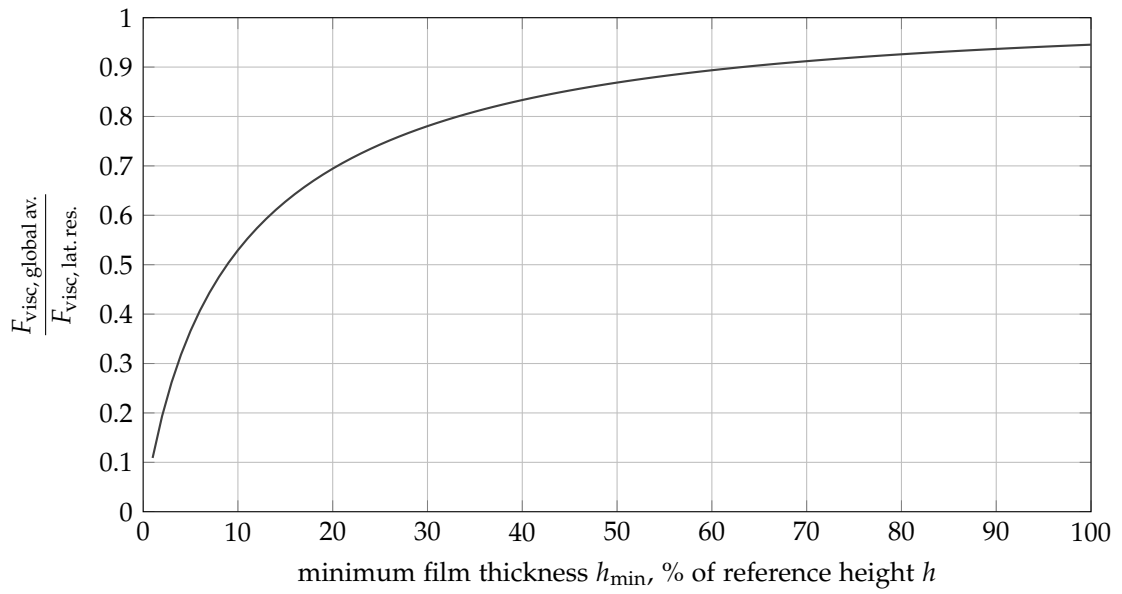


Figure 5.7: Underestimation of viscous lubricant friction due to film thickness averaging as a function of surface separation, arithmetic example.



---

## MODELING LUBRICATION AND FRICTION OF RADIAL LIP SEALS

---

Mixed lubrication approaches for calculating the frictional losses of dynamic seals are currently based on classical *hard* surface mixed lubrication models comprising partial lubricant film rupture and a Coulomb-type boundary friction component (see Figure 6.1 according to POLL [Pol00], and SHI AND SALANT [SS00], SHI AND SALANT [SS01], SHEN AND SALANT [SS06], ÖNGÜN ET AL. [ÖABD08], SCHMIDT [SAP10], SALANT [Sal10], SCARAGGI AND CARBONE [SC12], and GUO ET AL. [GJS<sup>+</sup>13]). These models are principally capable of explaining the classical Stribeck curve-like transition from partial to full-film lubrication: with increasing product of sliding velocity and viscosity the hydrodynamic load-carrying capacity of the lubricant film improves until the transition or lift-off point is reached where the Coulomb boundary friction component vanishes and the overall friction is then purely viscous. However, as described in Section 4.2 and Chapter 5, these lubrication approaches are obviously not capable of adequately covering the frictional phenomena observed with *soft* low-elastic modulus sliding partners such as elastomeric seal lip surfaces.

### 6.1 REVISITING THE CONCEPT OF SOFT MICRO-ELASTOHYDRO-DYNAMIC ASPERITY LUBRICATION

Given the above described difficulties encountered with standard (*hard* surface, or *isoviscous-rigid*<sup>1</sup>) mixed lubrication models, an alter-

---

<sup>1</sup> The term *isoviscous-rigid*, as used by HAMROCK ET AL. [HSJ04], refers to the lubrication of hard surfaces when the contact pressure is low and, therefore, both the elastic deformations of the (hard) contact partners, as well as the pressure dependency of the lubricant viscosity are negligibly small which is the case, e. g., in journal bearings. By contrast, the term *isoviscous-elastic* refers to the lubrication of soft contacts, where the contact pressures are low as well (of the order of few MPa), so that the lubricant viscosity can be considered isoviscous, too; however, due to the low elastic modulus of the contact partners, the lubricant film formation is appreciably influenced by elastic deformations which can occur not only at the macro scale (as is the case, e. g., in soft journal bearings), but at the asperity level as well, when the contact lacks a macroscopic hydrodynamic pressure and fluid film formation mechanism (as is the case with soft rough conformal surfaces in parallel sliding which are found, e. g., in radial lip seal contacts).

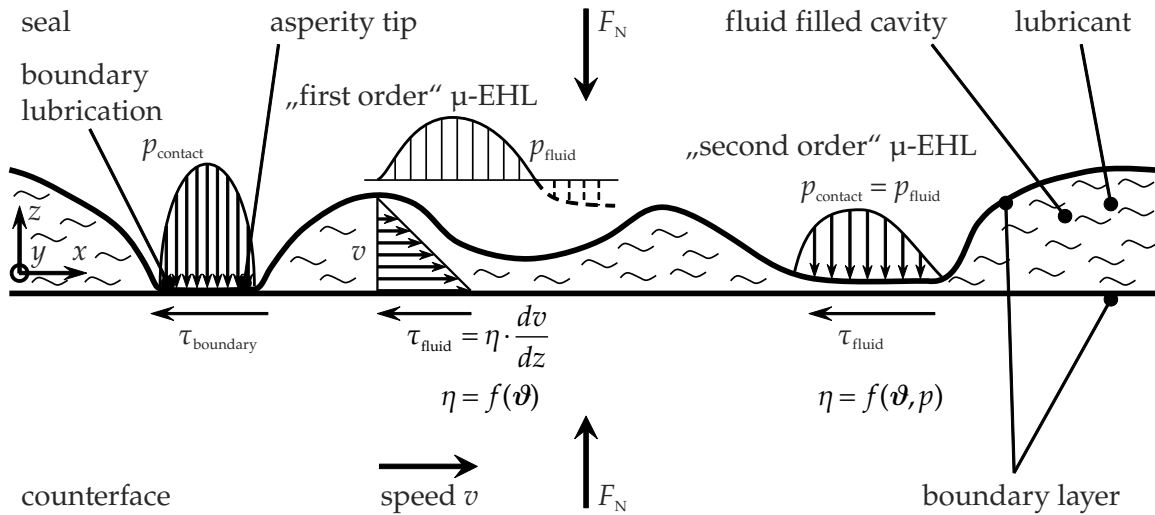


Figure 6.1: Lubrication regimes according to POLL [Poloo].

native lubrication model [Gab89, Gab91] is adopted, essentially relying on the assumption that the lubrication of *soft* rough surfaces can be described by micro- or submicron-scale soft elastohydrodynamic (soft-EHL, i. e. isoviscous-elastic) lubrication at the asperity level (“second order”  $\mu$ -EHL in Figure 6.1). The overall seal radial force is thus balanced by the joint action of both the (mesoscale) hydrodynamic pressure generation within the drag flow over the rough deformable surface (“first order”  $\mu$ -EHL in Figure 6.1) as well as the structural response of the flattened and tangentially deformed asperities which are sliding on a thin soft-EHL oil film at nearly any nonzero sliding velocity. The thickness of this oil film is determined applying well-established soft-EHL central film thickness formulae. Under the assumption of a perfectly smooth counterface the overall friction thus entirely originates from the lubricant: in addition to the viscous friction contribution of the oil-filled surface roughness (mesoscale), the viscous shear stresses resulting from the thin under-asperity soft-EHL oil films (submicron-scale) may contribute significantly to the overall friction. It is interesting to note that this asperity lubrication mechanism, i. e., the treatment of rubber asperities as an elastohydrodynamic problem, had first been proposed by JAGGER AND WALKER [JW67] as early as 1966, and later successfully applied by McCLUNE AND TABOR [MT78]. It was not until 1989, however, that GABELLI [Gab89] revisited this approach, implementing the soft (isoviscous-elastic) EHL central film thickness formula which had been presented by CHITTENDEN ET AL. in 1986 [CDT87].



## 6.2 DETERMINISTIC MODEL OF SEAL LIP SURFACE

In order to provide a basic geometric description of the seal lip surface roughness, in a first step the seal lip is characterized using optical interference surface profilometry (WYKO NT1100, VEECO, Institute of Measurement and Automatic Control (IMR), Leibniz Universität Hannover, Germany) with lateral sampling intervals of  $0.84\ \mu\text{m}$  and  $0.98\ \mu\text{m}$  in circumferential and axial direction, respectively.

Depending on the roughness characteristics and the optical properties of the specimen, the raw data obtained with optical surface profilometers always contains missing data or pixel values that are spiking both unrealistically high or low; upon inspection of the raw data these obvious outliers must be marked as invalid<sup>2</sup> in order to exclude them from subsequent fits. MATLAB routines developed at the IMR are used for the “stitching” (i. e., missing data interpolation) of the corresponding surface raw data matrix. Global curvature removal is performed by fitting a second-order bipolynomial to the surface data and then subtracting it<sup>3</sup>. The choice of a quadratic bipolynomial was based on the inherent curvature of the seal lip (in axial direction) as well as the entire seal ring (in circumferential direction). In order to remove the waviness component, a Gauss filter is then applied to the surface data, using a cut-off wavelength of  $80\ \mu\text{m}$ .

From the final roughness data the root mean square height  $S_q$  and root mean square slopes  $\Delta_{\text{r.m.s.,x/y}}$  are computed. The root mean square deviations of a continuous and a discrete surface from the reference datum (least squares mean plane) are given by (see, e. g., DONG ET AL. [DSS94a])

$$S_q = \sqrt{\frac{1}{l_x l_y} \int_0^{l_y} \int_0^{l_x} z^2(x, y) dx dy} \approx \sqrt{\frac{1}{MN} \sum_{j=1}^N \sum_{i=1}^M z^2(x_i, y_j)} \quad (6.1)$$

where  $l_x$  and  $l_y$  are the side lengths of the sampling area and  $(M \times N)$  is the size of the sampling matrix in  $x$ - and  $y$ -direction, respectively. The slope computation is carried out using the 7-point-formula

$$\left(\frac{dz}{dx}\right)_i = \frac{1}{60s_x} [45(z_{i+1} - z_{i-1}) - 9(z_{i+2} - z_{i-2}) + (z_{i+3} - z_{i-3})] \quad (6.2)$$

<sup>2</sup> In MATLAB, this can be done, e. g., by assigning them the “missing” default value *NaN* (Not a Number).

<sup>3</sup> For a discussion of the polynomial order the reader may refer, e. g., to DE CHIFFRE ET AL. [DCLT<sup>+</sup>00].

$$\left(\frac{dz}{dy}\right)_j = \frac{1}{60s_y} [45(z_{j+1} - z_{j-1}) - 9(z_{j+2} - z_{j-2}) + (z_{j+3} - z_{j-3})] \quad (6.3)$$

as recommended in CHETWYND [Che78], HAMROCK ET AL. [HSJ04], and DIN EN ISO 4287 [ISO4287]. Here,  $s_x$  and  $s_y$  are the sampling intervals in  $x$ - and  $y$ -direction, respectively. The root mean square slope in either direction is then given by

$$\Delta_{\text{r.m.s.,}x} = \sqrt{\frac{1}{M-6} \sum_{i=4}^{M-3} \left(\frac{dz}{dx}\right)_i^2} \quad , \quad (6.4)$$

$$\Delta_{\text{r.m.s.,}y} = \sqrt{\frac{1}{N-6} \sum_{j=4}^{N-3} \left(\frac{dz}{dy}\right)_j^2} \quad . \quad (6.5)$$

As shown in McCool [McC86b], the root mean square height, root mean square slope, and root mean square curvature are equivalent to the spectral moments  $(m_0)^{1/2}$ ,  $(m_2)^{1/2}$ , and  $(m_4)^{1/2}$ , respectively, according to NAYAK [Nay71], which had been used by GABELLI [Gab89, Gab91].

Using these parameters, a sinusoidal roughness model according to Figure 6.2 is set up with amplitude  $a$ , effective wavelengths  $\lambda_{\text{r.m.s.,}x}$  and  $\lambda_{\text{r.m.s.,}y}$ , and radii of curvatures  $R_x$  and  $R_y$  in circumferential and axial direction, respectively (Table 6.1). It is worth noting that the root mean square wavelength  $\lambda_{\text{r.m.s.}}$ —as a hybrid roughness parameter—combines amplitude and spacing information. It is a weighted average and considers a profile as a series of harmonics in which the amplitudes are weighted in proportion to their frequencies. It is thus a parameter that is a measure of the spacings between local peaks and valleys, taking into account their relative amplitudes and individual spatial frequencies [Gri01].

It should be noted that “characteristic wavelengths” used in roughness modeling are commonly based on the correlation length  $\beta^*$  introduced through the work of PEKLENIK [Pek68]. The correlation lengths are derived from the auto-correlation function (ACF), which (as summarized, e. g., in GRIFFITHS [Gri01]) is a means of defining the statistical features of profile spacings. It is a measure of the longitudinal similarity between two identical but shifted profiles. For a particular shift length the correlation value is obtained by multiplying the shifted and unshifted profile values ordinate by ordinate and then calculating the average. For a random profile, the ACF will decay quickly to zero but if the profile has a periodic component, the ACF will oscillate (this can be seen, e. g., in the ACF of fine-turned surfaces, where the length over which the ACF oscillates corresponds to the feedrate). The distance over which the correlation (which can be

Table 6.1: Parameters of the roughness model.

---

Amplitude <sup>a</sup> :	$\sqrt{2} S_q$	(6.6)
--------------------------	----------------	-------

Effective wavelengths <sup>b</sup> :	$\lambda_{r.m.s.,x/y} = 2\pi \frac{S_q}{\Delta_{r.m.s.,x/y}}$	(6.7)
--------------------------------------	---	-------

Radii of curvatures <sup>c</sup> :	$R_{x/y} = \frac{1}{\sqrt{2} S_q} \cdot \left( \frac{\lambda_{r.m.s.,x/y}}{2\pi} \right)^2$	(6.8)
------------------------------------	---	-------

---

<sup>a</sup> BAGLIN [Bag86a]; <sup>b</sup> GRIFFITHS [Gri01]; <sup>c</sup> KARAMI ET AL. [KES87]

modeled using an exponential function, see, e. g., PEKLENIK [Pek68]) decays to a certain percentage of its value at the origin (typically 10 % or 50 % as proposed by Peklenik [Pek68]) is termed the correlation length ( $\beta_{0.10}^*$  or  $\beta_{0.50}^*$ , PEKLENIK originally used the symbols  $\lambda_{0.1}$  and  $\lambda_{0.5}$ ) and two points separated along the surface by a distance equal to the correlation length are regarded as (statistically) independent. The non-isotropic properties of the surface can be seen from the polar coordinate representation of the  $\beta_\theta^*$  distribution as suggested by PEKLENIK [Pek68], which is in the first approximation an ellipse. In the notation used by PATIR [Pat78], the corresponding ellipticity ratio is  $\gamma = \beta_x^*/\beta_y^*$ . As further detailed by PATIR [Pat78], this ellipse can also be considered as the locus of all points whose heights have the same correlation with the height of a point located at the center of the ellipse. Therefore, asperities should have roughly elliptical shapes with the given ellipticity ratio. The parameter  $\gamma$ , which is the ratio of the  $x$  and  $y$  correlation lengths, shows the degree of non-isotropy of a rough surface. A value of  $\gamma = 1$  corresponds to an isotropic surface, while the limiting cases  $\gamma = 0$  and  $\gamma = \infty$  correspond to one-dimensional transverse or longitudinal ridges. As already noted by PATIR [Pat78], the above definition of the correlation length  $\beta^*$ , which is based on the choice of a specific decay value of the ACF, is somewhat arbitrary. Therefore, the root mean square wavelength  $\lambda_{r.m.s.}$  was chosen in this work as an alternative approach that was deemed more rigorous as it goes without such arbitrary choices.

In order to assess the validity of the above described roughness modeling approach, the actual elastomer contact roughness was studied in situ on the optical test rig using the total internal reflection contact visualization technique detailed in Section 3.2.1. Due to total internal reflection at the sapphire–air interfaces, areas without contact remain dark in the reflectance images, whereas the actual elastomer–sapphire contacts are optically coupled and, therefore, result in bright areas. A corresponding white light reflectance image of the sealing contact is depicted in Figure 6.3 (dry conditions, 100× magnification, lateral imaging resolution of 0.85 μm in both directions). As detailed in Section 4.1, in order to provide a clearer image of the elastomer

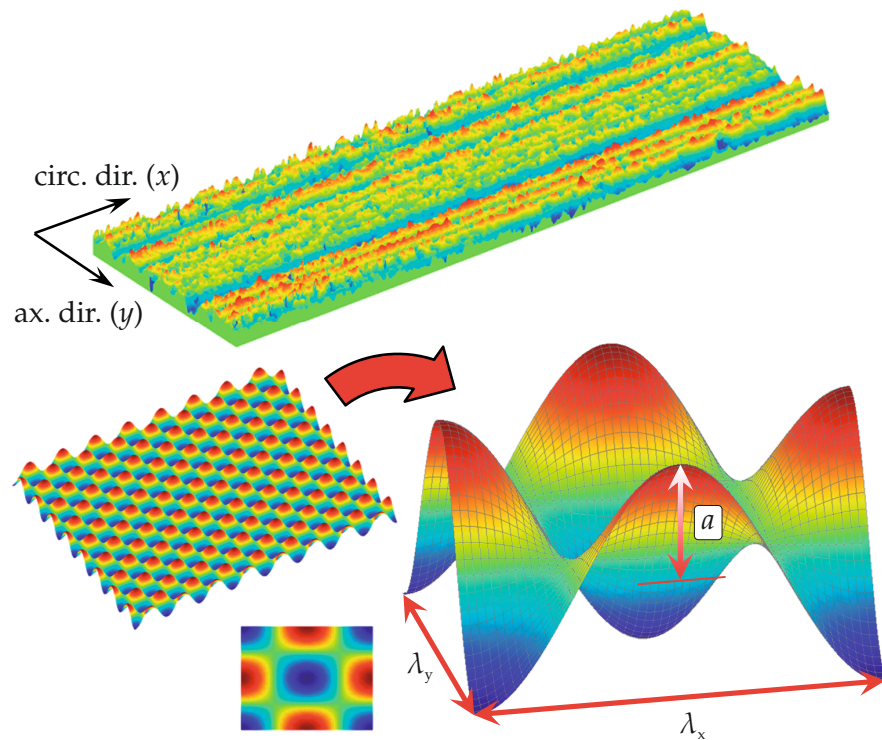


Figure 6.2: Deterministic roughness model. Reproduced from WENNEHORST AND POLL [WP14].

contact roughness, i. e., without including the circumferential surface structure of the counterface, for this image the (short-term run) seal was mounted on a smooth part of the sapphire hollow shaft. Due to the incidence angle of the illuminating light being oblique with respect to both the horizontal and the vertical symmetry plane of the sapphire hollow shaft, the overall brightness distribution of this image is slightly skewed to the lower right. It is worth noting that this overall brightness variation completely results from the illumination technique and does not reflect circumferential seal lip contact pressure fluctuations.

The total internal reflection image clearly reveals the actual elastomer contact roughness, the character of which obviously originates from the initial wear of the seal lip material (injection-molded FKM with a mineral filler), during which near-surface filler particles and filler particle agglomerates are worn away. In the above described roughness model, the asperity spacings amount to  $8.5\ \mu\text{m}$  in the diagonal and approximately  $12\ \mu\text{m}$  in both the circumferential and axial direction, respectively. Given the scale bar of  $25\ \mu\text{m}$ , which is depicted in Figure 6.3, it is very interesting to note that this range of asperity spacings obviously provides a fairly realistic estimate of the actual areal contact spot density. Therefore, following the concept of functional filtering [TS78, Tri98], the resolution of the surface measurement is deemed appropriate to allow sufficiently accurate mod-

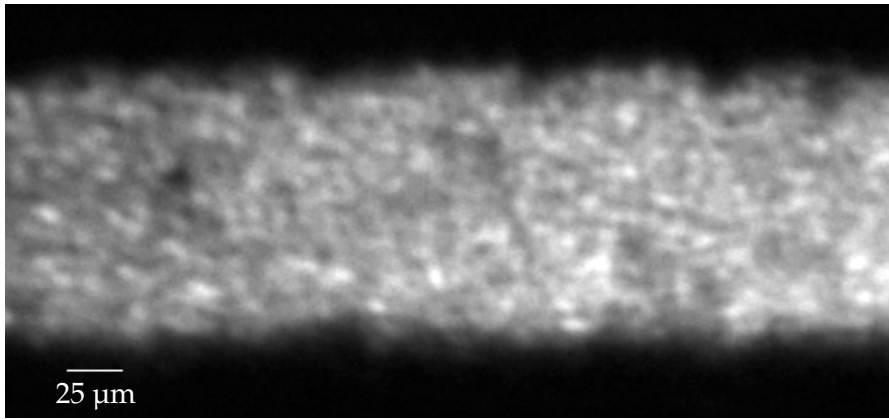


Figure 6.3: White light total internal reflection image of actual seal lip contact roughness, short-term run seal. Reproduced from WENNEHORST AND POLL [WP14].

eling of those roughness components that will govern the physical behavior of the contact.

The spacing of the model asperities is described by the effective wavelength utilizing both the root mean square height  $S_q$  and the root mean square slopes  $\Delta_{\text{r.m.s.},x/y}$  (see equation (6.7) in Table 6.1). Provided the sampling area is sufficiently large, the amplitude parameter  $S_q$  is rather insensitive to the sampling interval<sup>4</sup>. The root mean square slope, however, strongly depends on the sampling resolution and decreases significantly with increasing size of the sampling interval<sup>5</sup>. Therefore, when increasing the size of the sampling interval, the effective wavelength will increase, leading to both an increase of the asperity radii of curvatures and a reduction of the number of asperities in contact per unit area (asperity density).

If, by way of a theoretical example, the size of the sampling interval is artificially increased by using every third data point of the original seal lip surface topography (thereby increasing the sampling interval to approximately  $2.52 \mu\text{m}$  in circumferential and  $2.94 \mu\text{m}$  in axial direction, respectively), the root mean square height  $S_q$  changes by only 0.52%. The root mean square slopes, however, are reduced significantly to approximately 49% of the original value in circumferential and 59% in axial direction, respectively. Thus, the effective wavelengths increase to approximately  $25 \mu\text{m}$  in circumferential and  $20 \mu\text{m}$  in axial direction, respectively, which amounts to roughly twice the original values. Given the asperity spacings of this modified roughness pattern, amounting from  $16 \mu\text{m}$  in the diagonal to  $25 \mu\text{m}$  in circumferential direction, this coarser structure does obviously not provide a realistic estimate of the actual contact spot density seen in Figure 6.3. Nevertheless, both the asperity density, which directly relates to the normal load carried by each asperity, and the asperity radii of

<sup>4</sup> See, e. g., DONG ET AL. [DSS94a].

<sup>5</sup> See, e. g., DONG ET AL. [DSS94b].

curvatures are important parameters of micro-elastohydrodynamic asperity lubrication. Therefore, in Section 6.4.2, a coarser model will be used in a sensitivity analysis assessing the impact of roughness measurement resolution on the lubrication model results.

### 6.3 SOFT MICRO-EHL FILM THICKNESS COMPUTATION

The lubrication of the soft rough seal lip surface is described by micro- or submicron-scale soft (i. e. isoviscous-elastic) elastohydrodynamic lubrication at the asperity level. As long as the mesoscale hydrodynamic pressure generation within the drag flow over the rough surface alone is not sufficient to balance the entire external load, at nearly any nonzero sliding velocity the flattened and tangentially deformed asperities are sliding on a thin soft-EHL oil film. The thickness of this oil film is determined applying the soft-EHL central film thickness formula developed by CHITTENDEN ET AL. [CDT87] according to equations (6.9) to (6.12), which had been previously implemented by GABELLI [Gab89, Gab91]

$$H_{\text{cen}} = 8.28 \left( 1.0 - e^{\left( -0.86 \left( \frac{R_s}{R_e} \right)^{\frac{2}{3}} \right)} \right) \cdot U_e^{0.65} \cdot W_e^{-0.21}, \quad (6.9)$$

including the dimensionless groups

$$\text{Central film thickness: } H_{\text{cen}} = h_{\text{cen}}/R_e, \quad (6.10)$$

$$\text{Speed parameter: } U_e = \eta u_e / (E' R_e), \quad (6.11)$$

$$\text{Load parameter: } W_e = F / (E' R_e^2), \quad (6.12)$$

where

$h_{\text{cen}}$  (dimensional) central film thickness,

$R_e$  effective radius of curvature in the direction of lubricant entrainment (undeformed geometry),

$R_s$  effective radius of curvature in direction of lubricant side-leakage (undeformed geometry),

$\eta$  dynamic viscosity,

$E'$  equivalent elastic constant,

$u_e$  mean entrainment velocity,

$F$  normal load.

When applied to the radial lip seal contact, the direction of lubricant entrainment coincides with the circumferential (i. e.,  $x$ -) direction, and the direction of lubricant side-leakage coincides with the

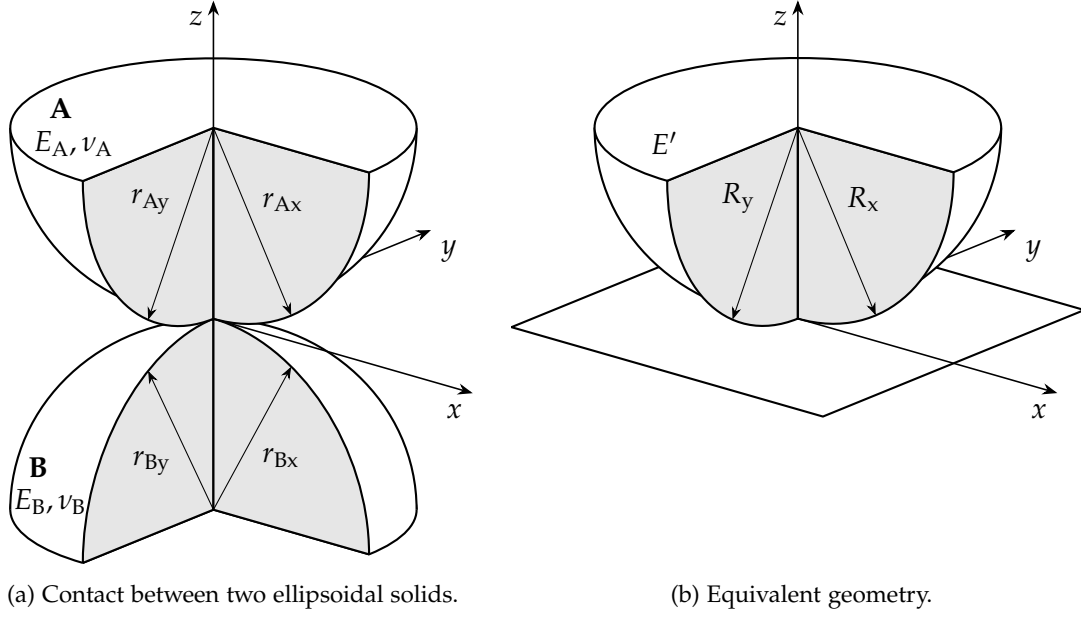


Figure 6.4: Geometry of point contacts according to CHITTENDEN ET AL. [CDT87].

axial (i. e.,  $y$ -) direction (see Figure 6.2). The effective radii of curvature  $R_e$  and  $R_s$  (i. e.,  $R_x$  and  $R_y$ , respectively) in these directions are derived from the general case of two contacting ellipsoidal solids as illustrated in Figure 6.4 according to CHITTENDEN ET AL. [CDT87].

The two contacting bodies, (A) and (B), shown in Figure 6.4 (a) are represented by an equivalent ellipsoid near a plane, as shown in Figure 6.4 (b). If the principal radii of curvature of the undeformed solids are  $(r_{Ax}, r_{Ay})$  and  $(r_{Bx}, r_{By})$ , it may be shown that to give the same separation close to the point of contact the equivalent ellipsoid has principal radii of curvature  $(R_x, R_y)$  at the contact point given by [CDT87]:

$$\frac{1}{R_x} = \frac{1}{r_{Ax}} + \frac{1}{r_{Bx}}, \quad (6.13)$$

$$\frac{1}{R_y} = \frac{1}{r_{Ay}} + \frac{1}{r_{By}}. \quad (6.14)$$

If the seal counterface is considered to be smooth the equivalent radii of curvature equate to the radii of curvature of the elastomer asperities given by equation (6.8) (see Table 6.1).

The equivalent elastic constant  $E'$  is derived from the Young's modulus of elasticity and the Poisson's ratio of the two contacting solids ( $E_A, \nu_A$ , and  $E_B, \nu_B$ ) using the relation [CDT87]:

$$\frac{2}{E'} = \frac{1 - \nu_A^2}{E_A} + \frac{1 - \nu_B^2}{E_B}. \quad (6.15)$$

The mean entrainment velocity  $u_e$ , finally, is given as the mean surface velocity [CDT87]:

$$u_e = \frac{1}{2}(u_A + u_B). \quad (6.16)$$

#### 6.4 FINITE-ELEMENT-BASED LUBRICATION MODELS

The following sections summarize the results of lubricant friction computations obtained with finite-element-based lubrication models of significantly different complexity. Both approaches, however, rely on the assumption of a rough seal lip surface sliding against a smooth counterface. This assumption, in the present study, is legitimate since both seal friction and optical lubricant film thickness measurements had been conducted simultaneously on a transparent sapphire hollow shaft featuring a surface roughness of approximately  $0.03 \mu\text{m}$  ( $R_q$ ). It is, however, worth noting that this roughness value was chosen for comparability with real run-in seal counterfaces made of steel<sup>6</sup>. Due to the fact that radial lip seal counterface roughness thus can easily be orders of magnitude smaller than seal lip surface roughness (few microns), the idealization of a smooth counterface is believed to be applicable to most practical situations. In cases where the counterface roughness cannot be neglected, the reader may refer to GABELLI [Gab89, Gab91] who modeled the combined surface roughness with statistical distribution functions applying a generalized form of the Greenwood–Tripp stochastic model for contact of two rough surfaces [GT70].

##### 6.4.1 Preliminary study neglecting hydrodynamic effects

In a first step, a drastically simplified approach has been studied neglecting hydrodynamic pressure build-up, pressure gradient effects and cavitation. Viscosity is considered to be constant throughout the entire fluid film, irrespective of local frictional heating beneath the flattened asperities. There is no fluid–structure coupling; the elastomer roughness is only normally deflected without being subject to tangential deformation due to pressure and shear. The elastomer roughness unit cell (Figure 6.2) deflection under the mean seal contact pressure is determined using the commercial finite element software ABAQUS. The elastomer is modeled as a neo-Hookean material, as described in Section 3.3. Hybrid elements are used in order to avoid volumetric locking of the finite element mesh at large compressive strains, which is a common problem particularly in the case of nearly incompressible materials [SM09]. In a next step, by means of additional MATLAB scripting, the flattened roughness model is lifted ac-

<sup>6</sup> See Section 1.1.3.



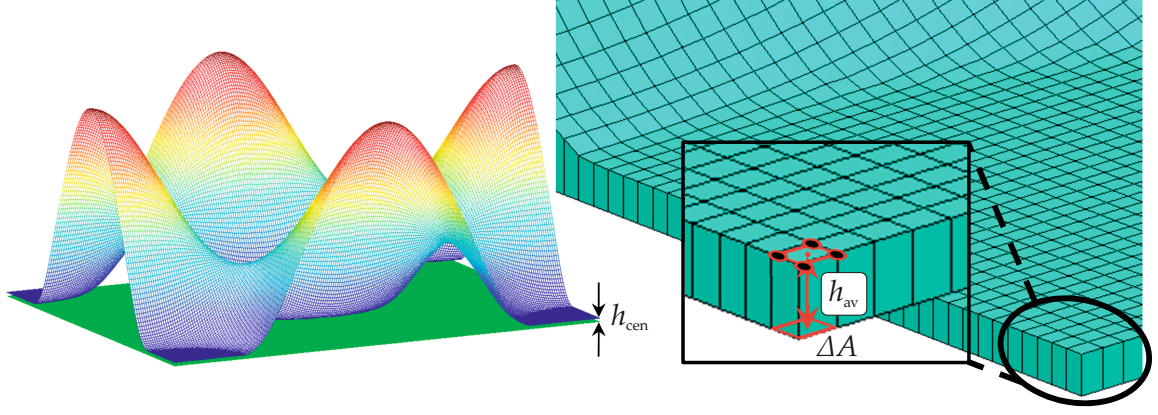


Figure 6.5: Roughness unit cell, computation of viscous lubricant friction (simplified approach). Reproduced from WENNEHORST AND POLL [WP14].

ording to the central film thickness. Then, the viscous friction torque resulting from the entire sealing contact zone is computed from the single roughness unit cell by summing all viscous friction increments over the domain according to Figure 6.5 and equation (6.17)

$$T_{\text{visc,contact}} = \left(\frac{d}{2}\right) \cdot \frac{d \cdot \pi \cdot b}{A_{\text{RUC}}} \cdot \sum_i \left( \frac{\Delta A_i \cdot \eta \cdot u}{h_{\text{av},i}} \right). \quad (6.17)$$

Using the results of the finite element analysis, the height coordinates of the deformed surface mesh are interpolated on a rectangular grid with equidistant spacing in each direction (see Figure 6.5), thereby introducing a constant shaft surface area increment  $\Delta A$ . As illustrated in Figure 6.5, for all  $i$  shaft surface area increments  $\Delta A$  on the computational domain (the roughness unit cell covering a shaft surface area  $A_{\text{RUC}}$ ), the average lubricant film thickness  $h_{\text{av},i}$  is derived from the height of the four corresponding surface nodes. The viscous lubricant friction originating from the entire roughness unit cell is then obtained by summing up all the viscous friction increments originating from the  $i$  average lubricant film thickness values and the shaft surface area increments  $\Delta A_i$ . The ratio of the entire nominal sealing contact area ( $d \cdot \pi \cdot b$ ) to  $A_{\text{RUC}}$  gives the number of cells within the sealing contact which is used to sum up the viscous friction increments from the roughness unit cells to the total viscous friction force originating from the entire sealing contact zone. The corresponding viscous friction torque is obtained by multiplication with the shaft radius ( $d/2$ ).

Finally, the viscous friction torque originating from the seal contact vicinity is added. It is derived from the measured lubricant film thickness profiles (see Figure 5.3 in Section 5.2). Its contribution to the overall measured seal friction torque is shown in Figure 6.6. Even though it does not constitute a major component of the overall friction, in order to accurately describe the frictional characteristics of

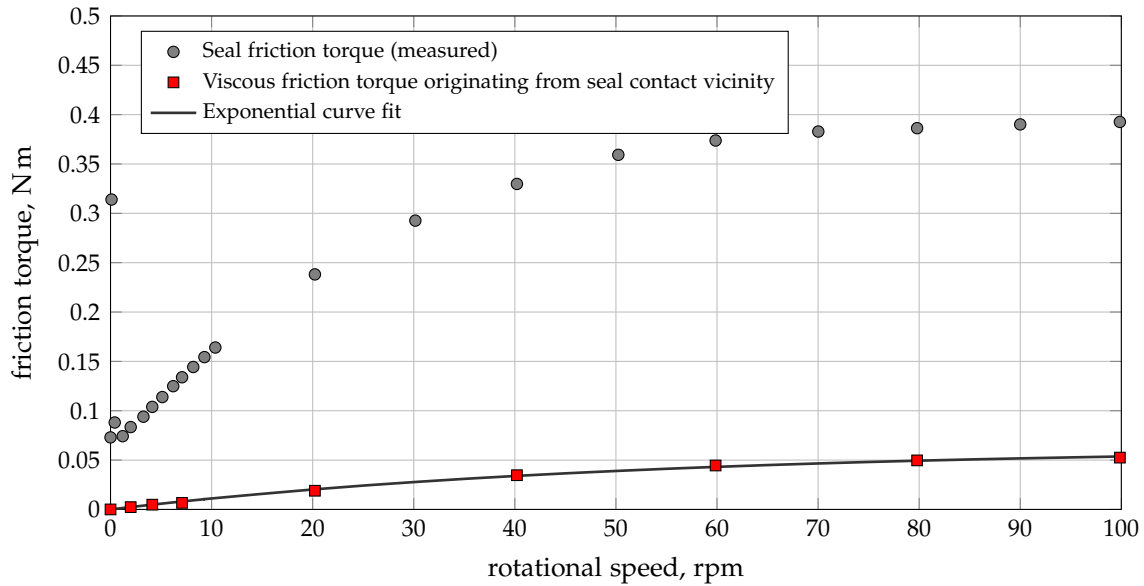


Figure 6.6: Viscous friction torque originating from seal contact vicinity (based on measured lubricant film thickness profiles). Reproduced from WENNEHORST AND POLL [WP14].

the entire sealing system its contribution obviously must be included in the friction computation.

As shown in Figure 6.7, the computed viscous lubricant friction and the measured seal friction agree fairly well, irrespective of the numerous simplifications described above. As expected, at higher sliding velocities, beyond the friction minimum, the computed friction systematically overestimates the real friction: having neglected mesoscale hydrodynamic pressure generation within the drag flow through the deformed surface roughness, there is no net lifting force counteracting the external normal load (seal radial force). Thus, due to the load parameter  $W_e$  being constant, the central EHL film thickness is underestimated resulting in unrealistically high viscous shear stresses. At the same time, due to the normal deflection of the asperities being constant, the central film thickness area under the flattened asperities (“asperity contact spot size”) is overestimated leading to unrealistically high total viscous friction values.

As described in WENNEHORST AND POLL [WP09c] (see Section 4.2.2), at very low sliding velocities below the friction minimum (see close-up in Figure 6.7), the system is subject to significant stick-slip leading to a pronounced friction maximum due to the additional rubber friction component. It is interesting to note that at such low sliding speeds the predicted soft micro-EHL central film thickness is of the order of only several nanometers and thus well below the roughness of the counterface ( $R_q \approx 0.03 \mu\text{m}$ ). Therefore, as illustrated in Figure 6.8, with decreasing sliding velocity the rigid counterface roughness increasingly interacts with the flattened elastomer asperities. Under such severe conditions, on the nanoscale more complex models are

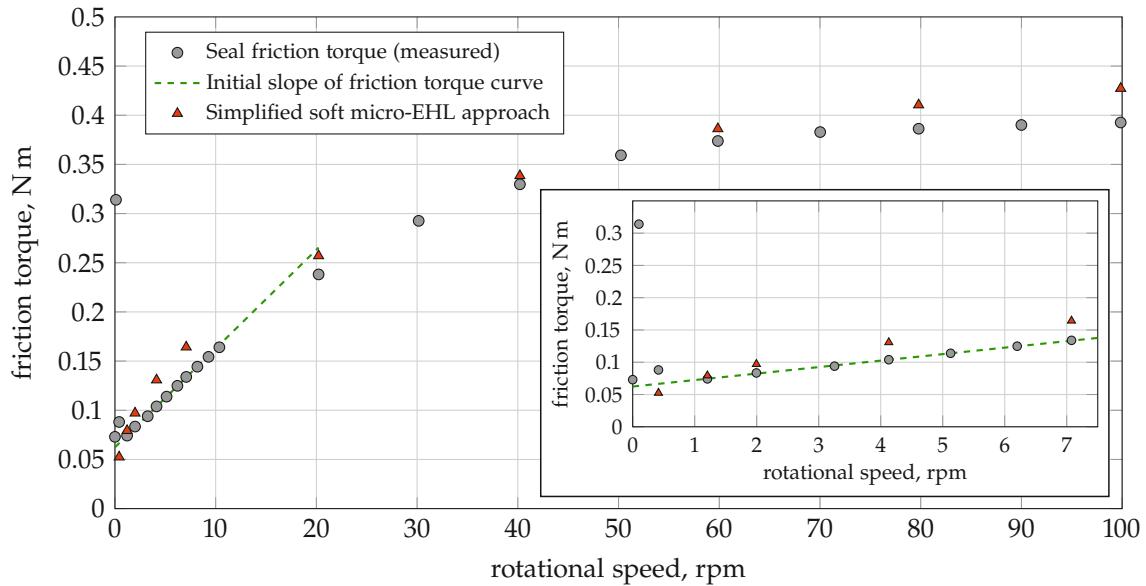


Figure 6.7: Comparison of measured overall friction torque and soft micro-EHL computation of viscous lubricant friction (simplified approach); short-term run seal, temperature-corrected viscosities. Reproduced from WENNEHORST AND POLL [WP14].

needed in order to explain the observed frictional phenomena. These models would have to include viscoelastic and hysteresis losses in the rubber due to local deformations caused by the passage of counterface asperities<sup>7</sup>.

It should be noted that within this concept the solid body friction losses in the rubber can be induced across a thin coherent elastohydrodynamic lubricant film. Therefore, even though the friction torque curve might, at first sight, resemble a classical Stribeck curve, the so-called *mixed friction regime* does not necessarily involve partial rupture of the lubricant film and a corresponding Coulomb-like friction component, nor does the so-called *viscous*, or, *hydrodynamic regime* necessarily involve a complete first order hydrodynamic unloading, i. e., hydrodynamic lift-off, of the compressed elastomer surface asperities. With increasing second order under-asperity soft micro-EHL central film thickness (which is dominated by the product  $u \cdot \eta$  of sliding velocity and viscosity, see equation (6.9)), the influence of the counterface roughness will gradually decay until smooth sliding prevails which is dominated nearly completely by viscous lubricant friction<sup>8</sup>.

<sup>7</sup> The reader may refer, e.g., to SCARAGGI AND PERSSON [SP14], or to KLÜPPEL AND HEINRICH [KH00], HEINRICH ET AL. [HKV00], PERSSON [Per01], KLÜPPEL ET AL. [KMLGH03], LINDNER [Lin05], LE GAL ET AL. [LGYK05], LE GAL [LG07], LE GAL AND KLÜPPEL [LGK08a, LGK08b], HEINRICH AND KLÜPPEL [HK08], DIMAKI AND POPOV [DP12], WANGENHEIM [Wan12], and LI ET AL. [LPD<sup>+</sup>13].

<sup>8</sup> It is interesting to note the similarity of this concept with the amplitude reduction approach used by MORA [MSLCL12, Mor14] who modeled the traction properties of tyres on wet roads. The contact of the tyre and the wet road was treated as a *macroscale* elastohydrodynamic problem with water (or the slurry formed by wa-

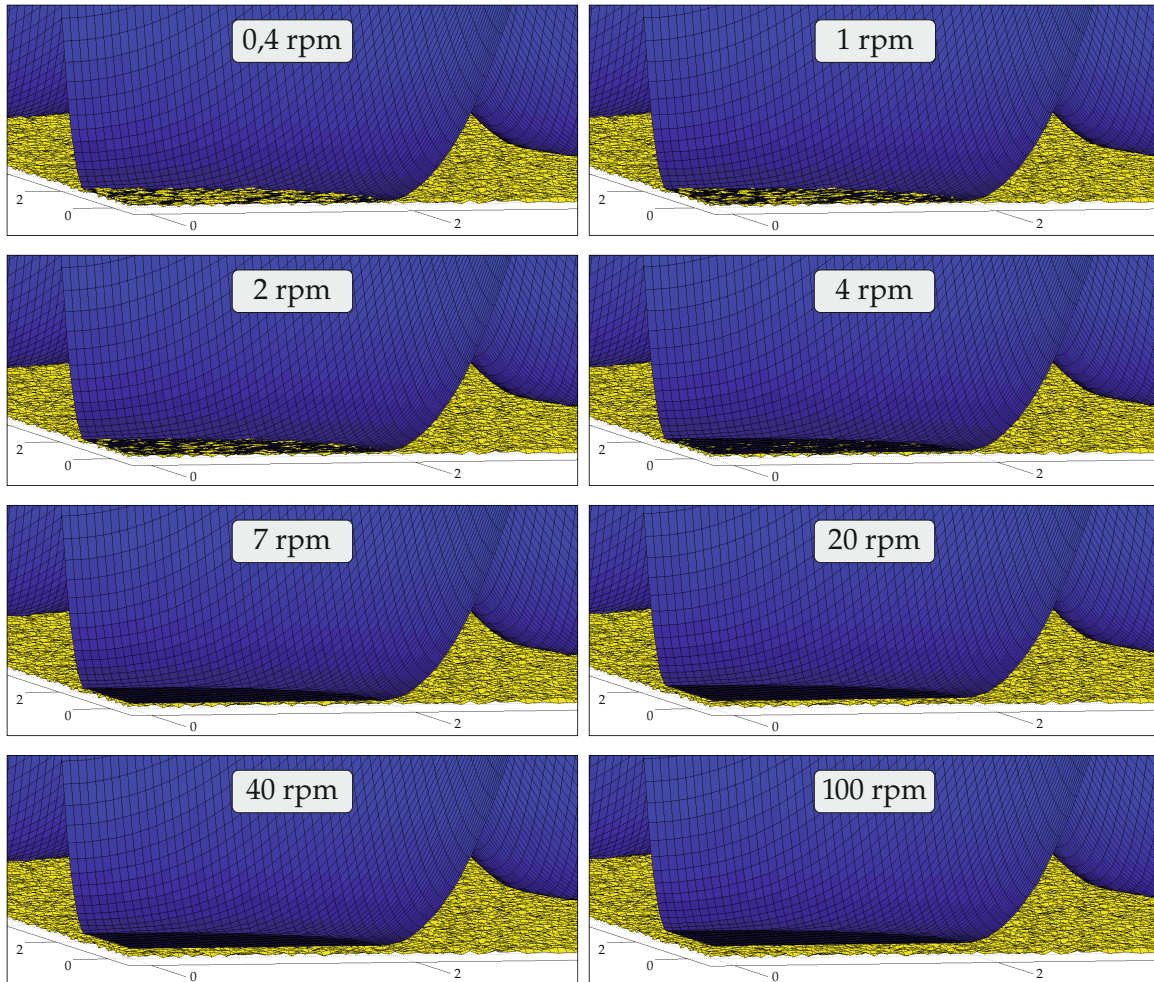


Figure 6.8: Soft micro-elastohydrodynamic lubricant film formation in elastomer asperity contacts (simplified approach; view from inside the elastomer into a quarter of the asperity contact ellipse); with decreasing product  $u \cdot \eta$  of sliding velocity and viscosity the counterface roughness increasingly interacts with the elastomer causing additional solid body friction losses in the rubber as shown in the close-up in Figure 6.7.

### 6.4.2 Sensitivity analysis

In order to further investigate the impact of the roughness measurement resolution on the results of the micro-EHL model, a sensitivity analysis was carried out using a larger roughness unit cell. As discussed in Section 6.2, when increasing the size of the sampling interval by a factor of three, due to the decreasing slope, the effective wavelengths increase to approximately  $25\ \mu\text{m}$  in circumferential and  $20\ \mu\text{m}$  in axial direction, respectively, which amounts to roughly twice the original values. At the same time the root mean square height  $S_q$  stays virtually constant. For the sake of simplicity, the roughness unit cell used in the sensitivity analysis will, therefore, use the same amplitude, and the wavelengths will be exactly twice the original values. Thus, both the total number of roughness unit cells within the sealing contact zone and the asperity density will reduce to one-fourth, the latter leading to a fourfold increase in normal load per asperity contact. According to equation (6.8) (see Table 6.1), the asperity radii of curvatures will also be increased by a factor of four. Using these new parameters, equations (6.9) to (6.12) yield a central EHL film thickness increase by a factor of  $(1/4)^{0.65} \cdot (4/16)^{-0.21} \cdot 4$ , equaling 2.17. Therefore, the fluid shear stresses within the central film thickness region will decrease by the same factor. At the same time, the asperity contact spot size increases approximately by a factor 5, according to the finite element analysis. Given the reduced asperity density, the total area of asperity contact will increase by a factor of 1.25. Therefore, the viscous lubricant friction originating from the micro-EHL central film thickness region will reduce to about 60 % of its original value. When including the viscous friction components originating from both the entire mesoscale surface roughness as well as the seal contact sides, the total seal friction torque amounts to approximately 62 % of the original value at  $2\ \text{min}^{-1}$ , 66 % at  $40\ \text{min}^{-1}$ , and 68 % at  $100\ \text{min}^{-1}$ , respectively. Therefore, the roughness measurement resolution significantly influences the results of the micro-EHL model. It should, however, be emphasized that, as demonstrated in Section 6.2, the above described sensitivity analysis is based on a roughness representation featuring an unrealistically low asperity density. Thus, the seal friction computation based on the original roughness model will be much more realistic.

### 6.4.3 Fully coupled fluid–structure interaction approach

In order to account for first order (mesoscale) hydrodynamic pressure generation as well as normal and tangential asperity deformations

---

ter and wear debris, respectively) acting as the lubricant. The elastohydrodynamic lubricant film filters out certain components of the road roughness spectrum, and, therefore, directly influences the solid body friction losses in the rubber.

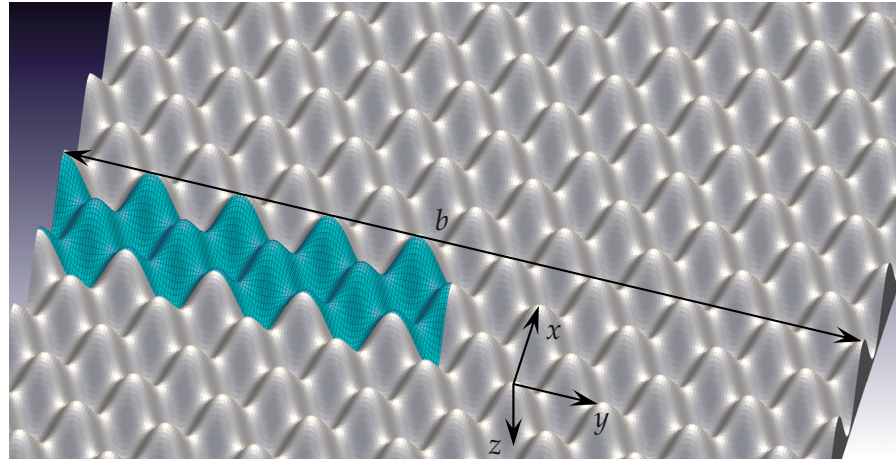


Figure 6.9: Structural model of elastomer seal lip. Reproduced from WENNEHORST AND POLL [WP14].

due to pressure and shear, a fully coupled fluid–structure interaction (FSI) model of the lip seal contact has been developed, incorporating second order soft micro-elastohydrodynamic asperity lubrication as a boundary condition submodel.

The lubrication model is set up using the finite element-based open source multiphysical simulation software ELMER. Currently, the simplified model utilizes globally averaged values of lubricant viscosity and contact pressure. The three-dimensional structural model of the elastomer seal lip according to Figure 6.9 (deterministic roughness model according to Section 6.2) thus encompasses only one half of the seal contact width in axial ( $y$ ) direction and a single wavelength in circumferential ( $x$ ) direction, making use of axial symmetry and imposing circumferential periodicity.

Again, the seal counterface is assumed to be perfectly smooth. The elastomer is modeled as a hyperelastic neo-Hookean material. The final resolution of the finite element mesh (41 472 8-node hexahedra) was determined by means of an additional mesh refinement study, gradually increasing the number of elements until the relative change of the model output parameters was negligibly small. The average dimensions of surface elements within the contact zones were approximately  $0.6\ \mu\text{m}$  in circumferential and  $0.45\ \mu\text{m}$  in axial direction, respectively.

The lubricating oil is considered to be incompressible; in order to determine the pressure distribution, the Reynolds equation<sup>9</sup>

$$\frac{\partial}{\partial x} \left( h^3 \frac{\partial p}{\partial x} \right) + \frac{\partial}{\partial y} \left( h^3 \frac{\partial p}{\partial y} \right) = 12\tilde{u}\eta \frac{\partial h}{\partial x} \quad (6.18)$$

with

$$\tilde{u} = \frac{u_A + u_B}{2} = u_e = \text{constant}$$

is solved on the fluid–structure interface. Inter-asperity cavitation is accounted for by means of the well-established Swift–Stieber cavitation zone formation conditions<sup>10</sup>

$$\frac{\partial p}{\partial x} = \frac{\partial p}{\partial y} = 0, \quad p = p_{\text{cav}}. \quad (6.19)$$

As will be discussed later, in this specific case their shortcoming of not being fully mass conservative is of minor importance. Starting from an initial surface separation the pressure field is solved and used as input for the elasticity solver. After each iteration the global radial (vertical) force balance is evaluated; from the difference of external load and hydrodynamic lifting force the soft-EHL central film thickness is derived, taking the operating parameters, the surface micro-geometry and the effective elastic properties of the contact partners into account (Table 6.2).

The momentary overall circumferential viscous friction force is utilized to calculate the average specific frictional heat, allowing for adjustment of oil film temperature and viscosity via the empirical thermal coupling scheme described in Section 4.3 (see also WENNEHORST ET AL. [WEP11]). The upper boundary of the seal lip model is then consecutively moved downward. The soft micro-EHL oil film is artificially enforced restraining the vertical displacement of the interface nodes according to the present central film thickness value. Utilizing force-feedback and an optimization routine, the displacement of the

<sup>9</sup> A comprehensive derivation of the Reynolds equation from the full set of the Navier-Stokes equations has been given, e. g., by HAMROCK ET AL. [HSJ04], see pp. 181 to 207. Equation (6.18) is the standard reduced form of the Reynolds equation for hydrodynamic (and soft elastohydrodynamic) lubrication. Here, the fluid properties do not vary significantly throughout the conjunction and thus may be considered to be constant, and the motion is pure sliding. Moreover, when applied to the configuration of the elastomer lip seal contact, only the seal counterface at  $z = 0$  moves. Thus, in the notation used in Figure 6.4,  $u_A = 0$  and  $u_B = u$ , so that the right-hand side of equation (6.18) becomes  $6u\eta \frac{\partial h}{\partial x}$ .

<sup>10</sup> These cavitation boundary conditions are also frequently referred to as Reynolds cavitation boundary conditions. For a detailed review of different models and algorithms, respectively, that are available to take into account the effect of cavitation in hydrodynamic lubrication, the reader may refer, e. g., to BRAUN AND HANNON [BH10] or SHEN AND KHONSARI [SK13].

Table 6.2: Model key parameters (short-term run seal).

Shaft diameter	$d$	0.082	m
Reference viscosities at 40 °C and 100 °C	$\nu_{40/100}$	171.92/13.35	mm <sup>2</sup> /s
Lubricant density at 15 °C	$\rho_{15}$	902	kg/m <sup>3</sup>
Equivalent elastic constant	$E'$	11.75	MPa
Seal radial force	$F_r$	14.3	N
Root mean square roughness of seal lip surface	$S_q$	4.37	μm
Effective wavelength in circumferential direction	$\lambda_{r.m.s.,x}$	12.24	μm
Effective wavelength in axial direction	$\lambda_{r.m.s.,y}$	11.84	μm
Number of undulations across seal contact	$N_y$	9	

upper boundary is iteratively adjusted until the steady-state convergence criteria of all sub-systems and the global coupled system are met so that the external seal radial force is accurately balanced by the combined reaction of this asperity EHL contact and the hydrodynamic lift. The basic concept of this iterative solution process is illustrated in Figure 6.10.

In order to provide an illustration of the final deformed configuration, in Figure 6.11 the seal contact of the short-term run seal is depicted at a rotational speed of 7 min<sup>-1</sup>. In this example, the shading corresponds to the nodal contact force.

In Figure 6.12, the computed viscous lubricant friction torque is compared to the measured seal friction torque. As expected, accounting for hydrodynamic pressure generation, cavitation as well as both normal and tangential deformations of the elastomer surface asperities, the fully coupled fluid–structure interaction model provides a far more accurate estimate of seal friction than the simplified approach. In both the simplified and the fully coupled approach the maximum fluid shear stresses consistently stay below the critical shear stress for shear thinning. It is worth noting that at the time the fluid–structure interaction model was set up, no special finite element formulation for the treatment of nearly incompressible materials was available. A comparative test case indeed revealed a stiffer structural response at the largest compressive strains when compared to the ABAQUS hybrid element formulation. As an important implication of this different numerical behavior, at very low sliding speeds, when hydrodynamic



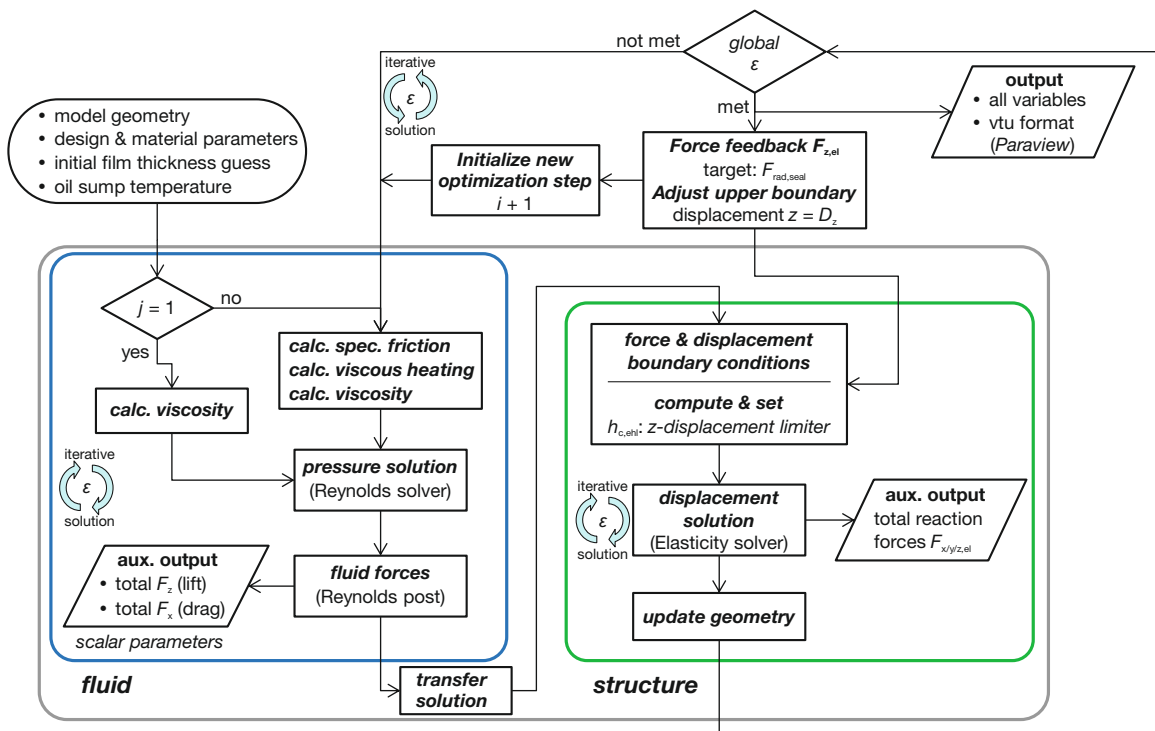


Figure 6.10: Soft micro-EHL FSI simulation flow chart. Reproduced from WENNEHORST AND POLL [WP14].

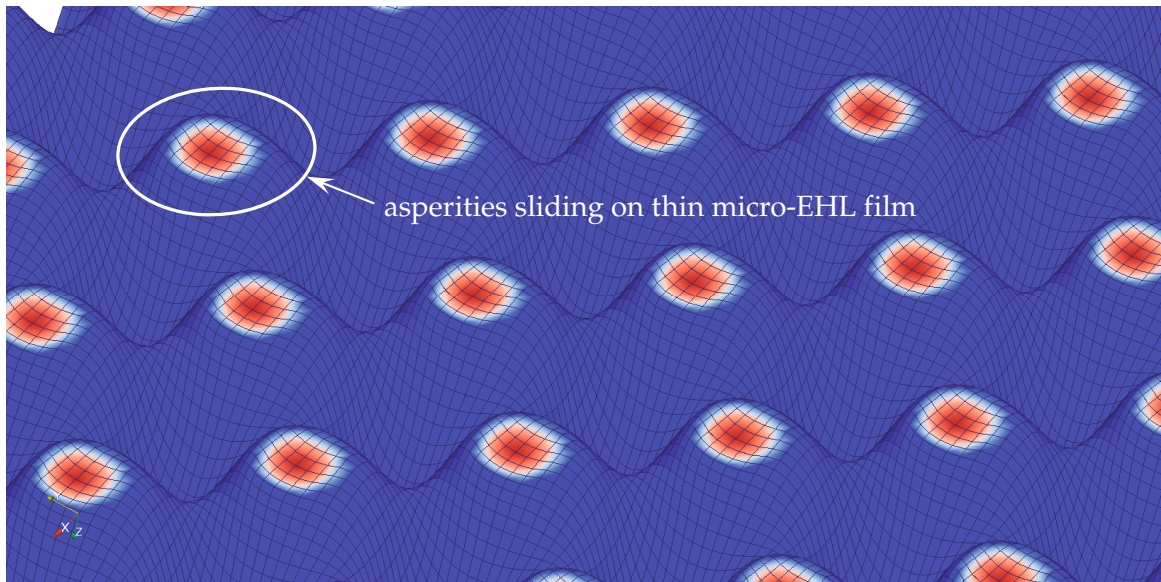


Figure 6.11: Deformed configuration at  $7 \text{ min}^{-1}$  (short-term run seal), shading corresponding to nodal contact force. Reproduced from WENNEHORST AND POLL [WP14].

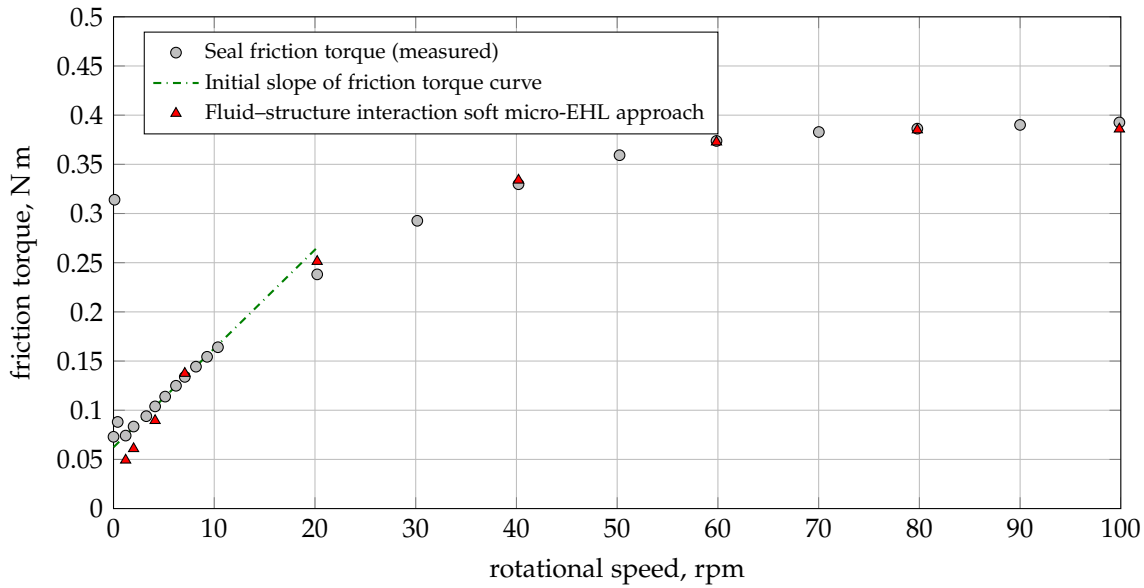


Figure 6.12: Comparison of measured overall friction torque and FSI soft micro-EHL computation of viscous lubricant friction, short-term run seal (fully coupled FSI model including empirical thermal coupling scheme according to ENGELKE [Eng11] and WENNEHORST ET AL. [WEP11]). Reproduced from WENNEHORST AND POLL [WP14].

pressures (counteracting the external load) are low, asperity normal deflection and “contact spot” size will be too small, leading to an underestimation of viscous lubricant friction.

In Figure 6.13, the ratio  $r_h$  of the hydrodynamic lifting force to the external load (seal radial force) is depicted. It is interesting to note that at a rotational speed of approximately  $1 \text{ min}^{-1}$  (corresponding to approximately  $5 \text{ mm s}^{-1}$ ), where minimum seal friction was observed, the hydrodynamic lifting force is negligibly small, indicating clearly that first order (mesoscale) micro-elastohydrodynamic lubrication does not (yet) suffice to cause any substantial unloading (i. e., lift) of the compressed elastomer roughness. Therefore, even though the seal friction is at a minimum, the seal must be considered as operating deep within the mixed lubrication regime.

The lubricant film formation mechanism of standard mixed lubrication approaches (comprising partial lubricant film rupture and a corresponding Coulomb-type friction component) largely relies on first order hydrodynamic effects; therefore, the computed friction minimum can be expected to be located at a higher sliding velocity. Evidence for this supposed systematic shift may be found in the results of SCHMIDT [Sch11] who modeled the friction and wear characteristics of hydraulic seals using a standard mixed lubrication approach based on the flow factor method. In order to verify the mixed lubrication model, the friction curves measured in tribometer tests (ball against three tilted elastomer plates) were compared with the friction curves obtained with the corresponding simulation model. The tested mate-

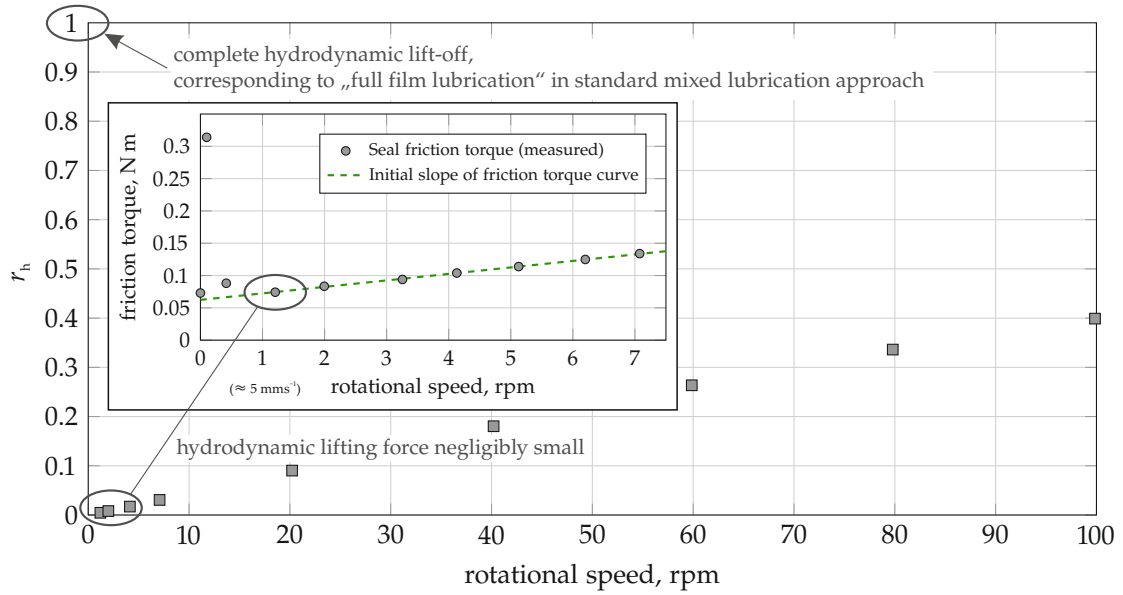


Figure 6.13: Ratio of hydrodynamic lifting force to external load, short-term run seal. Reproduced from WENNEHORST AND POLL [WP14].

rial was ultra-high-molecular-weight polyethylene (UHMW-PE), and a mixture of water and glycol was used as lubricant. In the tribometer tests, at a lubricant temperature of  $25^\circ\text{C}$  and a normal load of  $10\text{ N}$ , minimum friction was observed at a sliding velocity of approximately  $4.5\text{ mm s}^{-1}$ . The computed friction minimum, however, was located at approximately  $100\text{ mm s}^{-1}$ .

These results further underline that the revisited *second order* soft micro-elastohydrodynamic asperity lubrication mechanism is obviously capable of giving a physically sound explanation of both low-speed lubricant film formation as well as the frictional characteristics of lubricated soft rough conformal contacts in parallel sliding which inherently lack a macroscopic hydrodynamic pressure and fluid film formation mechanism. As discussed at the end of Section 6.4.1, the second order soft micro-elastohydrodynamic asperity lubrication mechanism may effectively attenuate the viscoelastic and hysteresis losses in the rubber induced by the passage of counterface asperities until the viscous lubricant friction component prevails and the overall friction increases again. It is, however, important to notice that, with regard to the underlying lubricant film formation mechanism, this transition is completely different from what is assumed when applying the concept of Stribeck curves.

In addition to the neo-Hookean hyperelastic material, further computations were carried out with a linear elastic approach in order to assess the impact of the elastomer material model on the results of the FSI soft micro-EHL model. The results of these computations are depicted in Figure 6.14 according to WENNEHORST AND POLL [WP15].

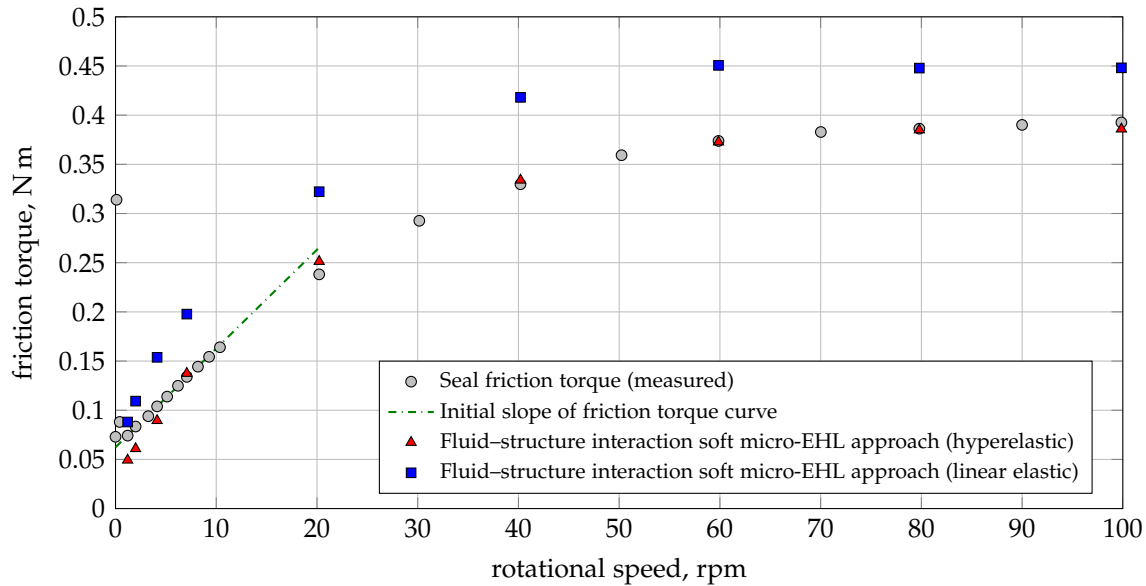


Figure 6.14: Impact of the elastomer material model on the results of the FSI soft micro-EHL seal friction computations, short-term run seal. Reproduced according to WENNEHORST AND POLL [WP15].

As expected (see Figure 3.7), the linear elastic material yields larger asperity contact spot sizes<sup>11</sup> and, therefore, leads to a systematic overestimation of seal friction compared to the hyperelastic material. With increasing rotational speed this overestimation tends to slightly decrease due to the gradual build-up of first order hydrodynamic lift (see Figure 6.13) which increasingly contributes to the total load support.

#### 6.4.4 Application to the run-in seal

In order to further assess the applicability of the above described second order soft micro-elastohydrodynamic asperity lubrication approach, additional friction computations were carried out for the run-in seal. Again, the seal lip surface roughness of the test seal was characterized using non-contacting optical profilometry. Because the white light interferometer (WYKO NT1100, see Section 6.2) was not available, the roughness measurement was carried out with a laser scanning microscope (KEYENCE VK-X200, Institute of Measurement and Automatic Control (IMR), Leibniz Universität Hannover, Germany). The lateral sampling interval was approximately  $0.7\ \mu\text{m}$  in both circumferential and axial direction and, therefore, comparable with the previous measurements. The corresponding parameters of the bi-sinusoidal roughness model as well as its geometric representa-

<sup>11</sup> This is consistent with results reported by SCARAGGI AND CARBONE [SC12].

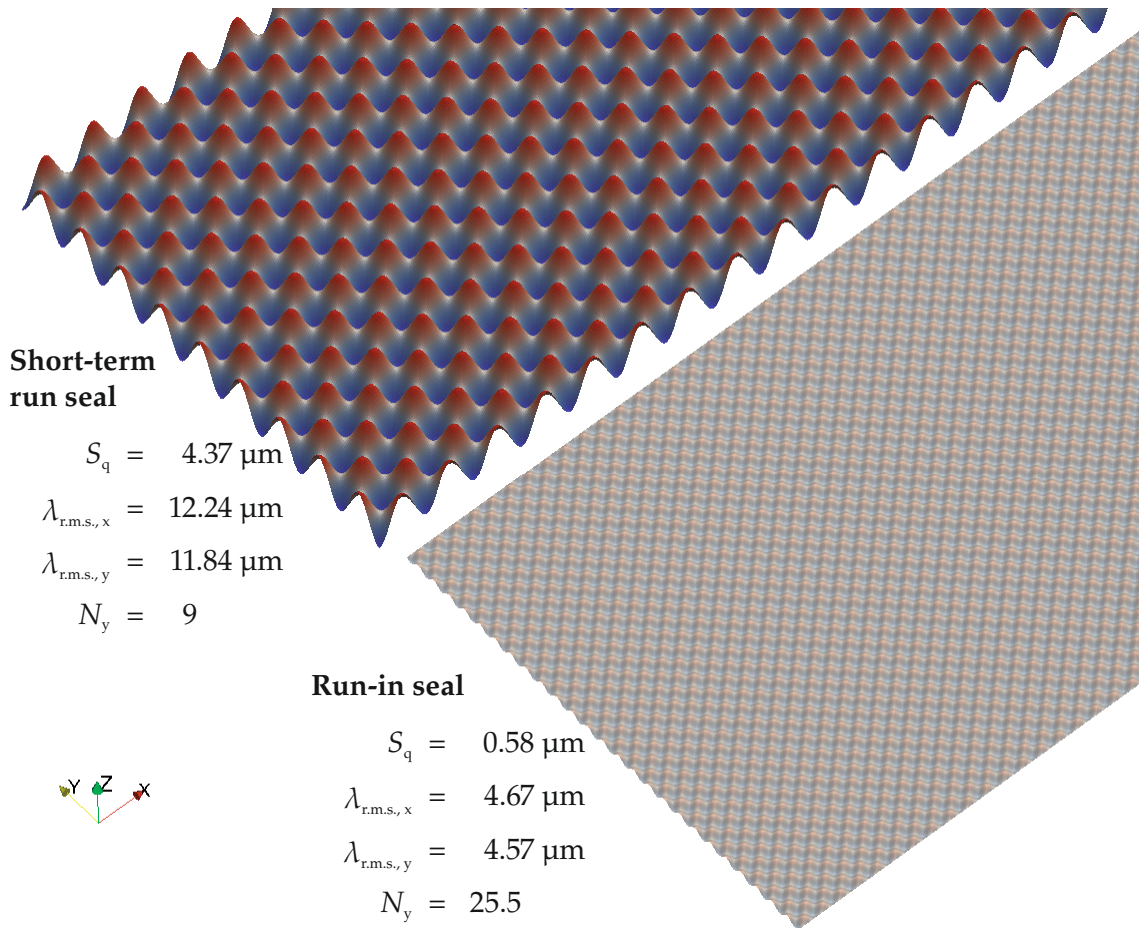


Figure 6.15: Bi-sinusoidal roughness model of run-in seal in comparison with corresponding model of short-term run seal. Reproduced according to WENNEHORST AND POLL [WP15].

tion are shown in Figure 6.15 in comparison with the short-term run seal.

With regard to the key parameters of the soft micro-elastohydrodynamic asperity lubrication model it is important to remember that the seal radial force did not differ among the short-term run and the run-in test seals (see Table 6.2 and Section 3.3). Given the reduced root mean square wavelengths and the correspondingly increased asperity density of the run-in seal, the load carried by a single asperity of the run-in seal is, therefore, appreciably smaller compared to the short-term run seal. At the same time the ratio of amplitude to wavelength of the run-in seal is smaller, compared to the short-term run seal, which further aids in the build-up of the hydrodynamic lubricant film. Thus, at a given constant seal radial force, due to the altered roughness characteristics the overall lubricant film formation of the run-in seal will be improved compared to the short-term run seal. It is further interesting to note that the model asperities of the run-in seal are still nearly circular in shape. Therefore, the run-in

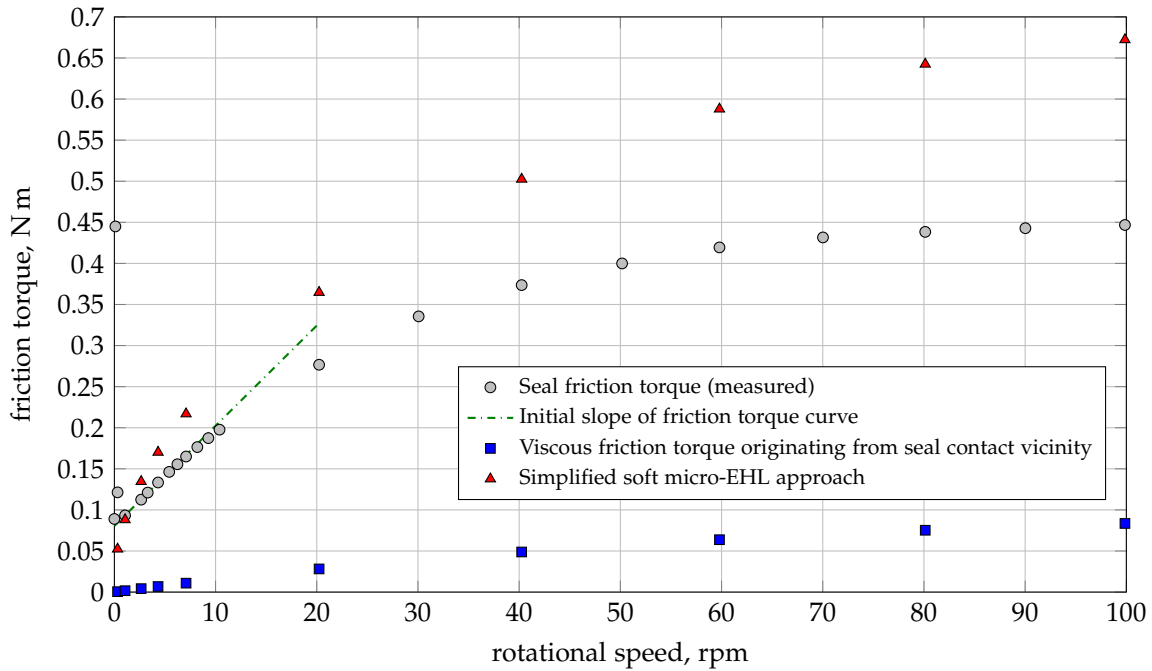


Figure 6.16: Comparison of measured overall friction torque and soft micro-EHL computation of viscous lubricant friction (simplified approach); run-in seal, temperature-corrected viscosities.

process, at least with this seal elastomer compound, did not induce axially oriented asperities with an ellipticity ratio smaller than one, as previously observed by KAMMÜLLER [Kam86].

In Figure 6.16, the computational results based on the simplified approach (neglecting first order hydrodynamic effects) are compared to the measured seal friction torque. As expected, at higher sliding velocities (beyond the linear region of the measured friction torque curve), when using the simplified soft micro-EHL approach neglecting first order hydrodynamic effects, the systematic overestimation of the seal friction torque is noticeably greater for the run-in seal compared to the short-term run seal (see Figure 6.7). This provides further indirect evidence of the improved lubricant film build-up characteristics of the run-in seal that have been demonstrated through the results of the LIF lubricant film thickness measurements described in Section 4.2.1.

As shown in Figure 6.17, for the run-in seal, too, the fully coupled FSI soft micro-EHL model provides a far more accurate estimate of the seal friction torque than the simplified approach. As explained above, the linear elastic material leads to a systematic overestimation of seal friction compared to the hyperelastic material. However, due to the improved hydrodynamic load bearing capacity and the correspondingly reduced radial asperity deformations (i. e., deformations in  $z$  direction), with increasing rotational speed this overestimation is less pronounced compared to the short-term run seal. This follows

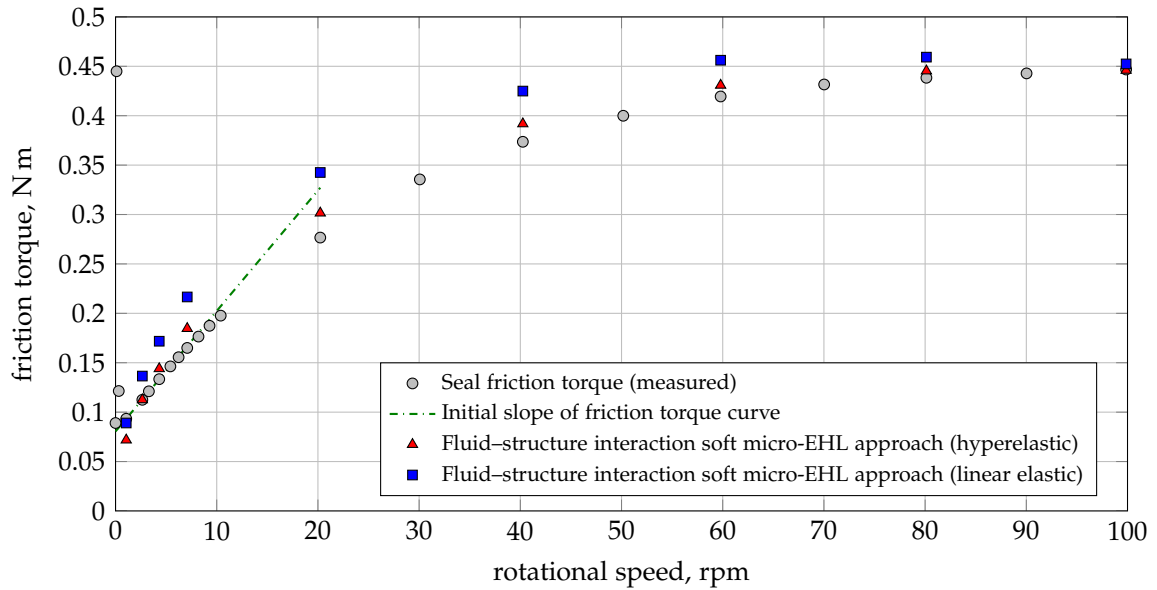


Figure 6.17: Comparison of measured overall friction torque and FSI soft micro-EHL computation of viscous lubricant friction, run-in seal (fully coupled FSI model including empirical thermal coupling scheme according to ENGELKE [Eng11] and WENNEHORST ET AL. [WEP11]). Reproduced according to WENNEHORST AND POLL [WP15].

also directly from the ratio  $r_h$  of the hydrodynamic lifting force to the external load (seal radial force) which is depicted in Figure 6.18 for both seals, additionally including the results obtained with the different material modeling approaches. In contrast to the seal lip surface roughness characteristics, which strongly influence the build-up of first order hydrodynamic lift, the latter depends only weakly on the choice of the elastomer material modeling approach. Regarding the enhanced load bearing capacity of the run-in seal, which amounts to approximately 85% at a rotational speed of  $100 \text{ min}^{-1}$  (corresponding to a sliding velocity of approximately  $0.5 \text{ m s}^{-1}$ ), it should be remembered that the corresponding low-speed measurements were carried out at room temperature using a lubricating oil with relatively high reference viscosities. Therefore, as shown in Figure 4.15, at a rotational speed of  $100 \text{ min}^{-1}$  the maximum temperature within the sealing contact zone of the run-in seal was only  $30^\circ\text{C}$  with a corresponding dynamic viscosity of about  $300 \text{ mPa s}$ . At more realistic oil sump temperatures and sliding velocities, due to frictional heating the lubricant viscosity within the sealing contact zone will be drastically reduced to a small fraction of this value. For example, as shown by ENGELKE [Eng11] (for standard oil seals) and OTTINK [Ott14] (for the seal type used here), based on an oil sump temperature of  $80^\circ\text{C}$ , at sliding velocities of  $5 \text{ m s}^{-1}$  to  $10 \text{ m s}^{-1}$  the temperature within the sealing contact zone may easily exceed  $100^\circ\text{C}$ . Under these conditions, according to the temperature–viscosity characteristics of the mineral base oil used here (see Figure 3.9), the dynamic viscosity will

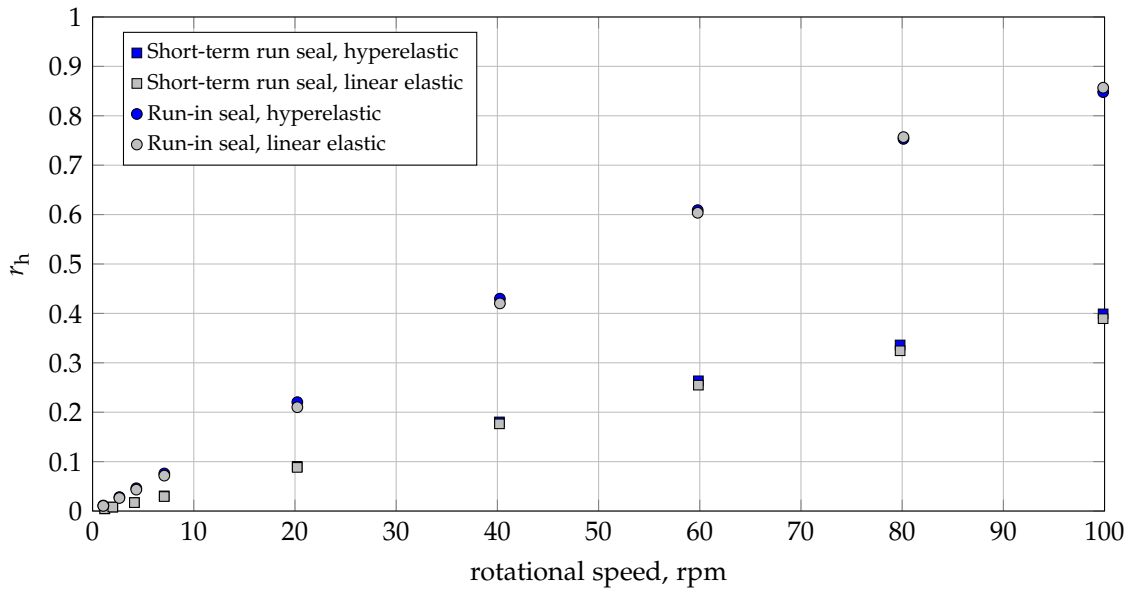


Figure 6.18: Ratio of hydrodynamic lifting force to external load, comparison of short-term run seal and run-in seal. Reproduced according to WENNEHORST AND POLL [WP15].

be on the order of only 10 mPa s. However, both first order as well as second order micro-elastohydrodynamic lubricant film build-up strongly depend on the product  $u \cdot \eta$  of sliding velocity and viscosity. Therefore, even under realistic conditions of high sliding velocities, in many practical situations the drop of the lubricant viscosity within the sealing contact zone can be assumed to prevent  $r_h$  (the ratio of hydrodynamic lifting force to external load) from approaching one, i. e., the seal will continue to operate under mixed lubrication conditions. When the sliding velocity is further increased, the fluid shear stress may locally (especially within the second order under-asperity lubricant films) exceed the critical shear stress for the onset of shear thinning; this impedes the lubricant film formation further. Moreover, when the fluid shear stress is larger than the asperity contact pressure, the lubricant film may rupture locally due to shear cavitation.

The lubricant film formation of the run-in seal is illustrated in Figure 6.19 for the rotational speed steps used in Figure 6.18. The cross-sections of a single asperity depicted herein are based on the actual deformed geometry of the run-in seal lip structural model as computed with the fully coupled FSI soft micro-EHL approach. As shown in Figure 6.19, at very low sliding velocities, where minimum friction was observed, the lubrication of the contraformal Hertzian asperity contacts is nearly completely governed by second order micro-EHL. With increasing speed, however, first order micro-EHL effects become more and more important, and the corresponding asperity



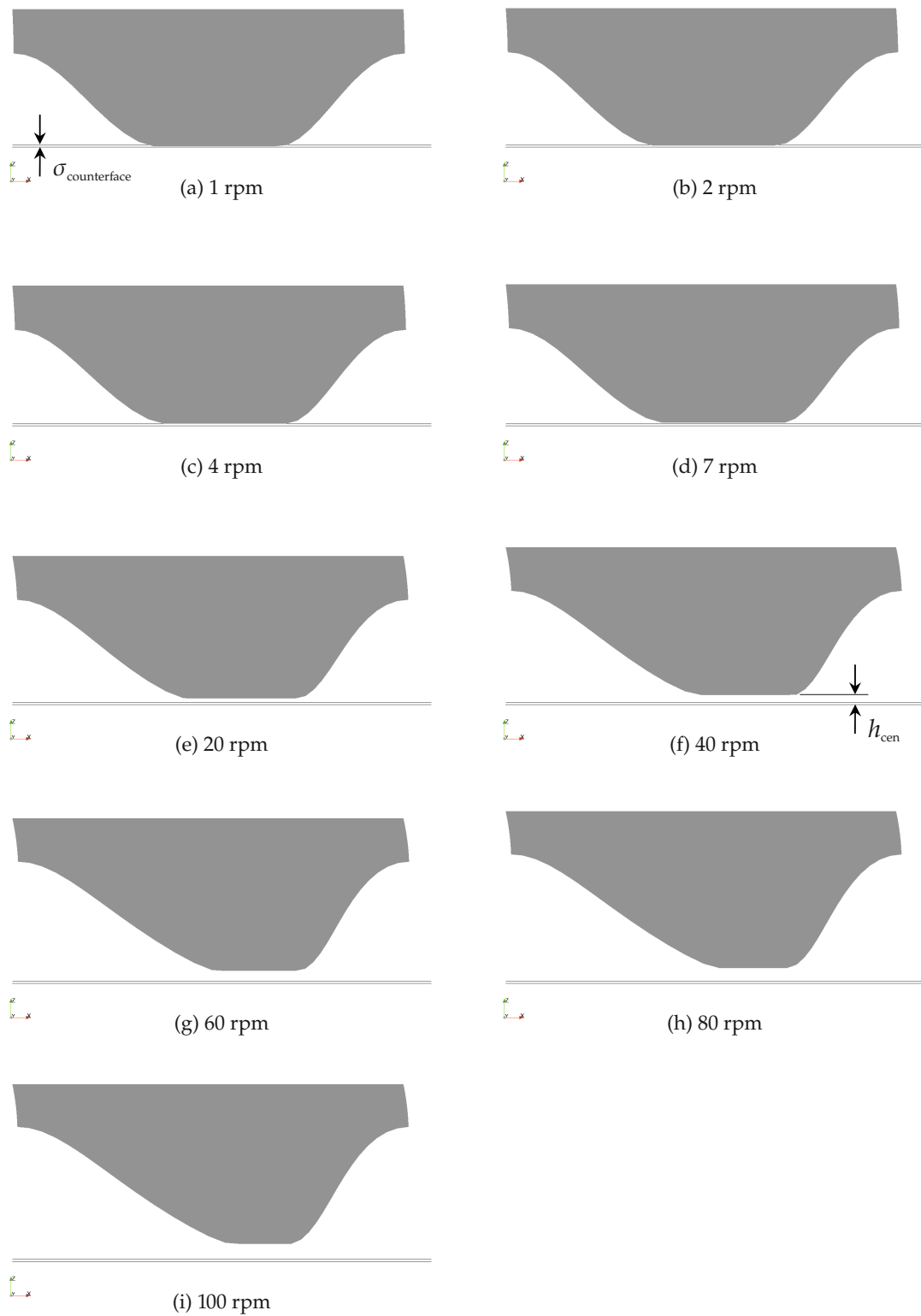


Figure 6.19: Lubricant film formation of run-in seal. Cross-sections of a single asperity, based on actual deformed geometry of seal lip structural model as computed with fully coupled FSI soft micro-EHL approach. Reproduced according to WENNEHORST AND POLL [WP15].

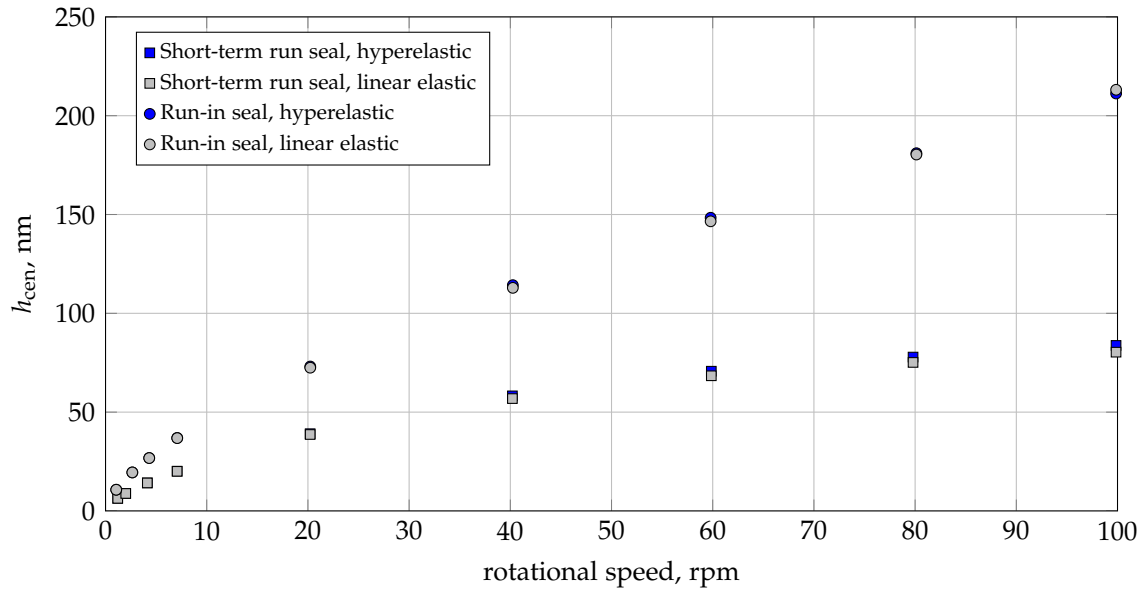


Figure 6.20: Second order under-asperity central elastohydrodynamic lubricant film thickness of short-term run seal and run-in seal.

micro-wedge formation contributes increasingly to the overall hydrodynamic load bearing capacity of the lubricant film<sup>12</sup>.

The enhanced first order hydrodynamic load bearing capacity of the run-in seal can also be seen indirectly from Figure 6.20, where the build-up of the second order under-asperity central elastohydrodynamic lubricant film thickness  $h_{\text{cen}}$  is shown for both the short-term run and the run-in seal. At higher rotational speeds beyond approximately  $40 \text{ min}^{-1}$  to  $60 \text{ min}^{-1}$ , due to the correspondingly reduced asperity normal load the central EHL film thickness increase of the run-in seal is noticeably steeper compared to that of the short-term run seal. The second order central EHL film thickness depends only weakly on the choice of the elastomer material modeling approach, and the qualitative trends are consistent with the results obtained for the ratio  $r_h$  of hydrodynamic lifting force to external load (see Figure 6.18).

Figure 6.21 shows the computed dynamic lubricant viscosity within the sealing contact zone. As explained in Section 4.3, it is based on the seal under-lip excess temperature which is empirically coupled to the specific seal friction via the iterative scheme proposed by ENGELKE [Eng11]. Starting out from a slightly lower oil sump temperature prior to the experiments, the overall viscosity level during the measurements with the run-in seal is higher compared with the short-term run seal. Nevertheless, the qualitative trends of both seals are very similar. As expected, the impact of the elastomer material mod-

<sup>12</sup> It is interesting to note the similarity with the experimental results of FOWELL ET AL. [FMSK14].

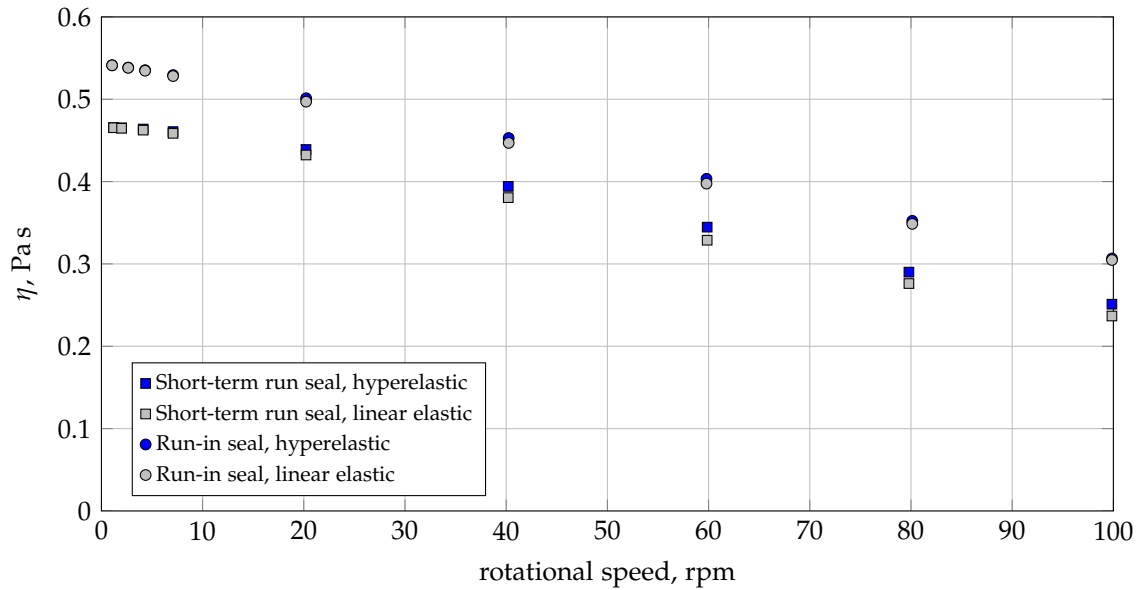


Figure 6.21: Computed dynamic lubricant viscosity within sealing contact zone of short-term run seal and run-in seal.

eling approach on the results of the viscosity computations is more pronounced for the short-term run seal. This is consistent with the results of the seal friction computations shown in Figures 6.14 and 6.17.

Figure 6.22 shows the maximum fluid shear stress  $\tau_{\max} = \eta \cdot u / h_{\min}$  resulting from the smallest gap height and, therefore, directly relating to the second order under-asperity elastohydrodynamic lubricant film thickness  $h_{\text{cen}}$ . For both the short-term run seal and the run-in seal the impact of the elastomer material modeling approach on the computational results is small, being qualitatively consistent with those obtained for the second order under-asperity central elastohydrodynamic lubricant film thickness  $h_{\text{cen}}$  and the dynamic lubricant viscosity  $\eta$  shown in Figures 6.20 and 6.21. In contrast to the short-term run seal, the maximum fluid shear stress within the sealing contact zone of the run-in seal passes through a maximum located at a rotational speed of approximately  $60 \text{ min}^{-1}$ . For the given set of operating parameters (i. e., sliding velocities, oil sump temperatures and thermal viscosity characteristics), and given the very similar viscosity decay rate of the short-term run and the run-in seal according to Figure 6.21, this maximum follows directly from the enhanced first order hydrodynamic load support observed with the run-in seal which, as described above and shown in Figures 6.19 and 6.20, becomes operative at rotational speeds of approximately  $40 \text{ min}^{-1}$  to  $60 \text{ min}^{-1}$ . The maximum fluid shear stresses consistently stay below the critical shear stress for shear thinning; they are also consistently below the mean asperity contact pressure which is of the same order as the critical shear stress for shear thinning. Therefore, under the given

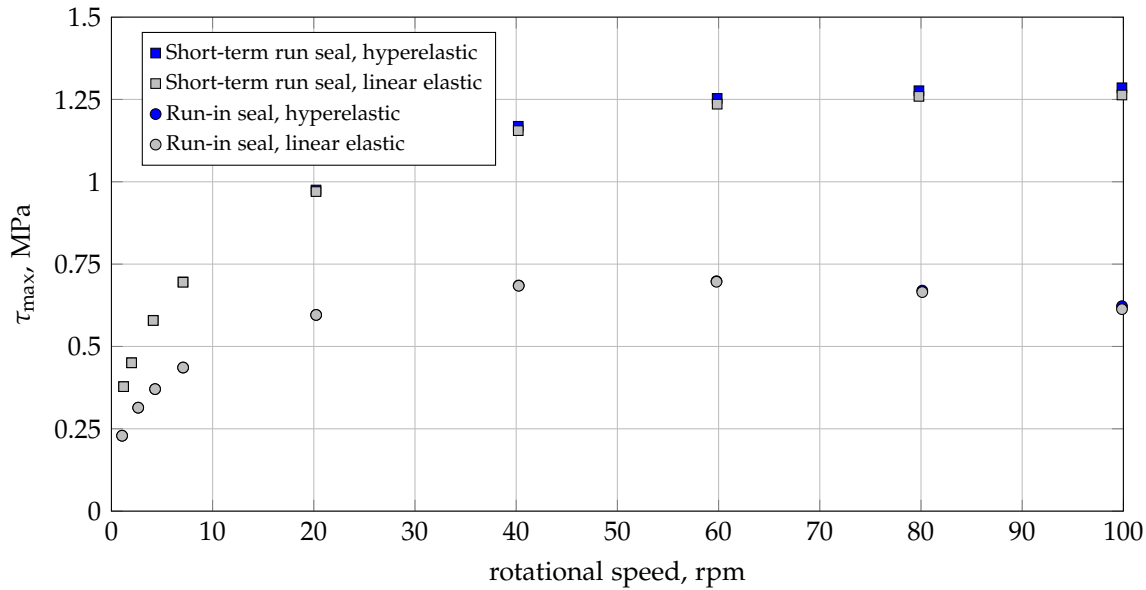


Figure 6.22: Maximum fluid shear stress within contact zone of short-term run seal and run-in seal.

conditions the lubricant can be considered to behave Newtonian, and shear cavitation is not expected to occur.

#### 6.4.5 Further validation on a steel shaft

So far the computational results obtained with the second order soft micro-elastohydrodynamic mixed lubrication approach have been compared to the results of seal friction measurements carried out on the optical test rig (see Section 3.1), using a transparent sapphire hollow shaft as the seal counterface. As explained in Section 3.1, due to its high thermal conductivity being similar to that of steel, sapphire was chosen instead of glass in order to avoid heat accumulation within the sealing contact zone and a corresponding unrealistic drop of the lubricant viscosity. The surface finish of the sapphire hollow shaft was chosen to be comparable with real run-in seal counterfaces (see also Section 6.4), and its wettability was confirmed to be comparable to that of steel counterfaces made of 100Cr6 bearing steel. Thus, based on the good comparability between the sapphire model system and the real application, the empirical thermal coupling scheme described in Section 4.3, providing the seal under-lip excess temperature as a function of specific seal friction, was deemed applicable for both steel and sapphire counterfaces. Therefore, when using a counterface made of steel with a comparable roughness, seal friction computations based on the above FSI second order soft micro-EHL model can be expected to be of comparable accuracy.

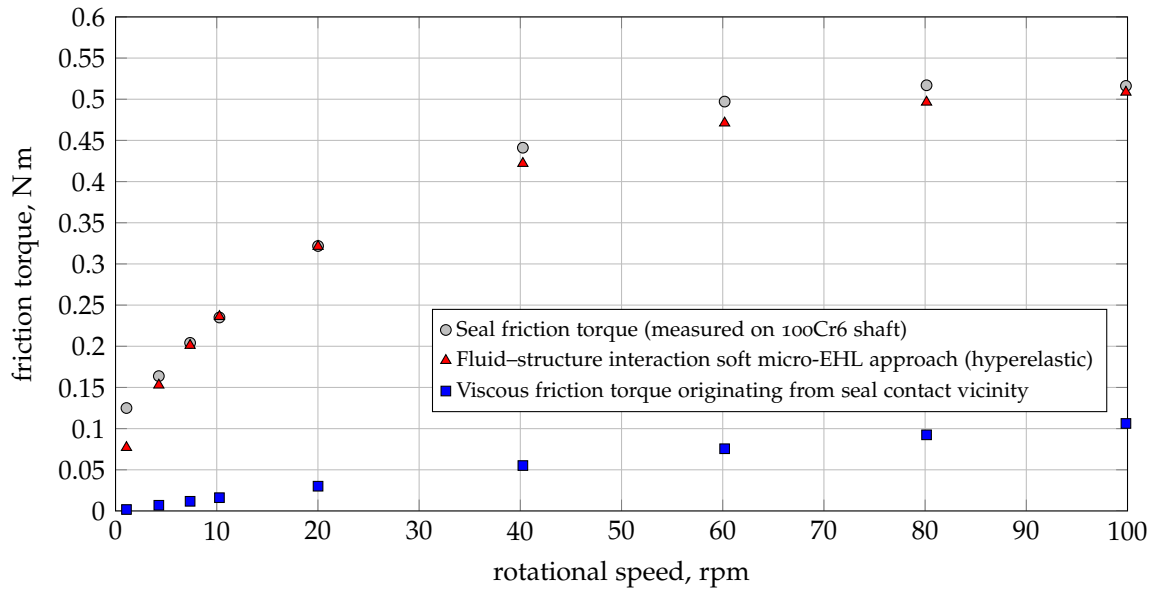


Figure 6.23: Comparison of seal friction torque measured on 100Cr6 counterface and FSI soft micro-EHL computation of viscous lubricant friction, run-in seal (fully coupled FSI model including empirical thermal coupling scheme according to ENGELKE [Eng11] and WENNEHORST ET AL. [WEP11]).

In order to assess the validity of this assumption, a further series of seal friction measurements in the range of  $1 \text{ min}^{-1}$  to  $100 \text{ min}^{-1}$  were made with the run-in seal and a counterface made of 100Cr6. The steel shaft was ground to a roughness of  $0.14 \mu\text{m}$  ( $S_q$ ). When measured in circumferential direction, i. e., in the direction of sliding, the roughness was considerably smaller, amounting to  $0.03 \mu\text{m}$  ( $R_q$ ) and, therefore, equaling the roughness of the sapphire hollow shaft<sup>13</sup>. As in the previous speed step experiments, the oil sump temperature was measured in the direct vicinity of the sealing contact. As shown in Figure 6.23, for the 100Cr6 counterface the FSI soft micro-EHL model predicts seal friction to an accuracy being indeed comparable to that obtained with the sapphire counterface.

<sup>13</sup> In contrast to the brittle fracturing of sapphire yielding an isotropic surface roughness structure, plunge grinding of the steel shaft yields an anisotropic surface roughness structure. Here, the axially measured roughness, directly relating to the grain size of the grinding wheel, can be noticeably larger compared to that measured in circumferential direction, i. e., along the grinding grooves. As noted in Section 1.1.3, with regard to the radial lip seal system this was previously described by KUNSTFELD [Kun05].



---

## CONCLUSION AND OUTLOOK

---

The experimental results of this work clearly show, and confirm previous findings, that the friction of elastomeric radial lip seals may be at a minimum under conditions where speed-dependent first order hydrodynamic lubricant film build-up effects are far too small to completely separate the seal lip surface asperities from the shaft. Thus, when passing through such a friction minimum, there is no transition to full-film lubrication in the classical sense, and the friction curve is, therefore, something very different from what is usually referred to as a “Stribeck” curve. Obviously, the seals are consistently running in a mode of mixed lubrication, where the elastomer seal lip surface asperities are still compressed, but, at the same time, are in a continuously lubricated sliding condition without indication of dry contact.

Semiempirical computations of the viscous lubricant friction component based on measured average lubricant film thickness profiles further demonstrate that the resulting viscous friction component alone consistently underestimates the measured seal friction. By accounting for the impact of film thickness averaging effects on the results of these semiempirical computations, it is argued that the flattened elastomer asperities and the counterface may be separated by thin micro-elastohydrodynamic lubricant films. The thickness of these second order films is expected to be appreciably smaller than the contact roughness of the elastomer seal lip surface, and the viscous lubricant friction originating from such films could make up for the difference observed between the measured seal friction and the results of the semiempirical computations.

In view of the experimental and semiempirical results, a finite element based fluid–structure interaction soft micro-elastohydrodynamic mixed lubrication model has been developed comprising elastic deformations of the elastomer surface asperities, inter-asperity cavitation and coupling of frictional heating, lubricant film temperature and lubricant viscosity. The computed seal friction agrees well with the experimental results. Even at the lowest sliding speeds, when the first order hydrodynamic lifting force is negligibly small, the soft micro-elastohydrodynamic asperity lubrication mechanism is obviously capable of giving a physically sound explanation of both

low-speed lubricant film formation as well as the frictional characteristics of lubricated soft rough surfaces in parallel sliding. This contrasts remarkably with widely adopted mixed lubrication approaches comprising local rupture of the lubricant film and a corresponding Coulomb-type boundary friction component. In the approach described in this work, there is no need for additional empirical parameters, such as the boundary friction coefficient, which require additional experimental effort prior to any computation. Instead, the model entirely relies on geometry and material parameters that can be determined separately.

It is shown that at the lowest sliding velocities, when the thickness of the second order under-asperity lubricant films is below the roughness of the counterface, the hard substrate roughness increasingly interacts with the flattened elastomer asperities, giving rise to a steep increase in seal friction. Under such severe conditions, on the nanoscale more complex models are needed in order to explain the observed frictional phenomena. These models would have to include viscoelastic and hysteresis losses in the rubber due to local deformations caused by the passage of counterface asperities. Within the proposed mixed lubrication concept the solid body friction losses in the rubber can be induced across a thin coherent elastohydrodynamic lubricant film. Therefore, even though the friction torque curve might, at first sight, resemble a classical Stribeck curve, the so-called *mixed friction regime* does not necessarily involve partial rupture of the lubricant film and a corresponding Coulomb-type friction component, nor does the so-called *viscous*, or, *hydrodynamic regime* necessarily involve a complete first order hydrodynamic unloading, i. e., hydrodynamic lift-off, of the compressed elastomer surface asperities. With increasing thickness of the second order under-asperity lubricant films, the influence of the counterface roughness, i. e., the rubber solid body friction component, will gradually decay until smooth sliding prevails which is dominated nearly completely by viscous lubricant friction. As further demonstrated, the build-up of the second order under-asperity lubricant films is tightly linked to the first order hydrodynamic micro-wedge formation on the level of the seal lip surface roughness.

Ongoing work is focused on further improving the accuracy of the computational approach. With regard to very low sliding speeds, this involves the implementation of hybrid finite element formulations allowing for a more accurate treatment of nearly incompressible materials undergoing large compressive strains. To capture the first order hydrodynamic effects more accurately at high sliding speeds, a fully mass conservative cavitation algorithm is used. Experimental and theoretical work focuses on a deeper understanding of the impact the elastomer material properties and the surface micro-geometries have



on the asperity lubrication mechanism and on the characteristics of the rubber solid body friction component.

The findings of this dissertation are not limited to the elastomer shaft seal application, but may also prove useful for studies of other soft rough conformal sliding contacts as, e.g., found in biotribological systems such as natural synovial joints and artificial joint replacements.



---

## BIBLIOGRAPHY

---

- [ACP00] AMABILI, M. ; COLOMBO, G. ; PRATI, E.: Leakage of radial lip seals at large dynamic eccentricities. In: *Proc. 16th Int. Conf. on Fluid Sealing: Successful Sealing* BHR Group Limited, Bury St. Edmunds; Professional Engineering Publishing, 2000 (BHR Group Conference Series Publication No. 42), p. 321–334
- [Adr91] ADRIAN, R.J.: Particle-imaging techniques for experimental fluid mechanics. In: *Annual Review of Fluid Mechanics* 23 (1991), Issue 1, p. 261–304
- [ASTM2502] *ASTM D 2502–92 (reapproved 2004). Standard Test Method for Estimation of Molecular Weight (Relative Molecular Mass) of Petroleum Oils From Viscosity Measurements.* Philadelphia, USA, 2004
- [AWA68] ANNO, J.N. ; WALOWIT, J.A. ; ALLEN, C.M.: Microasperity lubrication. In: *Journal of Lubrication Technology* 90 (1968), Issue 2, p. 351–355
- [Azu06] AZUSHIMA, A.: In situ 3D measurement of lubrication behavior at interface between tool and workpiece by direct fluorescence observation technique. In: *Wear* 260 (2006), Issue 3, p. 243–248
- [Bag86a] BAGLIN, K.P.: Elastohydrodynamic pressure rippling in cylinders finished with a circumferential lay. In: *Proceedings of the Institution of Mechanical Engineers, Part C: Journal of Mechanical Engineering Science* 200 (1986), Issue 5, p. 335–347
- [Baio7] BAIR, S.S.: *High pressure rheology for quantitative elastohydrodynamics.* Amsterdam: Elsevier, 2007
- [Bar96] BARZ, M.: *Die Schmierfilmbildung in fettgeschmierten schnelllaufenden Spindellagern,* Leibniz Universität Hannover, Doctoral Thesis, 1996
- [Bau08] BAUER, F.: *PTFE-Manschettendichtungen mit Spiralrille: Analyse, Funktionsweise und Erweiterung der Einsatzgrenzen,* Universität Stuttgart, Doctoral Thesis, 2008
- [Bav97] BAVEL, P.G.M. van: *The Leakage-free Operation of Radial Lip Seals,* University of Eindhoven, Doctoral Thesis, 1997

- [BH73] BRINK, R.V. ; HORVE, L.A.: Wave Seals – A Solution to the Hydrodynamic Compromise. In: *ASLE Lubrication Engineering* 29 (1973), Issue 6, p. 265–270
- [BH10] BRAUN, M.J. ; HANNON, W.M.: Cavitation formation and modelling for fluid film bearings: a review. In: *Proceedings of the Institution of Mechanical Engineers, Part J: Journal of Engineering Tribology* 224 (2010), Issue 9, p. 839–863
- [Bin91] BINNINGTON, P.G.: *The Measurement of Rotary Shaft Seal Film Thickness*, University of Durham, Doctoral Thesis, 1991
- [BLP10] BAART, P. ; LUGT, P.M. ; PRAKASH, B.: Non-Newtonian Effects on Film Formation in Grease-Lubricated Radial Lip Seals. In: *Tribology Transactions* 53 (2010), Issue 3, p. 308–318
- [BLP14] BAART, P. ; LUGT, P.M. ; PRAKASH, B.: On the normal stress effect in grease-lubricated bearing seals. In: *Tribology Transactions* 57 (2014), Issue 5, p. 939–943
- [Buho6] BUHL, S.: *Wechselbeziehungen im Dichtsystem von Radial-Wellendichtring, Gegenlaufläche und Fluid*, Universität Stuttgart, Doctoral Thesis, 2006
- [CDT87] CHITTENDEN, R.J. ; DOWSON, D. ; TAYLOR, C.M.: The lubrication of elliptical conjunctions in the isoviscous-elastic regime with entrainment directed along either principal axis. In: *Tribology Series, Proceedings of the 13th Leeds-Lyon Symposium on Tribology* Vol. 11, North Holland, 1987, 247–260. – Paper VIII(ii)
- [Che78] CHETWYND, D.G.: Slope measurement in surface texture analysis. In: *Journal of Mechanical Engineering Science* 20 (1978), Issue 3, p. 115–119
- [CIJL94] CANN, P. ; IOANNIDES, E. ; JACOBSON, B. ; LUBRECHT, A.A.: The lambda ratio—a critical re-examination. In: *Wear* 175 (1994), Issue 1, p. 177–188
- [CR92] CR: Book 1: Fundamentals of elastomeric lip seals. In: *Elastomeric lip seal handbook*. Second edition. CR Industries, 1992
- [CSH91] CHIBA, K. ; SHIMOMURA, T. ; HIRABAYASHI, H.: Sealing phenomena of a lip-type seal for an automotive air conditioning compressor / SAE. 1991 (910532). – SAE Technical Paper. – SAE Int., Engine and Drivetrain Sealing, SP-866

- [CSY98] CHIBA, K. ; SAGEHASHI, R. ; YOSHINO, A.: The Relationship Between Deposit Formation and Oil Leakage of Lip-Type Seal for Automotive Air Conditioner Compressor. In: *International Compressor Engineering Conference* Purdue University, School of Mechanical Engineering, 1998, p. 249–254
- [DCLT<sup>+</sup>00] DE CHIFFRE, L. ; LONARDO, P. ; TRUMPOLD, H. ; LUCCA, D.A. ; GOCH, G. ; BROWN, C.A. ; RAJA, J. ; HANSEN, H.N.: Quantitative characterisation of surface texture. In: *CIRP Annals-Manufacturing Technology* 49 (2000), Issue 2, p. 635–652
- [Debo5] DEBLER, C.: *Bestimmung und Vorhersage des Verschleißes für die Auslegung von Dichtungen*, Leibniz Universität Hannover, Doctoral Thesis, 2005
- [DGP03] DEBLER, C. ; GRONITZKI, M. ; POLL, G.: Investigation into the sealing contacts of reciprocating elastomeric seals — correlation of calculations with contact force measurements and optical observations. In: FLITNEY, R. (Ed.): *Proc. 17th International Conference on Fluid Sealing*, BHR Group, Cranfield, 2003, p. 169–186
- [DIN3761–9] DIN 3761 Teil 9. Radial-Wellendichtringe für Kraftfahrzeuge; Prüfung; Radialkraft-Messgerät-Digital (DIN 3761 part 9. Rotary shaft lip type seals for automobiles; test; radial force measuring instrument digital). 1984
- [DIN51563] DIN 51563:2011-04 (Testing of Mineral Oils and Related Materials – Determination of Viscosity Temperature Relation – Slope  $m$ ). 2011
- [DIN51757] DIN 51757:2011-01 (Testing of mineral oils and related materials – Determination of density). 2011
- [DP12] DIMAKI, A.V. ; POPOV, V.L.: The method of reduction of dimensionality and its application to simulation of elastomer friction under complex dynamic loads. In: *Physical Mesomechanics* 15 (2012), Issue 5–6, p. 319–323
- [DSS94a] DONG, W.P. ; SULLIVAN, P.J. ; STOUT, K.J.: Comprehensive study of parameters for characterising three-dimensional surface topography — III: Parameters for characterising amplitude and some functional properties. In: *Wear* 178 (1994), Issue 1, p. 29–43
- [DSS94b] DONG, W.P. ; SULLIVAN, P.J. ; STOUT, K.J.: Comprehensive study of parameters for characterising three-dimensional surface topography — IV: parameters for

- characterising spatial and hybrid properties. In: *Wear* 178 (1994), Issue 1, p. 45–60
- [DTA07] DHUNPUT, A. ; TEODORESCU, M. ; ARCOUMANIS, C.: Investigation of cavitation development in the lubricant film of piston-ring assemblies. In: *Journal of Physics: Conference Series* Vol. 85, IOP Publishing, 2007, p. 012005
- [DWH10] DAUBNER, A. ; WINTER, M. ; HAAS, W.: Erweiterte Methode zur Simulation der Temperatur im Reibkontakt mittels CHT. In: *Tribologie und Schmierungstechnik* 57 (2010), Issue 2, p. 25–30
- [Eng11] ENGELKE, T.: *Einfluss der Elastomer-Schmierstoff-Kombination auf das Betriebsverhalten von Radialwellendichtringen*, Leibniz Universität Hannover, Doctoral Thesis, 2011
- [EPSD11] ENGELKE, T. ; POLL, G.W.G. ; SCHÜLLER, M. ; DEWITZ, I.: Näherungsverfahren für die Berechnung von Reibmoment und Kontakttemperatur von Elastomer-Wellendichtungen. In: 52. *GfT-Tribologie-Fachtagung "Reibung, Schmierung und Verschleiß"*, Göttingen, Germany, 2011. – Paper 58
- [FF78] FORD, R.A.J. ; FOORD, C.A.: Laser-based fluorescence techniques for measuring thin liquid films. In: *Wear* 51 (1978), Issue 2, p. 289–297
- [Fin01] FINNEY, R.H.: Finite Element Analysis. In: GENT, A.N. (Ed.): *Engineering with Rubber — How to Design Rubber Components*. 2nd Edition. HanserGardner Publications, Inc., Cincinnati, 2001, Chapter 9, p. 257–305
- [Fli82] FLITNEY, R.: PTFE Lip Seal Investigation / BHRA fluid engineering. Cranfield, Bedford, England, 1982. – RR 1804
- [Fli14] FLITNEY, R.: Chapter Three – Rotary Seals. In: FLITNEY, R. (Ed.): *Seals and Sealing Handbook*. Sixth Edition. Oxford: Butterworth-Heinemann, 2014. – ISBN 978-0-08-099416-1, p. 105–288
- [FMSK14] FOWELL, M.T. ; MYANT, C. ; SPIKES, H.A. ; KADIRIC, A.: A study of lubricant film thickness in compliant contacts of elastomeric seal materials using a laser induced fluorescence technique. In: *Tribology International* 80 (2014), p. 76–89

- [FP01] FERZIGER, J.H. ; PERIC, M.: *Computational Methods for Fluid Dynamics*. 3rd Ed. Springer, 2001
- [Fre00] FRENZEL, U.K.: *Rückenstrukturierte Hydraulikstangendichtungen aus Polyurethan*, Universität Stuttgart, Doctoral Thesis, 2000
- [Fri94] FRITZSCHE, R.: *Ein Beitrag zur Untersuchung des Verhaltens von Radialwellendichtungen aus Elastomer- und Polytetrafluoräthylen-Material bei speziellen Betriebsbedingungen*, Universität Kaiserslautern, Doctoral Thesis, 1994
- [Gab89] GABELLI, A.: Micro-elastohydrodynamic lubricant film formation in rotary lip seal contacts. In: *Tribology Series, Proceedings of the 15th Leeds-Lyon Symposium on Tribology* Vol. 14, Elsevier, 1989, p. 57–68
- [Gab91] GABELLI, A.: *Deformation, stresses and elastohydrodynamic film formation in soft contacts*, Chalmers Tekniska Högskola, Göteborg, Sweden, Doctoral Thesis, 1991
- [GAC07] GORRINO, A. ; ANGULO, C. ; CANALES, J.: Theoretical analysis of the pumping effect of rotary hydrodynamic seals with elastomeric lips. In: *Tribology International* 40 (2007), Issue 5, p. 896–905
- [Gaw81] GAWLINSKI, M.J.: Lip Motion and Its Consequences in Oil Lip Seal Operation. In: *Proc. 9th Int. Conf. on Fluid Sealing*, BHRA, 1981. – Paper D2
- [GIM96] GABELLI, A. ; IOANNIDES, E. ; MIGLIETTA, E.: Increased Life Performance of Rolling Element Bearings in Gearboxes and Transmissions. In: *Proc. of Int. Conf. on Gears*, Verein Deutscher Ingenieure, 1996 (VDI-Bericht 1230), p. 631–645
- [GJL<sup>+</sup>14] GUO, F. ; JIA, X. ; LONGKE, W. ; SALANT, R.F. ; WANG, Y.: The effect of wear on the performance of a rotary lip seal. In: *Journal of Tribology* 136 (2014), Issue 4, p. 041703
- [GJS<sup>+</sup>13] GUO, F. ; JIA, X. ; SUO, S. ; SALANT, R.F. ; WANG, Y.: A mixed lubrication model of a rotary lip seal using flow factors. In: *Tribology International* 57 (2013), p. 195–201
- [GK84] GAWLINSKI, M. ; KONDERLA, P.: Dynamic analysis of oil lip seals. In: *Proc. 10th Int. Conf. on Fluid Sealing* BHRA The Fluid Engineering Centre, BHRA, 1984, p. 139–155. – Paper C4

- [GMEI08] GABELLI, A. ; MORALES-ESPEJEL, G.E. ; IOANNIDES, E.: Particle damage in Hertzian contacts and life ratings of rolling bearings. In: *Tribology Transactions* 51 (2008), Issue 4, p. 428–445
- [GP92] GABELLI, A. ; POLL, G.: Formation of lubricant film in rotary sealing contacts. Part I: Lubricant film modeling. In: *Transactions of the ASME. Journal of Tribology* 114 (1992), Issue 2, p. 280–287
- [GPP92] GABELLI, A. ; PONSON, F. ; POLL, G.: Computation and measurement of the sealing contact stress and its role in rotary lip seal design. In: NAU, B.S. (Ed.): *Fluid Sealing. Proc. 13th Int. Conf. on Fluid Sealing, Brugge, Belgium*. Springer (Copyright Holder: Kluwer Academic Publishers, Dordrecht), 1992, p. 21–39
- [Gri01] GRIFFITHS, B.: *Manufacturing surface technology: Surface integrity and functional performance*. London, UK: Penton Press, 2001 (Manufacturing engineering modular series). – p. 124
- [Gro06] GRONITZKI, M.: *Untersuchungen zur Funktion und Auslegung von Rechteckdichtungen für Drehdurchführungen*, Leibniz Universität Hannover, Doctoral Thesis, 2006
- [GT70] GREENWOOD, J.A. ; TRIPP, J.H.: The contact of two nominally flat rough surfaces. In: *Proceedings of the Institution of Mechanical Engineers* 185 (1970), Issue 1, p. 625–633
- [Gui90] GUILBAULT, G.G.: General Aspects of Luminescence Spectroscopy. In: GUILBAULT, G.G. (Ed.): *Practical fluorescence* Vol. 3. 2nd edition. Marcel Dekker New York Basel Hong Kong, 1990, Chapter 1, p. 6
- [Haa86] HAAS, W.: *Berührungsfreie Wellendichtungen für flüssigkeitsbespritzte Dichtstellen*, Universität Stuttgart, Doctoral Thesis, 1986
- [Har62] HARRICK, N.J.: Use of frustrated total internal reflection to measure film thickness and surface reliefs. In: *Journal of Applied Physics* 33 (1962), Issue 9, p. 2774–2775
- [HB04] HAJJAM, M. ; BONNEAU, D.: Elastohydrodynamic analysis of lip seals with microundulations. In: *Proceedings of the Institution of Mechanical Engineers, Part J: Journal of Engineering Tribology* 218 (2004), Issue 1, p. 13–22



- [HB06a] HAJJAM, M. ; BONNEAU, D.: Influence of the roughness model on the thermoelastohydrodynamic performances of lip seals. In: *Tribology International* 39 (2006), Issue 3, p. 198–205
- [HB06b] HAJJAM, M. ; BONNEAU, D.: Non-Newtonian effects on elastohydrodynamic behaviour of rotary lip seals. In: *Proc. IMechE Part J: J. Engineering Tribology* 220 (2006), p. 79–85
- [HH99] HIDROVO, C.H. ; HART, D.P.: Development of a Dual Purpose Visualization Technique for the Study of Rotating Shaft Seals. In: *Proceedings of the 3rd ASME/JSME Joint Fluids Engineering Conference July 18–23, 1999, San Francisco, California, 1999*
- [HH01] HIDROVO, C.H. ; HART, D.P.: Emission reabsorption laser induced fluorescence (ERLIF) film thickness measurement. In: *Measurement Science and Technology* 12 (2001), Issue 4, p. 467–477
- [HH02] HIDROVO, C.H. ; HART, D.P.: 2D thickness and temperature mapping of fluids by means of a two-dye laser induced fluorescence ratiometric scheme. In: *Journal of Flow Visualization and Image Processing* 9 (2002), Issue 2&3, p. 171–191
- [HI65] HIRANO, F. ; ISHIWATA, H.: The Lubricating Condition of a Lip Seal. In: *Proceedings of the Institution of Mechanical Engineers, Conference Proceedings Vol. 180, 1965*, p. 187–196
- [HIK61] HIRANO, F. ; ISHIWATA, H. ; KAMBAYOSHI, H.: Friction and sealing characteristics of oil seals. In: *Proc. Int. Conf. on Fluid Sealing*, British Hydromechanics Research Association, 1961
- [HK08] HEINRICH, G. ; KLÜPPEL, M.: Rubber friction, tread deformation and tire traction. In: *Wear* 265 (2008), p. 1052–1060
- [HKV00] HEINRICH, G. ; KLÜPPEL, M. ; VILGIS, T.A.: Evaluation of Self-Affine Surfaces and their Implication to Frictional Dynamics as Illustrated with a Rouse Material. In: *Comput. & Theor. Polym. Sci.* 10 (2000), p. 53–61
- [HLPR11] HOLLEN, J. von ; LEIS, A. ; POLL, G. ; REITHMEIER, E.: Einfluss von Beschädigungen der Gegenlauffläche auf das tribologische Verhalten von Radialwellendichtringen und Verfahren zur messtechnischen Detektion und

Charakterisierung. In: *Tribologie und Schmierungstechnik* 58 (2011), Issue 2, p. 16–22

- [HLWB88] HOULT, D.P. ; LUX, J.P. ; WONG, V.W. ; BILLIAN, S.A.: Calibration of Laser Fluorescence Measurements of Lubricant Film Thickness in Engines / SAE Int., Warrendale, PA. 1988 (881587). – SAE Technical Paper
- [HLWB89] HOULT, D.P. ; LUX, J.P. ; WONG, V.W. ; BILLIAN, S.A.: Calibration of laser fluorescence measurements of lubricant film thickness in engines. In: *SAE Transactions* 97 (1989), p. 576–584
- [Hor76] HORVE, L.A.: How to select radial lip seals. In: *Power Transmission Design* 11 (1976), p. 48–50
- [Hor84] HORVE, L.A.: The effect of operating parameters upon radial lip seal performance / SAE. 1984 (841145). – SAE Technical Paper
- [Hor87] HORVE, L.A.: A macroscopic view of the sealing phenomenon for radial lip oil seals. In: *Proc. 11th International Conference on Fluid Sealing, Cannes, France, 1987*, p. 710–731
- [Hor91] HORVE, L.A.: The Correlation of Rotary Shaft Radial Lip Seal Service Reliability and Pumping Ability to Wear Track Roughness and Microasperity Formation / SAE. 1991 (No. 910530). – SAE Technical Paper
- [HS85] HERMANN, W. ; SEFFLER, H.: New Knowledge of the Sealing Mechanism of Radial Shaft Sealing Rings. In: *Auto. Tech. Zeitschrift* 87 (1985), Issue 9
- [HS01] HARP, S.R. ; SALANT, R.F.: An Average Flow Model of Rough Surface Lubrication With Inter-Asperity Cavitation. In: *Journal of Tribology* 123 (2001), p. 134–143
- [HS02] HARP, S.R. ; SALANT, R.F.: Inter-asperity cavitation and global cavitation in seals: an average flow analysis. In: *Tribology International* 35 (2002), Issue 2, p. 113–121
- [HSJ04] HAMROCK, B.J. ; SCHMID, S.R. ; JACOBSON, B.O.: *Fundamentals of fluid film lubrication*. 2nd Edition. New York: Marcel Dekker, Inc., 2004
- [HWA66] HAMILTON, D.B. ; WALOWIT, J.A. ; ALLEN, C.M.: A theory of lubrication by microirregularities. In: *Journal of Basic Engineering* 88 (1966), Issue 1, p. 177–185

- [IC61] INY, E.H. ; CAMERON, A.: The Load Carrying Capacity of Synthetic Rubber Rotary Shaft Seals. In: *Proc. 1st Int. Conf. on Fluid Sealing*, BHRA, 1961. – Paper C1
- [IDBL07] INCROPERA, F.P. ; DEWITT, D.P. ; BERGMAN, T.L. ; LAVINE, A.S.: *Fundamentals of heat and mass transfer*. 6. edition. Wiley, 2007
- [ISMK95] INAGAKI, H. ; SAITO, A. ; MURAKAMI, M. ; KONOMI, T.: Development of Two-Dimensional Oil Film Thickness Distribution Measuring System / SAE. 1995 (952346). – SAE Technical Paper. – Engine Lubricants (SAE Int.): SP-1121
- [ISO4287] *DIN EN ISO 4287 (Geometrical Product Specifications (GPS) - Surface texture: Profile method - Terms, definitions and surface texture parameters (ISO 4287:1997 + Cor 1:1998 + Cor 2:2005 + Amd 1:2009); German version EN ISO 4287:1998 + AC:2008 + A1:2009)*. 2010
- [Jac91] JACOBSON, B.O.: *Tribology Series*. Vol. 19: *Rheology and Elastohydrodynamic Lubrication*. Elsevier Science, 1991
- [Jag57a] JAGGER, E.T.: Study of the lubrication of synthetic rubber rotary shaft seals. In: *Proceedings of the Conference on Lubrication and Wear, I. Mech. E.*, 1957, p. 409–415
- [Jag57b] JAGGER, E.T.: Rotary shaft seals: the sealing mechanism of synthetic rubber seals running at atmospheric pressure. In: *Proceedings of the Institution of Mechanical Engineers* 171 (1957), p. 597–616
- [Jas96] JASAK, H.: *Error Analysis and Estimation for the Finite Volume Method with Applications to Fluid Flows*, Imperial College, University of London, Doctoral Thesis, 1996
- [Jen91] JENISCH, B.: *Abdichten mit Radial-Wellendichtringen aus Elastomer und Polytetrafluorethylen*, Universität Stuttgart, Doctoral Thesis, 1991
- [Joh78] JOHNSTON, D.E.: Using the frictional torque of rotary shaft seals to estimate the film parameters and the elastomer surface characteristics. In: *Proc. 8th International Conference on Fluid Sealing, Durham, England, 1978*. – Paper C1
- [Joh86] JOHNSTON, D.E.: Rotary shaft seals. In: *Tribology International* 19 (1986), Issue 4, p. 170–174

- [Joh99] JOHNSTON, D.E.: Design aspects of modern rotary shaft seals. In: *Proceedings of the Institution of Mechanical Engineers, Part J: Journal of Engineering Tribology* 213 (1999), Issue 3, p. 203–213
- [JV95] JOHNSTON, D.E. ; VOGT, R.: Rotary shaft seal friction, the influence of design, material, oil and shaft surface / SAE. 1995 (950764). – SAE Technical Paper
- [JW67] JAGGER, E.T. ; WALKER, P.S.: Second paper: Further studies of the lubrication of synthetic rubber rotary shaft seals. In: *Proceedings of the Institution of Mechanical Engineers* 181 (1966–67), Issue 9, p. 191–204
- [JW70] JAGGER, E.T. ; WALLACE, D.: Oil seal research. In: *Industrial Lubrication and Tribology* 22 (1970), Issue 2, p. 54–56
- [JW73] JAGGER, E.T. ; WALLACE, D.: Further experiments on the sealing mechanism of a synthetic rubber lip type seal operating on a rotating shaft. In: *Proceedings of the Institution of Mechanical Engineers* 187 (1973), Issue 1, p. 361–367
- [KAH80] KAWAHARA, Y. ; ABE, M. ; HIRABAYASHI, H.: An analysis of sealing characteristics of oil seals. In: *ASLE Transactions* 23 (1980), Issue 1, p. 93–102
- [KAHM78] KAWAHARA, Y. ; ABE, M. ; HIRABAYASHI, H. ; MATSUSHIMA, A.: Effect of Surface Condition of Lip on Sealing Phenomena of Oil Seals / SAE International. 1978 (No. 780405). – SAE Technical Paper
- [Kam86] KAMMÜLLER, M.: *Zur Abdichtwirkung von Radialwellendichtringen*, Universität Stuttgart, Doctoral Thesis, 1986
- [Kas87] KASSFELDT, E.: *Analysis and design of hydraulic cylinder seals*, Luleå University of Technology, Doctoral Thesis, 1987
- [KBW05] KOTTKE, P.A. ; BAIR, S.S. ; WINER, W.O.: Cavitation in creeping shear flows. In: *AIChE journal* 51 (2005), Issue 8, p. 2150–2170
- [KES87] KARAMI, G. ; EVANS, H.P. ; SNIDLE, R.W.: Elastohydrodynamic lubrication of circumferentially finished rollers having sinusoidal roughness. In: *Proceedings of the Institution of Mechanical Engineers, Part C: Journal of Mechanical Engineering Science* 201 (1987), Issue 1, p. 29–36

- [KFKK97] KANETA, M. ; FUJIMOTO, T. ; KANZAKI, Y. ; KAWAHARA, Y.: Oil film behaviour and friction characteristics in reciprocating rubber seals. Part 2: multiple contacts. In: *Proc. 15th Int. Conf. on Fluid Sealing* BHR, BHR Group, 1997
- [KH79] KAWAHARA, Y. ; HIRABAYASHI, H.: A study of sealing phenomena on oil seals. In: *ASLE Transactions* 22 (1979), Issue 1, p. 46–55
- [KH00] KLÜPPEL, M. ; HEINRICH, G.: Rubber Friction on Self-Affine Road Tracks. In: *Rubber Chem. Technol.* 73 (2000), p. 578–606
- [KKK97] KANZAKI, Y. ; KAWAHARA, Y. ; KANETA, M.: Oil film behaviour and friction characteristics in reciprocating rubber seals. Part 1: single contact. In: *Proc. 15th Int. Conf. on Fluid Sealing* BHR, BHR Group, 1997, p. 79–95
- [KMLGH03] KLÜPPEL, M. ; MÜLLER, A. ; LE GAL, A. ; HEINRICH, G.: Dynamic contact of tires with road tracks. In: *Proc. ACS Meeting*, 2003
- [KNMS93] KONOMI, T. ; NOHIRA, H. ; MURAKAMI, M. ; SANDA, S.: Effects of piston skirt profile on friction loss and oil film behaviour. In: *Proceedings of the Institution of Mechanical Engineers. Experimental and Predictive Methods in Engine Research and Development. International Conference*, 1993. – (IMechE 1993-10, C465/011/93)
- [Kra82] KRAUTER, A.I.: Measurement of oil film thickness for application to elastomeric Stirling engine rod seals. In: *Journal of Lubrication Technology* 104 (1982), Issue 4, p. 455–459
- [KTN<sup>+</sup>00] KANETA, M. ; TODOROKI, H. ; NISHIKAWA, H. ; KANZAKI, Y. ; KAWAHARA, Y.: Tribology of flexible seals for reciprocating motion. In: *Journal of Tribology* 122 (2000), Issue 4, p. 787–795
- [KTT<sup>+</sup>05] KANETA, M. ; TAKESHIMA, T. ; TOGAMI, S. ; NISHIKAWA, H. ; KANZAKI, Y.: Stribeck curve in reciprocating seals. In: *Proc. 18th Int. Conf. On Fluid Sealing*, 2005, p. 333–347
- [Kun05] KUNSTFELD, T.: *Einfluss der Wellenoberfläche auf das Dichtverhalten von Radial-Wellendichtungen*, Universität Stuttgart, Doctoral Thesis, 2005

- [Leb87] LEBECK, A.O.: Parallel sliding load support in the mixed friction regime. Part 2—Evaluation of the Mechanisms. In: *Journal of Tribology* 109 (1987), Issue 1, p. 196–205
- [Lei54] LEIN, J.: Mechanische Untersuchungen an Dichtungsringen für rotierende Wellen. In: *Konstruktion* 6 (1954), Issue 10, p. 384–389
- [LG07] LE GAL, A.: *Investigation and Modelling of Rubber Stationary Friction on Rough Surfaces*, Leibniz Universität Hannover, Doctoral Thesis, 2007
- [LGKo8a] LE GAL, A. ; KLÜPPEL, M.: Investigation and Modeling of Rubber Stationary Friction on Rough Surfaces. In: *J. Phys.: Condens. Matter* 20 (2008), p. 015007
- [LGKo8b] LE GAL, A. ; KLÜPPEL, M.: Modelling of Sliding Friction for Carbon Black and Silica Filled Elastomers on Road Tracks. In: *Wear* 264 (2008), p. 606–615
- [LGYK05] LE GAL, A. ; YANG, X. ; KLÜPPEL, M.: Evaluation of Sliding Friction and Contact Mechanics of Elastomers Based on Dynamic-Mechanical Analysis. In: *J. Chem. Phys.* 123 (2005), p. 014704
- [LHO91] LUX, J.P. ; HOULT, D.P. ; OLECHOWSKI, M.J.: Lubricant film thickness measurements in a diesel engine piston ring zone. In: *Lubrication Engineering* 47 (1991), Issue 5, p. 353–364
- [LHRP10] LEIS, A. ; HOLLEN, J. von ; REITHMEIER, E. ; POLL, G.W.G.: Auswirkungen stochastischer Strukturen von Gegenlaufflächen auf die Funktion von Radialwellendichtringen / Forschungskuratorium Maschinenbau e.V. Frankfurt a.M., 2010 (Nr. 307). – Forschungsheft
- [Lim01] LIMING, L.: Investigation of oil film on the contact surface of a flooded model helical lip seal. In: *Lubrication Engineering / Journal of the Society of Tribologists and Lubrication Engineers* 57 (2001), Issue 12, p. 15–21
- [Lim03] LIMING, L.: The effect of surface asperities on the friction coefficient of a flooded reciprocating model lip seal. In: *Proc. 17th Int. Conf. on Fluid Sealing* BHR Group, Kluwer Academic Publishers, 2003, p. 187–202
- [Lin87] LINDGREN, H.: Pressure distribution in scraper ring contacts. In: *Wear* 115 (1987), Issue 1, p. 31–40

- [Lin05] LINDNER, M.: *Experimentelle und theoretische Untersuchungen zur Gummireibung an Profilklotzen und Dichtungen*, Leibniz Universität Hannover, Doctoral Thesis, 2005
- [LLO66] LINES, D.J. ; LAWRIE, J.M. ; O'DONOGHUE, J.P.: Effect of Under-Lip Temperature on the Lubrication of Rotary Shaft Garter Spring Seals. In: *Proceedings of the Institution of Mechanical Engineers* 181 (1966), Issue 9, p. 185–190
- [LPD<sup>+</sup>13] LI, Q. ; POPOV, M. ; DIMAKI, A. ; FILIPPOV, A.E. ; KÜRSCHNER, S. ; POPOV, V.L.: Friction between a viscoelastic body and a rigid surface with random self-affine roughness. In: *Physical Review Letters* 111 (2013), Issue 3, p. 034301
- [LPM11] LEEUWEN, H. van ; PETTERSON, R. ; MEESTERS, K.: Cinderella in fluid film lubrication: stretch effects in radial lip seals. In: *Proceedings of the 38th Leeds–Lyon Symposium on Tribology: Energy and Health*, 2011
- [LS90] LEEUWEN, H.J. van ; STAKENBORG, M.J.L.: Visco-Elastohydrodynamic (VEHD) Lubrication in Radial Lip Seals: Part 2 — Fluid Film Formation. In: *Journal of Tribology* 112 (1990), Issue 4, p. 584–592
- [LS91] LEEUWEN, H.J. van ; STAKENBORG, M.J.L.: A new concept in rotary shaft seal lubrication: viscoelastohydrodynamic (VEHD) lubrication. In: *Proc. of the 17th. Leeds–Lyon Symposium on Tribology*, 1991, p. 373–380
- [LW97] LEEUWEN, H. van ; WOLFERT, M.: The sealing and lubrication principles of plain radial lip seals: an experimental study of local tangential deformations and film thickness. In: *Tribology Series* 32 (1997), p. 219–232
- [Mar09] MAROTO, J.A.: Computational analysis of the accuracy in the evaluation of the mean molecular weight of petroleum oils from the ASTM Standard D 2502-92. In: *Journal of Petroleum Science and Engineering* 69 (2009), Issue 1, p. 89–92
- [MAS07] MIZUTA, H. ; ANZUE, K. ; SATO, Y.: An experimental study on lubrication of radial shaft seals under pressure. In: *Proc. 19th International Conference on Fluid Sealing* BHR Group, 2007, p. 147–156
- [McC86b] McCOOL, J.I.: Comparison of models for the contact of rough surfaces. In: *Wear* 107 (1986), Issue 1, p. 37–60

- [MFC14] MYANT, C. ; FOWELL, M. ; CANN, P.: The effect of transient motion on Isoviscous-EHL films in compliant, point, contacts. In: *Tribology International* 72 (2014), p. 98–107
- [MFS07] MIZUTA, H. ; FURUYAMA, H. ; SATO, Y.: Measurement Method of Pumping Ability of Radial Lip Seals for Small Shaft Diameters / SAE. 2007 (2007-01-1521). – SAE Technical Paper
- [MHB07] MAOUI, A. ; HAJJAM, M. ; BONNEAU, D.: Analysis of three-dimensional non-axisymmetric elastic effects of the lip on the thermoelastohydrodynamic radial lip seal behaviour. In: *Proceedings of the Institution of Mechanical Engineers, Part J: Journal of Engineering Tribology* 221 (2007), Issue 8, p. 859–868
- [MHB08] MAOUI, A. ; HAJJAM, M. ; BONNEAU, D.: Effect of 3D lip deformations on elastohydrodynamic lip seals behaviour. In: *Tribology International* 41 (2008), p. 901–907
- [MN07] MAROTO, J.A. ; NIEVES, F.J. de l.: Computational aids for the estimation of the molecular weight of petroleum oils from kinematic viscosity measurements. In: *Petroleum Chemistry* 47 (2007), Issue 2, p. 87–91
- [Mor14] MORA, F.: *Modélisation multiéchelles d'un contact rugueux viscoélastique lubrifié*, I.N.S.A. Lyon, Doctoral Thesis, 2014
- [MPo8] MOFIDI, M. ; PRAKASH, B.: Influence of counterface topography on sliding friction and wear of some elastomers under dry sliding conditions. In: *Proceedings of the Institution of Mechanical Engineers, Part J: Journal of Engineering Tribology* 222 (2008), Issue 5, p. 667–673
- [MPPA08] MOFIDI, M. ; PRAKASH, B. ; PERSSON, B.N.J. ; ALBOHR, O.: Rubber friction on (apparently) smooth lubricated surfaces. In: *Journal of Physics: Condensed Matter* 20 (2008), Issue 8, p. 085223
- [MRS10] MYANT, C. ; REDDYHOFF, T. ; SPIKES, H.A.: Laser-induced fluorescence for film thickness mapping in pure sliding lubricated, compliant, contacts. In: *Tribology International* 43 (2010), Issue 11, p. 1960–1969
- [MS11] MIZUTA, H. ; SUGIMURA, J.: An experimental and theoretical study of the effect of lip surface roughness on lubrication of radial lip seals. In: FLITNEY, R. (Ed.): *Proc. 21st International Conference on Fluid Sealing*, BHR Group, 2011



- [MS13] MIZUTA, H. ; SUGIMURA, J.: Numerical Study of the Effect of Lip Surface Roughness on Lubrication of Radial Shaft Seals with a Simple Sinusoidal Model. In: *Tribology Online* 8 (2013), Issue 1, p. 104–110
- [MSLCL12] MORA, F. ; SAINOT, P. ; LE CHENADEC, Y. ; LUBRECHT, A. A.: Lubrication of 2D soft elastohydrodynamic contacts: Extension of the amplitude reduction theory. In: *Proceedings of the Institution of Mechanical Engineers, Part J: Journal of Engineering Tribology* 226 (2012), Issue 9, p. 769–774
- [MT78] McCLUNE, C.R. ; TABOR, D.: An interferometric study of lubricated rotary face seals. In: *Tribology International* 11 (1978), Issue 4, p. 219–227
- [Mül87] MÜLLER, H.K.: Concepts of sealing mechanism of rubber lip type rotary shaft seals. In: *Proc. 11th Int. Conf. on Fluid Sealing*, BHRA, 1987. – Paper K1
- [MWG00] MEINHART, C.D. ; WERELEY, S.T. ; GRAY, M.H.B.: Volume illumination for two-dimensional particle image velocimetry. In: *Measurement Science and Technology* 11 (2000), Issue 6, p. 809–814
- [MWS99] MEINHART, C.D. ; WERELEY, S.T. ; SANTIAGO, J.G.: PIV measurements of a microchannel flow. In: *Experiments in Fluids* 27 (1999), Issue 5, p. 414–419
- [Nak87] NAKAMURA, K.: Sealing mechanism of rotary shaft lip-type seals. In: *Tribology International* 20 (1987), Issue 2, p. 90–101
- [Nay71] NAYAK, P.R.: Random process model of rough surfaces. In: *Journal of Lubrication Technology* 93 (1971), Issue 3, p. 398–407
- [NK84] NAKAMURA, K. ; KAWAHARA, Y.: An Investigation of Sealing Properties of Lip Seals through Observations of Sealing Surfaces under Dynamic Condition. In: *Proc. 10th Int. Conf. on Fluid Sealing* BHRA The Fluid Engineering Centre, BHRA, 1984. – Paper C1
- [NKK85] NAKAMURA, K. ; KAWAHARA, Y. ; KANZAKI, Y.: An investigation of sealing mechanism of rotary lip seals under dynamic condition. In: *Proc. of the JSLE Int. Tribology Conference*. Tokyo, Japan, 1985, p. 805–810
- [NSG<sup>+</sup>05] NAKAOKA, S. ; SATO, Y. ; GONDO, S. ; SUGIMURA, J. ; YAMAMOTO, Y.: Experimental study on gas transporta-

tion in radial shaft seals. In: *Life Cycle Tribology – Proceedings of the 31st Leeds–Lyon Symposium on Tribology* Vol. 48, 2005 (Tribology and Interface Engineering Series), 517–523

- [ÖABD08] ÖNGÜN, Y ; ANDRÉ, M ; BARTEL, D ; DETERS, L: An axisymmetric hydrodynamic interface element for finite-element computations of mixed lubrication in rubber seals. In: *Proceedings of the Institution of Mechanical Engineers, Part J: Journal of Engineering Tribology* 222 (2008), Issue 3, p. 471–481
- [OFS87] OGATA, M. ; FUJII, T. ; SHIMOTSUMA, Y.: Study on fundamental characteristics of rotating lip-type oil seals. In: *Proc. of the 14th Leeds–Lyon Symposium on Tribology*, 1987, p. 553–560
- [Oli95] OLIVEIRA, S.J.R. de: *Das nichtnewtonsche Verhalten von Fluiden bei hohen Schergefällen als Erklärung der Schmierungs- und Dichtvorgänge bei Radialwellendichtungen*, Universität Hamburg Harburg, Doctoral Thesis, 1995
- [Ott83] OTT, G.W.: *Untersuchungen zum dynamischen Leckage- und Reibverhalten von Radial-Wellendichtungen*, Universität Stuttgart, Doctoral Thesis, 1983
- [Ott13] OTTINK, K.: *Wälzlagerdichtungen: Schutzdichtungen für Wälzlager II; Forschungsvorhaben Nr. 432 II der FVA / Forschungsvereinigung Antriebstechnik e.V. Frankfurt a.M., 2013 (Nr. 1053). – Forschungsheft*
- [Ott14] OTTINK, K.: *Betriebsverhalten von Wälzlagerschutzdichtungen — experimentelle Untersuchungen und Berechnungsansätze*, Leibniz Universität Hannover, Doctoral Thesis, 2014
- [OWP10] OTTINK, K. ; WENNEHORST, B. ; POLL, G.: Analysis of Rod Seals by Application of the Light Induced Fluorescence Method. In: *Sealing systems — cutting edge technology in the smallest envelope: 16th ISC, International Sealing Conference* Fachverband Fluidtechnik im VDMA e.V., 2010
- [Pat78] PATIR, N.: A numerical procedure for random generation of rough surfaces. In: *Wear* 47 (1978), Issue 2, p. 263–277
- [PAT<sup>+</sup>04] PERSSON, B.N.J. ; ALBOHR, O. ; TARTAGLINO, U. ; VOLOKITIN, A.I. ; TOSATTI, E.: On the nature of surface

- roughness with application to contact mechanics, sealing, rubber friction and adhesion. In: *Journal of Physics: Condensed Matter* 17 (2004), Issue 1, p. R1
- [PC78] PATIR, N. ; CHENG, H.S.: An average flow model for determining effects of three-dimensional roughness on partial hydrodynamic lubrication. In: *Journal of Lubrication Technology* 100 (1978), Issue 1, p. 12–17
- [PC79] PATIR, N. ; CHENG, H.S.: Application of average flow model to lubrication between rough sliding surfaces. In: *Journal of Lubrication Technology* 101 (1979), Issue 2, p. 220–229
- [Pek68] PEKLENİK, J.: Paper 24: New developments in surface characterization and measurements by means of random process analysis. In: *Proceedings of the Institution of Mechanical Engineers* 182 (1967–68), Issue 11, p. 108–126
- [Per01] PERSSON, B.N.J.: Theory of rubber friction and contact mechanics. In: *Journal of Chemical Physics* 115 (2001), Issue 8, p. 3840–3861
- [PG92] POLL, G. ; GABELLI, A.: Formation of lubricant film in rotary sealing contacts. Part II: A new measuring principle for lubricant film thickness. In: *Transactions of the ASME. Journal of Tribology* 114 (1992), Issue 2, p. 290–296
- [PGBQ92] POLL, G. ; GABELLI, A. ; BINNINGTON, P.G. ; QU, J.: Dynamic mapping of rotary lip seal lubricant films by fluorescent image processing. In: NAU, B.S. (Ed.): *Fluid Sealing. Proc. 13th Int. Conf. on Fluid Sealing, Brugge, Belgium*. Springer (Copyright Holder: Kluwer Academic Publishers, Dordrecht), 1992, p. 55–77
- [Pol00] POLL, G.W.G.: A Contribution to the Discussion on Radial Lip Seal Working Principles. In: *Radialwellendichtringe: III. Hamburger Dichtungstechnisches Kolloquium Dynamische Dichtungen*. Hamburg-Harburg, 2000
- [Pra87] PRATI, E.: A Theoretical-Experimental Method for Analyzing the Dynamic Behavior of Elastomeric Lip Seals. In: *Rubber Chemistry and Technology* 60 (1987), Issue 1, p. 176–189
- [PV06] PERSSON, B.N.J. ; VOLOKITIN, A.I.: Rubber friction on smooth surfaces. In: *The European Physical Journal E* 21 (2006), Issue 1, p. 69–80

- [Qu93] QU, J.: Experimental Study on the Sealing Effect Due to Rotational Oil Flow / SAE Int. Warrendale, PA, 1993 (930528). – SAE Technical Paper
- [Raj71] RAJAKOVICS, G.E.: On the Sealing Mechanism of Fluid Seals. In: *Proc. 5th Int. Conf. on Fluid Sealing*, BHRA, 1971. – Paper A6
- [RB91] RICHARDSON, D.E. ; BORMAN, G.L.: Using fiber optics and laser fluorescence for measuring thin oil films with application to engines / SAE Int. Warrendale, PA, 1991 (912388). – SAE Technical Paper
- [RCSG10] REDDYHOFF, T. ; CHOO, J.H. ; SPIKES, H.A. ; GLOVNEA, R.P.: Lubricant flow in an elastohydrodynamic contact using fluorescence. In: *Tribology Letters* 38 (2010), Issue 3, p. 207–215
- [Ruh01] RUHL, C.: *Ein Beitrag zur Wirkungsweise von Radialwellendichtungen unter Berücksichtigung von rauheitsinduzierter Hydrodynamik und radialen Verlagerungen der Gegenlauffläche*, Universität Kaiserslautern, Doctoral Thesis, 2001
- [Sal92] SALANT, R.F.: Numerical Analysis of the Flow Field Within Lip Seals Containing Microundulations. In: *Journal of Tribology* 114 (1992), p. 485–491
- [Sal97] SALANT, R.F.: Rotary lip seal operation with an ingested meniscus. In: *Journal of Tribology* 119 (1997), Issue 1, p. 205–210
- [Sal99] SALANT, R.F.: Theory of lubrication of elastomeric rotary shaft seals. In: *Proceedings of the Institution of Mechanical Engineers, Part J: Journal of Engineering Tribology* 213 (1999), Issue 3, p. 189–201
- [Sal01] SALANT, R.F.: Numerical models of rotary lip seal seals. In: *Tribology Series* 39 (2001), p. 685–696
- [Sal10] SALANT, R.F.: Soft elastohydrodynamic analysis of rotary lip seals. In: *Proceedings of the Institution of Mechanical Engineers, Part C: Journal of Mechanical Engineering Science* 224 (2010), Issue 12, p. 2637–2647
- [SAP10] SCHMIDT, T. ; ANDRÉ, M. ; POLL, G.: A transient 2D-finite-element approach for the simulation of mixed lubrication effects of reciprocating hydraulic rod seals. In: *Tribology International* 43 (2010), Issue 10, p. 1775–1785

- [SC12] SCARAGGI, M. ; CARBONE, G.: A Two-Scale Approach for Lubricated Soft-Contact Modeling: An Application to Lip-Seal Geometry. In: *Advances in Tribology 2012* (2012). <http://dx.doi.org/10.1155/2012/412190>. – DOI 10.1155/2012/412190
- [Sch11] SCHMIDT, T.: *Mischreibung und Verschleiß in Hydraulikdichtsystemen — Modellbildung, Simulation und experimentelle Analyse*, Leibniz Universität Hannover, Doctoral Thesis, 2011
- [Sch14] SCHULER, P.: *Einfluss von Grenzflächeneffekten auf den Dichtmechanismus der Radial-Wellendichtung*, Universität Stuttgart, Doctoral Thesis, 2014
- [SF74] SMART, A.E. ; FORD, R.A.J.: Measurement of thin liquid films by a fluorescence technique. In: *Wear* 29 (1974), Issue 1, p. 41–47
- [SF92] STEINHILPER, W. ; FRITZSCHE, R.: The sucking of air under the lip of radial shaft seals / SAE. 1992 (920718). – SAE Technical Paper
- [SF95] SALANT, R.F. ; FLAHERTY, A.L.: Elastohydrodynamic analysis of reverse pumping in rotary lip seals with microasperities. In: *Journal of Tribology* 117 (1995), Issue 1, p. 53–59
- [SHY00] SUGIMURA, J. ; HASHIMOTO, M. ; YAMAMOTO, Y.: Study of elastohydrodynamic contacts with fluorescence microscope. In: *Tribology Series* 38 (2000), p. 609–617
- [SIHW92] SHAW II, B.T. ; HOULT, D.P. ; WONG, V.W.: Development of Engine Lubricant Film Thickness Diagnostics Using Fiber Optics and Laser Fluorescence / SAE Int., Warrendale, PA. 1992 (920651). – SAE Technical Paper
- [SK13] SHEN, C. ; KHONSARI, M.M.: On the magnitude of cavitation pressure of steady-state lubrication. In: *Tribology Letters* 51 (2013), Issue 1, p. 153–160
- [SKS87] SPONAGEL, S. ; KILTHAU, G. ; SPIES, K.H.: Sealing mechanism of lip seals. In: *Proc. 11th Int. Conf. on Fluid Sealing*, BHRA, 1987. – Paper K4
- [SLH90] STAKENBORG, M.J.L. ; LEEUWEN, H.J. van ; HAGEN, E.A.M. ten: Visco-Elastohydrodynamic (VEHD) Lubrication in Radial Lip Seals: Part 1 — Steady-State Dynamic Viscoelastic Seal Behavior. In: *Journal of Tribology* 112 (1990), Issue 4, p. 578–583

- [SM09] STUPKIEWICZ, S. ; MARCINISZYN, A.: Elastohydrodynamic lubrication and finite configuration changes in reciprocating elastomeric seals. In: *Tribology International* 42 (2009), Issue 5, p. 615–627
- [SP14] SCARAGGI, M. ; PERSSON, B.N.J.: Theory of viscoelastic lubrication. In: *Tribology International* 72 (2014), p. 118–130
- [SPT06] SILVESTRI, M. ; PRATI, E. ; TASORA, A.: Radial lip seals efficiency under dynamic operating conditions. In: *Proceedings of the 5th International Conference on Tribology, AITC-AIT, 2006*
- [SPT07] SILVESTRI, M. ; PRATI, E. ; TASORA, A.: Frictional behavior of radial lip seals under dynamic operating conditions for different elastomer rings. In: *Proc. 19th International Conference on Fluid Sealing BHR Group, 2007*, p. 121–134
- [SS00] SHI, F. ; SALANT, R.F.: A mixed soft elastohydrodynamic lubrication model with interasperity cavitation and surface shear deformation. In: *J Tribol-T ASME* 122 (2000), Issue 1, p. 308–316
- [SS01] SHI, F. ; SALANT, R.F.: Numerical study of a rotary lip seal with a quasi-random sealing surface. In: *J Tribol-T ASME* 123 (2001), Issue 3, p. 517–524
- [SS06] SHEN, D. ; SALANT, R.F.: A transient mixed lubrication model of a rotary lip seal with a rough shaft. In: *Tribology Transactions* 49 (2006), Issue 4, p. 621–634
- [SSKN93] SANDA, S. ; SAITO, A. ; KONOMI, T. ; NOHIRA, H.: Development of Scanning Laser-Induced-Fluorescence Method for Analyzing Piston Oil Film Behavior. In: *Proceedings of the Institution of Mechanical Engineers. Experimental and Predictive Methods in Engine Research and Development. International Conference, 1993*
- [SSSY03] SATO, Y. ; SEKI, K. ; SUGIMURA, J. ; YAMAMOTO, Y.: Experiments and simple modelling of hydrodynamic lubrication in radial shaft seals. In: *Proc. 17th Int. Conf. on Fluid Sealing BHR Group, BHR, 2003*, p. 139–156
- [Sta88a] STAKENBORG, M.J.L.: *On the sealing and lubrication mechanism of radial lip seals*, University of Eindhoven, Doctoral Thesis, 1988

- [Sta88b] STAKENBORG, M.J.L.: On the sealing mechanism of radial lip seals. In: *Tribology International* 21 (1988), Issue 6, p. 335–340
- [STNY00a] SATO, Y. ; TODA, A. ; NAKAMURA, K. ; YAMAMOTO, Y.: A study on the fluid-flow and the film-thickness of radial shaft seals using fluorescent micro-capsule visualization and laser-induced fluorescent method. In: FLITNEY, R. (Ed.): *Proc. 16th Int. Conf. on Fluid Sealing, Brugge, Belgium, 18–20 September 2000* Vol. 42, Bury St. Edmunds; Professional Engineering Publishing, 2000 (BHR Group Conference Series Publication), p. 71–86
- [STNY00b] SATO, Y. ; TODA, A. ; NAKAMURA, K. ; YAMAMOTO, Y.: Measurement of the Lubricant Film Thickness of Radial Shaft Seals using Laser Induced Fluorescent Method. In: *Proc. Int. Tribology Conf. Nagasaki 2000, 2000*, p. 1897–1902
- [STON99] SATO, Y. ; TODA, A. ; ONO, S. ; NAKAMURA, K.: A Study of the Sealing Mechanism of Radial Lip Seal with Helical Ribs – Measurement of the Lubricant Fluid Behavior Under Sealing Contact / SAE. 1999 (1999-01-0878). – SAE Technical Paper
- [SU73] SCHNÜRLE, F. ; UPPER, G.: Influence of Hydrodynamics on the Performance of Radial Lip Seals. In: *ASLE Transactions* 16 (1973), Issue 4, p. 310–315
- [SWM<sup>+</sup>98] SANTIAGO, J.G. ; WERELEY, S.T. ; MEINHART, C.D. ; BEEBE, D.J. ; ADRIAN, R.J.: A particle image velocimetry system for microfluidics. In: *Experiments in Fluids* 25 (1998), Issue 4, p. 316–319
- [TH00] THIROUARD, B. ; HART, D.P.: Investigation of Oil Transport Mechanisms on the Piston Second Land of a Single Cylinder Diesel Engine, Using Two-Dimensional-Laser-Induced Fluorescence. In: *Laser Techniques Applied to Fluid Mechanics: selected papers from the 9th international symposium, Lisbon, Portugal, July 13–16, 1998*. Springer, 2000, p. 487–503
- [Tin80] TING, L.L.: Development of a laser fluorescence technique for measuring piston ring oil film thickness. In: *Journal of Lubrication Technology* 102 (1980), Issue 2, p. 165–170
- [TLF93] TOURNERIE, B. ; LÉPINE, M. ; FRÊNE, J.: Thickness Measurement Methods for Thin Lubricant Films. Applica-

- tion to A Radial Face Seal. In: *Tribology Series* 25 (1993), p. 577–592
- [TNFY98] TAKIGUCHI, M. ; NAKAYAMA, K. ; FURUHAMA, S. ; YOSHIDA, H.: Variation of Piston Ring Oil Film Thickness in an Internal Combustion Engine—Comparison between Thrust and Anti-Thrust Sides / SAE. 1998 (No. 980563). – SAE Technical Paper. – Engine Component Technology (SAE Int.): SP-1317
- [TO00] TAMURA, T. ; OBAYASHI, S.: A Consideration of the Leakage Mechanism of Radial Lip Seals. In: *Proc. Int. Tribology Conf. Nagasaki 2000*, 2000, p. 1909–1913
- [TR92] TANIMOTO, K. ; RABINOWICZ, E.: A fluorescence technique for measuring lubricant thickness on hard magnetic disks. In: *Tribology Transactions* 35 (1992), Issue 3, p. 537–543
- [Tri98] TRIPP, J.H.: Rough Surface Characterization. In: BHUSHAN, B. (Ed.): *Tribology Issues and Opportunities in MEMS*, Springer, 1998, p. 135–148
- [TS78] THOMAS, T.R. ; SAYLES, R.S.: Some problems in the tribology of rough surfaces. In: *Tribology International* 11 (1978), Issue 3, p. 163–168
- [TS92] TØNDER, K. ; SALANT, R.: Non-leaking lip seals: A roughness effect study. In: *Journal of Tribology* 114 (1992), Issue 3, p. 595–599
- [Upp68] UPPER, G.: *Dichtlippentemperatur von Radialwellendichtungen*, Universität Karlsruhe, Doctoral Thesis, 1968
- [Vis92] VISSCHER, M.: *The measurement of the film thickness and the roughness deformation of lubricated elastomers*, University of Eindhoven, Doctoral Thesis, 1992
- [Wan12] WANGENHEIM, M.: *Untersuchungen zu Reibmechanismen an Pneumatikdichtungen*, Leibniz Universität Hannover, Doctoral Thesis, 2012
- [Weno4b] WENNEHORST, B.: *Entwicklung einer optischen Einrichtung zur Untersuchung des dynamischen Dichtspalts von Stangen- und Wellendichtungen; English title: Design of an optical device for investigations into the dynamic sealing gap of rod an rotary shaft seals*, Institut für Maschinenkonstruktion und Tribologie (IMKT), Leibniz Universität Hannover, Diplom thesis, 2004



- [Wen08] WENNEHORST, B.: Wälzlagerdichtungen: Schutzdichtungen für Wälzlager; Forschungsvorhaben Nr. 432 I der FVA / Forschungsvereinigung Antriebstechnik e.V. Frankfurt a.M., 2008 (Nr. 876). – Forschungsheft
- [WEP11] WENNEHORST, B. ; ENGELKE, E. ; POLL, G.W.G.: Modelling radial lip seal friction — A multi-scale mixed lubrication approach. In: FLITNEY, R. (Ed.): *Proc. 21st International Conference on Fluid Sealing*, BHR Group, Cranfield, 2011
- [WH91] WONG, V.W. ; HOULT, D.P.: Experimental survey of lubricant-film characteristics and oil consumption in a small diesel engine / SAE Int., Warrendale, PA. 1991 (910741). – SAE Technical Paper
- [WM05] WERELEY, S.T. ; MEINHART, C.D.: Micron-resolution particle image velocimetry. In: BREUER, K.S. (Ed.): *Microscale Diagnostic Techniques*. Springer, 2005, p. 51–112
- [WM10] WERELEY, S.T. ; MEINHART, C.D.: Recent advances in micro-particle image velocimetry. In: *Annual Review of Fluid Mechanics* 42 (2010), p. 557–576
- [Wol87] WOLF, A.: *Untersuchungen zum Abdichtverhalten von druckbelastbaren Elastomer- und PTFE-Wellendichtungen*, Universität Stuttgart, Doctoral Thesis, 1987
- [Wol93] WOLLESEN, V.: *Temperaturbestimmung in der Dichtzone von Radialwellendichtringen als Randbedingung für die Modellierung des Dichtvorgangs*, Universität Hamburg Harburg, Doctoral Thesis, 1993
- [WP06] WENNEHORST, B. ; POLL, G.W.G.: Optische Untersuchungen zu Vorgängen im Dichtspalt von Wellendichtungen. In: *Radialwellendichtringe: VI. Hamburger Dichtungstechnisches Kolloquium Dynamische Dichtungen*. Hamburg-Harburg, 2006
- [WP07] WENNEHORST, B. ; POLL, G.W.G.: Einfluss von Schmierstoffkontaminationen auf Lebensdauer und Betriebseigenschaften von Wälzlagern. In: *Tribologie und Schmierungstechnik* 54 (2007), Issue 5, p. 11–17
- [WP08] WENNEHORST, B. ; POLL, G.W.G.: Optical Investigations into the Dynamic Sealing Gap of Radial Shaft Seals. In: BARTZ, W.J. (Ed.): *Lubricants, materials and lubrication engineering: 16th International Colloquium Tribology, 15–17 January 2008, Ostfildern, Germany*, TAE, Technische Akademie Esslingen, 2008

- [WP09c] WENNEHORST, B. ; POLL, G.W.G.: Investigations into the tribological characteristics of radial lip seals — LIF and friction measurements. In: FLITNEY, R. (Ed.): *Proc. 20th International Conference on Fluid Sealing, 7–9 October 2009, Nottingham (UK)*, BHR Group, 2009, p. 213–229
- [WP14] WENNEHORST, B. ; POLL, G.W.G.: Soft micro-elastohydrodynamic lubrication and friction at rough conformal contacts. In: *Proceedings of the Institution of Mechanical Engineers, Part J: Journal of Engineering Tribology* 1350650114558322 (2014). <http://dx.doi.org/10.1177/1350650114558322>. – DOI 10.1177/1350650114558322. – Published online before print November 4, 2014
- [WP15] WENNEHORST, B. ; POLL, G.W.G.: Bi-sinusoidal roughness modeling for soft micro-elastohydrodynamic asperity lubrication in rough conformal contacts. In: *Proceedings of the 42nd Leeds–Lyon Symposium on Tribology*. Lyon, France, 2015
- [WS03] WEIMAR, H.-J. ; SPICHER, U.: Crank-Angle Resolved Oil Film Thickness Measurement Between Piston Ring And Cylinder Liner In A Spark Ignition Engine. In: *Proc. ASME Internal Combustion Engine Division 2003 Spring Technical Conference*, 2003
- [WSLW16] WENK, J.F. ; STEPHENS, L.S. ; LATTIME, S.B. ; WEATHERLY, D.: A multi-scale finite element contact model using measured surface roughness for a radial lip seal. In: *Tribology International* 97 (2016), p. 288–301
- [WTJF98] WELLER, H.G. ; TABOR, G. ; JASAK, H. ; FUREBY, C.: A tensorial approach to computational continuum mechanics using object-oriented techniques. In: *Computers in Physics* 12 (1998), Issue 6, p. 620–631
- [WYHC11] WEN, C. Y. ; YANG, A. S. ; HUANG, F. J. ; CHANG, H. T.: New deflected-helix ribbed lip seal with enhanced sealing performance. In: *Tribology International* 44 (2011), Issue 12, p. 2067–2073
- [WYTT11] WEN, C.-Y. ; YANG, A.-S. ; TSENG, L.-Y. ; TSAI, W.-L.: Flow analysis of a ribbed helix lip seal with consideration of fluid–structure interaction. In: *Computers & Fluids* 40 (2011), Issue 1, p. 324–332
- [ZLS<sup>+</sup>12] ZHOU, Q. ; LI, Z. M. ; SANG, S. J. ; TANG, J. P. ; AN, Q.: A numerical simulation method for hydrodynamic lubrication of lip seal. In: *Proceedings of the Institution*

*of Mechanical Engineers, Part J: Journal of Engineering Tribology* 226 (2012), Issue 2, p. 99–110

- [ZLTA<sub>13</sub>] ZHOU, Q. ; LI, Z. ; TANG, J. ; AN, Q.: Thermoelastohydrodynamic analysis of auto water pump bearing seal. In: *Proceedings of the Institution of Mechanical Engineers, Part J: Journal of Engineering Tribology* 227 (2013), Issue 10, p. 1101–1116
- [ZTL<sup>+</sup><sub>05</sub>] ZOU, Q. ; TIAN, Y. ; LIU, X. ; WEN, S. ; WEN, S. ; BARBER, G.C.: Study of flow characteristics of lubricant in spiral-groove bearings by the fluorescent method. In: *Tribology Transactions* 48 (2005), Issue 2, p. 259–263
- [ZW<sub>12</sub>] ZHU, D. ; WANG, Q.J.: On the  $\lambda$  ratio range of mixed lubrication. In: *Proceedings of the Institution of Mechanical Engineers, Part J: Journal of Engineering Tribology* 226 (2012), Issue 12, p. 1010–1022



## COLOPHON

This document was typeset in L<sup>A</sup>T<sub>E</sub>X using the typographical look-and-feel `classicthesis` developed by André Miede.



# LEBENS LAUF

## PERSÖNLICHE DATEN

Name            Bengt Wennehorst  
Geburtsdaten   22.07.1977 in Hannover  
Nationalität    deutsch  
Familienstand   verheiratet, ein Kind

## BERUFSTÄTIGKEIT

seit 07/2005    Wissenschaftlicher Mitarbeiter und Doktorand  
am Institut für Maschinenkonstruktion und Tri-  
bologie der Leibniz Universität Hannover  
01 – 06/2005    Wissenschaftliche Hilfskraft mit Abschluss am In-  
stitut für Maschinenkonstruktion und Tribologie  
der Leibniz Universität Hannover

## STUDIUM

1998 – 2004    Maschinenbaustudium an der Leibniz Universität  
Hannover  
Abschluss: Diplom-Ingenieur

## GRUNDWEHRDIENST

1997 – 1998    Grundwehrdienst im Heeresmusikkorps I,  
Hannover

## SCHULE

1990 – 1997    Humboldtschule Hannover  
Abschluss: Abitur  
1988 – 1990    Orientierungsstufe Martensplatz  
1984 – 1988    Grundschule Wettbergen